# Ph.D. Dissertation

Hadeer Waleed Qasim

**2024**

# Organocatalytic Urethane Synthesis – A Computational Study

Ph.D. Dissertation

*Hadeer Waleed Qasim*

Supervisor:

Dr. Béla Fiser

Antal Kerpely Doctoral School of Materials Science & Technology at the Faculty of Materials & Chemical Engineering

Institute of Chemistry

University of Miskolc

2024

*"And be patient for the decision of your lord, for indeed, you are in our eyes. And exalt with praise of your lord[Allah] when you arise."*

***The Noble Qur'an [Chapter 27- At-Tur, Verse 48]***

Supervisor's Recommendation for

**Hadeer Waleed Qasim**

for her doctoral dissertation entitled as

**Organocatalytic Urethane Synthesis – A Computational Study**

I take great pride and pleasure in working with Hadeer Waleed Qasim over the last four years. During this period I have seen her perform well with her colleagues, exercising excellent communication skills, and consistently improving. She was involved in a good number of projects, and already contributed to 15 articles, 6 of which were first author publications accepted in international scientific journals with a ranking of D1, Q1 and Q3. She has participated in 11 different conferences over the years where she presented her work via both oral and poster presentations. During her PhD studies Hadeer spent several weeks in Poland at the University of Lodz which proves that she is able to work in international environments. During her doctoral studies at the University of Miskolc, she proposed two general reaction mechanisms for catalytic urethane formation in the presence of amine and acid catalysts. She was involved in both computational and experimental studies which also proves her ability to carry out research in various frameworks.

Hadeer is a very conscientious scholar who takes projects from their inception and carries them to their completion. She is very active and works well alone as well as in a group environment. Hadeer has a very pleasant personality and it is easy to work with her, because of her amazingly positive attitude and eagerness to stick tightly to deadlines. She is always eager to learn and acquire new knowledge and develop new skills.

All the results published in Hadeer's publications and in her doctoral thesis are her own results and are the indicators of her independent scientific work.

**Based on all of this, I am confident that Hadeer Waleed Qasim is capable of conducting independent research, and I recommend that she be awarded a PhD degree.**

Miskolc, 4 April 2024 Dr. Béla Fiser

# CONTENTS

# ACKNOWLEDGMENT

First and foremost, praise and thank **God**, the Almighty, for His showers of blessings throughout my research work to complete my dissertation successfully.

I would like to express my deep and sincere gratitude to my supervisor **Dr. Béla Fiser**. I do not consider him as my supervisor just but I consider him as my brother, he was like my second family. He did not make me feel that I was far from my family he always supported me not just in scientific things but also my daily life. Also, this thesis would not have been possible without such excellent supervision, he was patient with me, taught me a new field (computational chemistry), and let me love this field. Thank you for the care and attention you have given me over the years, and for celebrating my successes with me.

I would like to thank **Prof. Dr. Béla Viskolcz** for his conscientious guidance and for supporting my doctoral work throughout.

I am grateful and lucky to had a chance to meet and learn from one of the great Hungarian minds **Prof. Imre G. Csizmadia**.

I deeply thank **Dr. Zsolt Fejes** for helping me during my research and carrying out the experimental parts and for everything he taught me during my study period.

Last but not least I acknowledge with a deep sense of reverence, my thanks to my parents **Waleed** and **Sameerah** for their sacrifices, love, caring, and prayers, and for devoting their lives to making me reach this point. Hope I can repay some of your sacrifices and hope to never disappoint you.

I would like to thank from the bottom of my heart my soul mate **Raha**, she is not only my sister, she is my companion, my best friend, she is the person from whom I draw support to complete my days, the person who sacrificed a lot for me, she always trusted on me and encouraged me. Thanks, sister without you I would not have been able to complete my life and career. Also, I am very thankful to my brother-in-law **Kawa**.

I am very much thankful to my brothers **Ahmad** and **Omar** who always supported me morally and encouraged me. They are always there for me when I need them. Thanks to my niece (**Laya**) and nephews (**Adam**, and **Ayham**) for making life more beautiful and full of joy. Thanks to my sister in law.

Thanks to all of my friends who directly or indirectly helped me. Thanks to **Dr. Rachid** for supporting me and being a good friend.

This research was supported by the National Research, Development and Innovation Fund (Hungary) within the TKP2021-NVA-14 project. The GITDA (Governmental Information-Technology Development Agency, Hungary) is gratefully acknowledged for allocating computing resources used in this work. Further calculations have been carried out using resources provided by the Wroclaw Centre for Networking and Supercomputing. This research was funded in part by the National Science Centre, Poland under the MINIATURA 7 call within the project reg. No: 2023/07/X/ST4/01433.

## شكر وتقدير

أولًا وقبل كل شيء، احمد الله تعالى وأشكره على نعمة التي أنعم بها علي طوال فترة دراستي لإتمام اطرروحة الدكتوراة بنجاح.

أود أن أعرب عن امتناني العميق والصادق لمشرفي **Dr. Béla Fiser**. أنا لا أعتبره مشرفي فقط ولكني أعتبره أخي، كان مثل عائلتي الثانية. لم يجعلني أشعر بأنني بعيد عن عائلتي، لقد كان يدعمني دائمًا ليس فقط في الأمور العلمية ولكن أيضًا في الحياة اليومية. كما أن هذه الأطروحة لم تكن ممكنة لولا هذا الإشراف الرائع منه، فقد كان صبورا معي وعلمني مجالا جديدا (computational chemistry) وجعلني أحب هذا المجال. أشكره على الرعاية والاهتمام الذي قدمه لي على مر السنين، وعلى الاحتفال بنجاحاتي معي.

أود أن أشكر **Prof. Dr. Béla Viskolcz** على توجيهاته الحكيمة وعلى دعم عملي طوال الوقت في مرحلة الدكتوراه.

أنا ممتن ومحظوظ لأنني أتيحت لي الفرصة للقاء والتعلم من أحد العقول المجرية العظيمة **Prof. Imre G. Csizmadia**

أشكر **Dr. Zsolt Fejes** على مساعدتي أثناء بحثي ومساعدتي في الجزء العملي واشكره على كل ما علمني إياه خلال فترة دراستي.

أخيرًا وليس آخرًا، أتقدم بالشكر الجزيل إلى والداي **وليد وسميرة** على تضحياتهما وحبهما واهتمامهما وصلواتهما، وعلى تكريس حياتهما لاجلي لكي اتمكن من الوصول إلى ما انا علية اليوم. آمل أن أتمكن من تسديد بعض تضحياتهم وأتمنى ألا أخيب ظنهم أبدًا.

أود أن أشكر من أعماق قلبي توأم روحي **رها**، إنها ليست أختي فقط، هي رفيقتي، أعز صديقاتي، هي الشخص الذي أستمد منه القوة لإكمال أيامي، الشخص الذي ضحى كثيرًا لاجلي، كانت تثق بي دائمًا وتشجعني. شكرا أختي لولاك لم أكن لأتمكن من إكمال حياتي ومسيرتي. واشكر زوج اختي **كاوه**.

وأنا ممتن جدًا لاخوتي **أحمد وعمر** الذان قدمو لي الدعم المعنوي وكانو دائما يشجعوني. اشكرهم لوجودوهم دائمًا بجانبي عندما أحتاج إليهم. شكراً لابنة أختي **(ليا)** وأبناء أخي **(آدم وأيهم)** لأنهم بولادتهم جعلوا الحياة أجمل ومليئة بالفرح. اشكر زوجة اخي.

أشكر كل أصدقائي الذين كانو دعم لي. واخص بالذكر **الدكتور رشيد**.

تم دعم هذا البحث من قبل الصندوق الوطني للبحث والتطوير والابتكار (هنغاريا) ضمن مشروع TKP2021-NVA-14. إن GITDA (الوكالة الحكومية لتنمية تكنولوجيا المعلومات، المجر) معترف بها بامتنان لتخصيص موارد الحوسبة المستخدمة في هذا العمل. تم إجراء المزيد من الحسابات باستخدام الموارد المقدمة من مركز Wroclaw للشبكات والحوسبة الفائقة. تم تمويل هذا البحث جزئيًا من قبل المركز الوطني للعلوم في بولندا بموجب دعوة MINIATURA 7 ضمن نطاق المشروع. رقم: X/ST4/01433/07/2023.

# TABLE OF FIGURES

# TABLE OF TABLES

# TABLE OF ABBREVIATION

| | |
|---|---|
| PU | Polyurethane |
| CAGR | Compound Annual Growth Rate |
| TPUs | Thermoplastic Polyurethanes |
| PUD | Waterborne Polyurethane Dispersion |
| NCO | Isocyanate |
| PUB | Polyurethane Binders |
| CASE | Coatings, Adhesives,Sealants And Elastomers |
| WPUs | Waterborne Polyurethanes |
| PUDs | Polyurethane Dispersions |
| EMI | Electromagnetic Interference Shielding |
| TDI | toluene diisocyanate |
| MDI | methylene diphenyl diisocyanate |
| HDI | hexamethylene diisocyanate |
| HMDI | hydrogenated methylene diphenyl diisocyanate |
| Pmdi | polymeric methylene diphenyl diisocyanate |
| MDA | 4,4'-methylenedianiline |
| TDA | toluenediamine |
| $CO_2$ | carbon dioxide |
| CFCs | chlorofluorocarbons |
| HFCs | hydrogenated fluorocarbons |
| HCFCs | hydrogenated chlorofluorocarbons |
| Cat. | Catalysts |
| DMHP | dimethyl hydrogen phosphate |
| MSA | methanesulfonic acid |
| TFMSA | trifluoromethanesulfonic acid |
| $NH_3$ | ammonia |
| DBU | 1,8-diazabicyclo[5,4,0]undec-7-ene |
| APIM | 1-(3-aminopropyl)imidazole |
| 1-MIM | 1-methylimidazole |
| DMCHA | *N,N*-dimethylcyclohexanamine |
| DMP | 1,4-dimethylpiperazine |
| DABCO | 1,4-diazabicyclo[2.2.2]octane |
| PMDETA | *N,N,N',N'',N''*–pentamethyldiethylenetriamine |
| DMPDA | *N,N*-dimethyl-1,3-propanediamine |
| 1,2-DMI | 1,2-dimethylimidazole |
| NEM | *N*-ethylmorpholine |
| DMEE | 2-(2-dimethylaminoethoxy)ethanol |
| DMAEE | bis[2-(*N,N*-dimethylamino)ethyl]ether |
| N-MM | 4-methylmorpholine |
| DMDEE | 2,2-dimorpholinodiethylether |
| DMEA | 2-dimethylaminoethanol |
| Eq | Equation |

| | |
|---|---|
| BO | Born-Oppenheimer |
| PES | Potential Energy Surface |
| PEC | Potential Energy Curve |
| 2D | Two Dimensional |
| G | Gibbs Free Energy |
| S | Entropy |
| H | Enthalpy |
| T | Temperature |
| P | Pressure |
| DFT | Density Functional Theory |
| CC | Coupled-Cluster |
| HF | Hartree–Fock |
| MP | Møller–Plesset |
| LSDA | Local Spin Density Approximation |
| SPWL | Slater Perdew-Wang Local |
| PZ | Perdew-Zunger |
| VWN | Vosko-Wilk-Nusair |
| PW | Perdew-Wang |
| GGA | Generalized Gradient Approximation |
| PBE | Perdew-Burke-Ernzerhof |
| B88 | Becke88 |
| BLYP | Becke, Lee–Yang–Parr |
| meta-GGAs | Meta-Generalized Gradient Approximation |
| TPSS | Tao–Perdew–Staroverov–Scuseria |
| B3LYP | Becke, 3 parameter, Lee-Yang-Parr |
| Myz | Minnesota Functionals |
| BHandHLYP | Becke, Half-and-Half, Lee-Yang-Parr |
| STO-Ng | Slater Type Orbital, with n – Number of Primitive Gaussian Functions |
| cc-Pvdz | Correlation-Consistent Valence Double Zeta |
| cc-Pvtz | Correlation-Consistent Valence Triple Zeta |
| cc-Pvqz | Correlation-Consistent Valence Quadruple Zeta |
| QCISD(T) | Quadratic Configuration Interaction with Single, Double and Triple Excitations |
| ZPE | Zero-Point Correction |
| HLC | Higher-Level Correction |
| DMDEE | 2,2-dimorpholinodiethylether |
| Qg3MP2BHandHLYP | quasi-G3MP2BHandHLYP |
| PA | Proton Affinity |
| SMD | Solvation Model Density |
| PCM | Polarizable Continuum Model |
| THF | Tetrahydrofuran |
| MeCN | Acetonitrile |
| $\varepsilon_r$ | Dielectric Constant |
| R | Reactant |
| RC | Reactant Complex |

| | |
|---|---|
| TS | Transition State |
| IM | Intermediate |
| PC | Product Complex |
| P | Product |
| Å | Angstrom |
| $\Delta_r H$ | Relative Enthalpy |
| $\Delta_r E_0$ | Zero-Point Corrected Relative Energy |
| $\Delta_r G$ | Relative Gibbs Free Energy |
| RNH2 | Primary Amine |
| R2NH | Secondary Amine |
| R3N | Tertiary Amines |
| $R_2C = N\text{-}R$ | Secondary Ketimine |
| $PA_{calc}$ | Computed Proton Affinities |
| $PA_{exp}$ | Measured Proton Affinities |
| PhNCO | Phenyl isocyanate |
| BuOH | Butan-1-ol |
| MeOH | Methanol |
| DMIPA | *N,N*-dimethylpropane-2-amine |
| TMPD | *N,N,N',N'*-tetramethylpentane-1,5-diamine |
| DMAEDMED | *N*-[2-(dimethylamino)ethyl]-N',N'-dimethylethane-1,2-diamine |
| 1N | Aromatic Nitrogen |
| 2N | Aliphatic Nitrogen |

## 1. Introduction

The field of polymer science emerged to develop new materials for growing civil and military needs. It tends to be more interdisciplinary than most sciences, combining chemistry, chemical engineering, and other fields as well[1,2]. The first polymers used were natural products, especially cotton, starch, proteins, and wool. The first synthetic polymers were made early in the twentieth century[3]. In 1937 one of the most special polymer types with versatile properties was discovered[4] **(Figure 1)**. This special type of polymer is polyurethane (PU), which was developed by Otto Bayer to compete with nylon[5,6]. Bayer's invention ranks among the most important breakthroughs in polymer science. At the beginning of the 1950s, researchers were able to use PUs to produce soft foam plastic. In the early 1960s, synthetic PU adhesive, PU flexible fiber, and others types were developed [7]. From the mid-1960s to the 1990s, the development of polyurethanes significantly increased and it became unavoidable in many applications[8,9]. In 2018 the PU market reached 59.5 billion USD globally and it is expected to grow between 2019 and 2026 by 5.8% CAGR (compound annual growth rate)[10,11] (**Figure 1**).

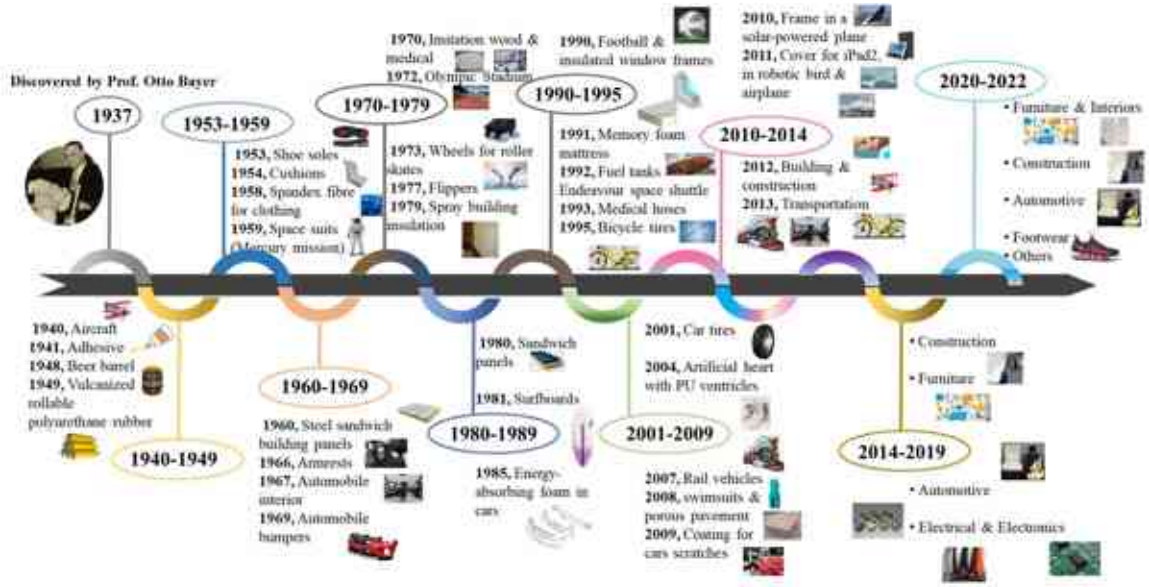


***Figure 1.*** *Timeline of major developments in the history of polyurethane.*

Polyurethane is used in a large array of industries as flexible, and rigid foams, elastomers, and thermoplastic materials[12]. Most of the PU types are designed to make life more comfortable and products more durable[13,14].

## 1.1 Polyurethane Chemistry

Polyurethanes (PU) are a special group of heterochain polymers (**Figure 2**).

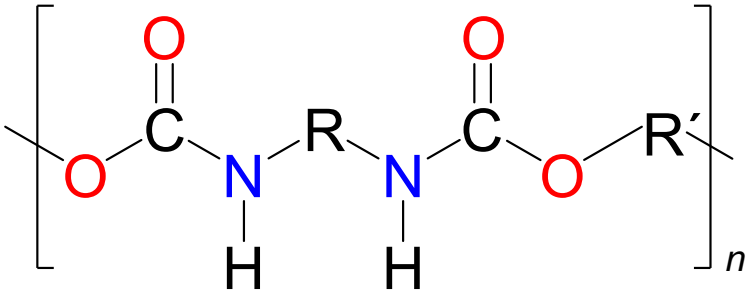


***Figure 2**. Schematic structure of polyurethane.*

Urethane group (-NH-COO-) is formed by the reaction of isocyanate (NCO) and hydroxyl (OH) groups[15,16] (**Figure 3**).

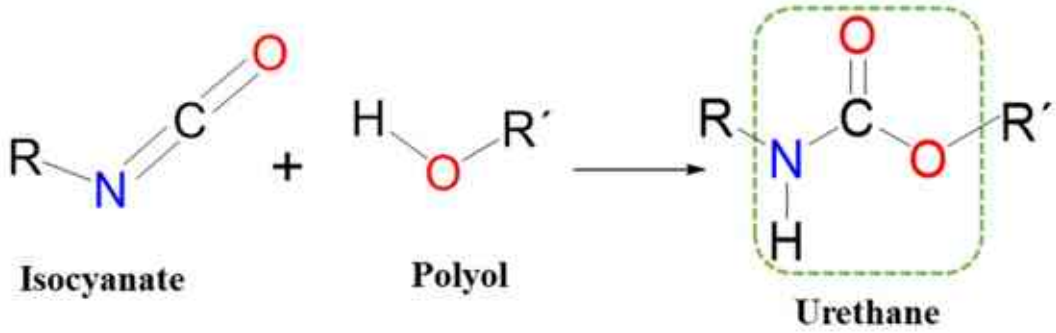


***Figure 3**. Schematic representation of urethane formation.*

### 1.1.1 Isocyanates

Isocyanate is a chemical that contains at least one isocyanate group (-N=C=O) in its structure. In PU synthesis two types of isocyanates, aromatic and aliphatic ones are used. Aromatic isocyanate is the most common type applied in the PU industry such as toluene diisocyanate (TDI), methylene diphenyl diisocyanate (MDI), and their oligomers for increased functionality and cross-linking. Mostly their application focuses on rigid and thermoset polyurethane[17]. To ultraviolet light and outdoor weathering resistance, aliphatic polyisocyanates such as hexamethylene diisocyanate (HDI) and hydrogenated MDI (HMDI) can be applied. These are also used in coatings as they blend well with pigments, and retain a gloss aspect[18]. However, these aliphatic molecules are less reactive and more expansive compared to their aromatic counterparts[19].

The reactions between a diisocyanate, a linear long-chain polyol, and a low-molecular-weight chain extender will lead to the production of elastomers. The properties of the elastomers are determined mainly by the chain structure, the degree of branching of the polymeric intermediate, and the

stoichiometric balance of the components. To achieve optimal mechanical strength, the ratio of NCO groups compared to OH groups usually has to be kept in the range of 1.0–1.1. As the ratio falls below 1.0, the mechanical strength, hardness, and resilience decrease, and elongation and compression set to increase very sharply[20].

#### 1.1.1.1 Methylene Diphenyl Diisocyanate (MDI)

Methylene diphenyl diisocyanate (MDI) is the generic name of a product used in industrial settings. Monomeric 4,4'-MDI is a white to pale yellow solid at room temperature, with a molecular weight of 250 (g/mol) (**Figure 4**). It has a boiling point of >300 °C at 101.3 kPa, and a melting point of 39–43 °C, and a vapor pressure of <1 mPa at 20 °C. It has a transient existence in water; thus, its water solubility is only notional. However, monomeric MDI is soluble in octane, benzene, and kerosene[21]. Although monomeric MDI is also available, but polymeric MDI (pMDI) is the primary technical/commercial form of methylene diphenyl diisocyanate, and pMDI is actually a mixture that contains 25–80% of monomeric 4,4'-MDI as well as oligomers containing 3–6 rings and other minor isomers, such as the 2,2'-MDI (**Figure 4**). The exact composition of pMDI varies with the manufacturer. pMDI is a dark reddish brown liquid with an indefinite melting point around 0 °C and a vapor pressure of <1 mPa at 20 °C. MDI is highly reactive in the environment or when taken up by organisms and is rapidly hydrolysed to form 4,4'-methylenedianiline (MDA), which reacts with excess MDI to yield insoluble oligurias and polyureas[22] .

MDI is used for polyurethane elastomer synthesis which has a wide variety of applications (rollers, packing, rubber vibration insulators, synthetic leather, spandex fibers, rubber shoe soles *etc*.). Polymeric MDI is applied to make rigid and flexible foams, foundry resin sand binders, and heat insulating materials [22] (**Figure 4**).

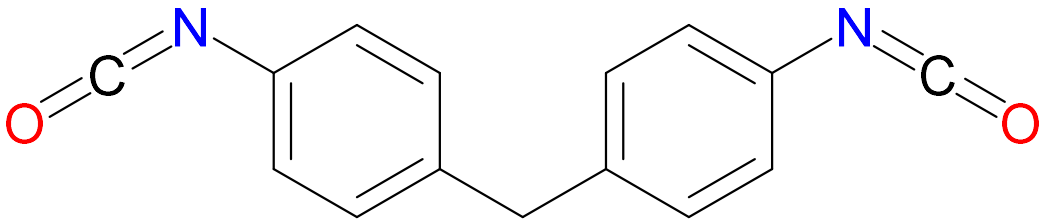

4,4'-methylenediphenyl diisocyanate (4,4'-MDI)

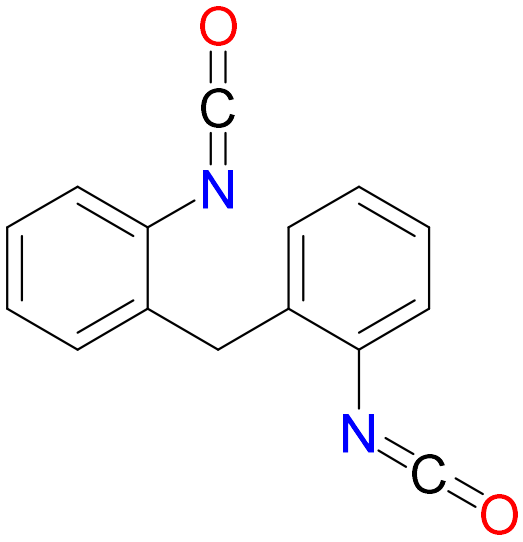

2,2'-methylenediphenyl diisocyanate (2,2'-MDI)

***Figure 4.*** *Chemical structure of 4,4'-MDI, and 2,2'-MDI.*

1.1.1.2. Toluene diisocyanate (TDI)

Toluene diisocyanate (TDI) (**Figure 5**) is one of the most common and most volatile aromatic isocyanates used in the production of polyurethane polymers. It is commonly a colorless or pale-yellow liquid consisting of a mixture of 2,4- and 2,6-TDI isomers which will polymerize readily in air (**Figure 5**). It has a high vapor pressure (3.33Pa at 25 °C; boiling point 115-120 °C) and must be strictly controlled to prevent fugitive emission losses to the atmosphere. TDI liquid must be managed carefully, because below 8-14 °C, it will begin to freeze, creating special problems in outdoor handling activities for much of the year[23].

The amine raw materials are generally manufactured by the hydrogenation of the corresponding nitro compounds; in this case, toluenediamine (TDA) is synthesized from dinitrotoluene, which then converted to toluene diisocyanate (TDI)[24].

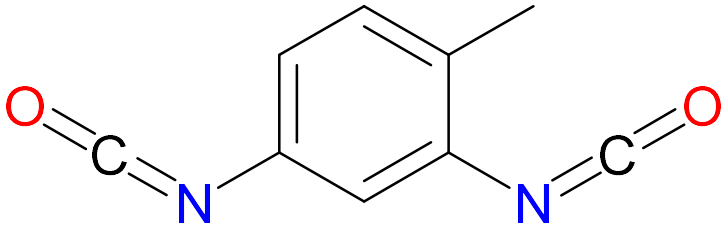


2,4-Toluene diisocyanate (2,4-TDI)

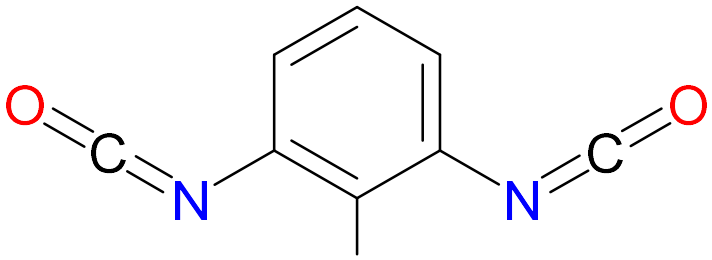


2,6-Toluene diisocyanate (2,6-TDI)

***Figure 5.*** *Chemical structure of 2,4-TDI, and 2,6-TDI.*

### 1.1.2 Polyols

Polyols are the second main components used in polyurethane production. Polyols compose the biggest number of starting materials that can be used to design PU. These species are generally structures containing two or more hydroxyl groups. This group of molecules can be divided into high and low-molecular-weight polyols. If the applied polyol has a high molecular weight, with long alkyl segments, flexible or elastic polyurethanes can be created, due to their linear chains allowing free rotation accompanied by low functionality and a low degree of cross-linking. While, if the applied polyol has a low molecular weight, rigid polyurethanes will be produced. Due to their short chains and high functionality an increase in their viscosity will occur which leads to highly branched and cross-linked polyurethane[25]. The reactivities are not the same for all hydroxyl groups. Primary alcohols react readily at 25–50°C, while the secondary and tertiary alcohols are about 0.3 and 0.005 times less reactive than the primary ones, respectively[26].

Polyols are very important components of polyesters and polyurethanes. As chain extenders, they control to a large extent the mechanical, thermal, and physical property of the polymer and can reduce the overall cost[26].

Most of the polyols that are used in the production of PUs are derived from petroleum feedstock. However, the increasing concern over the environmental impact and the availability of petroleum has motivated the development of bio-and renewable raw material-based polymers.

Thus, the application of renewable and sustainable chemicals, such as green and bio-based polyols, have been increased significantly in the production of PUs[27–29].

Thus, there are many reactions involved in polyurethane synthesis such as the reaction of isocyanate with alcohols, water, urethane, urea, and carboxylic acid[30,31].

### 1.1.3 Reaction of Isocyanates and Alcohols

The reaction of isocyanate with alcohol is one of the most important reactions in the synthesis of polyurethane. This exothermic reaction will lead to the formation of urethane bonds (**Figure 6**)[32]. Where the oxygen (nucleophilic) of the alcohol group will react with the carbon (partially positive) of the isocyanate group[33]. This leads to the transfer of a proton from the hydroxyl group to the nitrogen of the isocyanate group, and thus, urethane bond will be formed[34].

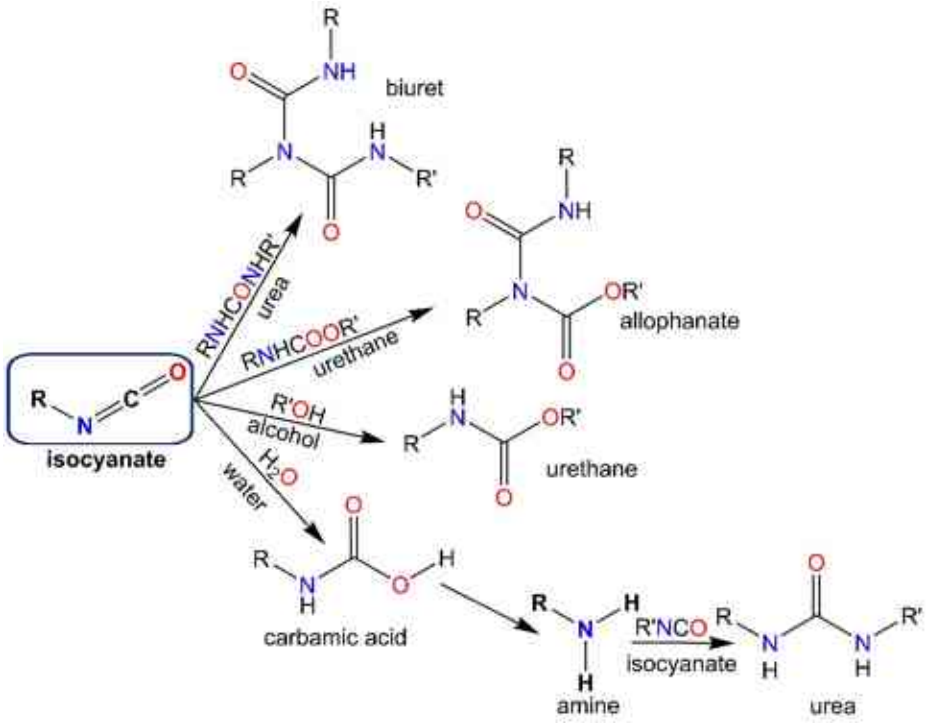


***Figure 6.*** *Possible reactions of isocyanate (NCO) with various reaction partners.*

### 1.1.4 Reaction of Isocyanate with Water

The reaction of isocyanate with water is an important sidereaction in urethane formation besides the isocyanate-alcohol reaction[35]. The isocyanate-water reaction is more exothermic than the reaction with alcohol. In PU synthesis water is commonly used as a blowing agent[36]. The reaction between the isocyanate and water will lead to the formation of an intermediate carbamic acid which decomposes to form amine and carbon dioxide ($CO_2$)[37]. Then, the resulting amine will react with another isocyanate and urea will be generated[38] (**Figure 6**).

### 1.1.5 Reaction of Isocyanates and Urethane

The reaction between isocyanate and urethane will lead to the formation of an allophanate[39,40]. As the hydrogen atom will be linked to the nitrogen atom, therefore, the urethane group can be considered HXR. The formation of allophanate work at high temperature (> 110 ºC) and it is a reversible reaction[41] (**Figure 6**).

### 1.1.6 Reaction of Isocyanates and Urea

Isocyanates can react with urea as well to yield a biuret[42]. The reaction of the isocyanate with urea is an equilibrium reaction, similar to the isocyanate-urethane reaction. High temperatures (>110 °C) are needed to form a biuret[39] (**Figure 6**).

## 1.2 Other Raw Materials Used for the Synthesis of Polyurethanes

The properties of polyurethanes are affected by the chemical structure and the functionality of isocyanates and polyols[43]. However, other materials can also affect polyurethane synthesis such as catalysts, chain extenders, crosslinkers, surfactants, and blowing agents[44]. Chain extenders are used in polyurethane synthesis, and have a low molecular weight which affects the thermal, and mechanical properties, morphology, and cellular structure of polyurethane. Also, they increase the block length of the rigid segment. Chain extenders are diols or diamines, and they can be aromatic or aliphatic[45,46]. Meanwhile, the cross-linkers are important for polyurethane to control the mechanical strength and rigidity of the polyurethane properties. Cross-linking is a chemical process that leads to creating a covalent bond between the polymeric chains leading to forming an interconnected network. Using aromatic or cyclic cross-linkers various properties of the products can be finetuned such as thermal stability, resistance to fire, and mechanical strength compared to the aliphatic cross-linkers[47]. Surfactants are often used in the manufacture of polyurethane foams. It is used to enhance the distribution of the isocyanate and polyol to promote a homogenous phase and provide stability in developing cellular structures. The mechanisms for surfactants work in two-step. First, it affects the raw material mixture by lowering the surface tension. Second, provides emulsification for the whole system[48]. Meanwhile, besides their application in foaming purposes, they are also used for nonfoaming, which will allow the release of air and function as a wetting agent, where this step is necessary for the development of coatings to evenly cover a surface and prevent delamination[49]. Blowing agents are important for the properties of the foam produced. The final characteristics of the produced foam are controlled by the quantity, quality, and nature of a blowing agent[50]. The classification of the blowing agents includes the physical and chemical blowing agents. Different blowing agents are used in the polyurethane technology

such as chlorofluorocarbons (CFCs), hydrogenated fluorocarbons (HFCs), hydrogenated chlorofluorocarbons (HCFCs), low-boiling saturated and unsaturated hydrocarbons, and water which led to the formation of carbon dioxide[51].

### 1.2.1 Catalysts

The term catalysis was coined by Berzelius over 150 years ago, and it comes from the Greek words ″kata″ meaning down and ″lyein″ meaning loosen[52]. Berzelius wrote that the term catalysis meant "the property of exerting on other bodies an action which is very different from chemical affinity. By means of this action, they produce decomposition in bodies and form new compounds into the composition of which they do not enter″[53]. Many years later in 1895, Ostwald came up with the definition that we use until today: ″a catalyst is a substance that changes the rate of a chemical reaction without itself appearing in the products″[54],[55]. In 1998 the foundation for green chemistry was laid down including twelve principles[56]. Two of these principles are energy efficiency and the use of catalysts. As in this work, the system deals with catalytic urethane formation which eventually leads to better energy efficiency.

Catalysis plays a fundamental role in industrial chemical transformations. More than 85% of synthetic chemicals are made through catalytic processes since catalysts promote more energetically favorable reactions in comparison to non-catalytic ones, thus, allowing the use of milder reaction conditions. Catalysts have a significant influence on polymerization reaction mechanisms (*e.g.* free-radical, cationic, anionic, and insertion polymerization). Among others, Ziegler–Natta as well as metallocene catalysts which have been successfully introduced in the industry for the production of polymers for new applications has to be mentioned[57]. Catalysts come in a multitude of forms, ranging from atoms and molecules to large structures like zeolites or enzymes. Moreover, they may be used in different surroundings: in gas, liquid, or at the surface of solid materials[58]. Catalysts can be classified according to their physical state, chemical nature, or the nature of the reactions that they catalyze. In the following section, three types will be differentiated: biocatalysts, homogeneous, and heterogeneous catalysts (**Figure 7**)[59,60].

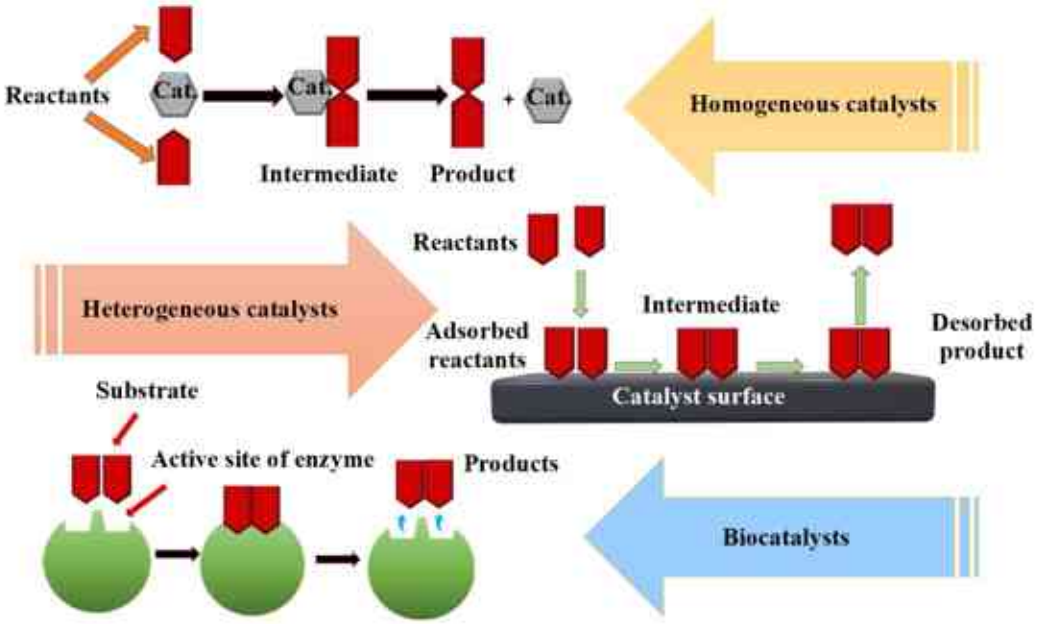


***Figure 7.*** *Common catalyst types: homogeneous, heterogeneous, and biocatalysts.*

Biocatalysis is the use of natural catalysts, such as enzymes, to carry out chemical transformations on organic compounds. Enzymes are highly specific and efficient catalysts (**Figure 7**). Thus, using biocatalysts in a reaction will give a predominant product, with high yield and shorter reaction time which will make the reaction ecofriendly[61]. Enzymes can be employed to obtain polymers of regular structure when high stereo-, regio- and chemoselectivity is needed. Furthermore, these special structures can be used succesfully in the production of new complex functional polymers based on natural compounds[62]. It is an important subspecialty of white biotechnology used in the manufacture of a large variety of chemical products required for the production of medicines and crop protectants, biodiesel, detergents, biosurfactants, food additives, functionalized biopolymers, and others[63]. Biocatalysis has developed into an industrially attractive technology and has been incorporated into mainstream organic synthesis[64]. Homogeneous catalysis, refers to a catalytic system in which the substrates for a reaction and the catalyst components are brought together in the same phase, usually in the liquid phase[65,66] (**Figure 7**). In heterogenous catalysis the substrates for a reaction and the catalyst are in a different phase, usually liquide and solid, respectively[67] (**Figure 7**). Heterogeneous catalysts are widely used in many important industrial applications such as hydrogenations, synthesis of ammonia, and ethylene oxidation because of simplifying the separation and purification steps[68–70].

Meanwhile, the right choice of the catalyst has a significant effect on polymer formation and on the time required for polymerization. The presence of the right catalysts accelerates polymerization[71]. Moreover, the catalyst can also affect the properties of the polymeric products

such as polyurethanes[72],[73]. In relation to PU synthesis, catalysts are often used to accelerate the reaction rate of polynucleophiles with isocyanate groups or to promote the trimerization of the isocyanate group to form cross-linked polymers. In the production of polyurethane, the amount of applied catalysts is small, but their impact is significant[74]. They can promote the foaming reaction. Polyurethane foam formation basically consists of two primary reactions, the first one is the urethane formation (gelling) which involves the reaction of the isocyanate with alcohol. This reaction leads to the formation of a cross-linked polymer, as several hydroxyl groups are used[75,76]. The second one is the urea formation (blowing), which is produced by adding water to isocyanates accompanied by the release of carbon dioxide as the blowing agent[77,78]. Furthermore, catalysts play an important role in the control and balance between the gelling and blowing reactions. They help to accurately control the relative reaction rates of the isocyanate with both alcohol and water. The imbalance between them is the reason for the foam collapse or formation of inappropriate cells that can be closed or opened prematurely[38,79]. Meanwhile, there are secondary reactions occur, when the isocyanate reacts with an urethane, amine, and urea, to produce allophanate, polyurea, and biuret, respectively[80–82].

Polyurethane catalysts mainly include organic acids, organic bases (amine catalysts), and organo-tin (organometallic) catalysts[83–86].

1.2.1.1 Organic Acid

Organic acid catalysts are a type of organic catalysts, which showed to a significant efficiency in urethane formation (alcohol−isocyanate) reaction[87]. The use of acid catalysis is expected to expand the range of metal-free polyurethane syntheses under both solution and bulk polymerization conditions[87]. Meanwhile, there are certain organic acids which are able to promote urethane formation under mild polymerization conditions and low catalyst loadings[88]. On the other hand, organic acid catalysts can extend the range of polymerizable monomers that have amides or additional functionalities that are sensitive to base catalysis[89] (**Figure 8**).

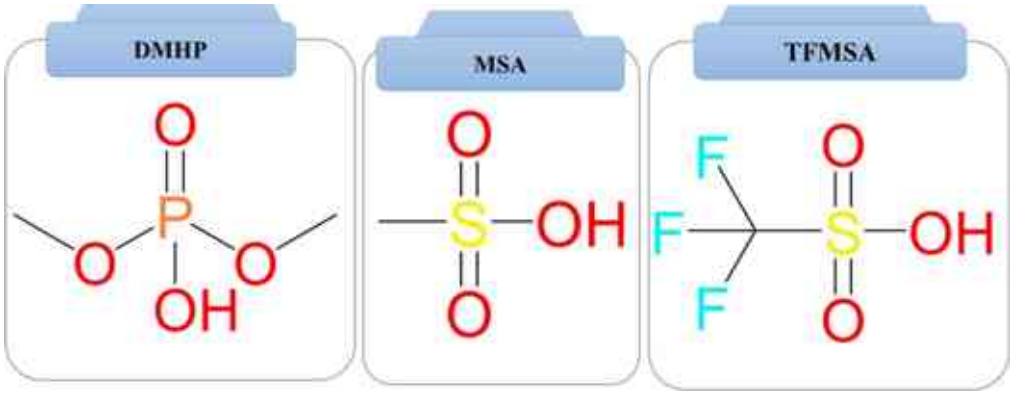


***Figure 8.*** *Structural features of organic acid catalysts commonly used in polyurethane synthesis. dimethyl hydrogen phosphate (DMHP), methanesulfonic acid (MSA), and trifluoromethanesulfonic acid (TFMSA).*

In a previous study, the investigations of the reaction between isocyanates and alcohols at high temperatures using organic acid catalysts were done, and the result showed that the use of organic acid catalysts was not as good as using tin catalysts[90]. Another study showed the ability to synthesize urethane bonds from the diisocyanates and diols in the presence of organic acid catalysts. They found that sulfonic acids were more efficient for polyurethane synthesis than dibutyltin dilaurate or 1,8-diazabicyclo[5.4.0]undec-7-ene. They figured that the employment of organic acid catalysts will lead to expanding the scope of metal-free polyurethane syntheses under both solution and bulk polymerization conditions, as it is effective for polymerizing sterically hindered secondary alcohols and isocyanates[87]. Meanwhile, another study showed that the use of sulfonic acid immobilized organic nanoparticles (nanoacid) exhibits considerable efficiency in catalysing urethane formation[88].

1.2.1.2 Organic Bases (amine catalysts)

Amine catalysts are a type of organic compounds derived from ammonia ($NH_3$) by replacing one or more of the hydrogen atoms with alkyl groups. There is primary, secondary, or tertiary amine depending on replacing one or more hydrogen atoms of ammonia with alkyl groups[91]. In the urethane synthesis the amine group activates the nitrogen-carbon double bond of the isocyanate group rapidly, depending on which of the competing species is close to the activated isocyanate site[85],[37]. There are many types of amines catalysts, and by considering their chemical structures, they can be essentially divided into aliphatic amines, cyclic amines, aromatic amines, alcohol amines, and ether amines (**Figure 9**)[86,91–96]. Previous studies proposed a mechanism for urethane formation in the presence of amine catalysts, but not the whole potential energy surface of the reaction was described[97,98].

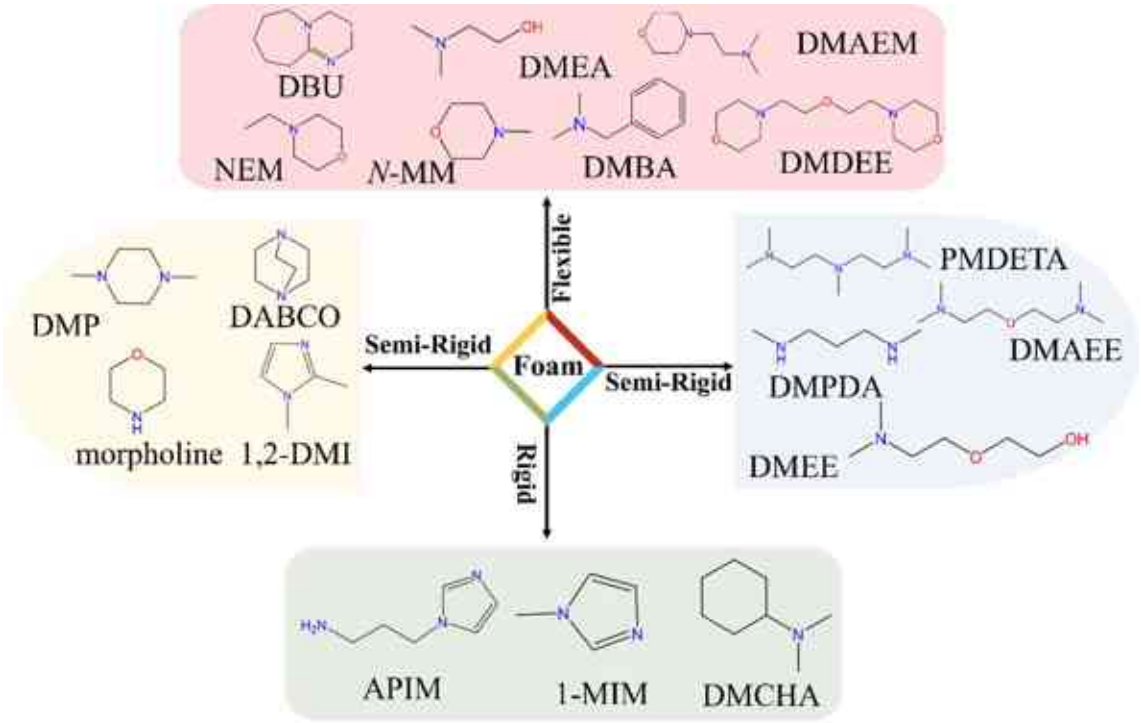


**Figure 9**. Structural features of common amine catalysts and their application. 1,8-diazabicyclo[5,4,0]undec-7-ene (DBU), 1-(3-aminopropyl)imidazole (APIM), 1-methylimidazole (1-MIM), N,N-dimethylcyclohexanamine (DMCHA), 1,4-dimethylpiperazine (DMP), 1,4-diazabicyclo[2.2.2]octane (DABCO), N,N,N',N",N"–pentamethyldiethylenetriamine (PMDETA), N,N-dimethyl-1,3-propanediamine (DMPDA), 1,2-Dimethylimidazole (1,2-DMI), and N-Ethylmorpholine (NEM), 2-(2-dimethylaminoethoxy)ethanol (DMEE), and bis[2-(N,N-dimethylamino)ethyl]ether (DMAEE), 4-methylmorpholine (N-MM), 2,2-dimorpholinodiethylether (DMDEE), 2-dimethylaminoethanol (DMEA).

1.2.1.3 Proton affinity

In the case of amine and acid catalysts, proton affinity is an important thermodynamic quantity because it describes the tendency of a structure to accept or donate a proton. Catalysts that donate or accept protons at specific reaction sites can direct the reaction towards desired pathways, lowering the activation energy barriers and enhancing the reactivity of the catalytic system. Proton affinity (PA) is computed as follows (Eq. 1)[99]:

$$PA = -\Delta H_r = -(H\,(\text{protonated structure}) - H\,(\text{neutral structure})) \quad \textbf{Eq.1}$$

## 1.3 Polyurethane Types

Having established the foundational importance of polyurethanes, we now explore the various types developed over the years and their unique applications.

### 1.3.1 Rigid Polyurethane Foams

Rigid PU foams are one of the most commonly used versatile and energy-saving insulation materials[100]. These foams can significantly reduce energy costs on the one hand and can make commercial and residential appliances more comfortable and efficient on the other[101]. To ensure a stable temperature as well as a reduced noise level for both home and commercial appliances, builders often resort to using polyisocyanurate and PU foams[102,103]. These foams have been proven to be effective as insulation materials, and hence have been applied in window insulations and wall and roof insulations as well as in barrier sealants for air and doors[104,105] (**Figure 9**).

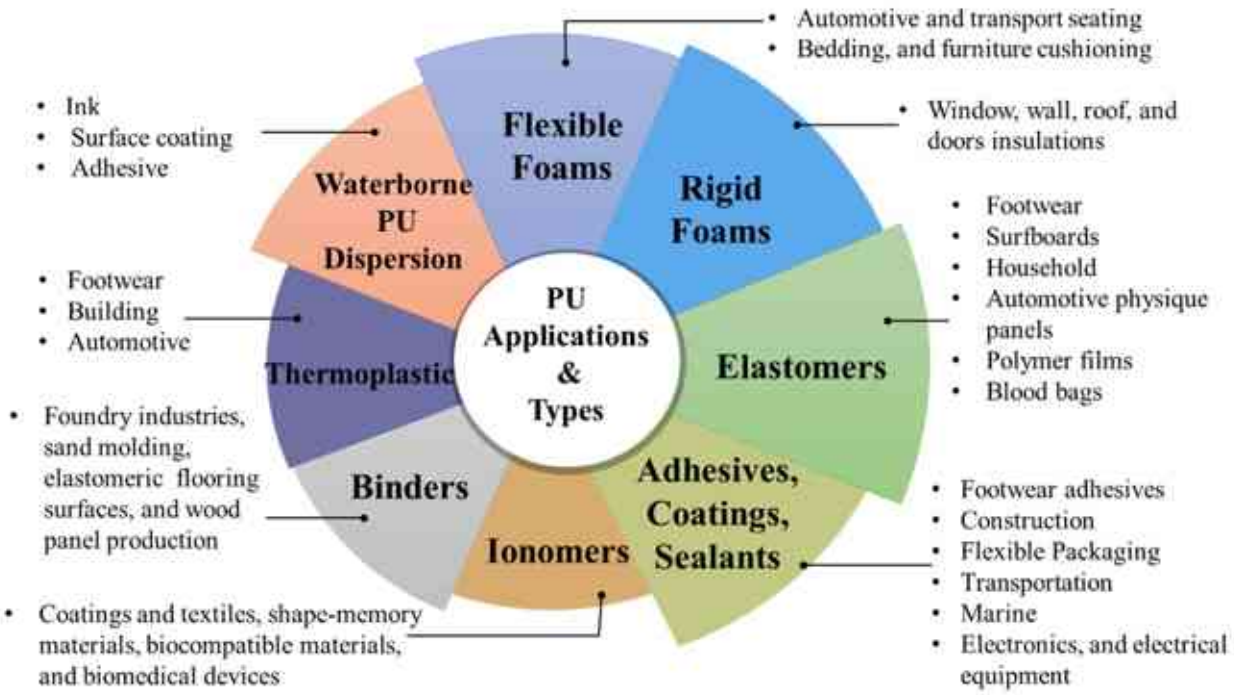


***Figure 10.*** *Main applications and types of polyurethanes.*

### 1.3.2 Flexible Polyurethane Foams

The use of flexible polyurethane foams has developed in the past 40 years on the basis of their ability to meet the requirements of the cushioning (mostly furniture), packaging, and safety products' markets[106] (**Figure 9**). This has been achieved through three predominant product types: slabstock foam, molded foam, and integral skin foam[107].

Slabstock foam has been developed to be used in lower density products and has found its main applications in cushioning and packaging (bedding, furniture cushioning, seats in public transport, textile backing (sportswear), carpet linings packaging *etc.*)[108]. The density not only has impact on the cost of the products, but also on their comfort[109].

Molded foam tends to occupy the interim range of densities for applications where some load-bearing requirement exists (*e.g.* automotive and transport seating)[110]. However, the division between this sector and the one occupied by integral skin formulations is somewhat blurred since skin formation is a natural property of polyurethane systems when moulded[111].

Integral skin foams are molded foams, which are manufactured either by injection into closed, vented molds (as in the case of steering wheels) or into open molds (as is the case with shoe soles)[112]. These foams are characterized by a high-density outer skin and a low density, softer core[113].

### 1.3.3. Thermoplastic Polyurethanes

Thermoplastic polyurethanes (TPUs) are linear, segmented block copolymers consisting of hard and soft segments[114,115] **(Figure 10**). The hard segments are rigid and highly polar and made from diisocyanate and short chain extender molecules such as diols or diamines[116]. Hard segments have high interchain interaction due to hydrogen bonding between the urethane/urea groups. The hydrogen bonding associations within the hard segments of the TPUs act as reinforcing filler for the soft matrix[117]. On the other hand, soft segments consist of long, linear flexible polyether or polyester chains which interconnect two hard segments[118]. In brief, the hard segments act as multifunctional tie points working as both physical crosslinks and reinforcing fillers, while the soft segments primarily influence the elastic properties of TPUs[119].

### 1.3.4. Polyurethane Ionomers

Ionomers are polymeric materials having a small number of ionic side groups in hydrophobic main chains[120] (**Figure 10**). Ionic fragments can be included in these polymers in the form of cationic, anionic, or zwitterionic groups in various concentrations[121]. Depending on the type of polymer, the ionic groups can be distributed along the main chain periodically, randomly, or as end groups. The concentration of ionic groups usually varies in the range of 1– 15 mol% and they can be completely or partially neutralized. Intensified interaction between ionic pairs and their clustering could increase the density of the nodes of their spatial polymer grid[122]. This feature leads to a high probability of self-organization with

the formation of various types of nano- and microstructures which contain ionic clusters and ion-conductive channels[123]. The resulting polymer network also causes strong changes in the mechanical properties of ionomers compare to the original non-ionic polymers[124,125].

### 1.3.5 Waterborne Polyurethane Dispersion

Waterborne polyurethane dispersion (PUD) consists of linear thermoplastic polyurethane chains dispersed in water due to the presence of ionic groups in the structure (i.e. polyurethane ionomer), which act as an internal emulsifier[126](**Figure 10**). Typically, an NCO-ended prepolymer ionomer is prepared first, which is readily dissolved in acetone. Afterwards, a chain extender, such as diamine, is added to react with the terminal NCO groups to increase the molecular weight of the polymer[127]. For facilitating the dispersion of the polyurethane in water, the acetone has to be removed to produce phase inversion and thus, obtain the polyurethane dispersion[128]. A major ingredient of the PUDs is the polyol (i.e. hydroxyl ended oligomer) as it provides their main properties such as flexibility, cross-linking ability, or thermosetting potential[129]. Several polyols can be used to manufacture PUDs such as polyesters, polyethers, polycarbonates and renewable source-based polyols[130].

### 1.3.6 Binders

PU binders (PUB) are often used to bond different types of fibers and other materials to each other. PUBs provide a permanent gluing effect between organic materials and long-strand lumbers, oriented strand boards, laminated veneer lumber, medium density fiberboards, particle boards, and straw boards[131] (**Figure 10**). As a binding material, the ratio of the hard-/ soft segments of PUs should be high, and good thermal stability is required[132]. Sometimes a specific or moderate acid number (not too high or not too low), weak crystallinity, limited molecular weight, and narrow particle distribution are preferred for a good quality binder[133]. To impart excellent chemical resistivity in PU binders, hybridization with acrylic polymer is also preferable[134].

## 1.4 Application of Polyurethanes (PU)

With versatility in the chemistry and constituent materials, polyurethanes find ubiquitous applications in almost all fields[135–138].

### 1.4.1 Coatings, Adhesives, Sealants and Elastomers (CASE) Industry

Polyurethane has taken over the CASE industry in the last few decades[139]. The wide variety of physical and chemical properties of PU can be finetuned and tailored according to the need of the end application or the product[140,141]. Adhesives based on PU offer very good bonding

strength and at the same time, polyurethane based sealants provide remarkable tight seals[142,143]. For polyurethane to be used in suitable coating applications it needs to have good adhesion, high chemical resistivity, excellent drying, low-temperature flexibility, and very good abrasion resistance[144,145]. Over the past two decades, there has been numerous research on the appropriate material for coating applications and polyurethane has always come out as one of the best paint and surface coating material[146,147].

### 1.4.2 Automotive Industry

The automotive industry has been one of the key application areas of polyurethanes[148,149]. PUs can be used to create comfortable seats, impact resistant front bumpers and rigid body for cars. Polyurethanes can also be found in the car doors, windows, and ceiling sections[150]. The biggest advantage of using polyurethane over metal or other materials is that apart from the comfort it reduces the weight of the car drastically and hence increases the fuel economy, making the car more efficient in its performance[151]. It is also being used for insulation and acoustic damping purposes. Polyurethane seats and cushions provide high comfort for the passengers[152].

### 1.4.3 Medical Applications

Due to the cost-effectiveness, toughness and longevity, PU has found usage for medical purposes[153,154]. The formerly mentioned properties (*e.g.* good mechanical properties, and biocompatibility) have helped this polymer to beat other materials such as metals, metal, alloys, and ceramic[155,156]. Polyurethanes are used in medical applications such as tubing, surgical drapes, catheters, hospital beddings, wound dressing, and many more[157,158]. However, the most frequent application of polyurethane in the medical field is for short period implants[159].

In one study crystalline prepolymers were used to improve the biodegradability of the polyurethane product in which water was applied as a chain extender[160]. A palpable increase in mechanical and degradation properties has been achieved compared to PU which is extended with ethylene glycol as a chain extender[161,162]. Furthermore, these properties were deemed suitable as joint endoprosthesis. Polyurethane has also found applications in drug delivery systems for the colon and intra-vaginal rings[163].

### 1.4.4 Textiles and Apparels

Since its inception, PU was considered as a good material for apparel. Initially, PU is converted into thin threads and then incorporated into nylon to make light and stretchable garments[164]. But with the advancement in research more and more improved garments have surfaced in the industry[165]. Spandex fibers and thermoplastic elastomers have heavily influenced new-age PU

apparels[166]. Due to the advancements in technology, the manufacturers have a whole new wide variety of PU-based products, such as faux leather, bra cups, and manmade skins, which have applications in various rigorous sports attire and in a large range of accessories. The textile industry has highly benefited from waterborne polyurethanes (WPUs) and polyurethane dispersions (PUDs) [167–169].

WPUs do not have harmful volatile organic compounds as their solvent counterparts and hence are environmentally friendly, worker friendly with low toxicity. They also showcase excellent properties such as permeability, abrasion resistance, softness (soft to touch surface). Also, crock fastness, fastness of washing, and soap fastness of reactive dyes, acid dyes, and direct dyes on dyed fabrics may be immensely improved by the use of WPU as finishing agents[170,171].

### 1.4.5 Marine Applications

Polyurethane has been a great addition to marine technology along with epoxy. Polyurethane based epoxy is not only an excellent building material but also excels in marine coatings too[172]. It protects from corrosion, water erosion and also manages the drag flow of the boat's hull by not allowing aquatic life to settle or grow on the ship[172]. This anti-fouling and algae protection have been one of the best utilities of the PU marine coatings. PU foams are also used in boats and ships because they provide outstanding insulation with very effective noise controlling or damping properties[173].

Boat parts made up of PU are generally lighter in weight than its metal counterpart hence increasing the efficiency of the boat engine and it also highly resistant to corrosion compared to the metals. Polyurethane also provides increased tear and abrasion resistance and load-bearing capacity even at lower temperatures[174]. Exploiting these properties, the marine industry has taken PU into various products such as cables and wire coatings, drive belts, hydraulic tubing as well as boat and ship construction. Recently polyurethane is being used as a removable media, i.e. removing organic substances from water[175].

Cyclodextrin PU has been reported for the removal of parabens from aqueous bodies. These types of PU can be produced by microwave-assisted synthesis, and they are usually insoluble in water and hence is very highly effective in the collection and removal of unwanted organic substances from aqueous systems[176]. It has been reported that cyclodextrin PU is also very good in the removal of phenol as well as Nile red dye from water [177]

1.4.6 Polyurethane Wood Composites

Polyurethane has stood out to be a very important material in the field of wood composites because the combined flexibility of wood and PU, lightweight and strength provide a suitable reinforcing material[178]. Recently polyurethane-based flat composites were produced by inculcating activated carbon to tackle the interference produced by electromagnetic waves or electromagnetic interference shielding (EMI)[179]. Activated carbon loading was done into PU for microwave adsorption and complex permittivity[180]. The composites made by this process performed better than polyethylene and polyester which need metal additives for higher performance. PU-wood composites can also be generated by using wood wastes[181,182].

## 1.5 The aim of this work

Considering the aforementioned details and the significance of polyurethane synthesis, as well as the important role of catalysts in polyurethane synthesis, and aiming to contribute to the principles of green chemistry, aims need to be established for the current dissertation. First and foremost, it is necessary to understand the urethane formation processes both with and without the presence of different catalysts. The following aims are set to be pursued:

1. The development of a computational protocol applicable to the study of catalytic and catalyst-free urethane formation reactions has to be carried out
2. The catalyst-free urethane formation reaction has to be studied and described.
3. The catalytic urethane formation reactions have to be studied and compared and corresponding general mechanisms envisaged.
4. The validity of the proposed mechanisms has to be verified.

# 2. Methods

## 2.1 Schrödinger Equation

The reaction mechanism of the urethane formation in the presence of organocatalysts consists of various elementary reaction steps including the formation of the reactant complex, transition states, intermediates, product complex, and the final product. All of the involved molecules have a particular structure and the corresponding thermodynamic properties can be calculated. To determine the energy of a molecule, the Schrödinger's wavefunction equation can be used (**Eq. 2**)[183] as follows:

$$\widehat{\boldsymbol{H}}\boldsymbol{\Psi} = \boldsymbol{E}\boldsymbol{\Psi} \qquad \textbf{Eq. 2}$$

where $\widehat{\boldsymbol{H}}$ is the Hamiltonian operator, $\boldsymbol{\Psi}$ is the wavefunction of all the spatial coordinates of nuclei and spatial and spin coordinates of electrons, and $\boldsymbol{E}$ is the energy[184].

By solving the Schrödinger equation a set of wave functions and a set of energy corresponding to the electron states allowed in that atom will appear[185]. The mathematical expressions of the wave functions can determine the probability of finding an electron in the area of a point near the nucleus. While, The movement of particles that form matter (molecules, electrons, and atoms) is studied by quantum mechanics[186].

The fundamental postulates of quantum mechanics are[187–189]:

1- The momentary state of a quantum chemical system is represented by the wavefunction which describes the probability distribution of its measurable properties. Thus, the non-relativistic time-independent Schrödinger equation **(Eq. 2)** will be applied to the energy of the ground state of a molecular system which does not depend on time.

2- The physical observables are represented with a linear Hermitian operator in the Hilbert space which gives the total energy of a system and defines the possible state vectors of the system. As the mathematical terms of the time-independent Schrödinger equation represent an *eigenvalue* equation ($\boldsymbol{\Psi}$= eigenfunction, and $\boldsymbol{E}$= eigenvalue) **(Eq. 2)** and since the Hermitian operator has real eigenvalues and expectation values, therefore, the Hermitian operator will be valid to the time-independent Schrödinger equation.

3- The measurable energy values are equal to the eigenvalues of the $\widehat{\boldsymbol{H}}$ operator.

4- A given physical observable of the general expectation value was described by the fourth postulate **(Eq. 3)**. $\hat{A}$ is the corresponding operator, and $\Psi^*$ is the conjugate form of the normalized wavefunction $\Psi$.

$$\langle A \rangle = \int_{-\infty}^{+\infty} \Psi^* \hat{A} \Psi dt \qquad \textbf{Eq. 3}$$

5- This postulate states that the time evolution of a system is governed by the Schrödinger equation **(Eq. 4)**.

$$i\hbar \frac{\partial \Psi(\tau,t)}{\partial t} = \hat{H}\Psi(\tau,t) \qquad \textbf{Eq. 4}$$

where $\hbar$ is the reduced Planck constant, and $\hat{H}$ is the total energy Hamiltonian operator.

6- Pauli exclusion principle can be deduced by the sixth postulate which is called the antisymmetry principle. To trade all coordinates of similar particles with half-integer spin (fermion) and symmetric for the exchange of all coordinates of identical particles with integer spin (bozon) the wave function of a microsystem must be antisymmetric.

In the expanded version of the Hamiltonian can be seen that the total energy of system in quantum mechanics contains kinetic and potential energy terms, the sum of all possible interactions between electrons and nuclei **(Eq. 5)**:

$$\hat{H} = -\sum_{i=1}^{N_{el}} \frac{\nabla_i^2}{2} - \sum_{A=1}^{M} \frac{\nabla_A^2}{2M_A} + \sum_{i=1}^{N_{el}} \sum_{j>i}^{N_{el}} \frac{1}{|r_i - r_j|} + \sum_{A=1}^{M} \sum_{B>A}^{M} \frac{Z_A Z_B}{|R_A - R_B|} + \sum_{i=1}^{N_{el}} \left( \sum_{A=1}^{M} \frac{-Z_A}{|r_i - R_A|} \right) \qquad \textbf{Eq. 5}$$

**First** **Second** **Third** **Fourth** **Fifth**

where $\nabla_i^2$ *and* $\nabla_A^2$ are the Laplacian operators which give the sum of second partial derivatives of a function, $M_A$ is the ratio of the mass of nucleus A to the mass of an electron, and $Z_A$ is the atomic number of nucleus A. The first and second terms correspond to the kinetic energy of all the electrons and nuclei, the third and fourth terms correspond to the Coulomb repulsion between electrons and nuclei respectively, and the last (fifth) term represents the Coulomb attraction between nuclei and electrons[190].

To simplify the wavefunction, various approaches were tested. In 1927 Max Born and Robert Oppenheimer's (BO) approximation made a huge change in the complexity of wavefunction. BO approximation is a description of the molecular spectra based on an approximate quantum mechanical treatment of electrons and nuclei in the molecules separately[191]. Thus, as the nuclei are much heavier than the electrons this helped to support the possibility of the dynamic decoupling. Therefore, in **(Eq. 5)**. the second term of the equation will be eliminated because the nuclei can be treated as static particles concerning electrons.

While, for the fourth term of the equation, repulsion between nuclei can be treated as a constant for a fixed configuration of the nuclei which led to a simpler equation **(Eq. 6)**. Thus, via the Born-Oppenheimer approximation only the ”electron related” part of the Hamiltonian is kept and the electronic Hamiltonian is acheived[192].

$$\widehat{H}_e = -\sum_{i=1}^{N_{el}} \frac{\nabla_i^2}{2} + \sum_{i=1}^{N_{el}} \sum_{j>i}^{N_{el}} \frac{1}{|r_i - r_j|} - \sum_{i=1}^{N_{el}} \left(\sum_{A=1}^{M} \frac{Z_A}{|r_i - R_A|}\right) \quad \textbf{Eq. 6}$$

## 2.2 Computational Chemistry

The first theoretical considerations originated for theoretical chemistry in the XVIII century. The development of the theoretical arguments into a vast body of concepts was in the XIX century[193]. Later a remarkable shift occurred where theoretical chemistry was commonly named atomistic modeling. There is a wide sense of the word "modeling" including computer-based approaches with different techniques that can even overlap with the computer-aided design of molecules or materials[194]. Today theoretical chemistry is an additional tool for chemists besides the various spectrum of available analytical methods during the operation of development[195]. Where the theory and experiments are competing to provide the existence of compounds not previously synthesized. Computational chemistry is strongly depends on approximations. By the development of computational tools the achievement of an approximate solution of the Schrödinger equation with extremely good precision and to predict molecular properties with an accuracy that is comparable to experiments became possible[196]. There are many different ways to use computational chemistry. Modeling the molecular system before synthesizing it in the laboratory helps to reduce the time, raw materials, and toxic waste that will appear with the synthesis of the compound. The system with the lowest energy is the most stable one[197]. The energy in a system is divided into kinetic and potential energy. The translational, vibrational, and rotational motion are the contributions to the kinetic energy. While the potential energy (defined by Coulomb's law) is separated into terms of bending, bond stretching, hydrogen bonds, conformational energy, *etc*.

The potential energy surface (PES) describes the total energy of a molecular system that differs with slight changes in its structure. It is a mathematical relationship that gives the resultant energy of a molecular structure as a function of its coordinates. In the diatomic molecule, a two-dimensional curve will result between the internuclear separation on the X-axis ( $\mathbf{r_e}$- is the equilibrium bond length (the lowest point of the curve)), and the energy at that bond distance on the Y-axis (**Figure 11**).

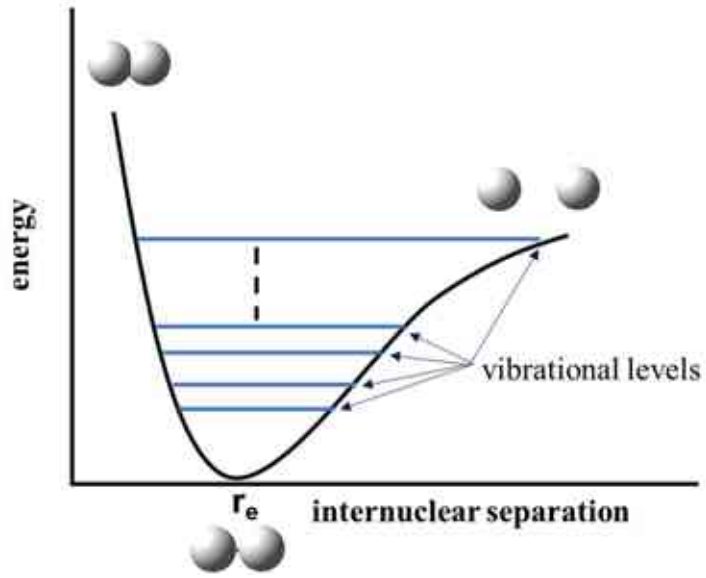


***Figure 11**. Potential energy curve for a diatomic molecule*

While, for the large system, the amount of degrees of freedom within the molecule will lead to PES with many dimensions. Since the 3N-6 is the degree of freedom for a molecule (where N is the number of atoms if N>2), the corresponding potential energy surface is also multi-dimensional[198]. In aPES each point will correspond to various values for the different bond angles, bond distances, and dihedral angles within the molecule. The potential energy curve (PEC) is represented by a 2D section of the PES. The determination, visualization, and comparison of the energy levels of the reaction pathways such as reactants, intermediates, transition states, and products are carried out with PEC. Studying the reaction dynamics, and obtaining the vibrational properties of the molecule is one of the numerous common reasons for doing a potential energy surface computation. In the case of a catalytic reaction mechanism, the reactants, intermediates, transition state, and products have to be found and the corresponding the potential energy curve can be drawn. On the PEC the minimum stationary points correspond to optimized geometries and are called minima. While the transition state structure between the reactants and products of a reaction can be defined as a stationary point on a potential energy surface. Which describes the rates of elementary reactions (elementary reactions are single-step reactions with a single transition state without intermediates) on a molecular scale. Transition state theory was formulated in 1935 by Erying and Polanyi to explain bimolecular reactions based on the relationship between kinetics and thermodynamics[199].

The properties of the molecule will be affected even with small changes in the structure. Therefore, before proceeding with properties predictions it will be necessary to locate the

equilibrium geometry for the molecular systems under examination. To do so the geometry optimization of the compounds should carried out[200]. A geometry optimization locates a point on a potential energy surface, starting with the initial geometry, and then, changing it till a lower-energy structure, a local minimum achieved. This lower energy corresponds to the conformer that is nearest to the starting geometry. The determination of the local minimum is carried out by varying the coordinates of nuclei and computing the corresponding electronic energy and nuclei repulsion energy. Computed energy and geometry optimization are time-consuming and complex. To carry this out, quantum chemical softwares are used[201]. In this study, the Gaussian 09 software package was employed. Several different theoretical methods are available in Gaussian 09, which can be used to compute the studied systems with differing accuracy, and model various chemical environments, and molecular states. Frequency calculation must be carried out after the geometry optimization. It will take into account the nuclear vibrations in molecular systems in their equilibrium states. The frequency calculation confirms that the structure is the right stationary point. The presence of an imaginary frequency means that the structure is a transition state and not a minimum[202].

## 2.3 Thermodynamic Parameters

Thermodynamic properties of molecules such as Gibbs free energy (*G*), entropy (*S*), enthalpy (*H*) can be computed. These parameters can be obtained with the help of partition functions [q(V,T)] which describe how the probabilities are partitioned among the various microstates such as rotation, vibration, transition, and electronic state. Thermodynamic state functions ($G$(T,p), $H$(T), $E_0$, $S$(T,p)) for all participated molecules in a reaction can be calculated, and thus, the corresponding thermodynamic properties of the reaction can be obtained[203].

The entropy (***S***) of the system is associated with the natural logarithm of the number of possible microstates (***W***) which was shown in 1868 by Boltzmann **(Eq. 7)**:

$$S = k_B \ln W \qquad \text{Eq. 7}$$

where $k_B$ is the Boltzmann constant ($1.38 \times 10^{-23}$ J/K). A system with a smaller number of possible microstates has a lower entropy[204]. While the entropy contribution through partition functions would be **(Eq. 8)**:

$$s = Nk_B + Nk_B \ln\left(\frac{q(V,T)}{N}\right) + Nk_B T\left(\frac{\partial \ln q}{\partial T}\right)V \qquad \text{Eq. 8}$$

***N*** is the particle number of molecules as a dimensionless quantity.

Enthalpy (***H***) is the total amount of the energy of the system. For a specific process, the change in enthalpy is a change in internal energy associated with the changing volume. Enthalpy is identified as the sum of the internal energy of the system (***E***) and the mathematical product of its pressure (**p**) and volume (***V***) **(Eq. 9)**[205,206]:

$$\boldsymbol{H(T) = E(T) + pV} \qquad \textbf{Eq. 9}$$

With the partition functions the enthalpy can be determined as follows **(Eq. 10):**

$$\boldsymbol{H - H(0) = \left(\frac{\partial \ln q}{\partial \beta}\right)_V + kTV \left(\frac{\partial \ln q}{\partial V}\right)_T} \qquad \textbf{Eq. 10}$$

where **β** is the most probable populations of the states of the system, related to the tempreture.

**q** is the partition function of the system.

Gibbs free energy (***G*(T,p)**) depends on the change in enthalpy (***H***) and a change in entropy (***S***) times temperature, at a constant pressure (**p**), and temperature (**T**)[207] **(Eq. 11)**.

$$\boldsymbol{G(T, p) = H(T) - TS(T, p)} \qquad \textbf{Eq. 11}$$

By using the partition function Gibbs free energy can be described via **(Eq. 12)**:

$$\boldsymbol{G - G(0) = -nRT \ln \frac{q}{N}} \qquad \textbf{Eq. 12}$$

where **R** is gas constatnt (8.314 J/K.mol), **T** is temperature, **q** is the partition function of the system, and **N** is the particle number of molecules as a dimensionless quantity.

## 2.4 Computational Chemistry Methods

The major purpose of computational chemistry is to find a solution to chemical problems via simulating the studied system but providing accurate, reliable, and comprehensive information at an atomic level. Quantum chemistry and molecular mechanics are the two main approaches in computational chemistry methods. In quantum chemistry, the electrons accounted are explicitly. The quantum chemistry methods calculate the interaction of electrons and nuclei by solving the time-independent electronic Schrödinger equation using the Born–Oppenheimer approximation. Quantum chemistry methods are divided into two important types, wavefunction and density functional theory (DFT) methods[208]. The wavefunction or *ab initio* methods are using a mathematical function to compute the electron distribution. The coupled-cluster (CC) technique is considered the theoretical gold standard of the wavefunction methods.

However, the computational cost for CC will increase with the system size[209]. Density functional theory methods use the electron density to determine the properties of the system. Unlike the case of wavefunction-based methods, DFT methods are suitable to deal with larger systems including those with more than thousands of electrons[210].

The main limitation of computational studies is the time required for the simulation, especially in case of large systems, it can be longer than the available resources. Furthermore, there are plenty of different methods available which work pretty well for certain systems and are very accurate, but not all of them are able to find all the critical points on the potential energy surface (PES). Therefore, in this work, three different DFT methods (B3LYP, BHandHLYP, and ωB97X-D) were tested. However, only BHandHLYP was suitable to find all critical points of the reaction on the PES. All in all, it can stated that there are no general methods for every application. In many cases, the methods can only deal with a well-defined set of chemical or physical problems. In our case, as it was proved by two different approaches (geometrical and thermodynamic validation) that G3MP2BHandHLYP is suitable to study organocatalytic urethane formations.

### 2.4.1 *Ab Initio*

The main goal of *ab initio* methods is to compute the stationary states of electrons in the electrostatic field of atomic nuclei (electronic structure). It is independent of experimental data. There is no need for fitting parameters or calibration. It can used for the hypothetical systems to compute the structure and mechanical properties[211]. The Hartree–Fock method (HF) is one the most common *ab initio* method and it divides the Schrödinger many-electron equation into one-electron equations[212,213]. The HF ab initio method goal is to find the dominant Slater determinant in the wave function system by optimizing the spatial form of the spin orbitals to minimize the energy of the wave function[214]. However, the electron correlation in the system can not be addressed with the HF method, this will lead to lower accuracy, but faster calculations. Therefore, post-Hartree-Fock methods were developed to reach higher accuracy. The main aim of the post-HF *ab initio* methods is to capture the part of the electron correlation missing from the original HF formulation[215]. There are two ways to do that. The first one is to try to correct the single determinant approximation. The second is to try through the perturbation theory to introduce correlation energy[216]. The Møller–Plesset (MP) perturbation theory (*e.g.* MP2, MP3, MP4, MP6) is the most popular example of the post-HF *ab initio* methods[217]. The coupled-cluster method (CC) is one of the most accurate formulations which is useful in a variety of fields ranging from quantum chemistry to nuclear physics, and material

sciences. This theory was presented in 1960 for computing nuclear binding energies in nuclei that could be treated in the first approximation by a single configuration of protons or neutrons. The CC method decomposes the wavefunction of a quantum many-body system in terms of amplitudes for exciting clusters of a finite number of particles[218,219].

### 2.4.2 Density Functional Theory

Density functional theory (DFT) was the predominant theory of the quantum mechanical simulation of periodic systems for the past 30 years[220]. Today it has been used widely to simulate various systems and to predict the electronic and molecular properties. The main advantage of the DFT methods is their low computational cost[221]. DFT is based on two theorems developed by Hohenberg and Kohn, which states that the energy of a molecule can be determined by using the electron density[222]:

***Theorem I:*** The characteristics of a molecule in the ground state electronic state are determined by electron density. This density is a unique function of the external potential.

***Theorem II:*** The electron density that minimizes the full energy of the system corresponds to the true ground state electronic density.

A straightforward proof of the first theorem was put forward by Wilson in 1965. Wilson's observation was that the positions and charges of the nuclei are determined by the electron density. The external potential in DFT is the Coulomb attraction between electrons and nuclei. The nuclei are considered fixed objects according to the Born-Oppenheimer approximation, which exercises their Coulomb potential to the electrons[223]. Therefore, the electronic Hamiltonian of the system can be written as **(Eq. 13)**:

$$\widehat{\boldsymbol{H}}_{\mathbf{e}} = \widehat{\mathbf{V}}_{\mathbf{k}}(\mathbf{n}) + \widehat{\mathbf{V}}_{\mathbf{ee}}(\mathbf{n}) + \widehat{\mathbf{V}}_{\mathbf{ext}}(\mathbf{n}) \qquad \textbf{Eq. 13}$$

where: $V_k -$ kinetic interaction operators

$V_{ee} -$ electron-electron interaction operators

$V_{ext} -$ external potential

The external potential ($V_{ext}$) can be represented as a function of the ground state electron density **(Eq. 14)**:

$$\widehat{\mathbf{V}}_{\mathbf{ext}}(\mathbf{n}) = \int \boldsymbol{n}\,(\boldsymbol{r})\,\boldsymbol{\Psi}^{*}(\boldsymbol{r})\boldsymbol{\Psi}(\boldsymbol{r})\mathbf{dr} \qquad \textbf{Eq. 14}$$

Thus, the electron density uniquely determines the Hamiltonian operator. This means that the total energy is a function of the density. Therefore, the energy will be **(Eq. 15)**:

$$\boldsymbol{E = \int \hat{V}_{ext}(n)\, n(r) + F[n(r)]} \qquad \textbf{Eq. 15}$$

where **F** indicates the functional relation, and consists of two $\hat{\mathbf{V}}_{\mathbf{k}}(\mathbf{n})$ and $\hat{\mathbf{V}}_{\mathbf{ee}}(\mathbf{n})$ terms.

Solving the Hohenberg-Kohn theorems for a real system was carried out with the collaboration between Kohn and Lu Jeu Sham (Kohn-Sham formalism)[224]. According to the Kohn-Sham formulism, the energy of a system can be determined by using the energy of an idealized system with noninteracting electrons and a deviation parameter. This theorem shows that the electron density could described by solving a set of equations involving a single electron. They have introduced a virtual non-interacting system, assuming that its ground state is equal to the density of the real interacting system[225].

The electron density of the ground state at a location is defined as the following **(Eq. 16)**:

$$\mathbf{n(r) = \sum_{i=1}^{n} \left|\varphi_i^{KS}(r)\right|^2} \qquad \textbf{Eq. 16}$$

where $\boldsymbol{\varphi_i^{KS}(r)}$ are the Kohn-Sham orbitals. Thus, the ground state of the system is represented as **(Eq. 17)**:

$$\boldsymbol{\hat{h}^{KS}(i)\varphi_i^{KS} = \varepsilon_i^{KS}\varphi_i^{KS}} \qquad \textbf{Eq. 17}$$

where $\boldsymbol{\hat{h}^{KS}(i)}$, and $\boldsymbol{\varepsilon_i^{KS}}$ are the Kohn-Sham Hamiltonian and corresponding energy of the Kohn-Sham orbital, respectively.

For the interacting real system, the Kohn-Sham Hamiltonian ($\boldsymbol{\hat{h}^{KS}(i)}$) is written as the following **(Eq. 18)**:

$$\boldsymbol{\hat{h}^{KS}(i) = \hat{V}_k[n(r)] + \hat{V}_{ee}[n(r)] + \hat{V}_{ext}[n(r)] + \hat{V}_{XC}[n(r)]} \qquad \textbf{Eq. 18}$$

where $\boldsymbol{\hat{V}_k[n(r)]}$ is the kinetic energy term, $\boldsymbol{\hat{V}_{ee}[n(r)]}$ electron-electron repulsion term, $\boldsymbol{\hat{V}_{ext}[n(r)]}$ external potential term, $\boldsymbol{\hat{V}_{XC}[n(r)]}$ exchange-correlation term $\boldsymbol{(\Delta_k^{corr}[n(r)] + \Delta_{ee}^{corr}[n(r)])}$.

The exchange-correlation functional ($\boldsymbol{\Delta_k^{corr}[n(r)] + \Delta_{ee}^{corr}[n(r)]}$) is corresponding to the exchange ($\boldsymbol{E^X[n(r)]}$, where $\boldsymbol{E^X}$ is the interactions between electrons of the same spin), and correlation energy terms ($\boldsymbol{E^C[n(r)]}$, where $\boldsymbol{E^C}$ is associated with the electron-electron interactions with opposite spin)[226]. However, in practice, DFT methods will need electron

exchange and correlation interaction approximations. There is an unlimited list of approximated functionals with varying complexity levels. Thus, Jacob's ladder of DFT is created by Perdew to show how the DFT is handling the $\widehat{V}_{XC}[n(r)]$ . Where the DFTs are categorized on rungs of a ladder according to their complexity **(Figure 12)**[227].

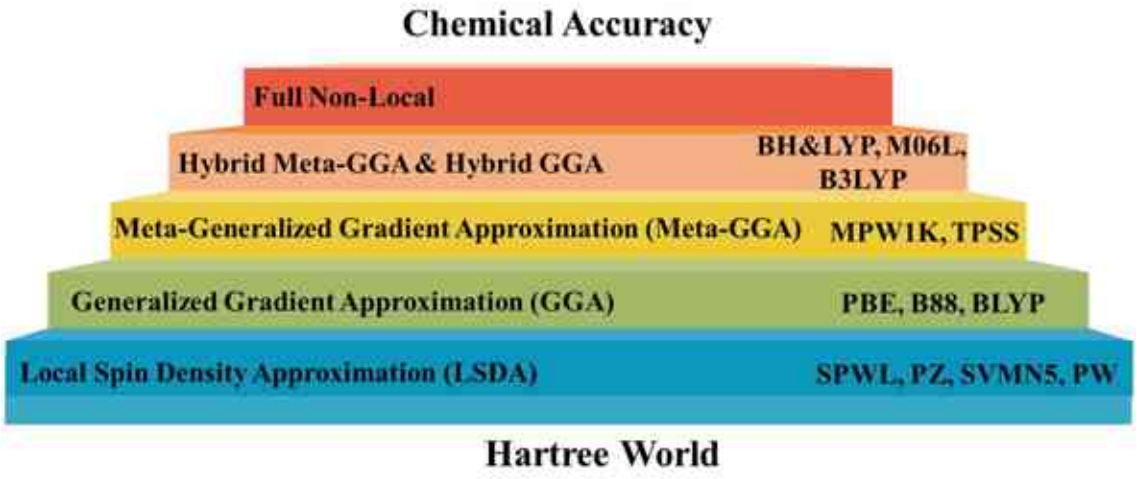


***Figure 12**. Jacob's ladder of density functional approximations.*

The local spin density approximation (LSDA) of Kohn and Sham is the mother of all approximations. A real inhomogeneous system with divided into infinite volumes by using the LSD approximation. The electron density in each of the volumes is considered constant. From the uniform electron gas model the exchange-correlation energy for the density within each volume can obtained. This will lead to writing the total exchange-correlation energy of the system as follows **(Eq. 19)**[228,229]:

$$E_{XC}^{LDA}(n) = \int n(r)dr\, E_{XC}^{unif}(n(r))dr \qquad \textbf{Eq. 19}$$

$E_{XC}^{unif}(n)$ is the exchange-correlation energy per particle of an electron gas with uniform spin densities.

LSD approximation demonstrated surprising accuracy for solid surfaces and solids, especially those with fast density variations. This was due to the exact characteristics that LSD approximation was inheriting from the uniform electron gas. The most typical LSDA functionals are the SPWL (Slater Perdew-Wang local), PZ (Perdew-Zunger), VWN (Vosko-Wilk-Nusair), and the PW (Perdew-Wang) functionals[228].

Although the LSD approximation was a common choice for solid-state physics, it was not popular with the plurality of quantum chemists. However, Jones and Gunnarsson, and others

proved that although LSDA yields reasonable molecular geometries and vibration frequencies, it causes extremely overestimated atomization energies. Therefore, by using the generalized gradient approximation (GGA) the errors in the atomization energy are significantly reduced. The generalized gradient approximation (GGA) functionals represent the second rung of Jacob's ladder, and their general form is as follows **(Eq. 20)**[230]:

$$E_X^{GGA}(n) = \int f^{GGA}(n(r), \nabla n(r))dr \qquad \text{Eq. 20}$$

The GGAs could lead to better results for the geometries and ground state energies than the LSDAs, mainly for weak and covalent systems. The most common gradient-corrected correlation functionals are the PBE (Perdew-Burke-Ernzerhof), B88 (Becke88), and BLYP (Becke, Lee–Yang–Parr)[231].

Meta-generalized gradient approximation (meta-GGAs) is the third rung of Jacob's ladder. This approximation will enhance the accuracy of GGAs by taking into account the local kinetic energy density. This leads to treating various chemical bonds (*e.g.* metallic, covalent, and weak) with more accurately compared to LSDAs and GGAs. The meta-GGA can written as follows **(Eq. 21)**[232]:

$$E_{XC}^{mGGA}(n) = \int f(n(r), \nabla n(r), \tau(r))\, d^3r \qquad \text{Eq. 21}$$

Popular meta-GGA functionals include MPW1K (a modified version of the Perdew-Wang gradient corrected exchange functional, with one parameter optimized to give the best fit to the kinetic data), and TPSS (Tao–Perdew–Staroverov–Scuseria)[233].

Jacob's ladder also contains one of the most common functionals represented in the fourth rung of the ladder, defined as hybrid functionals. The most well-known methods in this function are B3LYP and M06. The B3LYP (Becke, 3 parameter, Lee-Yang-Parr) was used in many studies and also became a reference for many researchers in the applied density functional theory because of its wide applicability ranges. The B3LYP method contains the linear combination of LSDA and BLYP functionals[234].

M06 is another popular hybrid functional method introduced by Truhlar and his co-workers. It is a member of the Minnesota Functionals (Myz) family. M06-L, M06-HF, and M06-2X are other methods in the Myz family which achieved popularity and appreciation for their good performance on different systems. The M06 is used to study main-group thermochemistry, organometallic thermochemistry, and kinetics, in organometallic, and noncovalent interactions[235].

Although there is a wide range of functionals, but there is no general functional for every application. In many cases, the functional can only deal with a well defined set of chemical or physical problems.

The need to create specific functionals that could deal with a set of problems was the major aim of the development of the DFT methods. Therefore, today various functionals are available for certain problems, but not a single one for all[236]. Therefore, this study shows that the BHandHLYP ( Becke, Half-and-Half, Lee-Yang-Parr) is the most effective DFT method than the other methods (*e.g.* B3LYP, $\omega$B97X-D) for synthesizing the urethane in the presence of organocatalysts, in combination with the 6-31G(d) basis set[237].

### 2.4.3 Basis Sets

A basis set is a mathematical description of the orbitals of a system. It is a set of mathematical functions building the quantum mechanical wavefunction for a molecular system. A basis set can be interpreted as restricting each electron to a particular region of space[238].

In computational a better accuracy of the electronic structure will be provided by the application of larger basis sets with a relatively high number of mathematical functions. Also, larger basis sets imposes fewer restrictions on electrons, however, with fewer restrictions more computational time will be required[239]. The most common basis set can be broadly classified into the following types; minimal basis sets STO-nG, where STO is a slater type orbital and n is the number of primitive Gaussian functions that comprise a single basis function. For example, in the minimal basis set STO-4G each atomic orbital is treated as a single slater type orbital (STO), which is approximated by a linear combination of 4 Gaussian functions (4G)[240]. The second type is the correlation-consistent basis sets such as cc-pVDZ (correlation-consistent valence double zeta), cc-pVTZ (correlation-consistent valence triple zeta), and cc-pVQZ (correlation-consistent valence quadruple zeta), *etc*[241]. Split-valence or Pople basis sets, in which valence orbitals are represented by two or more basis functions of various sizes such as split-valence double-zeta basis set (6-31G) where the core orbitals are created of 6 primitive Gaussian functions, and two basis functions (double-zeta) will describe the valence orbitals, each of them made from three Gaussians and one Gaussian. These can be improved by polarization (*) (6-31G*) and diffuse functions (+) (6-31+G*)[242–244].

### 2.4.4 Composite Methods

The composite methods are developed to provide an algorithm for obtaining accurate energies for reasonable cost. It combines robust levels of theory with smaller basis sets and

modest theories with larger basis sets to approximate the results obtained at a much higher level of theory[245]. Several different model chemistries were developed. In 1980 Pople and Curtiss proposed the first model chemistry called G1. Thereafter, improvements were achieved and better models G2 and G3 were designed. Conceptually each of these composite methods is similar. They just vary in what sets of compounds are used, which methods for the baseline and the corrections will be used, and which properties were employed in the ultimate fitting procedure[246]. These composite methods have an element of semi-empirical nature to them due to that the calculated energy is fitting to some experimental property[247]. In most cases, the Gaussian-n ($n \leq 4$, e.g. G3, G3MP2, G3MP2B3) families are applied with reasonable success. In this work, the G3MP2BHandHLYP composite method was applied, because of the necessity of the application of the BHandHLYP/6-31G(d) level of theory to obtain the proper geometries and thermochemical data. Furthermore, on the optimized structures, two single-point energy calculations have been performed at the MP2/GTMP2Large and QCISD(T)/6-31G(d) levels of theory[248–254]. All calculations were performed by using the Gaussian 09 program[255].

## 2.5 Applied Levels of Theory

The level of theory for a calculation is usually written as a method/basis set pair. The method could be Hartree-Fock, post-Hartree-Fock, density functional theory, *etc.* Each method differ in computational cost, resource requirements, and accuracy. Therefore, taking into account the size of the studied system, computational cost, and features of the previously discussed methods and basis sets, in this study different density functional methods were used such as B3LYP[232], BHandHLYP[237], and ωB97X-D[256], in combination with the 6-31G(d)[257–259] basis set **(Figure 13)**. However, just the BHandHLYP method was able to find all the critical points on the potential energy surfaces (PES) of the studied catalytic processes.

Thus, to further improve the accuracy of the results, the G3MP2BHandHLYP composite method[248,260,261] was applied and used in the discussion of the results. To achieve G3MP2BHandHLYP energies, geometry optimization and frequency calculation have been carried out at the BHandHLYP/6-31G(d) level of theory. Furthermore, on the optimized structures, two single-point energy calculations have been performed at the QCISD(T)/6-31G(d) and MP2/GTMP2Large levels of theory **(Figure 13)**. Thus, the G3MP2BHandHLYP total zero-point energy ($E_0$) has been computed as follows **(Eq. 22)**[248,260–262]:

$$E_0[\text{G3MP2BHandHLYP}] = E[\text{QCISD(T)/6-31G(d)}] -$$

$$E[\text{MP2/GTMP2Large}] + \Delta E(\text{HLC}) + \Delta E(\text{ZPE}) \quad \textbf{Eq. 22}$$

Where ZPE is the zero-point correction, while HLC is the higher-level correction. HLC is a linear function of the number of valence electrons with α and β spins, $-An_\beta - B$ ($n_\alpha - n_\beta$), with $n_\alpha \geq n_\beta$. The value of A is 10.041 m$E_h$, and B is 4.995 m$E_h$ ($E_h$−Hartree) for molecules.

The G3MP2BHandHLYP composite method was not applicable in case of larger species (*e.g.*, 2,2-dimorpholinodiethylether (DMDEE)), because computational cost of the calculations exceeded the available limit. Therefore, for those structures two sets of calculations were carried out. First, the whole system was calculated by using the BHandHLYP/6-31G(d) level of theory and then, a truncated system was created and on that two more calculations were carried out at the BHandHLYP/6-31G(d) and G3MP2BHandHLYP levels of theory. Thereafter, the G3MP2BHandHLYP energy of the whole system was estimated according to the quasi-G3MP2BHandHLYP (qG3MP2BHandHLYP) protocol by using the following equation **(Figure 13) (Eq. 23)**:

$$E_{\text{qG3MP2BHandHLYP}} = (E_{\text{whole,BHandHLYP}} - E_{\text{truncated,BHandHLYP}}) + E_{\text{truncated,G3MP2BHandHLYP}} \quad \textbf{Eq. 23}$$

Furthermore, an additional correction has been applied to handle zwitterionic structures within the proposed mechanisms to approximate the energy of the species. The applied correction was previously successfully used in the literature to handle a system within which a zwitterionic structure is formed in the case of an amino acid[[263]. To balance the effect of the formation of the zwitterionic intermediate IM, -24.9 kJ/mol and -38.1 kJ/mol was added to the was added to the relative Gibbs free energy and relative enthalpy[264], respectively.

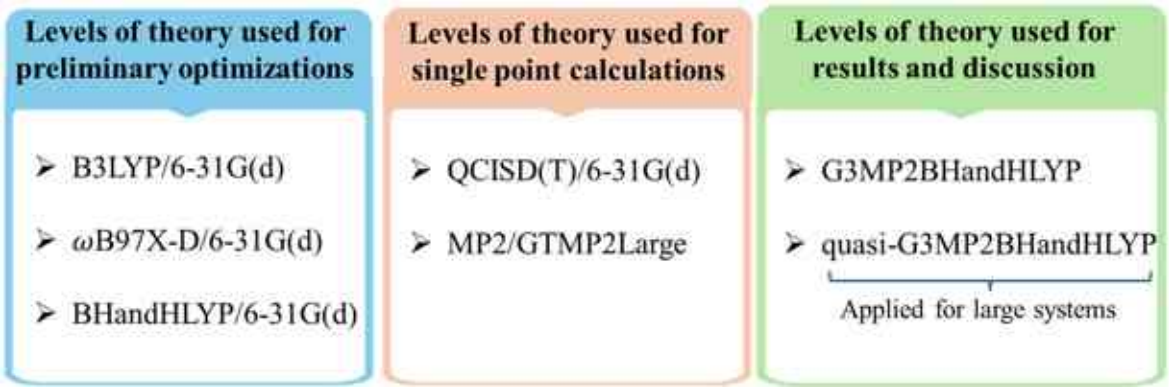


***Figure 13.*** *The applied level of theory.*

## 2.6 Solvent Models

The effects of the corresponding environmental factors such as solvent and temperature, must be considered when a chemical reaction is studied. Therefore, in computational studies of reaction mechanisms four different approaches are used to mimic the environment: implicit (or continuum), explicit, mixed (hybrid implicit/explicit) solvation models or gas phase calculations **(Figure 14)**[265,266].

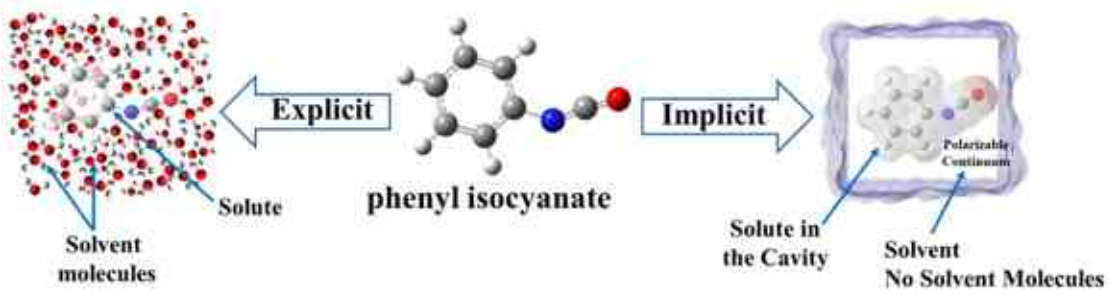


***Figure 14****. Schematic comparison of explicit and implicit solvation models.*

Explicit-solvent methods treat solvent molecules explicitly. It considers the movements and effects of the actual solvent molecules within a given region around the solute molecules. The disadvantage of this model is the computational cost, which could prevent the study of large systems, and long time scales[267].

The implicit model treated solvent as a continuous medium described by its macroscopic properties: bulk dielectric permittivity, possibly surface tension[268]. In the implicit solvent models, the electrostatics-based solute-solvent interactions will considered. The cavity will created when the solute is immersed into the continuum. Thus, inside this cavity, the charge distribution of the solute polarizes the continuum, leading to the back-polarizes the solute

charge distribution[269]. The implicit models have several advantages including that the computational costs are lower, and the scaling of calculations on parallel machines is better.

Implicit solvation models can be classified into different types such as the solvation model density (SMD) model is a universal solvation model, where D stands for ″density″, while “universal” means that this model can be applicable to any solute (charged or uncharged ) in any medium (solvent or liquid)[270]. Another type is the polarizable continuum model (PCM), which allows the *ab initio* calculation of the energy and the electronic properties of molecules dissolved in anisotropic and inhomogeneous solvents, the calculation of static and frequency-dependent polarizabilities and hyperpolarizabilities in solution, and the analytic optimization of solutes geometry[271]. In this work the solvation model density (SMD) model was used with considering the effects of two different solvents, tetrahydrofuran (THF, $\varepsilon_r$ = 7.4257) and acetonitrile (MeCN, $\varepsilon_r$ = 35.688)[248,260,261].

The hybrid implicit–explicit (hybrid cluster-continuum) solvation model approximate the solvent environment by using explicit solvent molecules together with implicit solvation. It will model the short-ranged interactions explicitly and long-range effects through the continuum model surrounding the cluster. Hybrid cluster-continuums are applied to handle various problems such as finetuning the activation-free energy barriers for ionic processes in solution, calculating the pKa in aqueous and nonaqueous solvents, and surface reactions[272,273].

Therefore, these models are important in quantum chemical research. Also, it is used for handling proper computational of organic reactions whether is happening in a polar environment or charged species are involved[274].

## 3. Results and Discussion

In this chapter, the formation of urethane from the reaction of isocyanate and alcohol in the presence of 18 bases (amine) catalysts **(Figure 9)** and 3 acid catalysts **(Figure 8)** is investigated. A general mechanism for urethane formation in the case of bases and acid catalysts is proposed. In the case amine catalyst system, two different alcohols were used (methanol, and butanol). All in all, density functional theory methods and composite methods are applied.

### 3.1 Mechanism

#### 3.1.1 Catalyst-Free Reaction Mechanism of Urethane Formation

The catalyst-free urethane bond formation goes through a concerted mechanism. First, a reactant complex (RC) is formed between the isocyanate and alcohol, where the former is an electrophile, and the latter is a nucleophile **(Figure 15)**. In the transition state (TS), the N=C=O group bends, activating the carbon for the formation of a new C-O bond, while the H-O bond breaks and the N-H forms to achieve the product (P) with the urethane bond.

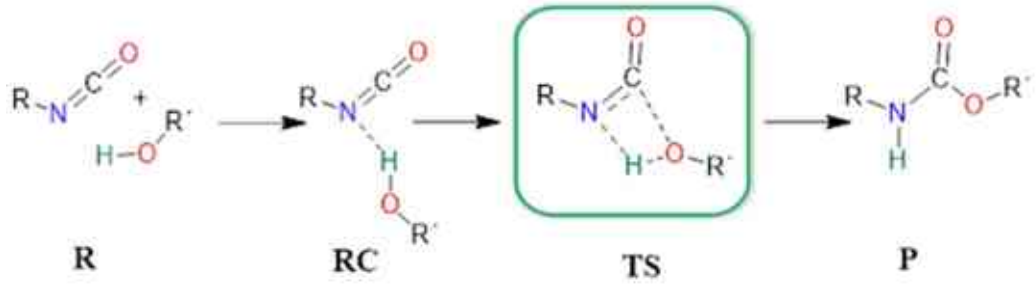


***Figure 15**. Schematic representation of the general catalyst-free reaction mechanism of isocyanates and alcohols. R—reactants, RC—reactant complex, TS—transition state, and P—product.*

#### 3.1.2 Urethane Formation Mechanism in the Presence of Catalysts

The proposed and studied catalytic urethane formation reaction mechanism contains seven steps **(Figure 16)**.

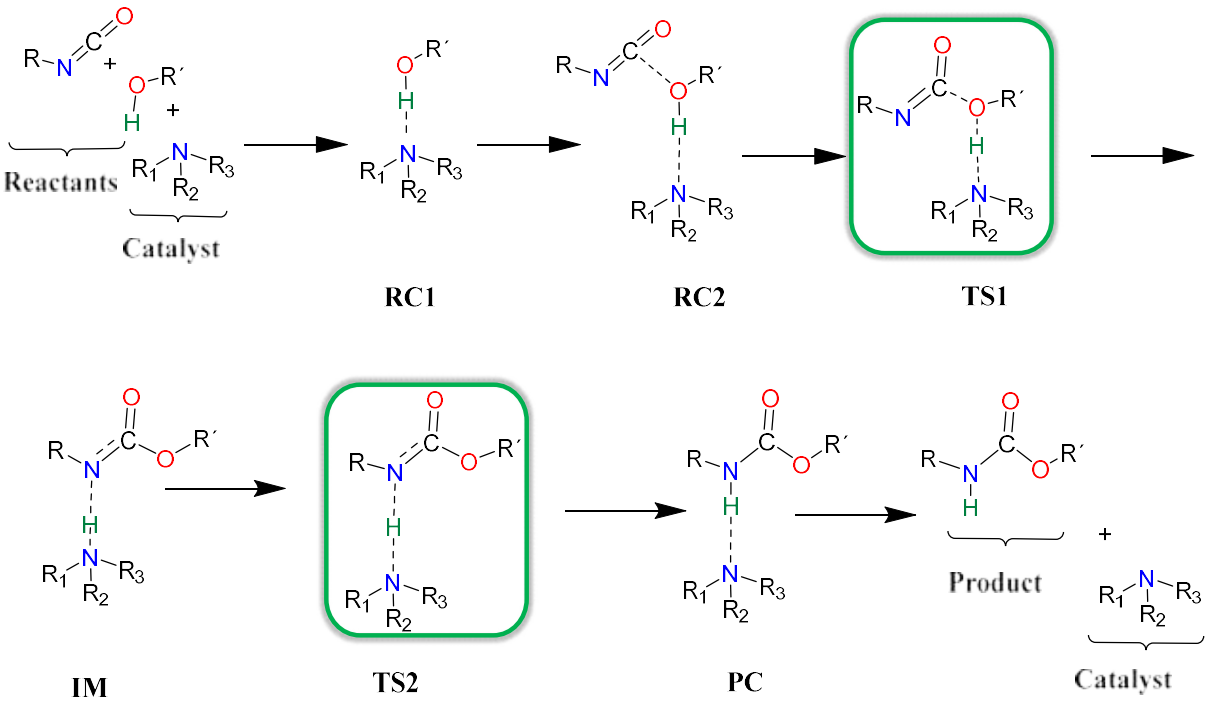


***Figure 16**. Schematic representation of the general amine -catalized urethane formation mechanism. RC—reactant complex, TS—transition state, and PC—product complex.*

It starts with the formation of a complex between the alcohol and the catalyst (RC1) because, under industrial conditions, the catalyst is first mixed into the polyols. In the next step, the isocyanate is mixed into the system and a three-molecule complex is formed (RC2). After the complex formation, a proton transfer occurs between the alcohol and the amine group of the catalyst (TS1). At the same time, a new C-O bond forms between the carbon of the NCO group and the oxygen of the alcohol, which leads to the formation of an intermediate (IM). Thereafter, the catalyst will return the proton through a transition state (TS2) and, thus, a product complex is formed (PC), where the urethane bond is complete and the catalyst is hydrogen-bonded to the product. In the final step, the catalysts and the product will be separated (P).

### 3.2 Urethane formation- reactions of phenyl isocyanate and methanol without and in the presence of amine catalysts[1]

The catalytic activities of eight different catalysts used in polyurethane synthesis have been compared using theoretical methods. The catalysts contain different amine, ketimine, and

[1] The following subchapter is based on: Hadeer Q. Waleed. *et al*. *Polymers*, 2022, 14, 8. https://doi.org/10.3390/polym14010008.

aromatic nitrogen functional groups. They are usually applied to synthesize polyurethanes with various mechanical properties (rigid and flexible foams, etc.) **(Figure 17)**.

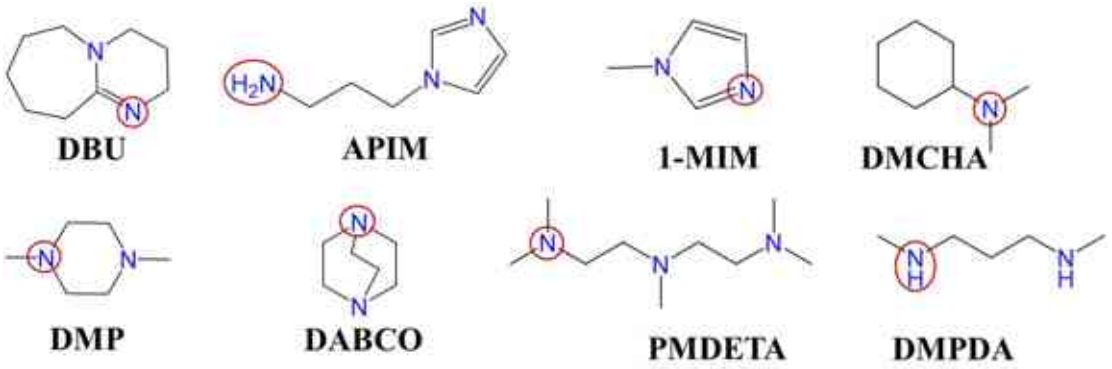


***Figure 17**. Chemical structures of the studied catalysts. 1,8-diazabicyclo[5,4,0]undec-7-ene (DBU), 1-(3-aminopropyl)imidazole (APIM), 1-methylimidazole (1-MIM), N,N-dimethylcyclohexanamine (DMCHA), 1,4-dimethylpiperazine (DMP), 1,4-diazabicyclo[2.2.2]octane (DABCO), N,N,N',N'',N''–pentamethyldiethylenetriamine (PMDETA), N,N-dimethyl-1,3-propanediamine (DMPDA). The catalytic nitrogen-containing groups which are considered in the calculations are highlighted with red circles.*

To determine the effect of the catalysts, a catalyst-free reaction has also been investigated.

### 3.2.1 Structural and Energetic Features of Model System (Methanol-Phenyl isocyanate)

The reaction of methanol and phenyl isocyanate has been selected as a first model to describe the energetic and structural features of the catalyst-free urethane formation. The structures of the corresponding reactant complex (RC), transition state (TS), and product (P) have been optimized **(Figure 15, Figure 18)** and the reaction mechanism has been characterized.

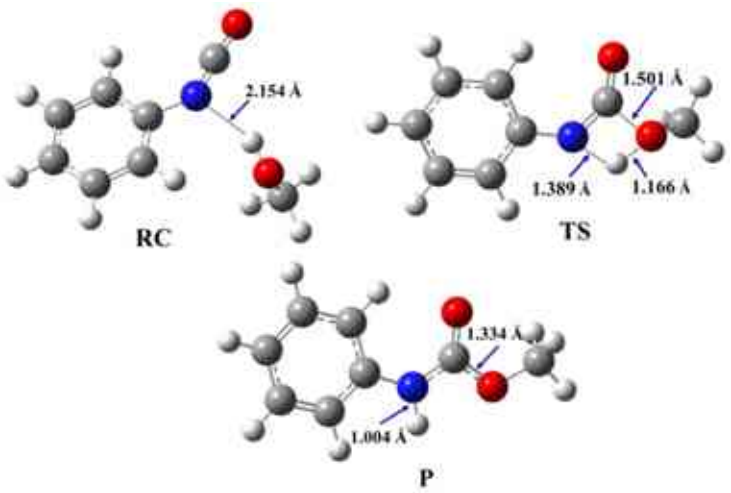


***Figure 18**. Three-dimensional structures of the reactant complex (RC), transition state (TS), and product (P) in the reaction of methanol and phenyl isocyanate, which are used as a model*

*of catalyst-free urethane formation. The structures have been optimized at the BHandHLYP/6-31G(d) level of theory in acetonitrile at 298.15 K and 1 atm.*

During the reaction between phenyl isocyanate and methanol, a reactant complex (RC) forms in the first step. It is stabilized by a hydrogen bond between the hydroxyl group of the methanol and the nitrogen of the isocyanate group with a corresponding distance of 2.154 Å **(Figure 18)**, while the relative enthalpy ($\Delta_r H$) is -6.65 kJ/mol compared to the sum of the separated reactants **(Table 1).**

***Table 1.*** *Relative enthalpy ($\Delta_r H$) of the reaction between phenyl isocyanate and methanol with and without catalysts, calculated using the G3MP2BHandHLYP composite method in acetonitrile, using the SMD implicit solvent model at 298.15 K and 1 atm. R—reactant, RC—reactant complex, TS—transition state, IM—intermediate, PC—product complex, and P—product.*

| | $\Delta_r H$ (kJ/mol) | | | | | | | |
|---|---|---|---|---|---|---|---|---|
| | **R** | **RC1** | **RC2** | **TS1** | **IM** | **TS2** | **PC** | **P** |
| **Catalyst-free system** | 0.00 | - | -6.65’ | 116.19 | - | - | - | -94.03 |
| **DBU** | 0.00 | -26.65 | -36.84 | -3.07 | -153.02# | -119.39 | -126.33 | -94.03 |
| **APIM** | 0.00 | -15.32 | -22.27 | 16.67 | -115.84# | -87.00 | -113.12 | -94.03 |
| **1-MIM** | 0.00 | -18.83 | -25.01 | 15.06 | -106.53# | -76.75 | -113.90 | -94.03 |
| **DMCHA** | 0.00 | -26.35 | -35.16 | -3.06 | -140.37# | -112.89 | -127.46 | -94.03 |
| **DMP** | 0.00 | -25.01 | -34.70 | 2.58 | -133.10# | -106.62 | -124.98 | -94.03 |
| **DABCO** | 0.00 | -24.94 | -33.37 | 1.81 | -132.76# | -106.20 | -121.82 | -94.03 |
| **PMDETA** | 0.00 | -26.21 | -35.90 | -2.58 | -136.89# | -109.85 | -118.24 | -94.03 |
| **DMPDA** | 0.00 | -18.52 | -26.63 | 8.24 | -129.69# | -101.26 | -119.00 | -94.03 |

’ RC for catalyst-free reaction. # Corrected relative enthalpy calculated according to ref.[251,263,264].

After this, in the TS, a proton from the hydroxyl group shifts to the nitrogen atom of the isocyanate, while a bond forms between the hydroxyl’s oxygen and the NCO’s carbon. The potential energy curve of the reaction **(Figure 19)** shows that the reaction needs to overcome a barrier of 116.19 kJ/mol to reach the final urethane product (P), which has a relative enthalpy ($\Delta_r H$) of -94.03 kJ/mol **(Table 1)**.

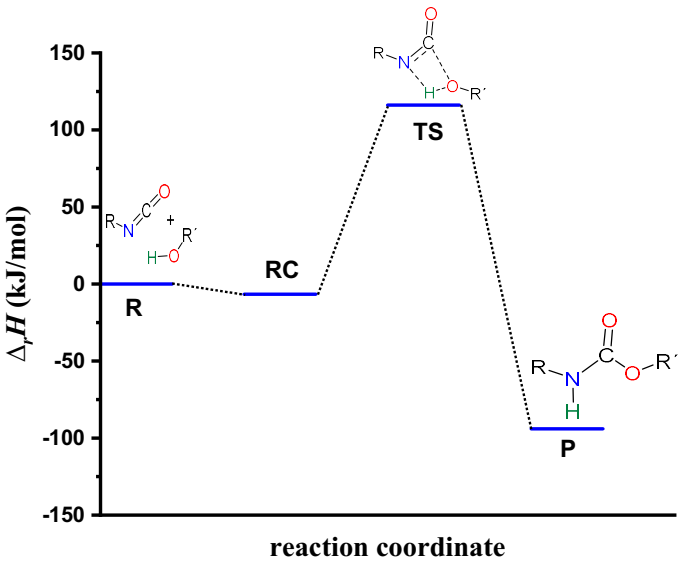


***Figure 19.*** *Energy profile (relative enthalpy ($\Delta_r H$)) of the phenyl isocyanate and methanol reaction calculated using the G3MP2BHandHLYP composite method in acetonitrile, using the SMD implicit solvent model at 298.15 K and 1 atm.*

### 3.2.2 Urethane Formation Reaction in the Presence of Nitrogen-Containing Catalysts

A varied set of nitrogen-containing catalysts have been selected from the literature[275–280]. Based on their applications, the catalysts can be divided into four groups as follows: DBU, APIM–DMCHA, DMP–PMDETA, and DMPDA, which are used in the synthesis of flexible, rigid, and semi-rigid foams, and others, respectively **(Figure 17 and Table 2)**.

***Table 2.*** *Structural features of the studied catalysts and their applications. $RNH_2$, $R_2NH$, $R_3N$, $R_2C$ = N-R: primary, secondary, tertiary amines, and secondary ketimine, respectively.*

| Catalysts | Resulted Polyurethane Type | Structural Property of PU | Functional Groups | | | | References |
|---|---|---|---|---|---|---|---|
| | | | $RNH_2$ | $R_2NH$ | $R_3N$ | $R_2C$ = N-R | |
| **DBU** | Flexible foam | Cyclic | | | • | • | [275] |
| **APIM** | Rigid foam | Aromatic, Linear | • | • | • | | [275] |
| **1-MIM** | Rigid foam | Aromatic | | • | • | | [276] |
| **DMCHA** | Rigid foam | Linear | | | • | | [277] |
| **DMP** | Semi-rigid | Cyclic | | | •• | | [278,279] |
| **DABCO** | Semi-rigid | Cyclic | | | •• | | [280] |
| **PMDETA** | Semi-rigid | Linear | | | ••• | | [275] |
| **DMPDA** | Other | Linear | | •• | | | [86] |

There are three linear, three cyclic, one aromatic, and one aromatic and linear structures. Catalyst DMCHA has only one, while all the others have at least two potential catalytic sites **(Table 2)**. Most of the catalysts have at least one tertiary amine group, except DMPDA, which contains only two secondary amines **(Figure 17)**. Secondary ketimine groups are also important, as occurs in catalyst DBU, while catalysts APIM and 1-MIM contain aromatic groups. Primary and secondary amine groups can be found only in catalysts APIM and DMPDA, and they are significant due to their potential reaction with isocyanates. However, only the catalytic activity of the species will be discussed.

### 3.2.2.1 Proton Affinity (PA) of the Studied Catalysts

As the proposed catalytic mechanism contains protonation steps, it is important to know the proton affinities (PA) of the catalysts. Only the nitrogen-containing groups of the catalysts are considered, and the corresponding PA values have been calculated **(Eq. 1) (Tables 3 and Table A1(Appendix A))**.

***Table 3.*** *Computed ($PA_{calc}$) and measured proton affinities ($PA_{exp}$) in kJ/mol. The calculations have been carried out at the G3MP2BHandHLYP level of theory in gas phase at 298.15 K and 1 atm. $RNH_2$, $R_2NH$, $R_3N$, $R_2C = N\text{-}R$: primary, secondary, tertiary amines, secondary ketimine, respectively. • side; •• middle amine group.*

| Catalysts | $PA_{calc}$ (kJ/mol) | | | | $PA_{exp}$ (kJ/mol)[281] |
|---|---|---|---|---|---|
| | $RNH_2$ | $R_2NH$ | $R_3N$ | $R_2C=N\text{-}R$ | |
| DBU | - | - | 937.50 | 1070.34 | - |
| APIM | 905.75 | 994.19 | 800.93 | - | - |
| 1-MIM | - | 983.68 | 785.51 | - | 959.6 |
| DMCHA | - | - | 998.68 | - | 983.6 |
| DMP | - | - | 984.84 | - | - |
| DABCO | - | - | 983.91 | - | 963.4 |
| PMDETA | - | - | 984.71 • 982.62 •• | - | - |
| DMPDA | - | 966.54 | - | - | 1035.2 |

In some cases, there are more than one amine group in the catalysts, but only one of them is considered during the catalytic mechanism. However, the proton affinity has been computed for all nitrogen-containing groups. The experimental and computational results are in fairly good agreement with each other **(Tables 3 and Table A1(Appendix A))**. In the case of catalyst DMCHA, the deviation between the calculated and experimental values was the lowest, only

15.08 kJ/mol. The deviation between the calculated and literature data is the highest, 68.66 kJ/mol, in the case of catalyst DMPDA. Catalyst 1-MIM has the lowest calculated proton affinity (785.51 kJ/mol) within the studied set of structures in the case of its tertiary amine group **(Tables 3 and Table A1(Appendix A))**, which makes it the best proton donor, as less energy is needed to remove the proton. It is followed by the tertiary amine group of catalyst APIM, which has just a slightly higher PA value (800.93 kJ/mol). The highest proton affinity belongs to the secondary ketimine of catalyst DBU (1070.34 kJ/mol), which makes it the best proton acceptor. Most of the calculated PA values are around or above 900 kJ/mol **(Tables 3 and Table A1(Appendix A))**. All in all, the proton affinities of the amine groups of the catalysts cover a wide range of almost 300 kJ/mol, between 785.5 and 1070.3 kJ/mol.

#### 3.2.2.2 Structural Features of Urethane Formation in the Presence of the Studied Catalysts

Even though the same reaction mechanism of phenyl isocyanate and methanol was considered in the presence of the studied catalysts **(Figure 16)**, the structural features vary slightly with the different catalysts **(Table 4, Figures 20, and Figures A1-A7(Appendix A))**.

***Table 4.*** *The N-H, O-H, and C-O bond lengths (Å) along the phenyl isocyanate (PhNCO) and methanol reaction pathway in the presence of the studied catalysts. N-H* for catalysts, while N-H** for PhNCO.*

| Catalysts | RC1 | | RC2 | | | TS1 | | | IM | | TS2 | | PC | |
|---|---|---|---|---|---|---|---|---|---|---|---|---|---|---|
| | N-H* | O-H | N-H* | O-H | C-O | N-H* | O-H | C-O | N-H* | N-H** | N-H* | N-H** | N-H* | N-H** |
| DBU | 1.813 | 0.980 | 1.828 | 0.979 | 3.033 | 1.604 | 1.021 | 1.884 | 1.041 | 1.779 | 1.242 | 1.316 | 1.888 | 1.027 |
| APIM | 1.848 | 0.977 | 1.853 | 0.977 | 3.026 | 1.653 | 1.011 | 1.869 | 1.092 | 1.605 | 1.168 | 1.437 | 1.920 | 1.026 |
| 1-MIM | 1.882 | 0.972 | 1.855 | 0.974 | 3.064 | 1.690 | 1.002 | 1.828 | 1.088 | 1.597 | 1.134 | 1.481 | 1.967 | 1.019 |
| DMCHA | 1.864 | 0.977 | 1.868 | 0.977 | 3.036 | 1.670 | 1.014 | 1.845 | 1.065 | 1.725 | 1.223 | 1.370 | 2.012 | 1.023 |
| DMP | 1.879 | 0.975 | 1.883 | 0.975 | 3.062 | 1.695 | 1.009 | 1.836 | 1.068 | 1.718 | 1.212 | 1.384 | 2.022 | 1.021 |
| DABCO | 1.851 | 0.976 | 1.827 | 0.980 | 3.078 | 1.657 | 1.013 | 1.857 | 1.073 | 1.670 | 1.211 | 1.372 | 1.996 | 1.023 |
| PMDETA | 1.870 | 0.976 | 1.872 | 0.976 | 3.053 | 1.669 | 1.012 | 1.845 | 1.070 | 1.703 | 1.213 | 1.381 | 1.987 | 1.023 |
| DMPDA | 1.849 | 0.978 | 1.850 | 0.978 | 3.052 | 1.653 | 1.013 | 1.866 | 1.077 | 1.660 | 1.203 | 1.387 | 1.927 | 1.026 |

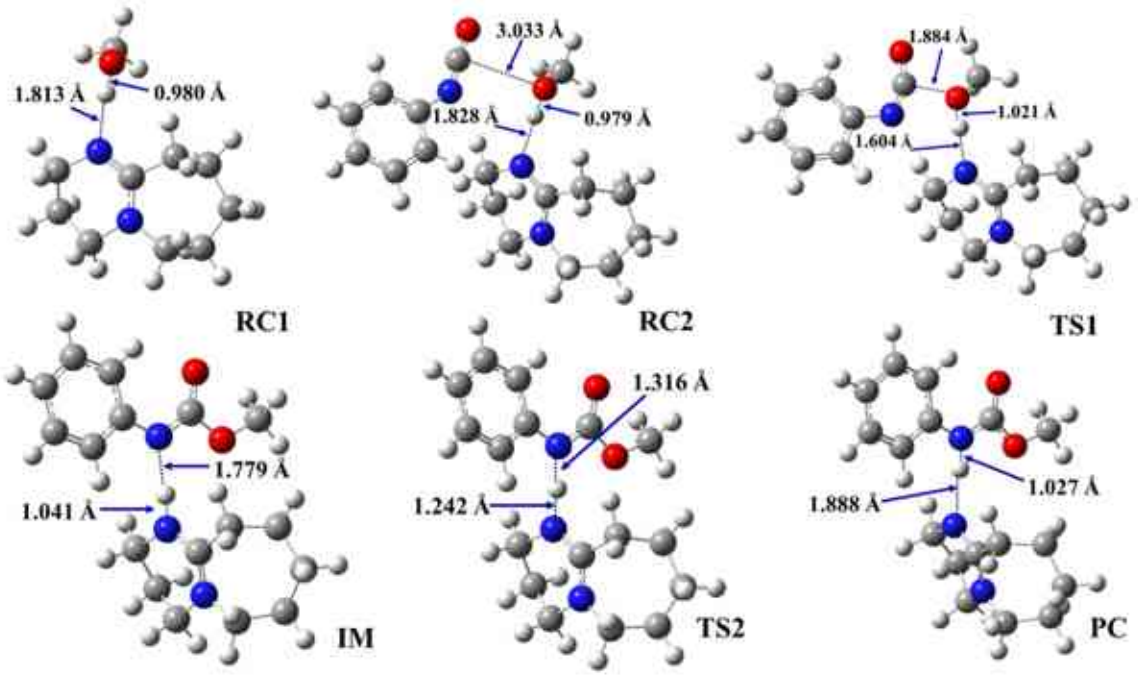


***Figure 20.*** *Optimized structures along the reaction pathway between phenyl isocyanate and methanol in the presence of 1,8-diazabicyclo[5,4,0]undec-7-ene (DBU), calculated at the BHandHLYP/6-31G(d) level of theory in acetonitrile at 298.15 K and 1 atm. RC—reactant complex, TS—transition state, IM—intermediate, and PC—product complex.*

In the first step, during which the RC1 forms, the distance between the catalyst's nitrogen and the methanol's hydroxyl hydrogen ranged between 1.812 and 1.882 Å **(Table 4, N-H*)**. In the second step, RC2, a three-molecule complex forms with the addition of PhNCO. A new interaction between the methanol's oxygen and the PhNCO's isocyanate group occurs, but only minor changes could be identified in the length of the previously established N-H*. The effect on the O-H bond length was even smaller and almost no change was observed between RC1 and RC2 **(Table 4)**. As the TS1 developed in the presence of the catalysts, the N-H slightly decreased while the C-O significantly decreased, by ~0.2 and ~1.2 Å, respectively. At the same time, the O-H increased in each case by ~0.3 Å **(Table 4)**. The structural changes take place according to the proposed steps, and it shows that the methanol's oxygen loses the proton while attaching itself to the isocyanate's N=C=O group. Thus, an IM is formed including the protonated catalyst (N-H*), which is hydrogen-bonded to the nitrogen of the adduct (N-H**), while the methoxy group (from the methanol) is attached to the carbon of the former isocyanate group (C-O) **(Figures 20 and Figures A1-A7(Appendix A))**. The N-H* distance was the lowest in this step for each catalytic process, and it was in the range of 1.041 and 1.092 Å, while N-H** ranged between 1.597 and 1.779 Å. In TS2, proton transfer occurs and, thus, the final urethane bond develops (N-H* increases, while N-H** decreases). Through this step, the PC

will be formed, which is a bimolecular complex of the catalyst and the final product (methyl phenylcarbamate).

### 3.2.2.3 Energetics of Urethane Formation in the Presence of Different Catalysts

The thermodynamic properties of the catalysed isocyanate–methanol reaction have been computed **(Tables 1, and Tables A2, A3(Appendix A))** and the corresponding energy profiles have been drawn **(Figures 21 and Figure A9(Appendix A))**. The most stable methanol-catalyst complex (RC1, $\Delta_r H$ = -26.65 kJ/mol) and trimolecular complex (RC2, $\Delta_r H$ = -36.84 kJ/mol) were formed in the presence of DBU catalyst, while the least stable ones were associated with APIM catalyst (RC1 and RC2, $\Delta_r H$ = -15.32 and -22.27 kJ/mol, respectively). The calculated barrier height significantly decreased ($\Delta\Delta_r H$ > 98 kJ/mol) in the presence of the studied set of catalysts compared to the catalyst-free reaction. The relative energy at TS1 was the lowest in case of DBU catalyst ($\Delta_r H$ = -3.07 kJ/mol) within the studied set of catalysts **(Table 1, Figure 21, and Figure A9(Appendix A))**.

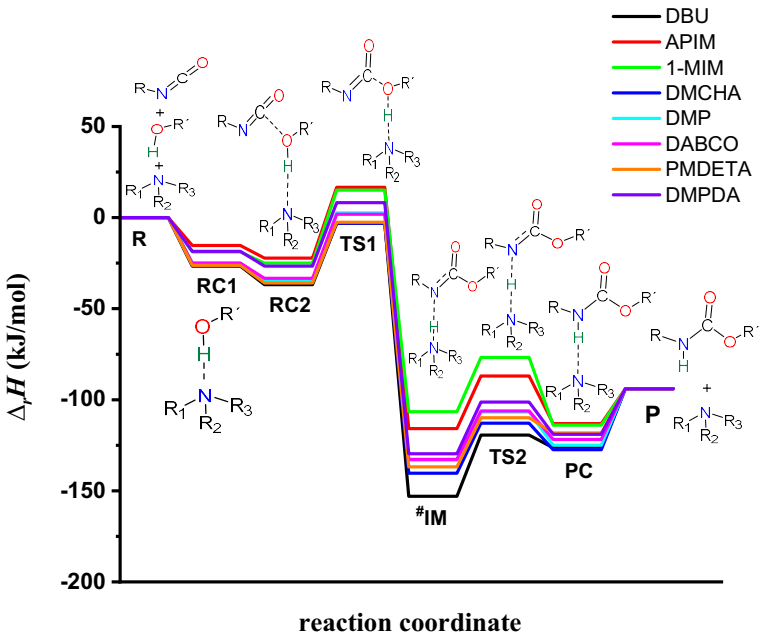


***Figure 21.*** *Energy profiles (relative enthalpy ($\Delta_r H$)) of the catalyzed urethane formation reactions calculated with the G3MP2BHandHLYP composite method in acetonitrile, using the SMD implicit solvent model at 298.15 K and 1 atm. #Corrected relative enthalpy of IM calculated according to Ref.*[251,263,264].

The relative energy of the IM was the highest in the presence of 1-MIM ($\Delta_r H$ = -106.53 kJ/mol), while this step was more preferred in the case of DBU. By applying DBU catalyst, TS2 (proton shift) had the lowest relative energy (($\Delta_r H$ = -119.39 kJ/mol) compared to the studied set of catalysts. Before the reaction completed, the product complex (PC) formed with a relative enthalpy range of -113.12 and -126.33 kJ/mol. After this, the product was achieved,

which had a relative energy of -94.03 kJ/mol. Therefore, along with the whole reaction mechanism, DBU catalyst was the most effective and provided the most favorable pathway, which can be associated with its high PA and cyclic structure.

### 3.3 Urethane formation- reactions of phenyl isocyanate and butan-1-ol without and in the presence of cyclic amine catalysts[2]

Three different cyclic amine catalysts **(Figure 22)** were studied, and their catalytic activity in urethane synthesis was compared by using kinetic measurements.


***Figure 22.*** *Chemical structures of the studied catalysts. 1,4-Diazabicyclo[2.2.2]octane (DABCO), 1,2-Dimethylimidazole (1,2-DMI), and N-Ethylmorpholine (NEM). The catalytic nitrogen-containing groups which are considered in the calculations are highlighted with red circles.*

Furthermore, the catalytic reactions were also examined by using computational tools to determine the step-by-step mechanisms with and without catalysts and to compare the reaction pathways **(Figure 22)**. Catalyst design and development will be possible by describing the catalytic urethane formation at the molecular level.

#### 3.3.1 Catalyst-Free Model Reaction (Butan-1-ol-Phenyl isocyanate)

The reaction of butan-1-ol and phenyl isocyanate has been selected as a second model to describe the energetic and structural features of the catalyst-free urethane formation. It can be seen that the catalyst-free reaction goes through a concerted step **(Figure 15)**. First, the reactant complex (RC), including PhNCO and BuOH, is formed. In the studied case, a hydrogen bond between the hydroxyl group of BuOH and the nitrogen of the NCO group of PhNCO formed with a corresponding distance of 2.182 Å **(Figure 23)**.

[2] The following subchapter is based on: Hadeer Q. Waleed. *et al. Polymers*, 2022, 14, 2859, https://doi.org/10.3390/polym14142859

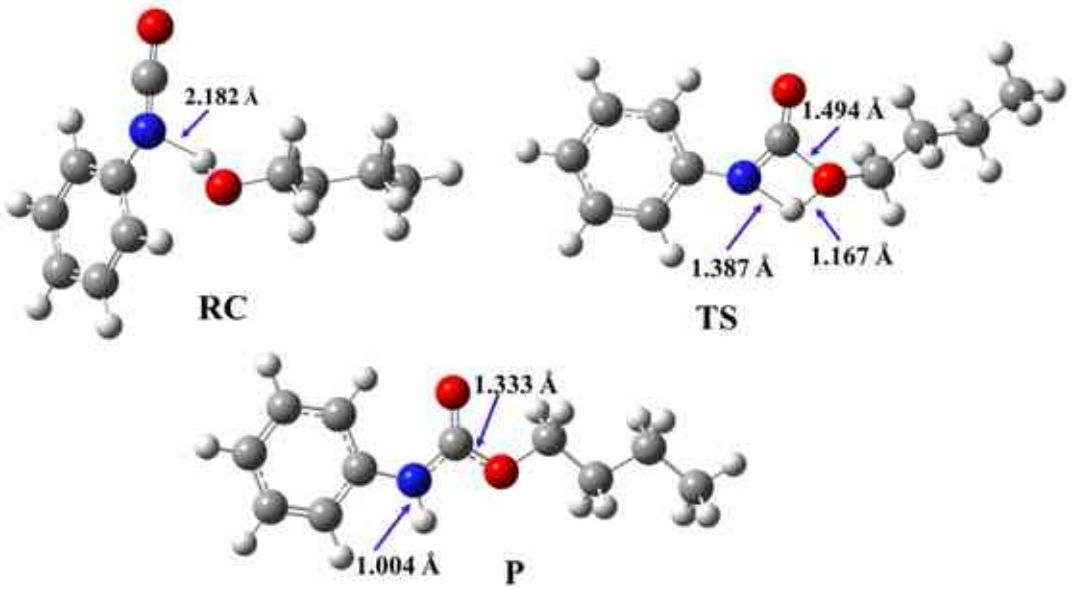


***Figure 23.*** *Three-dimensional structures of the reactant complex (RC), transition state (TS), and product (P) in the reaction of butan-1-ol and phenyl isocyanate, which are used as a model of catalyst-free urethane formation. The structures have been optimized at the BHandHLYP/6-31G(d) level of theory in acetonitrile at 298.15 K and 1 atm.*

In the next step, a transition state (TS) developed in which a proton transfer between the BuOH hydroxyl group and the nitrogen of the NCO group took place (1.387 Å), while a C-O bond was formed between the NCO's carbon and the butan-1-ol's oxygen (1.494 Å). The relative enthalpy of the TS compared to the entrance channel was 116.49 kJ/mol **(Table 5, and Figure 24)**, and after this, the final urethane product (P) was reached.

***Table 5.*** *Relative enthalpy ($\Delta_r H$) of the reaction between phenyl isocyanate and butan-1-ol with and without catalysts, calculated using the G3MP2BHandHLYP composite method in acetonitrile, using the SMD implicit solvent model at 298.15 K and 1 atm. R—reactant, RC—reactant complex, TS—transition state, IM—intermediate, PC—product complex, and P—product.*

| | $\Delta_r H$(kJ/mol) | | | | | | | |
|---|---|---|---|---|---|---|---|---|
| | **R** | **RC1** | **RC2** | **TS1** | **IM** | **TS2** | **PC** | **P** |
| **Catalyst-free system** | 0.0 | - | -8.97' | 116.49 | - | - | - | -94.84 |
| **DABCO** | 0.0 | -24.54 | -41.44 | -0.84 | -134.98[#] | -109.15 | -124.63 | -94.84 |
| **1,2-DMI** | 0.0 | -20.56 | -28.55 | 7.25 | -116.89[#] | -88.56 | -119.56 | -94.84 |
| **NEM** | 0.0 | -27.33 | -44.40 | -0.87 | -135.30[#] | -107.93 | -132.21 | -94.84 |

'RC for catalyst-free reaction. # Corrected relative enthalpy calculated according to ref.[251,263,264].

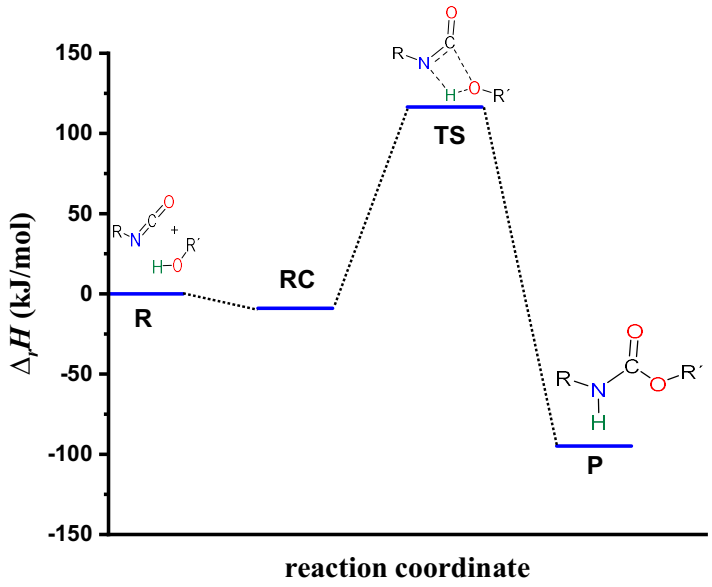


**Figure 24.** *Energy profile (relative enthalpy ($\Delta_r H$)) of the phenyl isocyanate and butan-1-ol reaction calculated using the G3MP2BHandHLYP composite method in acetonitrile, using the SMD implicit solvent model at 298.15 K and 1 atm.*

### 3.3.2 Proton Affinity (PA) of the Studied Catalysts

As proton transfers are crucial during the reactions, proton affinity (PA) was computed for all unique nitrogen that were considered catalytically active within the cyclic amine catalysts **(Ep. 1) (Figure 22, Table 6)**. The PAs of the catalytically active nitrogens were in a range of 973.2−1002.9 kJ/mol. The results showed that the difference between the calculated and data in the literature was 20.5 kJ/mol in the case of DABCO and 18.1 kJ/mol for 1,2-DMI. As the nitrogen of NEM had the lowest proton affinity (973.2 kJ/mol), after protonation, it was the most prone to donating its proton. Meanwhile, 1,2-DMI was the best proton acceptor, as it had the highest proton affinity (1002.9 kJ/mol).

***Table 6.*** *Computed ($PA_{calc}$) and measured proton affinities ($PA_{exp}$) of the tertiary amines of the studied catalysts: 1,4-diazabicyclo[2.2.2]octane (DABCO), 1,2-dimethylimidazole (1,2-DMI), and N-ethylmorpholine (NEM), in kJ/mol. The calculations were carried using the G3MP2BHandHLYP composite method in the gas phase at 298.15 K and 1 atm.*

| Catalysts | $PA_{calc}$ (kJ/mol) | $PA_{exp}$ (kJ/mol)[282] |
|---|---|---|
| **DABCO** | 983.9 | 963.4 |
| **1,2-DMI** | 1002.9 | 984.7 |
| **NEM** | 973.2 | - |

### 3.3.3 Structural Features of Urethane Formation in the Presence of the Studied Catalysts

The mechanism was also examined in the presence of catalysts **(Figure 16, Figures 25, and Figures B1, B2(Appendix B))**. It can be seen that additional structures were formed compared to the catalyst-free case.

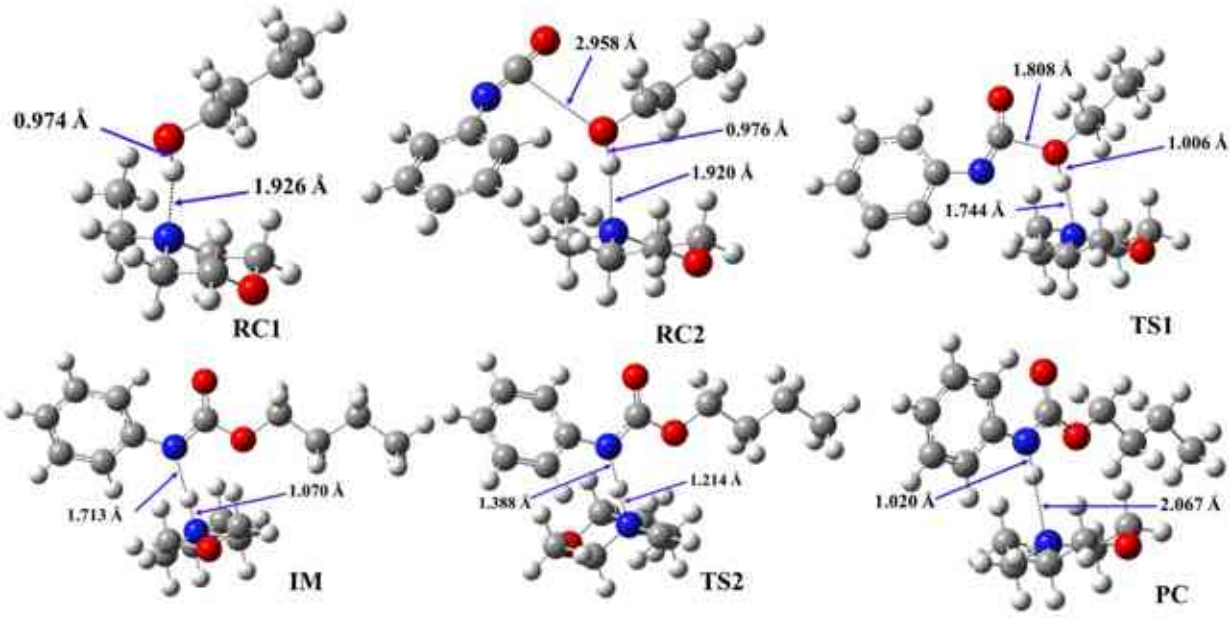


***Figure 25.*** *Optimized structures along the reaction pathway between phenyl isocyanate and butan-1-ol in the presence of NEM, calculated at the BHandHLYP/6-31G(d) level of theory in acetonitrile at 298.15 K and 1 atm. RC—reactant complex, TS—transition state, IM—intermediate, and PC—product complex.*

During the industrial urethane synthesis, the catalyst was mixed into the polyol. Thus, in the presence of catalysts, the reaction was mimicked by the formation of the first complex (RC1) between the catalyst and the alcohol. The distance between the catalyst's nitrogen and the hydroxyl hydrogen of butan-1-ol was in the range of 1.856 and 1.926 Å **(Table 7, N-H *)**. Then, isocyanate was added to the system, which led to the formation of a trimolecular complex (RC2). In the case of RC2, an interaction occurred between the oxygen of BuOH and the NCO group of the isocyanate, with the corresponding C-O distance being in the range of 2.958–3.073 Å, while a minor change in the length of the N-H * bond could be identified compared to the same interaction in RC1 **(Table 7)**.

***Table 7.*** *The N-H, O-H, and C-O bond lengths (Å) along the phenyl isocyanate (PhNCO) and butan-1-ol reaction pathway in the presence of the studied catalysts. N-H* for catalysts, while N-H** for PhNCO.*

| Catalysts | RC1 | | RC2 | | | TS1 | | | IM | | TS2 | | PC | |
|---|---|---|---|---|---|---|---|---|---|---|---|---|---|---|
| | N-H * | O-H | N-H * | O-H | C-O | N-H * | O-H | C-O | N-H * | N-H ** | N-H * | N-H ** | N-H * | N-H ** |
| DABCO | 1.856 | 0.976 | 1.835 | 0.979 | 3.073 | 1.661 | 1.012 | 1.853 | 1.074 | 1.668 | 1.207 | 1.367 | 1.998 | 1.023 |
| 1,2-DMI | 1.878 | 0.973 | 1.898 | 0.972 | 3.059 | 1.704 | 1.001 | 1.832 | 1.082 | 1.610 | 1.150 | 1.450 | 1.972 | 1.020 |
| NEM | 1.926 | 0.974 | 1.920 | 0.976 | 2.958 | 1.744 | 1.006 | 1.808 | 1.070 | 1.713 | 1.214 | 1.388 | 2.067 | 1.020 |

The formed complexes (i.e., RC1 and RC2) were the most favoured in the case of NEM ($\Delta_r H$ = -27.33 kJ/mol, and -44.40 kJ/mol, respectively), while in the presence of 1,2-DMI, they were the least stable ($\Delta_r H$ = -20.56 and -28.55 kJ/mol, for RC1 and RC2, respectively) compared to the other studied catalysts **(Table 5 and Figure 25)**. As the catalytic reaction mechanism included proton transfer steps, the proton affinity of the catalytic nitrogen influenced the relative enthalpy of the reaction steps (e.g., the reactant complex (RC1)), and by increasing the proton affinity, the corresponding thermodynamic property also changed **(Table B1, B2(Appendix B))**. After the formation of the reactant complexes, the reaction continued with TS1 in which a proton transfer occurred from the hydrogen of the OH group to the nitrogen of the catalyst, and the corresponding distance between these groups significantly decreased to the range of 1.661–1.744 Å in the studied systems. The potential energy curve showed that in the presence of NEM, the TS1 step had the lowest relative enthalpy ($\Delta_r H$ = 0.87 kJ/mol) within the studied set of catalysts **(Figure 26)**. The N=C=O group was bent activating the carbon for the formation of a new C–O bond, and this led to the formation of an intermediate (IM), where the distance between the hydrogen of the OH and the nitrogen of the catalyst significantly decreased, while a bond formed between the carbon of the N=C=O and the oxygen of the BuOH. The relative enthalpy of the IM is lowest in the presence of NEM (-135.30 kJ/mol). After the formation of the IM, the proton transfer occurred from the catalyst to complete the formation of the urethane bond. In this step, the N-H* increased, and the N-H** decreased compared to the IM. The relative enthalpy of TS2 was lowest in the presence of DABCO ($\Delta_r H$ = -109.15 kJ/mol) compared to the other two (*i.e.*, 1,2-DMI and NEM) catalysts.

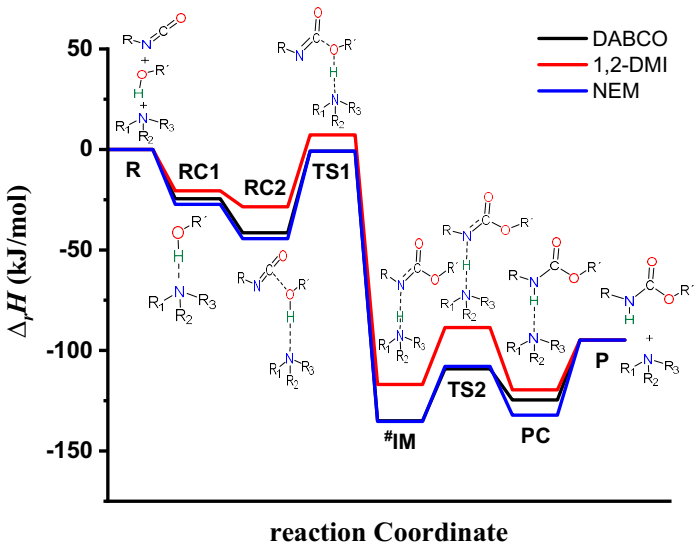


***Figure 26.*** *Energy profiles (relative enthalpy ($\Delta_rH$)) of the catalyzed urethane formation reactions calculated with the G3MP2BHandHLYP composite method in acetonitrile, using the SMD implicit solvent model at 298.15 K and 1 atm. #Corrected relative enthalpy of IM calculated according to Ref.*[251,263,264].

The penultimate step in the catalytic mechanism was the formation of the product complex (PC) in which a new bond formed between the hydrogen of the BuOH and the nitrogen of the N=C=O. The corresponding distance was significantly decreased, and it was in the range of 1.020–1.023 Å **(Table 7, Figures 25, and Figures B1, B2(Appendix B))**. This led to the final step in this mechanism, namely, the separation of the catalyst from the product. The relative enthalpy for the product was significantly reduced to -94.84 kJ/mol **(Table 5 and Figure 26)**. It was found that the presence of the catalyst in urethane formation significantly changed the reaction mechanism compared to the catalyst-free case. There was a multi-step pathway to form the product. The presence of catalysts significantly reduced the relative enthalpy, and the barrier height decreased ($\Delta\Delta_rH$ > 108 kJ/mol) compared to the catalyst-free reaction. By comparing the calculated activation energies (i.e., 26.5, 23.7, and 27.8kJ/mol) with measured values (*i.e.*, 18.1 ± 0.7, 20.3 ± 0.8, and 24.8 ± 0.8 kJ/mol)[250] for the DABCO-, 1,2-DMI-, and NEM-catalysed reactions, respectively **(Table 5)**, the highest difference was only 8.4 kJ/mol in the case of DABCO, while the lowest difference (3 kJ/mol) was experienced in the case of NEM. These results prove the validity of the proposed mechanism and verify the method selection as well.

### 3.4 Urethane formation-reactions of phenyl isocyanate and butan-1-ol without and in the presence of aliphatic tertiary amine catalysts[3]

Urethane formation in the presence of three tertiary amine catalysts (*N,N*-dimethylcyclohexylamine (DMCHA), 2-(2-dimethylaminoethoxy)ethanol (DMEE), and bis[2-(*N,N*-dimethylamino)ethyl]ether (DMAEE)) **(Figure 27)**[275,283] has also been analysed by using computational tools to understand the reactions from a mechanistic point of view. The activity of the catalysts has been compared by using theoretical methods. The catalyst-free system has also been studied computationally and used as a reference **(Figure 15)**. To mimic the experimental system as close as possible, the reaction of butan-1-ol and phenyl isocyanate has been selected as reactants to describe the energetic and structural features of the urethane formation **(Figures 15, 23, and 24)**.

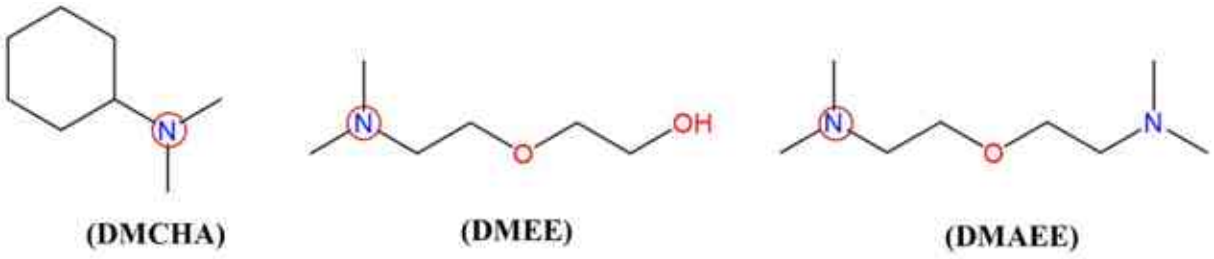


***Figure* 27.** *Chemical structures of the studied catalysts. N,N-dimethylcyclohexylamine (DMCHA), 2-(2-dimethylaminoethoxy)ethanol (DMEE), and bis[2-(N,N-dimethylamino)ethyl]ether (DMAEE). The catalytic nitrogen-containing groups which are considered in the calculations are highlighted with red circles.*

#### 3.4.1 Proton Affinity (PA) of the Studied Catalysts

As the suggested catalytic mechanism includes protonation steps, the proton affinities (PA) have been computed for all nitrogen containing groups **(Table 8)**. In the case of DMCHA the deviation between the calculated and literature data is 15.08 kJ/mol. DMEE has the lowest proton affinity (972.7 kJ/mol), which makes it the best proton donor, as less energy is needed for the deprotonation. While DMCHA has the highest proton affinity which makes it the best proton acceptor. All in all, the proton affinities of the tertiary amine groups of these catalysts are in the range of 972.7 and 998.7 kJ/mol **(Table 8)**.

[3] The following subchapter is based on: Hadeer Q. Waleed. et al. *Phys. Chem. Chem. Phys,* 2022,24, 20538-20545, https://doi.org/10.1039/D2CP00728B.

***Table 8.*** *Computed ($PA_{calc}$) and measured proton affinities ($PA_{exp}$) in kJ/mol. The calculations have been carried out at the G3MP2BHandHLYP composite method in gas phase at 298.15 K and 1 atm.*

| Catalysts | $PA_{calc}$ (kJ/mol) | $PA_{exp}$ (kJ/mol)[281] |
|---|---|---|
| **DMCHA** | 998.7 | 983.6 |
| **DMEE** | 972.7 | - |
| **DMAEE** | 973.5 | - |

### 3.4.2 Structural Features of Urethane Formation in the Presence of the Studied Catalysts

In contrast to the catalyst-free case, urethane formation in the presence of catalysts includes seven steps **(Figure 16, Figure 28, and Figures C1,C2 (Appendix C))**.

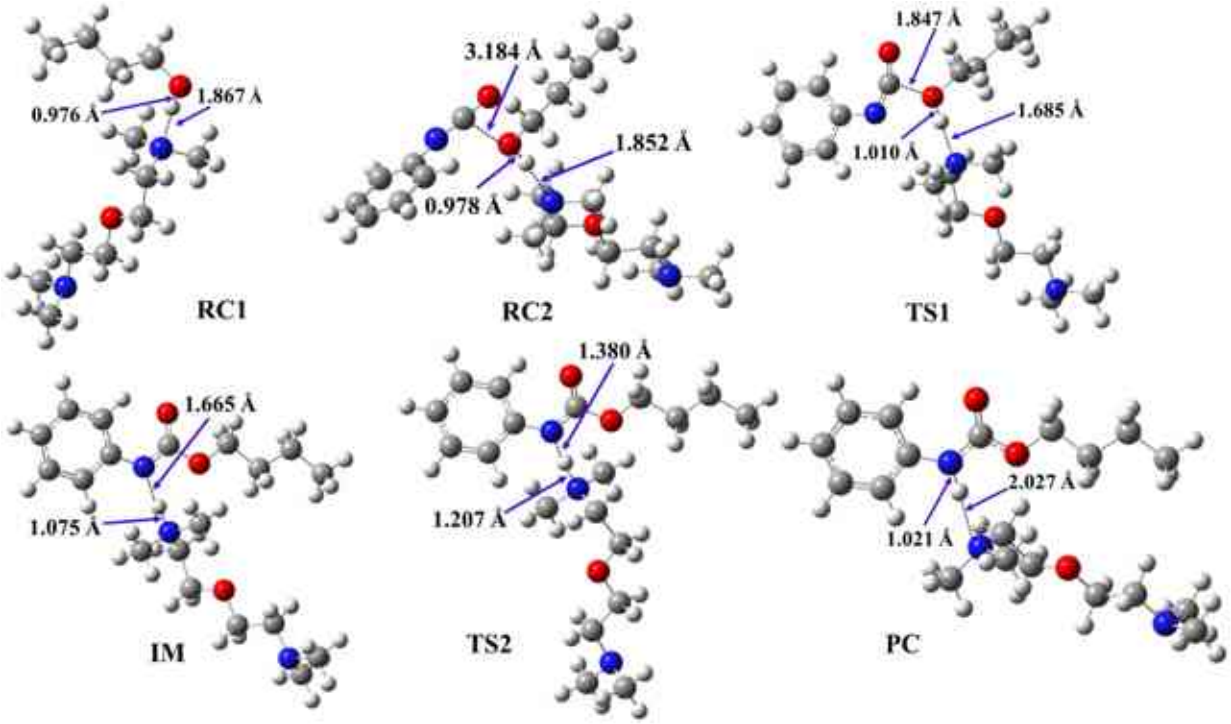


***Figure 28.*** *Optimized structures along the reaction pathway between phenyl isocyanate and butan-1-ol in the presence of DMAEE, calculated at the BHandHLYP/6-31G(d) level of theory in acetonitrile at 298.15 K and 1 atm. RC—reactant complex, TS—transition state, IM—intermediate, and PC—product complex.*

First, a complex (RC1) between the alcohol and the catalyst is forming, while the distance between the catalyst's nitrogen and the hydroxyl hydrogen of butan-1-ol is in the range of 1.867 and 1.883 Å **(Table 9, N-H*)**. This is supposed to mimic the industrial urethane synthesis, within which, first the catalyst is mixed into the polyol. Then, in the next step the isocyanate,

PhNCO, is added to the system, and RC2, a trimolecular complex is formed. In this step, a new interaction occurs between the butanol's oxygen and the isocyanate group, while only insignificant changes can be identified in the length of the previously established N-H*.

***Table 9.*** *The N-H, O-H, and C-O bond lengths (Å) along the phenyl isocyanate (PhNCO) and butan-1-ol reaction pathway in the presence of the studied catalysts (DMCHA, DMEE, and DMAEE). N-H* for catalysts, while N-H** for PhNCO.*

| Catalysts | RC1 | | RC2 | | | TS1 | | | IM | | TS2 | | PC | |
|---|---|---|---|---|---|---|---|---|---|---|---|---|---|---|
| | N-H * | O-H | N-H * | O-H | C-O | N-H * | O-H | C-O | N-H * | N-H ** | N-H * | N-H ** | N-H * | N-H ** |
| DMCHA | 1.883 | 0.976 | 1.868 | 0.978 | 3.038 | 1.691 | 1.011 | 1.842 | 1.068 | 1.710 | 1.221 | 1.371 | 2.016 | 1.022 |
| DMEE | 1.883 | 0.975 | 1.885 | 0.975 | 3.031 | 1.718 | 1.006 | 1.815 | 1.075 | 1.678 | 1.206 | 1.392 | 2.022 | 1.021 |
| DMAEE | 1.867 | 0.976 | 1.852 | 0.978 | 3.184 | 1.685 | 1.010 | 1.847 | 1.075 | 1.665 | 1.207 | 1.380 | 2.027 | 1.021 |

The effect on the O-H bond length is even smaller and almost no change is observed between RC1 and RC2 **(Table 9)**. The most stable butan-1-ol–catalyst complex (RC1) and trimolecular complex (RC2) are formed in the case of DMCHA ($\Delta_r H$ = -28.14 kJ/mol, and -47.16 kJ/mol, for RC1 and RC2, respectively). Meanwhile, DMEE–butan-1-ol is the least stable RC1 ($\Delta_r H$ = -27.33 kJ/mol), and DMAEE participates in the least stable trimolecular complex (RC2, $\Delta_r H$ = -38.67kJ/mol) **(Table 9 and Figure 29**).

***Table 10.*** *Relative enthalpy ($\Delta_r H$) of the reaction between phenyl isocyanate and butan-1-ol with and without catalysts, calculated using the G3MP2BHandHLYP composite method in acetonitrile, using the SMD implicit solvent model at 298.15 K and 1 atm. R—reactant, RC—reactant complex, TS—transition state, IM—intermediate, PC—product complex, and P—product.*

| | $\Delta_r H$ (kJ/mol) | | | | | | | |
|---|---|---|---|---|---|---|---|---|
| | **R** | **RC1** | **RC2** | **TS1** | **IM** | **TS2** | **PC** | **P** |
| **Catalyst-free system** | 0.00 | - | -8.97' | 116.49 | - | - | - | -94.84 |
| **DMCHA** | 0.00 | -28.14 | -47.16 | -5.94 | -143.73[#] | -116.14 | -130.65 | -94.84 |
| **DMEE** | 0.00 | -27.33 | -44.75 | -5.36 | -135.94[#] | -107.74 | -131.45 | -94.84 |
| **DMAEE** | 0.00 | -27.59 | -38.67 | -3.20 | -139.72[#] | -111.10 | -127.92 | -94.84 |

'RC for catalyst-free reaction. # Corrected relative enthalpy calculated according to ref.[251,263,264].

In the next step, TS1 is developing in the presence of the catalyst where a proton transfer between the alcohol and the amine group of the catalyst occurs, and the N=C=O group is being bent activating the carbon for the formation of a new C–O bond. Therefore, the N-H* and C-O distances are significantly decreased, and these are in the range of 1.685 – 1.718 Å, and 1.815 – 1.847 Å, for N-H* and C-O, respectively. At the same time, the O-H distance increased from 0.975 – 0.978 to 1.006 – 1.011Å. The potential energy curve showed that in the presence of

DMCHA the TS1 step has the lowest relative energy ($\Delta_r H$= -5.94 kJ/mol) within the studied set of catalysts **(Figure 29)**.

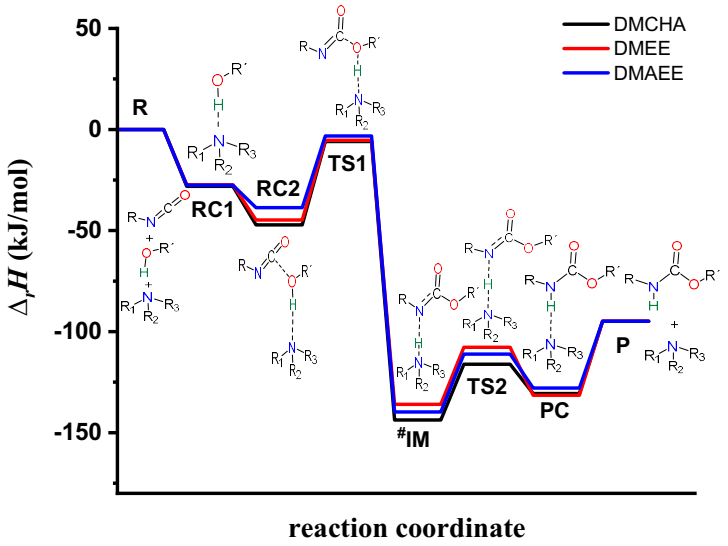


***Figure 29.*** *Energy profiles (relative enthalpy ($\Delta_r H$)) of the catalyzed urethane formation reactions calculated with the G3MP2BHandHLYP composite method in acetonitrile, using the SMD implicit solvent model at 298.15 K and 1 atm. #Corrected relative enthalpy of IM calculated according to Ref.*[251,263,264].

In the next step, an IM is formed which includes the protonated catalyst, hydrogen bonded to the nitrogen of the forming urethane bond, and the distance in this step is the lowest for N-H* and it is in the range of 1.068 and 1.075 Å for each catalyst, while a new C–O bond is formed between the carbon of the NCO group and the oxygen of the alcohol. In this step, the relative enthalpy is the lowest in the presence of DMCHA ($\Delta_r H$ = -143.73), which is followed by DMAEE (-139.72 kJ/mol) and DMEE (-135.94 kJ/mol). Thereafter, TS2 will occur, and the catalyst will return the proton to the nitrogen forming urethane group, and in this step N-H* increases, while N-H** decreases. At this step, the relative enthalpy is the lowest in the presence of DMCHA ($\Delta_r H$ = -116.14 kJ/mol) compared to the other two studied catalysts. Before the reaction completes, a product complex (PC) is forming, where the urethane bond is complete, and thus, the distance between N-H** significantly decreased **(Figure 28, and Figures C1, C2(Appendix C))**. In the final step the catalysts and the product will be separated (P), with the corresponding relative energy of -94.84 kJ/mol.

Taking into account the fact, that the catalyst is first mixed into the alcohol and a complex will be formed between the alcohol and the catalyst (RC1), the measured activation energy will be the difference between TS1 and RC1 **(Figure 29)**. The calculated enthalpy differences are

22.2, 21.9, and 24.4 kJ/mol, for the DMCHA, DMEE, and DMAEE catalysed reactions, respectively. These are in an excellent agreement with the experimentally determined values which are 25.8 ± 1.0, 23.9 ± 1.3, and 25.2 ± 0.7 kJ/mol, for the DMCHA, DMEE, and DMAEE catalysed reactions, respectively[252]. The highest difference was only 3.6 kJ/mol in the case of DMCHA, while the lowest difference (1.9 kJ/mol and 1.1 kJ/mol) was experienced in the case of DMEE, and DMAEE, respectively, which further proves the validity of the proposed mechanism and verify the method selection as well.

The PhNCO – butan-1-ol reaction was also studied in the presence of three additional catalysts, *N*,*N*-dimethylpropane-2-amine (DMIPA), *N*,*N*,*N'*,*N'*-tetramethylpentane-1,5-diamine (TMPD), and *N*-[2-(dimethylamino)ethyl]-*N'*,*N'*-dimethylethane-1,2-diamine (DMAEDMED) **(Figures C3-C5 (Appendix C))**, to investigate whether modifications further than the gamma positions from the catalytic centre causes any significant change in the catalytic activity. DMCHA was compared to DMIPA, while DMAEE was compared to TMPD, and DMAEDMED. The results showed that the relative energy difference for TS1 is less than 3.5 kJ/mol for each catalyst pairs **(Table C2(Appendix C))**. Thus, the change in the structure does not affect significantly the activity of the catalysts.

### 3.5 Urethane formation in the presence of 2,2-dimorpholinodiethylether (DMDEE) and 1,4-dimethylpiperazine (DMP)[4]

The catalytic activity of 2,2-dimorpholinodiethylether (DMDEE) and 1,4-dimethylpiperazine (DMP), two cyclic amines were studied **(Figure 30)** using computational methods and verifying the data with kinetic measurements. Industrially, DMDEE is a strong foaming catalyst. It can be prolonged the storage period of N=C=O components due to the steric hindrance of amino groups. DMDEE is a specifically suitable catalyst for one-component polyurethane rigid foam sealant systems. It is also used for polyether and polyester polyurethane soft foam, semi-rigid foam, *etc*.[284]. While 1,4-dimethylpiperazine (DMP) is a liquid crystalline compound melting at 105 ˚C, dissoluble in water, alcohol, glycerol, and glycols. In case of DMP, the nitrogen containing ring plays an essential role in biological research and the drug manufacturing industry. Furthermore, it is an important cyclic component in the industrial field as raw materials for hardener of epoxy resins, accelerators for rubber, and urethane catalysts. DMP is used as a catalyst that speeds up polyurethane formation[285]. However, to

[4] The following subchapter is based on: Hadeer Q. Waleed. *et al. Computational and Theoretical Chemistry*, 2023, 1221, 114045, **https://doi.org/10.1016/j.comptc.2023.114045**

the best of our knowledge, the atomistic details of urethane synthesis in the presence of DMDEE have never been studied before, while the catalytic effect of DMP has never been compared before with experimental values. Thus, important insights are gained by this combined experimental and computational study into their catalytic activity.

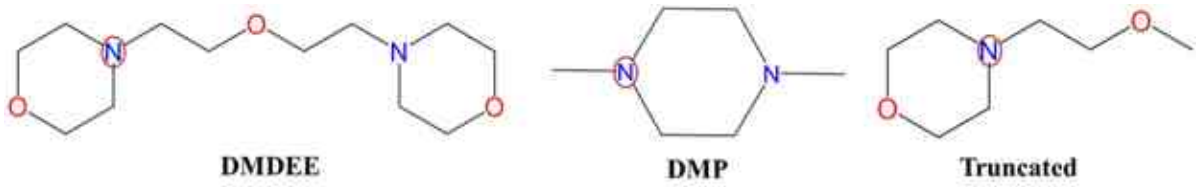


***Figure 30.*** *Chemical structures of the studied catalysts. 2,2-dimorpholinodiethylether (DMDEE), and 1,4-dimethylpiperazine (DMP). The catalytic nitrogen-containing groups which are considered in the calculations are highlighted with red circles.*

To describe the reactions from a mechanistic point of view, a recently proposed general urethane formation reaction mechanism without and with amine catalysts[250,252,253] was followed **(Figure 15, and Figure 16)**. The catalyst-free system has been studied computationally and used as a reference **(Figures 15, 23, and 24) (Table 11).**

***Table 11.*** *Relative enthalpy ($\Delta_r H$) of the reaction between phenyl isocyanate and butan-1-ol with and without catalysts, calculated using the G3MP2BHandHLYP composite method in acetonitrile, using the SMD implicit solvent model at 298.15 K and 1 atm. R—reactant, RC—reactant complex, TS—transition state, IM—intermediate, PC—product complex, and P—product.*

| | $\Delta_r H$ (kJ/mol) | | | | | | | |
|---|---|---|---|---|---|---|---|---|
| | **R** | **RC1** | **RC2** | **TS1** | **IM** | **TS2** | **PC** | **P** |
| **Catalyst-free system** | 0.0 | - | -8.97’ | 116.49 | - | - | - | -94.84 |
| ***DMDEE** | 0.0 | -27.27 | -54.65 | -5.03 | -133.12# | -109.29 | -135.34 | -94.84 |
| **DMP** | 0.0 | -26.43 | -35.81 | -2.79 | -135.69# | -109.27 | -129.23 | -94.84 |

’RC for catalyst-free reaction. *calculated using the qG3MP2BHandHLYP workflow. # Corrected relative enthalpy calculated according to ref.[251,263,264].

### 3.5.1 Proton Affinity (PA) of the Studied Catalysts

As the catalytic reaction mechanism include proton transfer steps, and one of the main factors which affect the activity of the catalysts is the proton affinity (PA) of the catalytic nitrogen, thus, PA of the catalytically active sites was also computed within the amine catalysts **(Figure 30, Table 12)**. As the nitrogen of DMP had lower proton affinity (984.84 kJ/mol), after protonation, it is more prone to donate the proton. Meanwhile, DMDEE is better proton acceptor, as it had higher proton affinity (1012.28 kJ/mol). These effected the relative energy

of the reaction steps (*e.g.,* IM, TS2) and by increasing proton affinity the corresponding relative energy is also increasing.

***Table 12.*** *Computed ($PA_{calc}$) of the amines of the studied catalysts, 2,2-dimorpholinodiethylether (DMDEE), and 1,4-dimethylpiperazine (DMP), in kJ/mol. The calculations were carried by using the G3MP2BHandHLYP composite method in the gas phase at 298.15 K and 1 atm.*

| Catalysts | $PA_{calc}$ (kJ/mol) |
|---|---|
| **DMDEE** | 1012.28 |
| **DMP** | 984.84 |

### 3.5.2 Structural Features of Urethane Formation in the Presence of the Studied Catalysts

In the presence of catalysts the urethane formation mechanism includes additional steps compared to the reaction without catalysts **(Figures 16, 31 and 32)**.

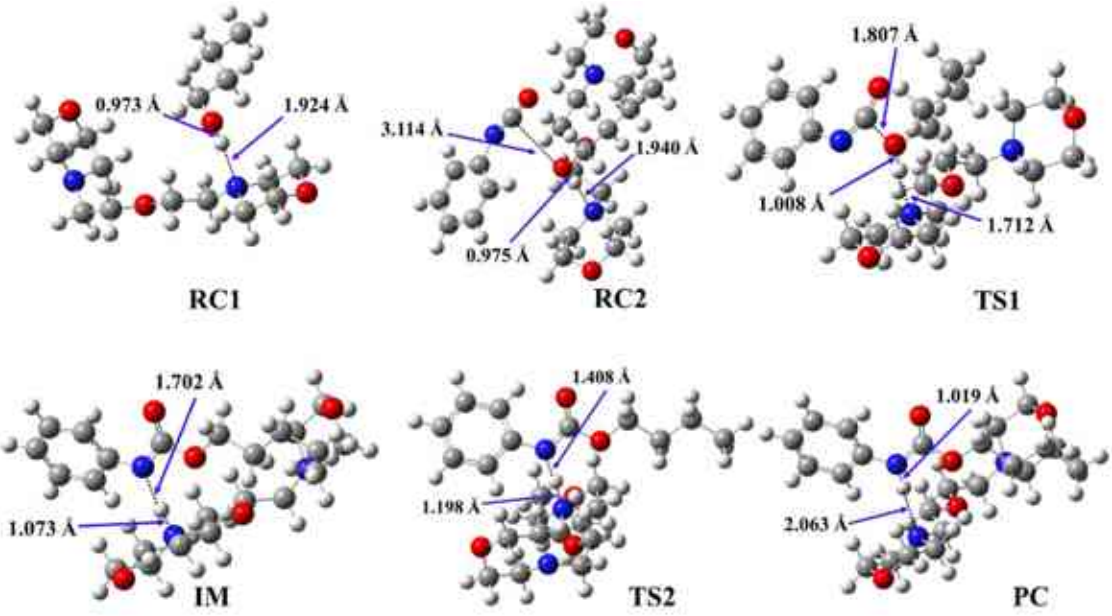


***Figure 31.*** *Optimised structures along the reaction pathway between phenyl isocyanate and butan-1-ol in the presence of 2,2-dimorpholinodiethylether (DMDEE) calculated at the BHandHLYP/6-31G(d) level of theory in acetonitrile. RC—reactant complex; TS—transition state; IM—intermediate; PC—product complex.*

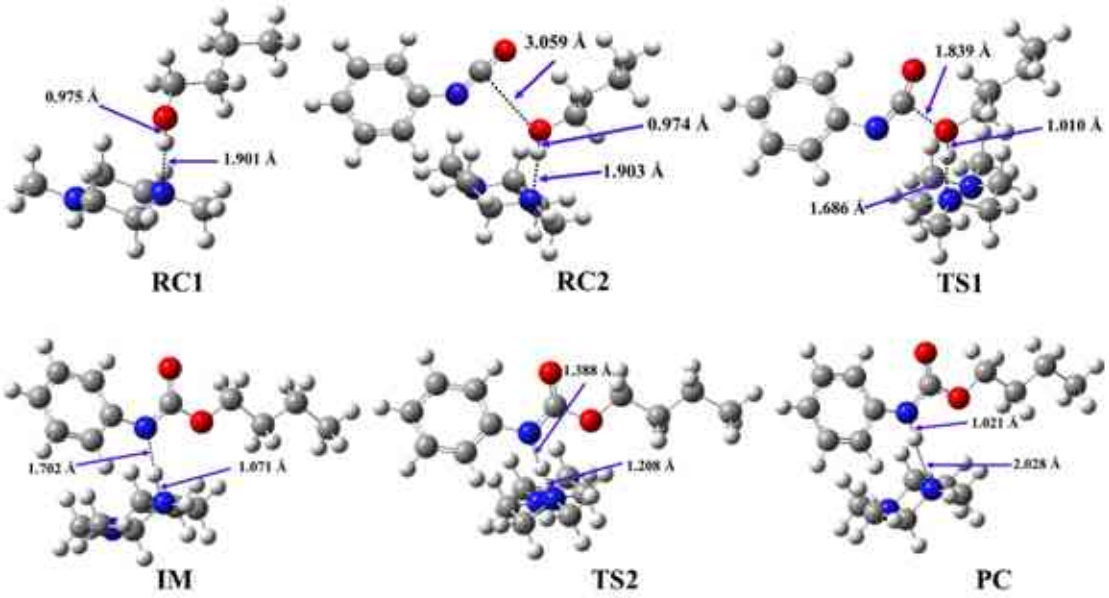


***Figure 32.*** *Optimised structures along the reaction pathway between phenyl isocyanate and butan-1-ol in the presence of 1,4-dimethylpiperazine (DMP) calculated at the BHandHLYP/6-31G(d) level of theory in acetonitrile. RC—reactant complex; TS—transition state; IM—intermediate; PC—product complex.*

First, the catalyst and alcohol are mixed during the industrial urethane synthesis, therefore, for modeling this experimental process, first the complex formation (RC1) between the catalyst and alcohol was computed **(Figures 31 and 32)**. It was found that the distance between the catalyst's nitrogen and the hydroxyl hydrogen of BuOH was in the range of 1.901 and 1.924 Å **(Table 13, N-H *)**. The next step is when the isocyanate is added to the system and a trimolecular complex (RC2) is formed, in this case, an interaction will occur between the carbon of the NCO group and the oxygen of the alcohol with the distance between them being in the range of 3.059–3.114 Å **(Table 13, C-O)** for the studied systems.

***Table 13.*** *N-H, O-H, and C-O bond lengths (Å) along the phenyl isocyanate (PhNCO) and butan-1-ol reaction pathway in the presence of the studied catalysts, 2,2-dimorpholinodiethylether (DMDEE), and 1,4-dimethylpiperazine (DMP) calculated at the BHandHLYP/6-31G(d) level of theory in acetonitrile at 298.15 K and 1 atm. N-H * for catalysts, while N-H ** for PhNCO.*

| Catalysts | RC1 | | RC2 | | TS1 | | | IM | | TS2 | | | PC | |
|---|---|---|---|---|---|---|---|---|---|---|---|---|---|---|
| | N-H * | O-H | N-H * | O-H | C-O | N-H * | O-H | C-O | N-H * | N-H ** | N-H * | N-H ** | N-H * | N-H ** |
| DMDEE | 1.924 | 0.973 | 1.940 | 0.975 | 3.114 | 1.712 | 1.008 | 1.807 | 1.073 | 1.702 | 1.198 | 1.408 | 2.063 | 1.019 |
| DMP | 1.901 | 0.975 | 1.903 | 0.974 | 3.059 | 1.686 | 1.010 | 1.839 | 1.071 | 1.702 | 1.208 | 1.388 | 2.028 | 1.021 |

After the trimolecular complex, a transition sate (TS1) will occur and through that a bond will form between the carbon of the NCO group and the oxygen of the alcohol group. Meanwhile, a proton is donated from the hydrogen of the OH group to the nitrogen of the

catalyst, and the corresponding distance between them is significantly reduced to the range of 1.686–1.712 Å. In the TS1 step, the lowest relative enthalpy was in the presence of DMDEE ($\Delta_r H$ = -5.03 kJ/mol) **(Figure 33, Table 11)**. TS1 is followed by an intermediate (IM) within which the distance between the hydrogen of the BuOH and the nitrogen of the catalyst was significantly reduced to the range of 1.071–1.073 Å. This leads to the next step where the second transition state (TS2) will form, within which the proton is donated back from the nitrogen of the catalyst to the nitrogen of the NCO group, with a corresponding distance in the range of 1.388–1.408 Å **(Table 13, N-H **)**. In the penultimate step of the catalytic mechanism, the product complex (PC) will form which will include a new bond between the nitrogen of the NCO group and hydrogen of the BuOH group with decreasing in the corresponding distance to the range of 1.019–1.021 Å **(Table 13, Figures 31 and 32)**. In the final stage of the catalytic mechanism the catalyst will separate from the product, which has a relative enthalpy of -94.84 kJ/mol **(Table 11 and Figure 33)**. All in all, it was found that in the presence of catalysts a multi-step pathway is feasible to reach the product. The barrier height of the reaction significantly decreased (>118 kJ/mol) in the presence of catalysts compared to the catalyst-free reaction. The relative enthalpy difference for TS1 was 121.5 kJ/mol in the presence of DMDEE, while in the case of DMP it was 119.3 kJ/mol compared to the catalyst-free reaction, respectively.

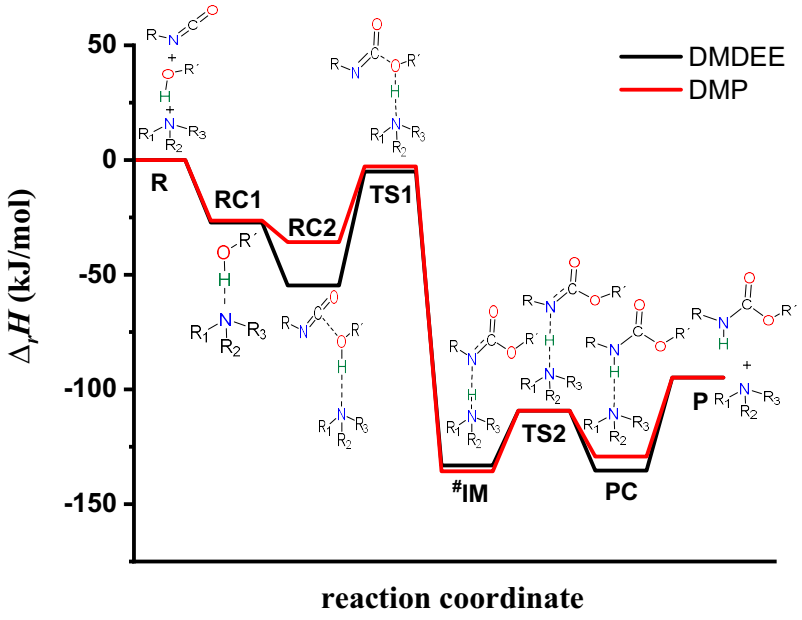


***Figure 33.*** *Energy profiles (relative enthalpy ($\Delta_r H$)) of the catalyzed urethane formation reactions calculated with the G3MP2BHandHLYP composite method in acetonitrile, using the SMD implicit solvent model at 298.15 K and 1 atm. #Corrected relative enthalpy of IM calculated according to ref.*[251,263,264].

In the experimental protocol, first the catalyst is mixed with the alcohol, where a complex will be formed between them (RC1), and thus, the measured activation energy will be the energy difference between TS1 and RC1 **(Figure 33)**. Thus, the corresponding relative enthalpy are 22.2 and 23.6 kJ/mol, for DMDEE and DMP, respectively **(Table 11, Figure 33)**. The differences compared to experimentally determined activation energy values are 11.2 kJ/mol in the case of DMDEE, and only 5.3 kJ/mol for the DMP catalyst[249]. These are not excellent, but still acceptable differences and can be used to further verify the validity of the suggested mechanism.

### 3.6 Urethane formation in the presence of morpholine, and 4-methylmorpholine[5]

The further understanding of the catalytic process is inevitable to achieve more environmentally friendly processes and thus, in this research, the reaction between PhNCO and BuOH is studied in the presence of two different cyclic amine catalysts **(Figure 34)**. These two cataysts, morpholine, and 4-methylmorpholine are synthetic organic liquids used mainly as an intermediate in the production of rubber chemicals, corrosion inhibitors, waxes and polishes, and optical brighteners. Due to their advantageous physicochemical, biological, and metabolic properties, as well as facile synthetic routes. The morpholine ring is a versatile and readily accessible synthetic building block, it is easily introduced as an amine reagent or can be built according to a variety of available synthetic methodologies[286].

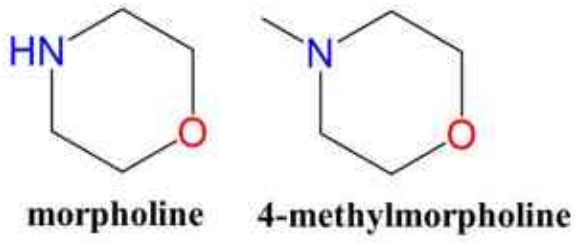


***Figure 34.*** *Chemical structures of the studied catalysts.*

The formation of the urethane linkage has been studied by using the butan-1-ol and phenyl isocyanate as reference models **(Figure 15)**. The catalyst-free system was investigated along with the catalytic process, the geometries were optimized, and the corresponding thermodynamic properties were calculated, and based on these the reactions were characterized **(Figures 23, and 24) (Table 14)**.

[5] The following subchapter is based on: Hadeer Q. Waleed. *et al*. *Sci Rep, 2023, 13, 17950,* https://doi.org/10.1038/s41598-023-44492-x

***Table 14.*** *Relative enthalpy ($\Delta_r H$) of the reaction between phenyl isocyanate and butan-1-ol with and without catalysts, calculated using the G3MP2BHandHLYP composite method in acetonitrile, using the SMD implicit solvent model at 298.15 K and 1 atm. R—reactant, RC—reactant complex, TS—transition state, IM—intermediate, PC—product complex, and P—product.*

| | $\Delta_r H$ (kJ/mol) | | | | | | | |
|---|---|---|---|---|---|---|---|---|
| | **R** | **RC1** | **RC2** | **TS1** | **IM** | **TS2** | **PC** | **P** |
| **Catalyst-free system** | 0.00 | - | -8.97' | 116.49 | - | - | - | -94.84 |
| **morpholine** | 0.00 | -22.95 | -31.41 | 5.31 | -125.44[#] | -97.44 | -120.47 | -94.84 |
| **4-methylmorpholine** | 0.00 | -25.21 | -34.89 | -0.58 | -132.26[#] | -105.96 | -127.37 | -94.84 |

'RC for catalyst-free reaction. # Corrected relative enthalpy calculated according to ref.[251,263,264].

### 3.6.1 Proton Affinity (PA) of the Studied Catalysts

Proton affinities (PAs) for the active nitrogens of the catalysts are also calculated **(Figure 34, Table 15)**. It was found that morpholine is better proton acceptor, as it had higher proton affinity (1523.95 kJ/mol). While, 4-methylmorpholine has a lower proton affinity (963.07 kJ/mol), after protonation, it is more prone to donate the proton.

***Table 15.*** *Computed ($PA_{calc}$) of the amines of the studied catalysts, morpholine, and 4-methylmorpholine, in kJ/mol. The calculations were carried by using the G3MP2BHandHLYP composite method in the gas phase at 298.15 K and 1 atm.*

| **Catalysts** | **$PA_{calc}$ (kJ/mol)** |
|---|---|
| **morpholine** | 1523.95 |
| **4-methylmorpholine** | 963.07 |

### 3.6.2 Structural Features of Urethane Formation in the Presence of the Studied Catalysts

Several additional steps will occur in the case of the mechanism of the phenyl isocyanate – butan-1-ol reaction in the presence of amine catalysts compared to the catalyst-free pathway **(Figure 16)** which was proposed before[253]. In this case, the first step will be the formation of the bimolecular reactant complex (RC1), and then a trimolecular complex will emerge (RC2). The hydrogen bond between BuOH and the catalytic amine is formed, and the corresponding N-H* distance is 1.889 Å in case of morpholine and a bit elongated to 1.906 Å when 4-methylmorpholine is considered **(Table 16, Figure 35)**.

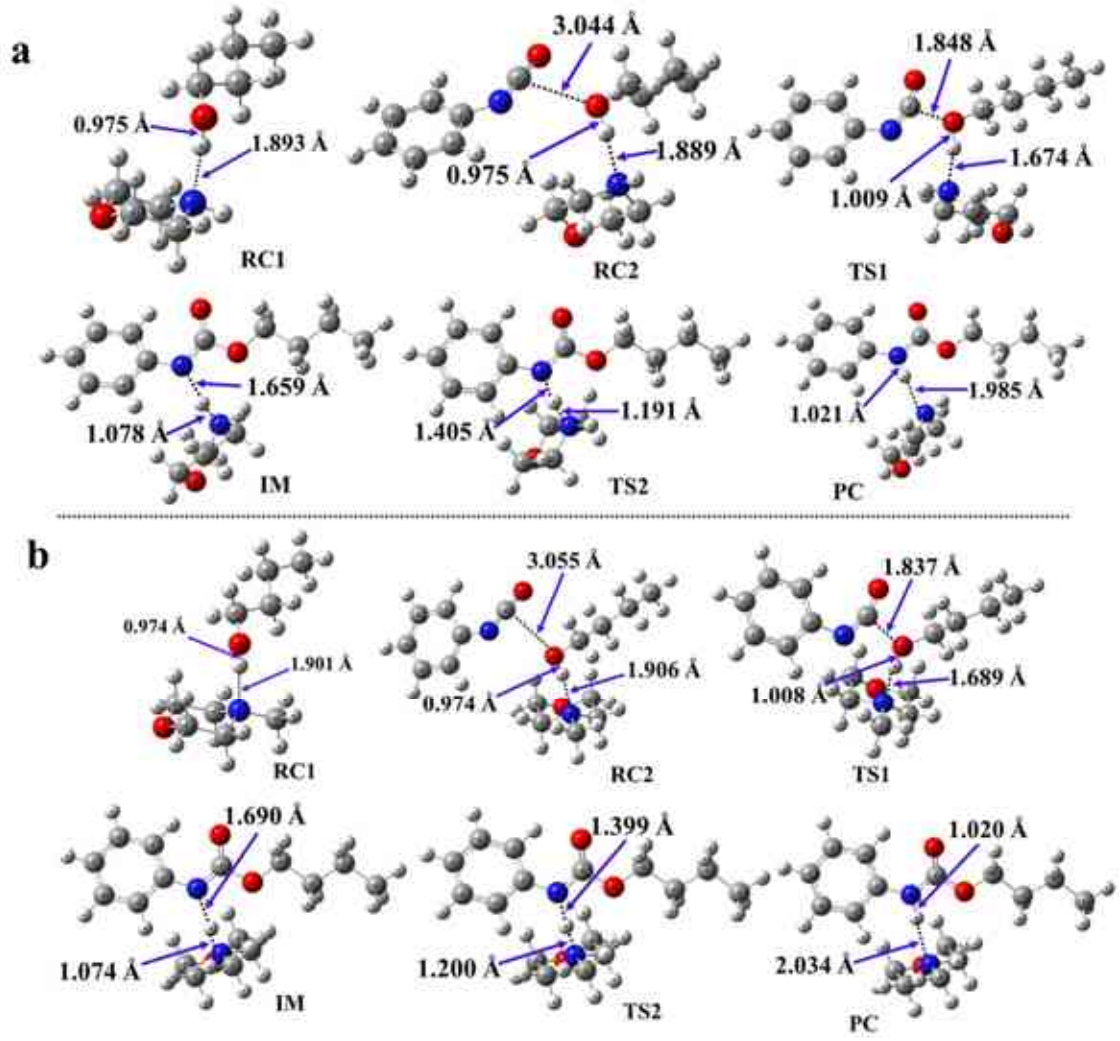


***Figure 35****. Optimised structures along the reaction pathway between phenyl isocyanate and butan-1-ol in the presence of catalysts: a) morpholine, and b) 4-methylmorpholine calculated at the BHandHLYP/6-31G(d) level of theory in acetonitrile. RC—reactant complex; TS—transition state; IM—intermediate; PC—product complex.*

***Table 16.*** *N-H, O-H, and C-O bond lengths (Å) along the phenyl isocyanate (PhNCO) and butan-1-ol reaction pathway in the presence of the studied catalysts, morpholine, and 4-methylmorpholine calculated at the BHandHLYP/6-31G(d) level of theory in acetonitrile at 298.15 K and 1 atm. N-H * for catalysts, while N-H ** for PhNCO.*

| Catalysts | RC1 | | RC2 | | | TS1 | | | IM | | TS2 | | PC | |
|---|---|---|---|---|---|---|---|---|---|---|---|---|---|---|
| | N-H * | O-H | N-H * | O-H | C-O | N-H * | O-H | C-O | N-H * | N-H ** | N-H * | N-H ** | N-H * | N-H ** |
| morpholine | 1.893 | 0.975 | 1.889 | 0.975 | 3.044 | 1.674 | 1.009 | 1.848 | 1.078 | 1.659 | 1.191 | 1.405 | 1.985 | 1.021 |
| 4-methylmorpholine | 1.901 | 0.974 | 1.906 | 0.974 | 3.055 | 1.689 | 1.008 | 1.837 | 1.074 | 1.690 | 1.200 | 1.399 | 2.034 | 1.020 |

To verify the proposed mechanism and the potential formation of the reactant complexes or intermediates, an extensive search for crystal structures in the Cambridge Structural Database (CSD)[287] was carried out. Crystal structures including morpholine and 4-methylmorpholine complexed with hydroquinone **(Figure 36 ″a″)** were found[288]. It can be seen that the

interaction (-OH---N-, hydrogen bond) between morpholine and the corresponding hydroxyl group in the crystal structure and in the case of the optimized reactant complex (RC1) is very similar to each other and the difference between the length of the hydrogen bonds is only 0.048 Å, while in the case of 4-methylmorpholine it is even smaller 0.031 Å. These promising similarities between the crystal structures and the computed reaction complexes further support the previously proposed complex 7-step mechanism.

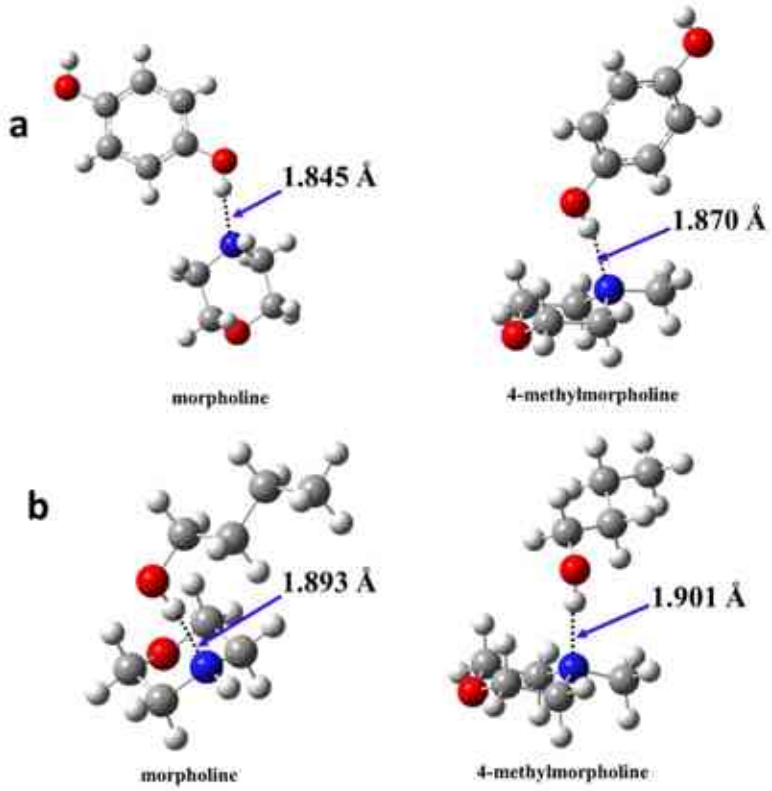


***Figure 36.*** *Comparison of morpholine and 4-methylmorpholine complexes: a - crystal structures*[288]*; b - optimized structures.*

Another interaction was established between the carbon of isocyanate and hydroxyl oxygen of BuOH. The corresponding C-O distance is 3.044 Å and 3.055 Å in case of morpholine and 4-methylmorpholine, respectively **(Figure 35)**. After the reactant complex formation, proton transfer occurs in TS1 from the hydroxyl group to the nitrogen of both morpholine and 4-methylmorpholine, and thus, the corresponding N-H* distances reduced to 1.674 Å and 1.689 Å, respectively **(Figure 35)**.

The relative enthalpy of TS1 is the lowest -0.58 kJ/mol when 4-methylmorpholine is considered, while in case of morpholine a increase of ~5 kJ/mol is experienced **(Figure 37)**. However, in both cases the relative enthalpy of the transition state significantly reduced compared to catalyst-free process.

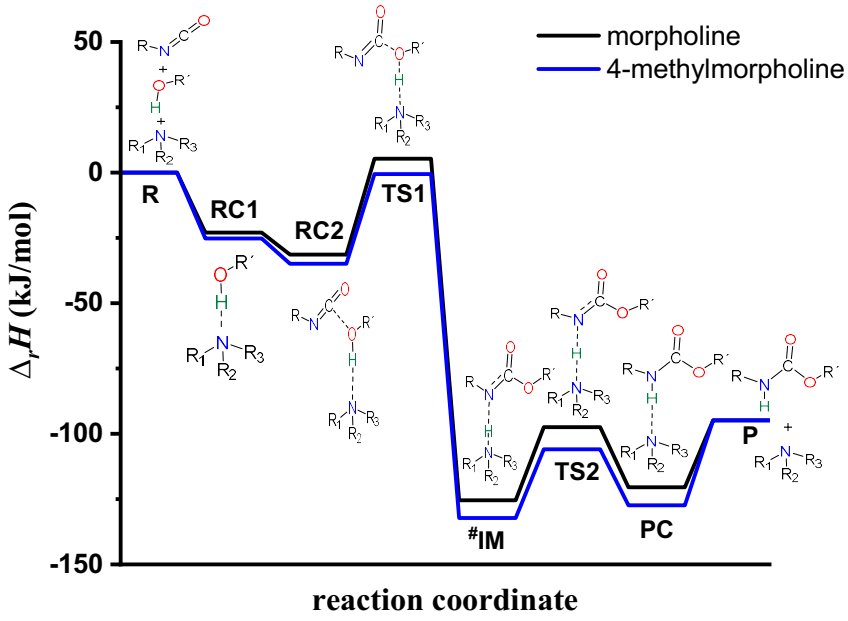


***Figure 37.*** *Relative enthalpy ($\Delta_r H$) profile of the studied catalysed urethane formation reactions in the presence of morpholine, and 4-methylmorpholine calculated at the G3PMP2BHandHLYP level of theory in acetonitrile using the SMD implicit solvent model, respectively. # Corrected relative enthalpy of IM calculated according to ref.* [263,264]

The catalysts are mixed first with the polyol in the experimental preparation steps and thus, RC1 is formed. Thereafter, the trimolecular complex is evolved by adding the isocyanate and the reaction proceeds. Therefore, to compute the barrier height for the first reaction step, the relative energy between TS1 and RC1 has to be computed. In the presence of morpholine and 4-methylmorpholine **(Table 14)**. In previous studies, kinetic experiments of urethane formation were carried out[249,250,252]. The results showed that in the case of cyclic catalysts the activation energy ($E_a$) cover a wider range between 24.8-25.8 kJ/mol, while in the case of linear catalysts it is around 23.9-25.2 kJ/mol. In the current work, the studied catalysts are cyclic structures and the calculated activation energies are 24.6 and 28.2 kJ/mol, for 4-methylmorpholine, and morpholine respectively, which is in good agreement with previous experimental data for similar catalysts. This indicates that morpholine is a bit less effective to prepare urethane compared to its methylated counterpart. A zwitterionic intermediate structure (IM) will form after TS1 within which a new bond will develop between the isocyanate's carbon and butan-1-ol. The corresponding relative enthalpy of the IMs are -87.34 and -94.16 kJ/mol, for the morpholine and 4-methylmorpholine catalyzed reaction, respectively **(Table 14)**.

The second transition state (TS2) will form where the proton transfer from the catalyst to the product occurs. In TS2, the distance between N-H** decreased, while the distance between N-H* increased compared to IM **(Table 16, Figure 35)**, and the relative enthalpy are differed

by ~10 kJ/mol in case of morpholine and 4-methylmorpholine. The TS2 structures including morpholine and 4-methylmorpholine have a relative energy of -97.44 kJ/mol and -105.96 kJ/mol, respectively.

It seems that IM is higher in enthalpy than TS2, $\Delta\Delta_r H_{[TS2\text{-}IM]}$=-10.10 kJ/mol and -11.79 kJ/mol in case of morpholine and 4-methylmorpholine, respectively **(Table 14)**, which needs to be explained. The most straightforward explanation is the solvent effect, which is caused by the zwitterionic nature of the intermediate. Despite numerous attempts, IM was not located in the gas phase, which is also related to its zwitterionic nature. Furthermore, calculations were also carried out in different solvents and it was found that by changing solvent the relative enthalpy of TS2 and IM is also changing **(Table 17**) similarly in the literature[289], but the IM remained higher than the corresponding transition state. Thus, the applied method is not suitable to handle the solvent effect precisely in case of the zwitterionic intermediate. Therefore, a correction was applied which was previously successfully used in the literature to handle a system within which zwitterionic structure is formed in case of an amino acid[264]. To balance the effect of the formation of the zwitterionic IM, -38.1 kJ/mol[263] was added to the relative enthalpy which shifted the uncorrected relative enthalpy ($\Delta\Delta_r H_{[TS2\text{-}IM]}$) between TS2 and IM from -10.10 kJ/mol and -11.79 to 28 and 26.31 kJ/mol in case of the morpholine and 4-methylmorpholine catalysed process, respectively. By applying the correction, the IM became lower in energy than TS2, and thus, the previous irregularity in the energy profile has been handled.

***Table 17.*** *Relative enthalpy ($\Delta\Delta_r H_{[TS2\text{-}IM]}$) for intermediate (IM) and TS2 in various media.*

| Medium | Dielectric constant (ε) | $\Delta\Delta_r H$ (kJ/mol) | |
|---|---|---|---|
| | | morpholine | 4-methylmorpholine |
| **Water** | 80 | -7.66 | -7.45 |
| **Acetonitrile** | 37.5 | -8.92 | -8.80 |
| **Tetrahydrofuran** | 7.58 | -6.56 | -8.78 |

The formation of the product complex (PC) is the penultimate step of the reaction, it is a bimolecular compound of the catalyst and product **(Figure 35)**. In the last step, the catalyst is separated from the product. The reaction is significantly changed in the presence of catalysts compared to the case of catalyst-free system **(Table 14)**. The product forms in multiple steps and the relative enthalpy is significantly reduced in case of the organocatalytic reaction. The

proton affinity of the catalytic site affects the relative enthalpy of the reaction steps (*e.g.*, TS1, IM, TS2) and by increasing proton affinity the corresponding relative enthalpy is also increasing and thus, the lower proton affinitiy can be associated with better catalytic effect. Considering the studied catalysts, 4-methylmorpholine is more effective to promote urethane formation than morpholine.

### 3.7 Stoichiometric reaction and catalytic effect of 2-dimethylaminoethanol in urethane formation[6]

Some of the studied catalysts contain reactive functional groups (e.g. OH) that can act as stoichiometric reactants with isocyanate and form urethane bonds. One of such structures are 2-dimethylaminoethanol (DMEA) which has a reactive functional group (OH). In the case of DMEA two different processes were considered and studied: catalytic and stoichiometric scenarios. Therefore, the computational study of urethane formation in the presence of 2-dimethylaminoethanol (DMEA) which has a reactive functional group is carried out (**Figure 38**).


***Figure 38.*** *Chemical structures of the studied 2-dimethylaminoethanol (DMEA) catalysts.*

#### 3.7.1 Urethane formation involving 2-dimethylaminoethanol (DMEA) as a catalyst

First, DMEA is considered as a catalyst for the model reaction between phenyl isocyanate (PhNCO) and butan-1-ol (BuOH). Previously the proposed reaction mechanism was considered. In this catalytic reaction **(Figure 16)**, a reaction complex (RC1) between the alcohol and the catalyst is formed first. This step was computed to model the experimental process, where a premix of a polyol and the catalyst is usually prepared beforehand. In the next step, the isocyanate is added to the system and trimolecular reaction complex is formed (RC2). This will lead to the formation of the first transition state structure (TS1) where the N=C=O group is being bent, activating the carbon of the isocyanate group for the formation of a new bond with the oxygen belonging to the hydroxyl

[6] The following subchapter is based on: Hadeer Q. Waleed. *et al*. *Phys. Chem. Chem. Phys.,* 2024, 26, 7103-7108, **https://doi.org/10.1039/D3CP05800J.**

group (C–O bond) with a distance of 1.829 Å (**Table 18**). At the same time a proton transfer occurs from the hydroxyl group of the alcohol to the nitrogen of the catalyst where the N-H* bond length decreased to 1.713 Å (**Table 18, and Figure 39**).

***Table 18.*** *O-H, C-O, and d N-H bond lengths (Å) along the butan-1-ol and phenyl isocyanate (PhNCO) reaction pathway in the case of 2-dimethylaminoethanol (DMEA) (catalytic system), calculated at the BHandHLYP/6-31G(d) theory level at (298.15 K and 1 atm) in acetonitrile. N-$H^{I}$ for DMEA, while N-$H^{II}$ for PhNCO.*

| | **O-H** | **C-O** | **N-$H^{I}$** | **N-$H^{II}$** |
|---|---|---|---|---|
| **RC1** | 0.975 | - | 1.883 | - |
| **RC2** | 0.977 | 3.232 | 1.871 | - |
| **TS1** | 1.007 | 1.829 | 1.713 | - |
| **IM** | - | 1.367 | 1.077 | 1.669 |
| **TS2** | - | 1.359 | 1.202 | 1.393 |
| **PC** | - | 1.336 | 2.014 | 1.022 |
| **P** | - | 1.333 | - | 1.004 |

Thus, an intermediate structure (IM) is reached. Thereafter, the proton is donated back from the nitrogen of the catalyst to the nitrogen of the isocyanate group through a transition state (**TS2**) while the corresponding distance N-H** is 1.393 Å. Thus, the urethane bond is complete, and a product complex (PC) is formed. The N-H* increased to 2.014 Å while the N-H** bond length decreased to 1.022 Å. At this point the final product (P) is formed by the separation from DMEA, and N-H** bond length further decrease to 1.004 Å (**Table 18, Figure 39**).

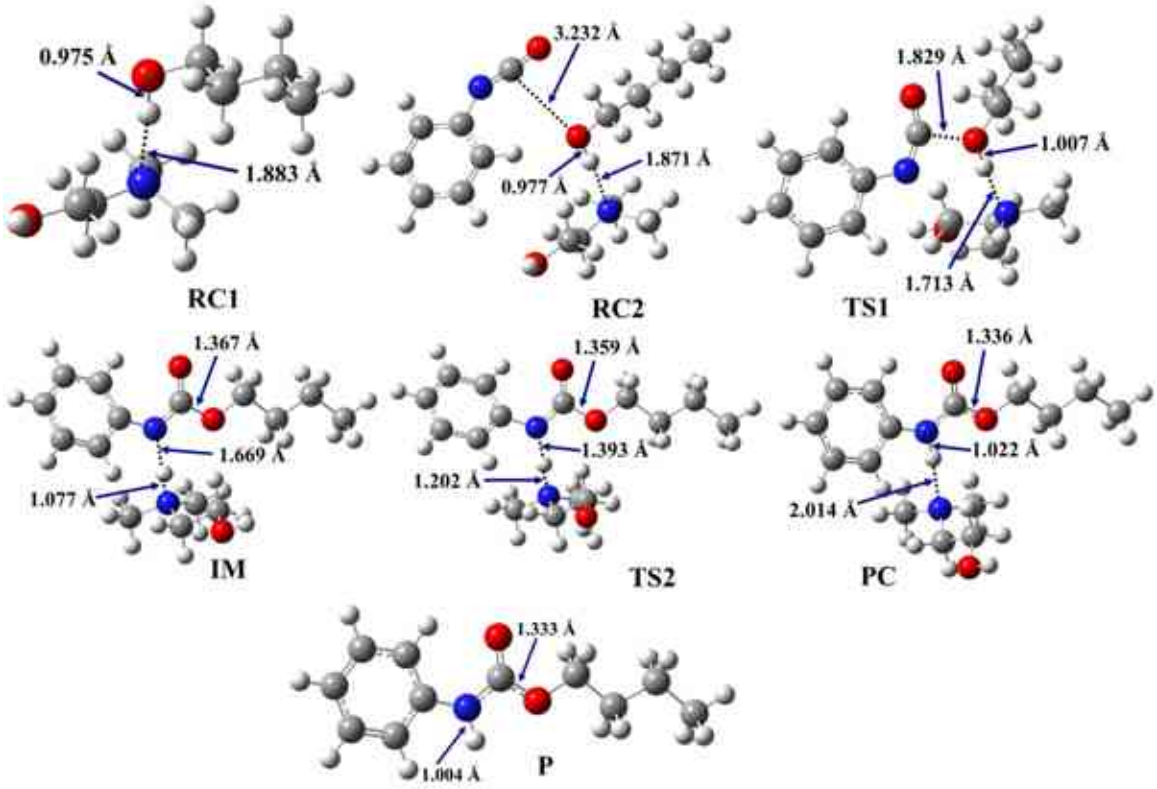


***Figure 39.*** *Optimised structures along the reaction pathway between phenyl isocyanate and butan-1-ol in the presence of 2-dimethylaminoethanol (DMEA) calculated at the BHandHLYP/6-31G(d) level of theory in acetonitrile. RC—reactant complex, TS—transition state, IM—intermediate, and PC—product complex.*

### 3.7.2 Urethane formation involving 2-dimethylaminoethanol (DMEA) as a reactant

New reaction mechanism was proposed for the stoichiometric reaction between DMEA and phenyl isocyanate (**Figure 40**).

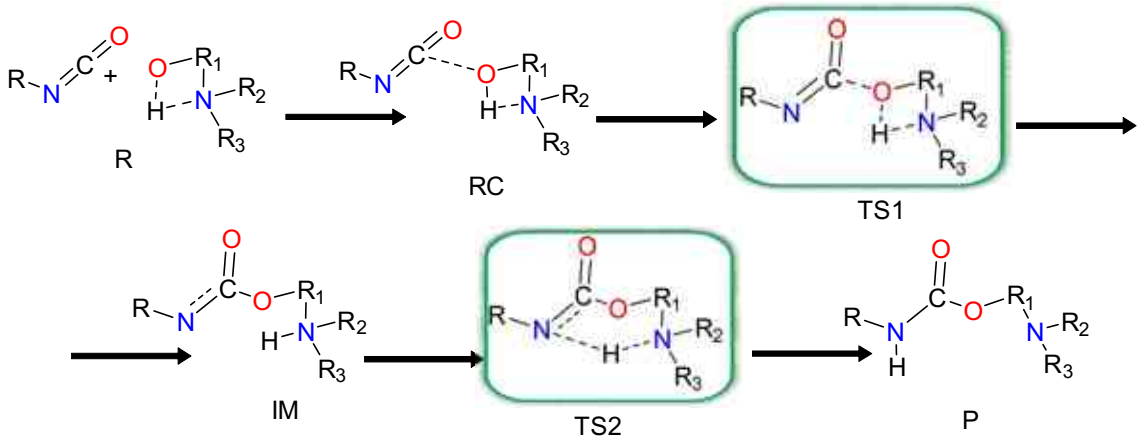


***Figure 40.*** *Schematic representation of the reaction mechanism of 2-dimethylaminoethanol (DMEA) - isocyanate autocatalytic process. R—reactant, RC—reactant complex, TS—transition state, IM—intermediate, and PC—product complex.*

The mechanism starts with the formation of a reaction complex (RC) with isocyanate. Leading to the first transition state (TS1) where the N=C=O group is activated and a new C–O bond is forming with a distance of 1.529 Å (**Table 19, Figure 41**).

***Table 19.*** *O-H, C-O, and d N-H bond lengths (Å) along the butan-1-ol and phenyl isocyanate (PhNCO) reaction pathway in the case of 2-dimethylaminoethanol (DMEA) (stoichiometric reaction), calculated at the BHandHLYP/6-31G(d) theory level at (298.15 K and 1 atm) in acetonitrile. N-H$^{I}$ for DMEA, while N-H$^{II}$ for PhNCO.*

| | | O-H | C-O | N-H$^{I}$ | N-H$^{II}$ |
|---|---|---|---|---|---|
| | RC | 0.962 | 3.118 | 2.308 | 2.455 |
| | TS1 | 1.065 | 1.529 | 1.539 | 2.392 |
| **DMEA** | IM | 2.304 | 1.402 | 1.051 | 1.798 |
| | TS2 | 2.329 | 1.387 | 1.206 | 1.374 |
| | P | - | 1.333 | - | 1.004 |

Meanwhile, the proton will be donated from the hydroxyl group of the DMEA to the nitrogen of the same molecule (N-H*) with the distance of 1.539 Å. After this step, the intermediate structure (IM) is formed where the created C-O bond has a distance of 1.402 Å and the distance between N-H* is only 1.051 Å **(Table 19, Figure 41)**.

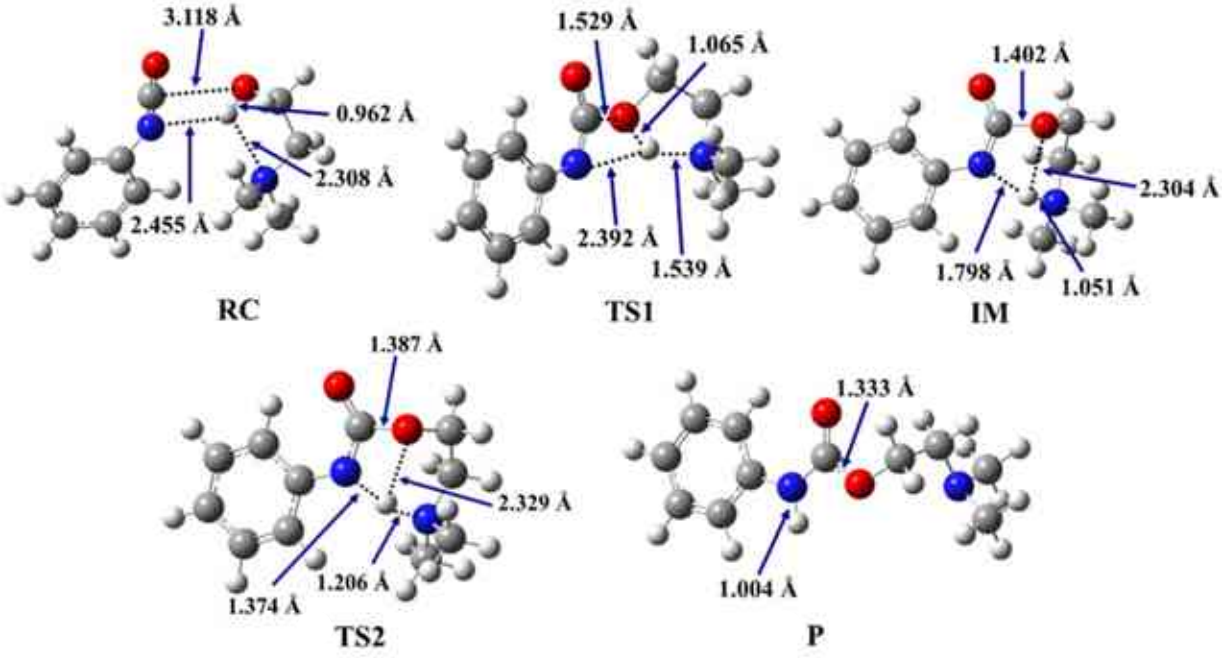


***Figure 41.*** *Optimised structures along the reaction pathway between phenyl isocyanate and 2-dimethylaminoethanol (DMEA) (stoichiometric reaction) calculated at the BHandHLYP/6-31G(d) level of theory in acetonitrile. RC—reactant complex, TS—transition state, IM—intermediate, and PC—product complex.*

This step will lead to the second transition state (TS2) where the proton is donated from the nitrogen of DMEA to the nitrogen of the isocyanate group with a distance of N-H** 1.374 Å **(Table 19, Figure 41)** and where the distance of N-H* is increased to 1.206 Å. That will lead to the final step where the product (P) is formed with N-H** equal to 1.004 Å.

### 3.7.3 Energetics of urethane formation in the presence of DMEA

The thermodynamic properties of the stoichiometric reaction and catalyzed phenyl isocyanate–butanol urethane formation with DMEA involvement have been computed **(Table 20, and Tables E1,E2(Appandix E))** and the corresponding energy profiles have been drawn **(Figure 42)**.

***Table 20.*** *Relative enthalpy ($\Delta_r H$) of the reaction between phenyl isocyanate (PhNCO) and butan-1-ol in the presence 2-dimethylaminoethanol (DMEA) (catalytic system), and DMEA with PhNCO (stoichiometric), calculated at the G3MP2BHandHLYP theory level at (298.15 K and 1 atm) in acetonitrile using the SMD implicit solvent model. R—reactant, RC—reactant complex, TS—transition state, IM—intermediate, PC—product complex, and P—product.*

| | $\Delta_r H$ (kJ/mol) | | | | | | | |
|---|---|---|---|---|---|---|---|---|
| | **R** | **RC1** | **RC2** | **TS1** | **IM** | **TS2** | **PC** | **P** |
| **Catalyst-free system** | 0.00 | - | -8.97’ | 116.49 | - | - | - | -94.84 |
| **Catalytic system** | 0.00 | -25.66 | -38.08 | -2.56 | -133.61[#] | -106.51 | -126.79 | -94.84 |
| **Stoichiometric system** | 0.00 | -22.19 | - | 38.63 | -89.29[#] | -57.27 | - | -95.23 |

’RC for catalyst-free reaction; # Corrected relative enthalpy calculated according to ref.[251,263,264].

The most stable molecular complex (RC1, $\Delta_r H$ = -25.66 kJ/mol) was formed in the case of the reaction within which DMEA is involved only as a catalyst. The lowest relative enthalpy of the transition state (TS1) was also experienced in case of the catalyzed isocyanate–butanol reaction ($\Delta_r H$ = -2.56 kJ/mol) and it was 41.2 kJ/mol lower compared to TS1 of the stoichiometric process ($\Delta_r H$ = 38.63 kJ/mol) **(Table 20, Figure 42)**.

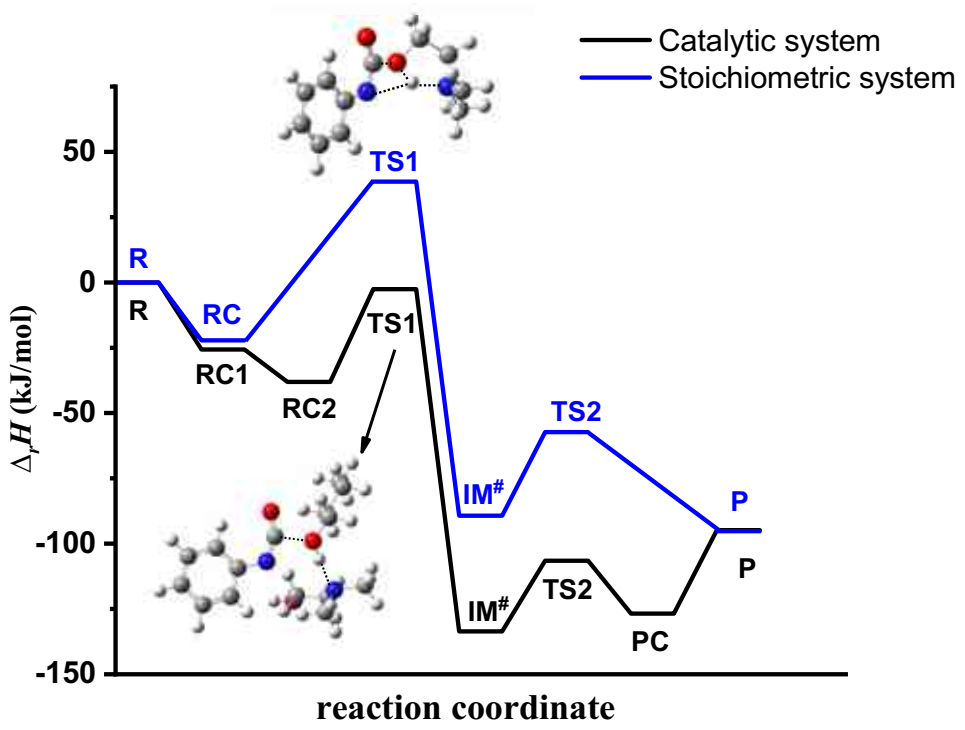


***Figure 42.*** *Relative enthalpy ($\Delta_r H$) profile of the studied catalysed urethane formation reactions in the presence 2-dimethylaminoethanol (DMEA). Phenyl isocyanate (PhNCO) and butan-1-ol (BuOH) (catalytic system, black line), or DMEA and PhNCO react (stoichiometric reaction, blue line). The energies were calculated at the G3PMP2BHandHLYP theory level at (298.15 K and 1 atm) in acetonitrile using the SMD implicit solvent model, respectively. #Corrected relative enthalpy of IM calculated according to Ref.* [251,263,264].

Otherwise, comparing the processes with the catalyst-free reaction of phenyl isocyanate-butanol, it was showed that the relative enthalpy in the case of the catalyst-free case was much higher ($\Delta_r H$(TS)= 116.49 kJ/mol)[249–252] compared to both catalytic and stoichiometric reactions **(Table 20)**. This indicate that the involvement of an amine in the reaction would lead to a more preferred process. To balance the effect of the formation of the zwitterionic IM, a correction (−38.1 kJ/mol) was employed and added to the relative enthalpy of the compound (IM) which led to a shift in the $\Delta_r H$ from -95.51 kJ/mol and -51.19 kJ/mol to -133.61 and -89.29 kJ/mol in both catalytic and stoichiometric processes, respectively. The relative enthalpy of the IM were the highest in the case of the stoichiometric system ($\Delta_r H$ = -89.29 kJ/mol), while this step was more preferred in the case of the catalyst system ($\Delta_r H$ = -133.61 kJ/mol). Meanwhile, in the TS2 step, the catalytic system had the lowest relative enthalpy ($\Delta_r H$ = -106.51 kJ/mol). In the case of the catalytic system, the reaction was completed by forming the product complex with a relative enthalpy of -126.79 kJ/mol. This step does not occur in the case of stoichiometric reaction. The final step for both reaction systems (catalytic and stoichiometric) will be the formation of the product, where the difference in the relative

enthalpy between the catalytic and stoichiometric reaction is 0.39 kJ/mol **(Table 20, Figure 42)**.

All in all, in the first process (catalytic system), DMEA acts as a catalyst when phenyl isocyanate and butan-1-ol will react, while in the second case, a stoichiometric reaction is considered when DMEA react with phenyl isocyanate. The rate determining step of the stoichiometric scenario is significantly higher compared to the catalytic reaction system. Therefore, 2-dimethylaminoethanol can be considered as a more effective catalyst than stoichiometric reactant. Furthermore, when the stoichiometric pathway occurs, after urethane bond formation between DMEA and isocyanate, the former will be prevented from free movement and thus, it will not be able to catalyze as many reactions as it could, and it will not be as effective. Therefore, more catalysts will be needed to achieve the same effect. On the other hand, the catalyst will not be released from the final product and thus, less risk is associated with it towards the end users.

### 3.8 Urethane formation in the presence of 4-[2-(dimethylamino)ethyl]morpholine, and *N,N*-dimethylbenzylamine.

The reaction between butan-1-ol (BuOH ) and phenyl isocyanate (PhNCO) is studied in the presence of two different amine catalysts 4-[2-(dimethylamino)ethyl]morpholine (DMAEM), and *N,N*-dimethylbenzylamine (DMBA)**(Figure 43)** using computational methods. The proposed mechanisms **(Figure 15 and 16)** has been used to understand the reactions from a mechanistic point of view. Furthermore, the comparison between two selected catalysts has been carried out where the DMAEM catalyst contains different aromatic and aliphatic nitrogen functional groups. While the DMBA catalyst contains just aliphatic nitrogen functional groups. The BuOH – PhNCO reaction has been used as a model to study urethane formation **(Figure 43)**.

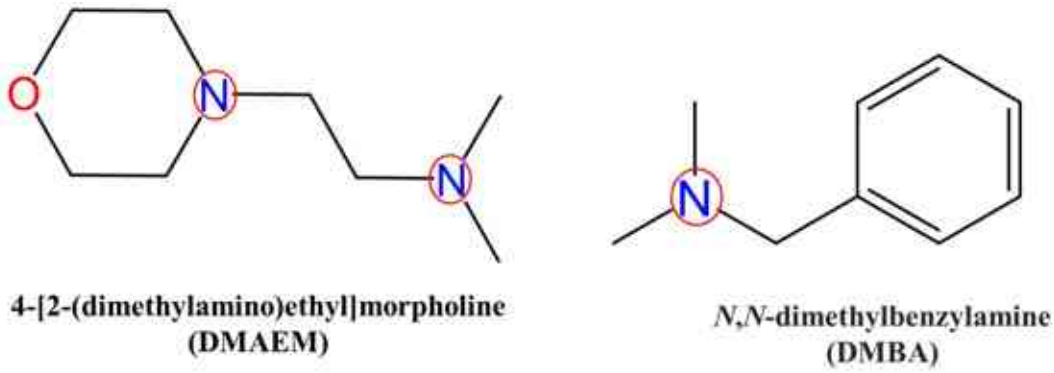


4-[2-(dimethylamino)ethyl]morpholine
(DMAEM)

*N,N*-dimethylbenzylamine
(DMBA)

***Figure 43.*** *Chemical structures of the studied 4-[2-(dimethylamino)ethyl]morpholine (DMAEM), and N,N-dimethylbenzylamine (DMBA) catalysts. The catalytic nitrogen-containing groups which are considered in the calculations are highlighted with red circles.*

### 3.8.1 Proton Affinity (PA) of the Studied Catalysts

A proton affinity (PA) was computed for all unique nitrogen that were considered catalytically active within the aromatic and aliphatic amine catalysts **(Ep. 1) (Figure 43, Table 21)**. The PAs of the catalytically active nitrogens were in a range of 968.10−987.37 kJ/mol. The difference between the calculated and data in the literature was 18.97 kJ/mol in the case of DMBA . As the nitrogen of DMAEM had the lowest proton affinity 968.10 kJ/mol), after protonation, it was the most prone to donating its proton. Meanwhile, DMBA was the best proton acceptor, as it had the highest proton affinity (987.37 kJ/mol).

***Table 21.*** *Computed ($PA_{calc}$) of the amines of the studied catalysts, 4-[2-(dimethylamino)ethyl]morpholine (DMAEM), and N,N-dimethylbenzylamine (DMBA), in kJ/mol. The calculations were carried by using the G3MP2BHandHLYP composite method in the gas phase at 298.15 K and 1 atm. 1N— aromatic nitrogen, 2N— aliphatic nitrogen.*

| Catalysts | $PA_{calc}$ (kJ/mol) | $PA_{exp}$ (kJ/mol)[282] |
|---|---|---|
| **DMAEM-1N** | 968.10 | - |
| **DMAEM-2N** | 972.59 | - |
| **DMBA** | 987.37 | 968.4 |

### 3.8.2 Structural Features of Urethane Formation in the Presence of the Studied Catalysts

The steps of the phenyl isocyanate – butan-1-ol reaction in the presence of the studied catalysts have been computed **(Figure 44, and Figures F1,F2(Appendix F))(Table 22)**. Additional structures (e.g., IM) have been formed compared to the catalyst-free pathway.

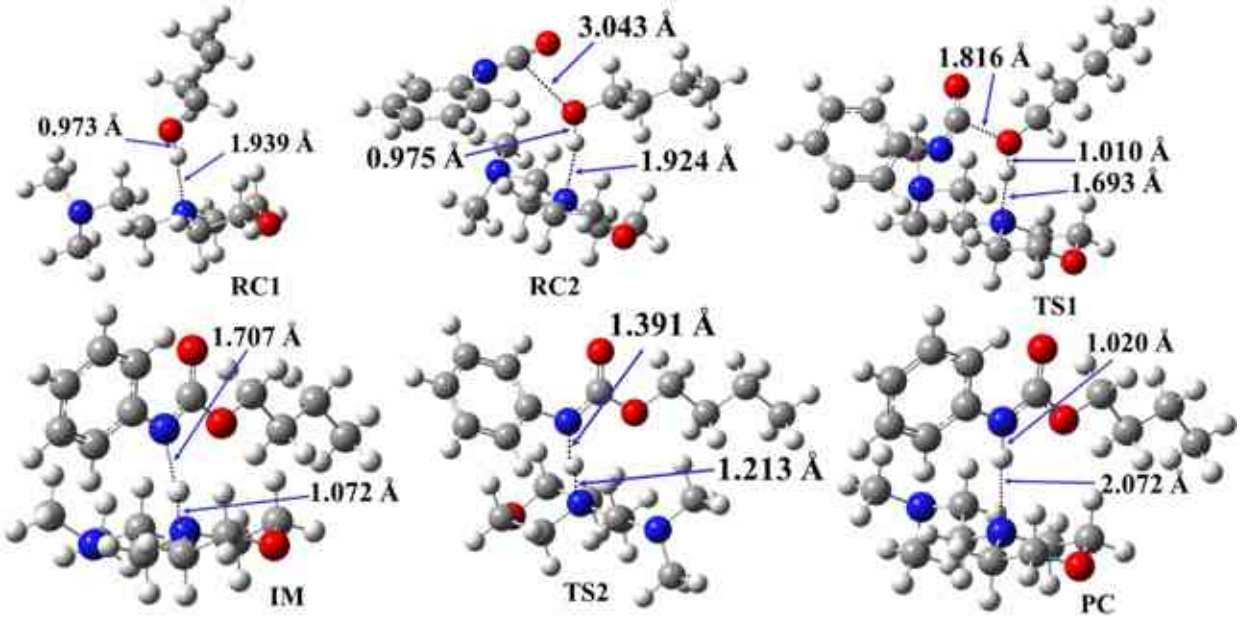


***Figure 44.*** *Optimised structures along the reaction pathway between phenyl isocyanate and butan-1-ol in the presence of 4-[2-(dimethylamino)ethyl]morpholine (DMAEM-1N) calculated at the BHandHLYP/6-31G(d) level of theory in acetonitrile. 1N—aromatic nitrogen, RC—reactant complex, TS—transition state, IM—intermediate, PC—product complex.*

In the first step, a reaction complex (RC1) between the butan-1-ol and the catalyst is formed first. The RC1 step was computed to model the experimental process, where catalysts are mixed first with the polyol. In the next step, the phenyl isocyanate is added to the system and a trimolecular reactant complex, RC2 was formed in this case. A hydrogen bond formed between the hydroxyl group of the butan-1-ol and the catalysts nitrogen and the corresponding N-H* distance is in the range of 1.853 Å-1.924 Å **(Figure 44, and Table 22)**. Another interaction was established between the isocyanate carbon and butan-1-ol hydroxyl oxygen. The C-O distance is in the range of 2.891 Å-3.051 Å.

***Table 22.*** *N-H, O-H, and C-O bond lengths (Å) along the phenyl isocyanate (PhNCO) and butan-1-ol reaction pathway in the presence of the studied catalysts, 4-[2-(dimethylamino)ethyl]morpholine (DMAEM), and N,N-dimethylbenzylamine (DMBA) calculated at the BHandHLYP/6-31G(d) level of theory in acetonitrile at 298.15 K and 1 atm. 1N— aromatic nitrogen, 2N— aliphatic nitrogen, N-H * for catalysts, while N-H ** for PhNCO.*

| Catalysts | RC1 | | RC2 | | | TS1 | | | IM | | TS2 | | PC | |
|---|---|---|---|---|---|---|---|---|---|---|---|---|---|---|
| | N-H * | O-H | N-H * | O-H | C-O | N-H * | O-H | C-O | N-H * | N-H ** | N-H * | N-H ** | N-H * | N-H ** |
| DMAEM-1N | 1.939 | 0.973 | 1.924 | 0.975 | 3.043 | 1.693 | 1.010 | 1.816 | 1.072 | 1.707 | 1.213 | 1.391 | 2.072 | 1.020 |
| DMAEM-2N | 1.881 | 0.976 | 1.869 | 0.978 | 2.891 | 1.690 | 1.011 | 1.826 | 1.075 | 1.666 | 1.207 | 1.382 | 2.020 | 1.021 |
| DMBA | 1.873 | 0.975 | 1.853 | 0.978 | 3.051 | 1.685 | 1.013 | 1.810 | 1.070 | 1.695 | 1.210 | 1.385 | 2.029 | 1.020 |

The reaction is going through two transition states and an intermediate. After the formation of the complex (RC), a proton transfer will occur in TS1 from the hydrogen of the hydroxyl group to the nitrogen of the catalyst and thus, the N-H* distance will be reduced compared to that of the reaction complex **(Table 22)**. Furthermore, a bond is forming between the butan-1-ol oxygen and the isocyanate's carbon. The relative enthalpy of the TS1 is lower ($\Delta_r H$ = –7.40 kJ/mol) when DMAEM-1N is considered, while in the case of DMAEM-2N, an increase of ~10 kJ/mol is experienced. Meanwhile, the DMBA catalyst has lower TS1 (-3.86 kJ/mol) than the DMAEM-2N **(Table 23)**.

***Table 23.*** *Relative enthalpy ($\Delta_r H$) of the reaction between phenyl isocyanate and butan-1-ol with and without catalysts, calculated using the G3MP2BHandHLYP composite method in acetonitrile, using the SMD implicit solvent model at 298.15 K and 1 atm. 1N— aromatic nitrogen, 2N— aliphatic nitrogen, R—reactant, RC—reactant complex, TS—transition state, IM—intermediate, PC—product complex,and P—product.*

| | $\Delta_r H$ (kJ/mol) | | | | | | | |
|---|---|---|---|---|---|---|---|---|
| | **R** | **RC1** | **RC2** | **TS1** | **IM** | **TS2** | **PC** | **P** |
| **Catalyst-free system** | 0.00 | - | -8.97' | 116.49 | - | - | - | -94.84 |
| **DMAEM-1N** | 0.00 | -27.56 | -52.41 | -7.40 | -137.58[#] | -106.34 | -129.85 | -94.84 |
| **DMAEM-2N** | 0.00 | -21.26 | -42.60 | 2.90 | -132.59[#] | -104.55 | -120.05 | -94.84 |
| **DMBA** | 0.00 | -23.62 | -37.43 | -3.86 | -140.21[#] | -113.21 | -132.99 | -94.84 |

'RC for catalyst-free reaction; # Corrected relative enthalpy calculated according to ref.[251,263,264].

Through TS1, an intermediate structure (IM) obtained within which a bond is formed between the isocyanate's carbon and the butan-1-ol's oxygen, while the protonated catalyst is hydrogen bonded to the nitrogen of the former isocyanate group **(Figure 44)**. To balance the effect of the formation of the zwitterionic IM, a correction (-38.1 kJ/mol) was employed and added to the relative enthalpy of the compound (IM) which led to a shift in the $\Delta_r H$ from -99.48 kJ/mol, -94.49 kJ/mol, and -102.11 kJ/mol to -137.58 kJ/mol, -132.59 kJ/mol, and -140.21 kJ/mol for DMAEM-1N, DMAEM-2N, and DMBA, respectively. The relative enthalpy of the IM were the highest in the case of the DMAEM-2N ($\Delta_r H$ = -132.59 kJ/mol), while this step was more preferred in the case of the DMBA ($\Delta_r H$ = -140.21 kJ/mol). The reaction was continued with TS2 within which the proton transferred from the catalyst to the isocyanate group. It can be seen that in TS2 the N-H** distance decreased compared to the IM **(Figure 44, and Table 22)**. The relative enthalpy of TS2 calculated in DMBA is -113.21 kJ/mol, which is lower than

in the case of DMAEM **(Table 23, Figure 45)**. The penultimate step in this reaction mechanism is the formation of the product complex (PC). It is a bimolecular complex of the final product **(Figure 45)**. The final step is the separation of the catalyst from the product.

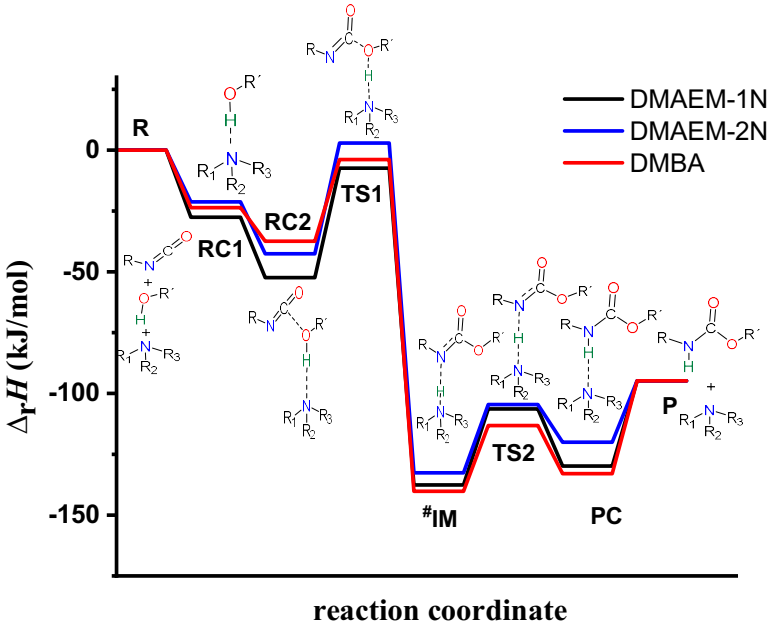


***Figure 45.*** *Relative enthalpy ($\Delta_r H$) profile of the studied catalysed urethane formation reactions in the presence 4-[2-(dimethylamino)ethyl]morpholine (DMAEM), and N,N-dimethylbenzylamine (DMBA) calculated at the G3PMP2BHandHLYP theory level at (298.15 K and 1 atm) in acetonitrile using the SMD implicit solvent model, respectively. 1N— aromatic nitrogen, 2N— aliphatic nitrogen. #Corrected relative enthalpy of IM calculated according to ref.* [251,263,264].

All in all, the presence of the catalyst changes significantly the reaction mechanism and the energetics of the reaction compared to the catalyst-free case, where the barrier height of the reaction significantly decreased (>123 kJ/mol) in the presence of catalysts **(Table 23)**. However, the aromatic amine catalyst has a slightly greater effect on the energetics of the catalytic reaction compared to the aliphatic amine catalysts **(Table 23, and Figure 45)**.

### 3.9 Urethane formation in the presence of acid catalysts

Besides the amine catalysts (organic bases), organic acids have also been shown to be an effective catalyst in urethane synthesis. However, there are not many studies used organic acids in urethane formation. Herein, the reaction between PhNCO and BuOH is studied in the presence of three different acid catalysts **(Figure 46)**. The computational tools have been used to understand the reactions from a mechanistic point of view. The reaction of butan-1-ol and phenyl isocyanate has been selected as reactants to describe the energetic and structural features of the urethane formation **(Figures 15, 23, and 24)**.

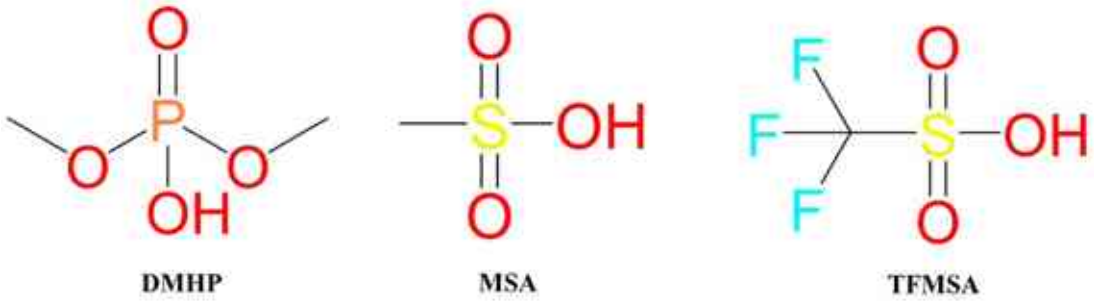


***Figure 46.*** *Chemical structures of the studied catalysts. dimethyl hydrogen phosphate (DMHP), methanesulfonic acid (MSA), and trifluoromethanesulfonic acid (TFMSA).*

### 3.9.1 Structural Features of Urethane Formation in the Presence of the Studied Catalysts

General mechanisms for urethane formation from isocyanate and alcohol in the presence of organic acid catalysts have been proposed (**Figure 47**).

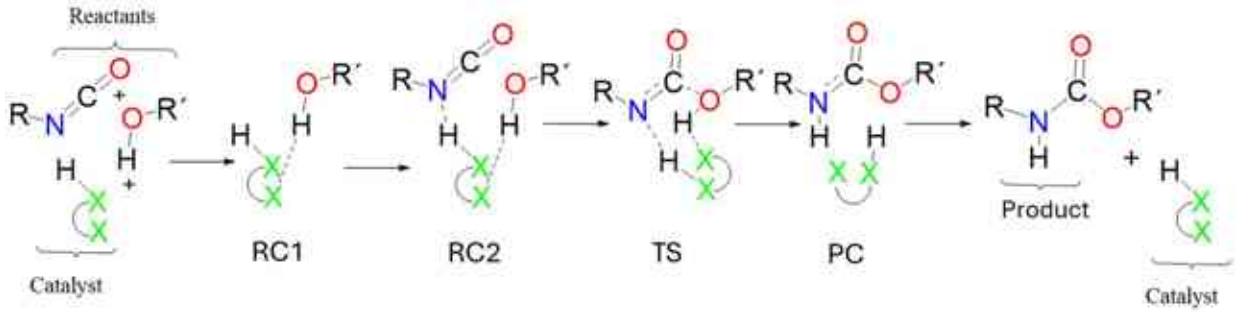


***Figure 47.*** *Schematic representation of the general organic acid-catalyzed urethane formation. RC—reactant complex, TS—transition state, and PC—product complex.*

First, a complex (RC1) between the alcohol and the catalyst is forming, while the distance between the catalyst's oxygen and the hydroxyl hydrogen of butan-1-ol is in the range of 1.830 and 2.048 Å **(Figure 48, and Figures G1,G2(Appendix G)) (Table 24, O-H*)**. This is supposed to mimic the industrial urethane synthesis, within which, first the catalyst is mixed into the polyol. Then, in the next step the isocyanate, PhNCO, is added to the system, and RC2, a trimolecular complex is formed. In this step, a new interaction occurs between the butanol's oxygen and the isocyanate group, while only insignificant changes can be identified in the length of the previously established O-H*.

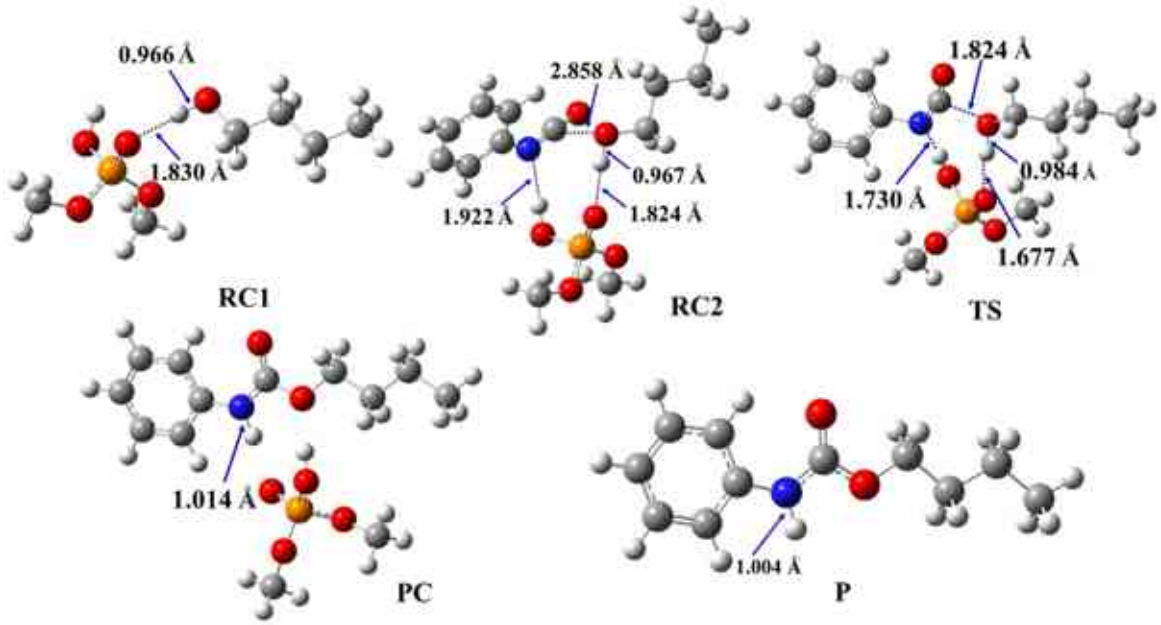


***Figure 48.*** *Optimised structures along the reaction pathway between phenyl isocyanate and butan-1-ol in the presence of dimethyl hydrogen phosphate (DMHP) calculated at the BHandHLYP/6-31G(d) level of theory in acetonitrile. RC—reactant complex, TS—transition state, PC—product complex, and P—product.*

**Table 24.** *N-H, O-H, and C-O bond lengths (Å) along the pathway of the phenyl isocyanate (PhNCO) and butan-1-ol reaction in the presence of the studied catalysts, dimethyl hydrogen phosphate (DMHP), methanesulfonic acid (MSA), and trifluoromethanesulfonic acid (TFMSA), calculated at the BHandHLYP/6-31G(d) level of theory in acetonitrile. O-H* for catalysts, while O-H** for butan-1-ol.*

| Catalysts | RC1 | | RC2 | | | | TS | | | | PC | | | P |
|---|---|---|---|---|---|---|---|---|---|---|---|---|---|---|
| | O-H* | O-H** | N-H | O-H* | O-H** | C-O | N-H | O-H* | O-H** | C-O | N-H | O-H* | O-H** | N-H |
| DMHP | 1.830 | 0.966 | 1.922 | 1.824 | 0.967 | 2.858 | 1.730 | 1.677 | 0.984 | 1.824 | 1.014 | 0.974 | 1.822 | 1.004 |
| MSA | 1.971 | 0.961 | 1.867 | 1.928 | 0.961 | 2.856 | 1.640 | 1.738 | 0.967 | 1.871 | 1.008 | 0.981 | 1.775 | 1.004 |
| TFMSA | 2.048 | 0.958 | 1.761 | 2.003 | 0.959 | 2.862 | 1.240 | 1.960 | 0.962 | 2.480 | 1.006 | 0.993 | 1.686 | 1.004 |

The effect on the O-H** bond length is even smaller and almost no change is observed between RC1 and RC2 **(Table 24)**. The most stable butan-1-ol–catalyst and trimolecular complex are formed in the case of DMHP ($\Delta_r H$ = -18.09 for RC1, and RC2, $\Delta_r H$ = -47.79 kJ/mol)). Meanwhile, TFMSA–butan-1-ol is the least stable one RC1 ($\Delta_r H$ = -6.94 kJ/mol), while MSA–butan-1-ol is the least trimolecular complex one (RC2, $\Delta_r H$ = -41.30 kJ/mol) **(Table 25 and Figure 49)**.

***Table 25.*** *Relative enthalpy ($\Delta_r H$) of the reaction between phenyl isocyanate and butan-1-ol with and without catalysts, calculated using the G3MP2BHandHLYP composite method in acetonitrile, using the SMD implicit solvent model at 298.15 K and 1 atm. R—reactant, RC—reactant complex, TS—transition state, PC—product complex, and P—product.*

| $\Delta_r H$ (kJ/mol) |
|---|

| | R | RC1 | RC2 | TS | PC | P |
|---|---|---|---|---|---|---|
| **Catalyst-free system** | 0.00 | - | -8.97' | 116.49 | - | -94.84 |
| **DMHP** | 0.00 | -18.09 | -47.79 | -15.31 | -133.12 | -94.84 |
| **MSA** | 0.00 | -8.66 | -41.30 | -8.44 | -125.01 | -94.84 |
| **TFMSA** | 0.00 | -6.94 | -45.94 | -42.85 | -130.46 | -94.84 |

'RC for catalyst-free reaction.

In the next step, TS develops in the presence of the catalyst where a proton transfer between the alcohol and the catalyst, also between the N=C=O and catalyst occurs, and the N=C=O group is being bent activating the carbon for the formation of a new C–O bond. Therefore, the O-H*, C-O and N-H distances are significantly decreased, and these are in the range of 1.677 – 1.960 Å, 1.824 – 2.480 Å, and 1.240 – 1730 Å for O-H*, C-O, and N-H respectively. At the same time, the O-H** distance increased. The potential energy curve showed that in the presence of TFMSA the TS step has the lowest relative enthalpy ($\Delta_r H$= -42.85 kJ/mol) within the studied set of catalysts **(Figure 49)**. The results showed that the barrier height of the reaction significantly decreased (>123 kJ/mol) in the presence of acid catalysts compared to the catalytic-free system **(Table 25)**.

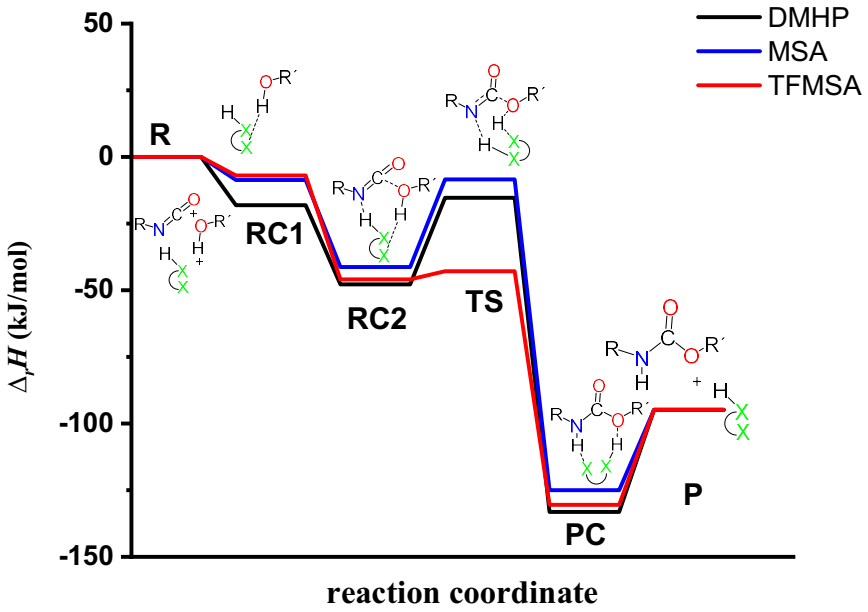


***Figure 49.*** *Relative enthalpy ($\Delta_r H$) profile of the studied catalysed urethane formation reactions in the presence of dimethyl hydrogen phosphate (DMHP), methanesulfonic acid (MSA), and trifluoromethanesulfonic acid (TFMSA) calculated at the G3PMP2BHandHLYP level of theory in acetonitrile using the SMD implicit solvent model, respectively.*

Before the reaction completes, a product complex (PC) is forming, where the urethane bond is complete, and thus, the distance between N-H significantly decreased **(Figure 48)**. In the final step the catalysts and the product will be separated (P), with the corresponding relative enthalpy of -94.84 kJ/mol. Where both the strength of a given acid and the nucleophilicity of its conjugate base play a vital role in the bifunctional catalysis of urethane formation.

## 4. Summary

Polyurethanes are some of the most versatile and unique polymers used in the industry for manufacturing a wide variety of products. Polyurethane is a macromolecular polymer including several urethane linkages that are formed by the reaction between -NCO groups (isocyanate) and -OH groups (polyol). Isocyanates and polyols are responsible for the different properties of PU products such as flexibility and hardness. The synthesis of polyurethanes from diisocyanates and polyols under industrial conditions requires a catalyst or often a combination of catalysts, which can be regarded as the most important component of the reaction system besides the starting materials. Therefore, one of the main development trends in PU synthesis is finding improved catalysts. The effect of a catalyst in the urethane bond formation lies in an increase in the rates of reactions, completion of the reactions, and establishment of a proper balance between the chain propagation reaction and the foaming proces. Therefore, several types of catalysts are used in urethane synthesis such as amine, acid, and organometallic catalysts.

In this doctoral dissertation, urethane formation in catalyst-free and catalytic processes was studied using computational chemical tools, and a general formation mechanism was proposed. All in all, urethane formation was studied in the presenece of 18 amine and 3 acid catalysts. An extensive method test was carried out and BHandHLYP/6-31G(d) was selected in combination with the SMD solvent model to describe all the different steps along the pathways of the catalytic urethane formation mechanism. Further improvements on the calculations were included using the G3MP2BHandHLYP composite calculation scheme. The applicability of the mechanism for amine catalysed urethane formation was tested in the case of the phenyl isocyanate (PhNCO)–methanol (MeOH) reaction. The catalytic activities of eight different catalysts used in polyurethane synthesis have been compared by adding them to the PhNCO–MeOH model system. As the studied catalytic mechanism contains protonation steps, the proton affinities (PA) of the catalysts have also been calculated and compared. All in all, the proton affinities of the amine groups of the catalysts cover a wide range of almost 300 kJ/mol, between 760.6 and 1070.34 kJ/mol. The energetics of the model reaction significantly changed in the presence of catalysts. The barrier height was reduced by >100 kJ/mol compared to the catalytic-free reaction. It was found that 1,8 diazabicyclo[5,4,0]undec-7-ene (DBU) catalyst was the most effective and provided the most favorable pathway, which can be associated with its high PA and cyclic structure. Meanwhile, the applicability of the mechanism for amine catalysed urethane formation in the case of the phenyl isocyanate (PhNCO)–butan-1-ol (BuOH) reaction was also tested. The catalytic activities of different cyclic amine catalysts (categorized into two groups: secondary and tertiary nitrogen functional groups) and aliphatic

catalysts used in polyurethane synthesis have been compared by adding them to the PhNCO–BuOH system. As proton transfers are crucial during the reactions, proton affinity (PA) was also computed for all unique nitrogen that was considered catalytically active within the cyclic amine catalysts. The PAs of the catalytically active nitrogens were in a range of 963.07−1523.95 kJ/mol. The effects of secondary and tertiary nitrogen functional groups have been analyzed. The results indicated that the catalysts within the tertiary nitrogen functional groups are the most effective and provided the most favorable pathway with the lowest enthalpy in the range of (TS1, $\Delta_r H$=-7.40-2.90 kJ/mol) compared to the secondary nitrogen functional group (1,2-dimethylimidazole (1,2-DMI) (TS1, $\Delta_r H$= 7.25 kJ/mol), and morpholine (TS1, $\Delta_r H$= 5.3 kJ/mol)). The results showed that in the case of cyclic catalysts the activation energy cover a range between 22.2-27.8 kJ/mol, while in the case of aliphatic catalysts, it is around 21.9-24.4 kJ/mol. The calculated thermodynamic properties have been compared to experimentally measured values and it was found that the highest difference was 11.2 kJ/mol, while the lowest difference was only 1.1 kJ/mol. Thus, the applied computational protocoll was successfully validated. In addition, a new general formation mechanism for catalytic urethane formation in the presence of three acid catalysts has been proposed and studied using theoretical methods. The mechanism includes one transition state and product complex. This route is different from the mechanism for catalytic urethane formation in the presence of amine catalysts. Meanwhile, it is slightly similar to the catalyst-free process as both have one transition state. However, the results showed that the barrier height of the reaction significantly decreased (>123 kJ/mol) in the presence of acid catalysts compared to the catalyst-free system.

It can be stated, that through this doctoral dissertation, a deeper understanding of the effect of catalysts on urethane formation is achieved. Meanwhile, the computed and measured thermodynamic properties were in good agreement with each other, which proves the validity of the proposed mechanism and verifies the method selection as well. Thus, a great theoretical tool has been achieved which can be used to describe similar systems in the future.

## 5. New scientific results

During my Ph.D. I studied the effect of organocatalysts on urethane formation using computational tools, and the following main conclusions are drawn as new scientific results:

### 1st Thesis

Method test has been carried out and a computational protocol applicable to the study of catalytic and catalyst-free urethane formation reactions has been selected. The protocol includes the G3MP2BHandHLYP composite method in combination with the SMD implicit solvation model. To keep the computational protocol as simple as possible, but finetune the energy of zwitterionic species, a correction has also been introduced and applied **(Figure 1T)**.

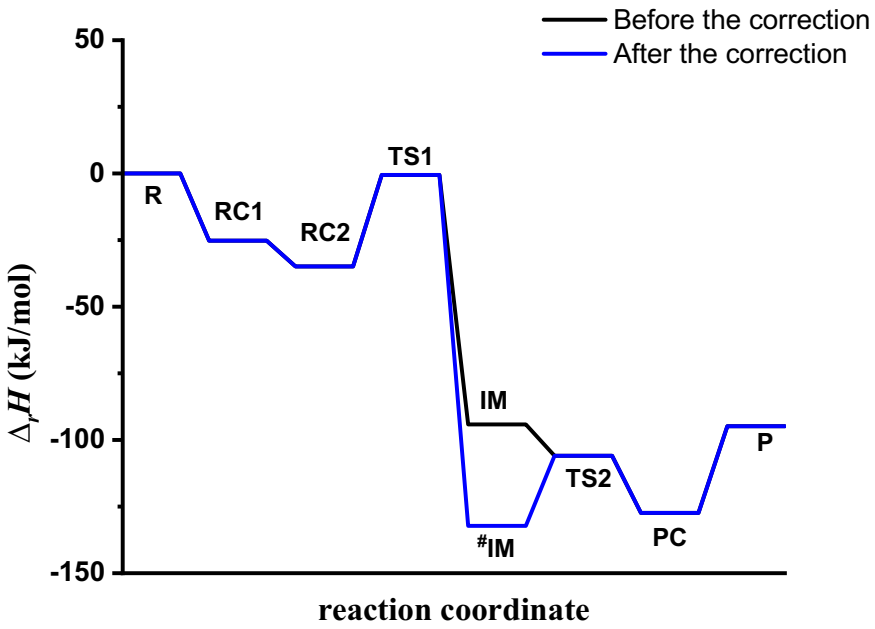


**Figure 1T** Relative enthalpy ($\Delta_r H$) profile of the phenyl isocyanate (PhNCO) and butan-1-ol (BuOH) reaction in the preseance of 4-methylmorpholine (catalyst) before (black line) and after the correction (blue line).

### 2nd Thesis

The catalyst-free reaction mechanism of phenyl isocyanate and alcohol (methanol (MeOH), and butan-1-ol (BuOH)) has been described by applying density functional theory and composite methods. It was found that the relative enthalpy difference in the barrier heights ($\Delta_r H_{[TSBuOH-TSMeOH]}$) when MeOH or BuOH are involved in the reaction with phenyl isocyanate is just 0.3 kJ/mol, which indicates that increasing the length of the aliphatic chain of the alcohol did not have a significant effect on urethane bond formation **(Figure 2T)**.

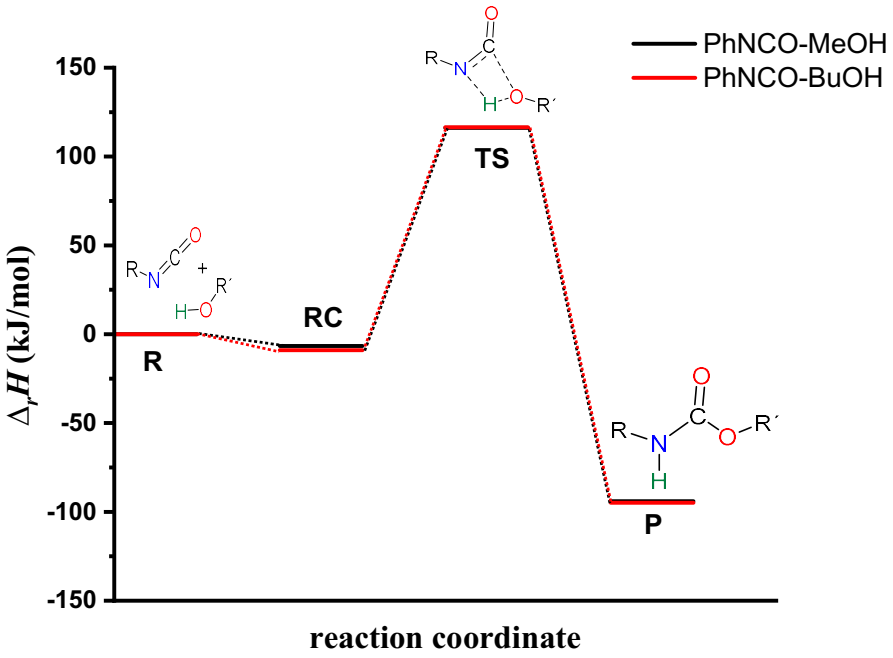


**Figure 2T** Relative enthalpy ($\Delta_r H$) profile of phenyl isocyanate (PhNCO) - methanol (MeOH) and PhNCO - butan-1-ol (BuOH) reactions, indicated with black and red lines, respectively. Calculated at the G3PMP2BHandHLYP theory level (298.15 K and 1 atm) in acetonitrile using the SMD implicit solvent model.

**3rd Thesis**

*A general mechanism for catalytic urethane formation in the presence of amine catalysts has been proposed and verified by using theoretical methods and literature data* ***(Figure 3T)***. The mechanism was tested in the cases of 18 catalysts. The proposed reaction mechanism of amine catalysed urethane formation contains seven steps. It starts with the formation of an alcohol-catalyst complex (RC1), which is followed by the formation of an alcohol-catalyst-isocyanate trimolecular complex (RC2). After these steps, a proton transfer occurs between the alcohol and the amine group of the catalyst (TS1). This leads to the next step where the intermediate (IM) will be formed. Thereafter, the catalyst will return the proton through a transition state (TS2), and thus, a product complex is formed (PC). In the final step, the catalysts and the product will be separated (P).

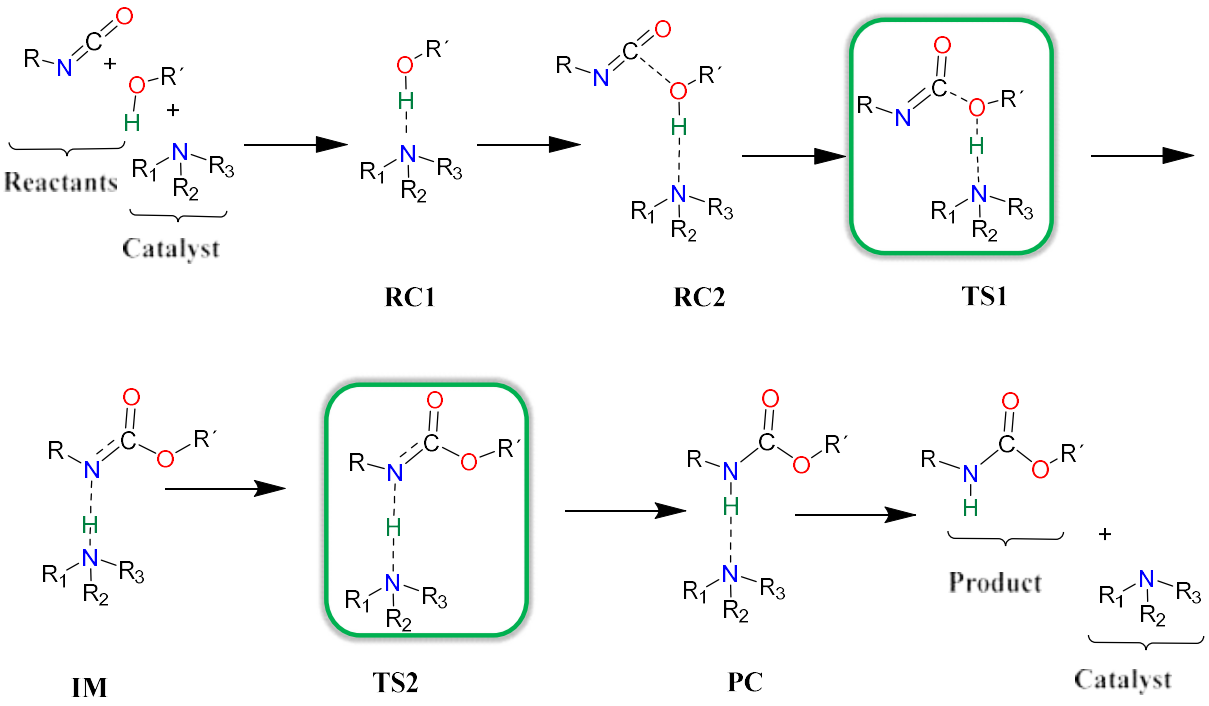


**Figure 3T** Schematic representation of the general amine -catalized urethane formation mechanism, where RC—reactant complex, TS—transition state, and PC—product complex.

**4th Thesis**

*A general mechanism for catalytic urethane formation in the presence of acid catalysts has been proposed and studied using theoretical methods* ***(Figure 4T)***. The proposed reaction mechanism of acid catalysed urethane formation contains five steps. First, a complex (RC1) between the alcohol and the catalyst is formed. Then, in the next step the isocyanate is added to the system, and RC2, a trimolecular complex is formed. After the complex formation, transition state (TS) develops and where a proton transfer between the alcohol and the catalyst, also between the N=C=O and catalyst occurs. Before the reaction completes, a product complex (PC) is forming, where the urethane bond is complete. In the final step, the catalysts and the product will be separated (P). The mechanism was tested in case of three different acid catalysts.

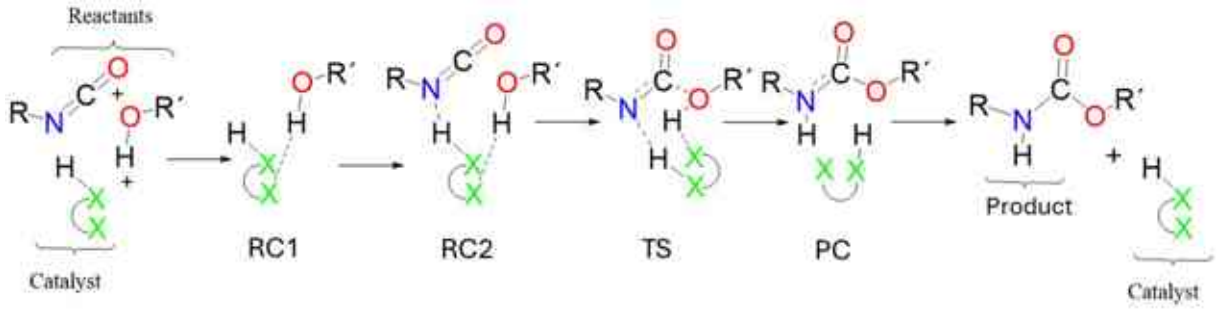


**Figure 4T** Schematic representation of the general organic acid-catalyzed urethane formation, where RC—reactant complex, TS—transition state, and PC—product complex.

**5th Thesis**

*A new reaction mechanism was proposed for the stoichiometric reaction between 2-dimethylaminoethanol (DMEA) and phenyl isocyanate* **(Figure 5T)**. By comparing the catalytic and stoichiometric processes, it was found that the catalytic process is more effective for urethane formation even if the difference in energy is not so high. Thus, DMEA can act as an effective catalyst and after some time, it can also react with free isocyanates and be built into the polymer chain which will reduce the volatile organic compound (VOC) content in the final product.

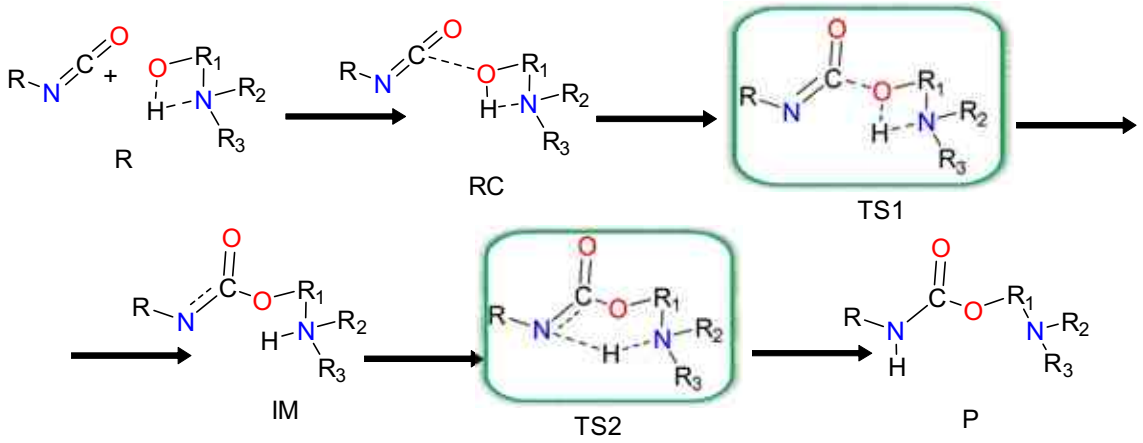


**Figure 5T** Schematic representation of the reaction mechanism of 2-dimethylaminoethanol (DMEA) - isocyanate stoichiometric reaction, where R—reactant, RC—reactant complex, TS—transition state, IM—intermediate, and PC—product complex.

## 6. Scientific publications

### Publications Related to the Subject of the Dissertation

1. **Hadeer Q. Waleed**, Marcell Csécsi, Rachid Hadjadj, Ravikumar Thangaraj, Dániel Pecsmány, Michael Owen, Milán Szőri, Zsolt Fejes, Béla Viskolcz, and Béla Fiser, ″Computational study of catalytic urethane formation,″ *Polymers*, **2022**, 14, 8, DOI: 10.3390/polym14010008. (Q1; IF=5.0)

   Number of Independent Citations: 5

2. **Hadeer Q. Waleed,** Dániel Pecsmány, Marcell Csécsi, László Farkas, Béla Viskolcz, Zsolt Fejes, and Béla Fiser, ″Experimental and theoretical study of cyclic amine catalysed urethane formation,″ *Polymers*, **2022**, 14, 2859, DOI: 10.3390/polym14142859. (Q1; IF=5.0)

   Number of Independent Citations: 1

3. **Hadeer Q. Waleed**, Marcell Csécsi,Vivien Konyhás, Zsanett R. Boros, Béla Viskolcz, Zsolt Fejes, and Béla Fiser, ″Aliphatic tertiary amine catalysed urethane formation – a combined experimental and theoretical study,″ *Phys. Chem. Chem. Phys*., **2022**, 24, 20538, DOI: 10.1039/d2cp00728b. (Q1; IF= 3.676)

   Number of Independent Citations: 2

4. **Hadeer Q. Waleed**, Rachid Hadjadj, Béla Viskolcz, and Béla Fiser, ″Effect of morpholine, and 4-methylmorpholine on urethane formation: a computational study,″ *Sci Rep*., **2023**, 13, 17950, DOI: 10.1038/s41598-023-44492-x. (D1; IF= 4.6)

   Number of Independent Citations: 0

5. **Hadeer Q. Waleed**, Béla Viskolcz, Zsolt Fejes, and Béla Fiser, ″Urethane formation in the presence of 2,2-dimorpholinodiethylether (DMDEE) and 1,4-dimethylpiperazine (DMP) – A combined experimental and theoretical study,″ *Computational and Theoretical Chemistry,* **2023***,* 1221, 114045, DOI: 10.1016/j.comptc.2023.114045. (Q3; IF= 2.8)

   Number of Independent Citations: 3

6. **Hadeer Q. Waleed**, Rachid Hadjadj, Béla Viskolcz, and Béla Fiser, ″Stoichiometric reaction and catalytic effect of 2-dimethylaminoethanol in urethane formation,″ *Phys. Chem. Chem. Phys,* **2024**, 26, 7103-7108, DOI:10.1039/D3CP05800J (Q1; IF= 3.676).

   Number of Independent Citations: 0

**Further Publications**

1. **Hadeer Q. Waleed**, Marcell Csécsi, Rachid Hadjadj, Ravikumar Thangaraj, Michael Owen, Milán Szőri, Zsolt Fejes, Béla Viskolcz, and Béla Fiser, ″The catalytic effect of DBU on urethane formation – A computational study,″ *Materials Science and Engineering*, **2021**, 46, 70–77, doi:org/10.32974/mse.2021.008.
2. **Hadeer Q. Waleed**, Fejes Zsolt, Viskolcz Béla, Fiser Béla, ″Experimental and theoretical study of urethane formation in the presence of amine catalyst,″ *Symposium on Polyurethane Innovation - SPI 2022, Conference publications,* **2022**, 203, 28-35.
3. **Hadeer Q. Waleed**, Béla Fiser, ″Polyurethane synthesis and classification - A mini-review,″ *Doktorandusz Almanach,* **2022**, 1, 116-127.
4. Mallouhi Julie, **Hadeer Q. Waleed**, Szőri-Dorogházi Emma, Owen Michael, Fiser Béla, ″Molecular dynamics study of the closed conformations of Candida rugosa lipase 2 (CRL),″ *Symposium on Polyurethane Innovation - SPI 2022, Conference Publications*, **2022**, 203, 82-90.
5. **Hadeer Q. Waleed**, Béla Fiser, ″The catalytic effect of 1,4-diazabicyclo[2.2. 2]octane (DABCO) on urethane formation - A computational study,″ *Doktorandusz Almanach*, **2023**, 1, 91-97.
6. **Hadeer Q. Waleed**, Edina Reizer, Béla Viskolcz, Béla Fiser, ″A computational study of the catalytic effect on urethane formation,″ *Symposium on Polyurethane Innovation – SPI 2023 - Conference Publications*, **2023**, 230, 19-27.
7. **Hadeer Q. Waleed**, Dalal K. Thbayh, Amal Zarrami, Julie Mallouhi, Pecsmány Dániel, Reizer Edina, Rachid Hadjadj, Fiser Béla, ″Hogyan tervezhetünk jobb polimereket szuperszámítógépek segítségével?,″ *HPC ECHO, Tudománytól Innovációig*, 2021, 10-12.
8. **Hadeer Q. Waleed**, Dalal K. Thbayh, Amal Zarrami, Julie Mallouhi, Pecsmány Dániel, Reizer Edina, Rachid Hadjadj, Fiser Béla, ″How can we design better

polymers with supercomputers?,″ *HPC ECHO, From Science to Innovation*, 2021, 10-12.

9. Rachid Hadjadj, Imre G. Csizmadia, **Hadeer Q. Waleed**, Dalal K. Thbayh, Béla Viskolcz, Béla Fiser, ″Monoethanolamine assisted CO2 hydrogenation to methanol – A computational study,″ Molecular Catalysis, Vol. 559, pp.114091, 2024. DOI: 10.1016/j.mcat.2024.114091. (Q2; IF= 4.6).

**Presentations and posters**

1. A Miskolci Egyetem Kémiai Intézetének (KI, MAK, ME) és a MAB Elméleti és Fizikai Kémiai Munkabizottságának közös rendezvénye
   Oral presentation/Online,Miskolc, Hungary, 2021.05.11.
   A Computational Study of Urethane Formation.
2. Symposium on Polyurethane Innovation SPI 2021
   Oral presentation/Online, Miskolc, Hungary, 2021.08.24.
   Computational Study of Urethane Formation in the Presence of Catalysts.
3. 37. Borsodi Vegyipari Nap
   Oral presentation/Online, Miskolc, Hungary, 2021.11.17.
   Catalytic Effect of Amine Catalysts on Urethane Formation - A Computational Study.
4. 25$^{th}$ Spring Wind Conference
   Poster presentation/Pécs, Hungary, 2022.06-08.05.
   Catalytic Effect of Tertiary Amine on Urethane Formation.
5. Symposium on Polyurethane Innovation SPI 2022
   Oral presentation/Miskolc, Hungary, 2022.11.11.
   Experimental and Theoretical Study of Urethane Formation in the Presence of Amine Catalyst.
6. 10$^{th}$ Visegrad Symposium on Biomolecular Interactions
   Poster presentation/Nove Hrady, Czech Republic, 2022.06.16.
   Experimental and Theoretical Study of Tertiary Amine Catalysed Urethane Formation.
7. Hungarian Science Day
   Oral presentation/Miskolc, Hungary, 2022.11.09.
   Polyurethane Catalysis by Tertiary Amines - A Combined Theoretical and Experimental Study.
8. 26$^{th}$ Spring Wind Conference

Oral presentation/Miskolc, Hungary, 2022.05-07.05.

Experimental and Theoretical Study of Urethane Formation in the Presence of Tertiary Amine Catalyst.

9. 11th Visegrad Symposium on Biomolecular Interactions

Poster presentation/Szidonia Castle, Hungary, 2023.20-23.06.

Amine Catalysed Urethane Formation – A Combined Experimental and Theoretical Study.

10. 10th Doctoral Symposium on chemistry

Poster presentation/Lodz, Poland, 2023.18-19.05.

Cyclic Amine Catalysed Urethane Formation- A Combined Experimental and Theoretical Study.

11. Symposium on Polyurethane Innovation SPI 2023

Oral presentation/Miskolc, Hungary, 2023.08.24.

A Computational Study of the Catalytic Effect on Urethane Formation.

12. Basics & Application of Computational Chemistry in Action (BACCA), Erasmus+ Blended Intensive Programme, virtual session

Oral presentation/Online, 2024.04.04

Organocatalytic Urethane Synthesis– A Computational Study.

## 7. References


1. Kanamori, T.; Sakai, K. Introduction to Polymer Science Involved in Membrane Preparation Technology. Nippon rinsho. Japanese J. Clin. Med. **1991**, 49 Suppl, 44–52, PMID: 1808297.
2. Saldívar-Guerra, E.; Vivaldo-Lima, E. Handbook of Polymer Synthesis, Characterization, and Processing; 2013, 1-622, doi:10.1002/9781118480793.
3. Billmeyer, F.W. Textbook of Polymer Science; 1963; Vol. 12; ISBN 0471031968.
4. Szycher, M. Structure–property relations in polyurethanes. Szycher's Handbook of Polyurethanes, 2nd ed.; CRC Press: Boca Raton, FL, USA; **2012**, 37-86, ISBN 9781439863138.
5. Yanping, Y. The Development of Polyurethane. Mater. Sci. Mater. Rev **2018**, 1, 1–8, doi:10.18063/msmr.v1i1.507.
6. Bayer, O. Das Di-Lsocganat-Poluadditionsverfahren (Polyurethane). Angew. Chemie **1947**, 59, 257–288, doi:org/10.1002/ange.19470590901
7. Das, A.; Mahanwar, P. A Brief Discussion on Advances in Polyurethane Applications. Adv. Ind. Eng. Polym. Res. **2020**, 3, 93–101, doi:10.1016/j.aiepr.2020.07.002.
8. Brzeska, J.; Piotrowska-Kirschling. A Brief Introduction to the Polyurethanes According to the Principles of Green Chemistry. Processes **2021**, 9, 1929, doi:10.3390/pr9111929.
9. Matsumura, S.; Soeda, Y.; Toshima, K. Perspectives for Synthesis and Production of Polyurethanes and Related Polymers by Enzymes Directed toward Green and Sustainable Chemistry. Appl. Microbiol. Biotechnol. **2006**, 70, 12–20, doi:10.1007/s00253-005-0269-2.
10. Polyurethanes Market Statistics, PU Share 2026 PDF Report Available online: https://www.gminsights.com/industry-analysis/polyurethane-PU-market-report (accessed on 8 September 2021).
11. Polyurethane Foam Market: Trends, Opportunities and Competitive Analysis Available online: https://www.lucintel.com/polyurethane-foam-market.aspx (accessed on 11 July 2022).
12. Sabrina, S.S.A.;Denilson, A.S.; Danielle, M.A. Physico-Chemical Analysis of Flexible Polyurethane Foams Containing Commercial Calcium Carbonate. Mater. Res. **2008**, 11, 433–438, doi:10.1590/s1516-14392008000400009.
13. Sonnenschein, M.F. Polyurethanes Science, Technology, Markets, and Trends; First Edit.; John Wiley & Sons, Inc., 2015; ISBN 9789896540821.
14. Shoaib, S.; Shahzad, M. K.; Nafisa, G.; Waqas, A.; Muhammad, S.; Jamil, T. A Comprehensive Short Review on Polyurethane Foam. Int. J. Innov. Appl. Stud **2014**, 12, 165–169.
15. Ionescu, M. Chemistry and Technology of Polyols for Polyurethanes , 2nd Edition; A Smithers Group Company Shawbury, 2016; Vol. 1; ISBN 9781910242988.
16. Zhang, X. D.; Neff, R. A.; Macosko C.W.. Foam Stability in Flexible Polyurethane Foam Systems. In Polymeric Foams: Mechanisms and Materials; 2004; pp. 139–172 ISBN 9780203506141.
17. Aqilahhamuzan, H.; Badri, K.H. The Role of Isocyanates in Determining the Viscoelastic Properties of Polyurethane. AIP Conf. Proc. **2016**, 1784, doi:10.1063/1.4966757.
18. Cocker, J.; Jones, K.; Leng, G.; Gries, W.; Budnik, L.T.; Müller, J.; Göen, T.; Hartwig, A. Hexamethylene Diisocyanate, 2,4-Toluene Diisocyanate, 2,6-Toluene Diisocyanate, Isophorone Diisocyanate and 4,4′-Methylene Diphenyl Diisocyanate - Determination of Hexamethylenediamine, 2,4-Toluenediamine, 2,6-Toluenediamine, Isophoronediamine and 4,4′-Me. MAK-Collection Occup. Heal. Saf. **2017**, 1415–1435, doi:10.1002/3527600418.bi82206e2217.
19. Ionescu, M. Chemistry and Technology of Polyols for Polyurethane Volume 2; 2016; Vol. 2; ISBN 978-1-84735-035-0.
20. Szycher, M.; D, P.; Szycher, M. Structure–Property Relations in Polyurethanes; 2012; ISBN 9781439863138.
21. Sekizawa, J.; Greenberg, M.M. Diphenylmethane Diisocyanate (MDI). IPCS Concise Int. Chem. Assess. Doc. **2001**, 1–31, ISBN 92 4 153027 8.
22. Mhike, M. Characterization of Methylene Diphenyl Diisocyanate Protein Conjugates, dissertation, Portland State University, 2014.
23. Parod, R.J. Toluene Diisocyanate; Third Edit.; Elsevier, 2014; Vol. 4; ISBN 9780123864543.
24. Pogacean, O.A.; Schiopu, I.; Neamtiu, I.; Gurzau, E.; Water, D.; Contamination, A. Assessment

of Human Exposure to Toluene Diisocyanate. **2011**.
25. Radeloff, M.A.; Beck, R.H.F. Polyols – More than Sweeteners. Sugar Ind. **2013**, 226–234, doi:10.36961/si14095.
26. Polyols Available online: https://polymerdatabase.com/Polymer Brands/Polyols.html (accessed on 17 October 2020).
27. Gama, N. V; Ferreira, A.; Barros-Timmons, A. Polyurethane Foams: Past, Present, and Future., doi:10.3390/ma11101841.
28. Tan, S.; Abraham, T.; Ference, D.; MacOsko, C.W. Rigid Polyurethane Foams from a Soybean Oil-Based Polyol. Polymer (Guildf). **2011**, 52, 2840–2846, doi:10.1016/j.polymer.2011.04.040.
29. Padsalgikar, A.D. Speciality Plastics in Cardiovascular Applications. In Plastics in Medical Devices for Cardiovascular Applications; Elsevier Inc., 2017; pp. 53–82 ISBN 9780323371223.
30. Thomas, S.; Datta, J.; Haponiuk, J. T.; Reghunadhan, A. Polyurethane Polymers: Blends and Interpenetrating Polymer Networks; Netherlands: Elsevier Science., 2017, ISBN 978-0-12-804039-3.
31. Jiang, L.; Ren, Z.; Zhao, W. ; Liu, W.; Liu, H.; Zhu, C. Synthesis and Structure/Properties Characterizations of Four Polyurethane Model Hard Segments. R. Soc. Open Sci. **2018**, 5, 180536, doi:10.1098/rsos.180536.
32. Sato, M.; Received The Rate of the Reaction of Isocyanates with Alcohols. I1 MASAO. Phys. Rev. Lett. **1961**, 6, 70–71, doi:10.1103/PhysRevLett.6.70.
33. Ephraim, S.; Woodward, A.E.; Mesrobian, R.B. Kinetic Studies of the Reaction of Phenyl Isocyanate with Alcohols in Various Solvents. J. Am. Chem. Soc. **1958**, 80, 1326–1328, doi:10.1021/ja01539a012.
34. Dyer, E.; Taylor, H.A.; Mason, S. J.; Samson, J. The Rates of Reaction of Isocyanates with Alcohols. I. Phenyl Isocyanate with 1- and 2-Butanol. **1949**, 4, 4106–4109, doi.org/10.1021/ja01180a064.
35. Chen, Z.; Yang, W.; Yin, H.; Yuan, S. Kinetics of Water–Isocyanate Reaction in N,N-Dimethylformamide. Chinese J. Chem. Eng. **2017**, 25, 1435–1441, doi:10.1016/j.cjche.2017.03.012.
36. Ozaki, S. Recent Advances in Isocyanate Chemistry. J. Synth. Org. Chem. Japan **1982**, 40, 285–295, doi:10.5059/yukigoseikyokaishi.40.285.
37. Delebecq, E.; Jean-Pierre, P.; Boutevin, B.; Ganachaud, F. On the Versatility of Urethane/Urea Bonds: Reversibility, Blocked Isocyanate, and Non-Isocyanate Polyurethane Etienne. Am. Chem. Soc. **2013**, 1–39, doi.org/10.1021/cr300195n.
38. De Souza, F. M.; Kahol, P. K.; Gupta, R.K. Introduction to Polyurethane Chemistry. ACS Symp. Ser. **2021**, 1380, 1–24, doi:10.1021/bk-2021-1380.ch001.
39. Han, J. L.; Yu, C. H.; Lin, Y. H.; Hsieh, K.H. Kinetic Study of the Urethane and Urea Reactions of Isophorone Diisocyanate. J. Appl. Polym. Sci. **2008**, 107, 3891–3902, doi:10.1002/app.
40. Zhao, Y.; Zhong, F.; Tekeei, A.; Suppes, G. J. Modeling impact of catalyst loading on polyurethane foam polymerization. Applied Catalysis A: General. **2014**, 17, 229-238, doi:org/10.1016/j.apcata.2013.09.055
41. Bernard, J.M. ; Schwarz, J.; Olier, P. Method For Preparing An Allophanate, Allophanate, And Low-Viscosity Composition Containing The Allophanate, US patent, 2012, US 2012/0016073 A1.
42. Carnaroglio, D.; Martina, K.; Palmisano, G.; Penoni, A.; Domini, C.; Cravotto, G. One-Pot Sequential Synthesis of Isocyanates and Urea Derivatives via a Microwave-Assisted Staudinger-Aza-Wittig Reaction. Beilstein J. Org. Chem. **2013**, 9, 2378–2386, doi:10.3762/bjoc.9.274.
43. Echeverria-Altuna, O.; Ollo, O.; Calvo-Correas, T.; Harismendy, I.; Eceiza, A. Effect of the Catalyst System on the Reactivity of a Polyurethane Resin System for RTM Manufacturing of Structural Composites. Express Polym. Lett. **2022**, 16, 234–247, doi:10.3144/EXPRESSPOLYMLETT.2022.19.
44. Touchet, T. J.; Cosgriff-Hernandez, E.M. Hierarchal Structure-Property Relationships of Segmented Polyurethanes; Elsevier Ltd, 2016; ISBN 9780081006221.
45. Tian, N.; Chao, H. Chain Extender Evaluation for Polyurethanes Derived: Polybutadiene from Hydroxyl-Terminated Resins.; 2010; Vol. 26;.
46. Ralph D. Priester, Jr.; Edwin J. Strojny.; Debra H. Stutts. Chan Extenders For Polyurethanes, US

patent, **1990**, US 4,931,487.
47. Ramkumar, S. C.; Murali, A.; Preethi, G.; Chandrasekaran, B.; Saravanan, P.; Jaisankar, S.N. Polycarbodiimide and Polyurethane Cross-Linkers for Leather Finishing. Leather Footwear J. **2017**, 17, 181–192, doi:10.24264/lfj.17.4.1.
48. Szycher, M. Szycher'S Handbook of Polyurethanes; Second Edi.; Taylor & Francis Group, LLC, 2013; ISBN 9781439863138.
49. Zhao, Y.; Zhong, F.; Tekeei, A.; Suppes, G.J. Modeling Impact of Catalyst Loading on Polyurethane Foam Polymerization. Appl. Catal. A Gen. **2014**, 469, 229–238, doi:10.1016/j.apcata.2013.09.055.
50. Wianowski, L.; Białkowska, A.; Dobrowolski, L.; Zarzyka, I. Physical Blowing Agents for Polyurethanes. Polimery/Polymers **2020**, 65, 83–94, doi:10.14314/POLIMERY.2020.2.1.
51. Jaf, L.; Al-Moameri, H.H.; Ayash, A.A.; Lubguban, A.A.; Malaluan, R.M.; Ghosh, T. Limits of Performance of Polyurethane Blowing Agents. Sustain. **2023**, 15, doi:10.3390/su15086737.
52. Jacob A. Moulijn ; Rutger A. van Santen. History of Catalysis. RSC eTextbook Collection, **1999**; pp. 3–28, doi:org/10.1039/9781849739900-00001
53. Yanping, Y. The Development of Polyurethane. Mater. Sci. Mater. Rev. **2018**, 1, 1–8, doi:10.18063/msmr.v1i1.507.
54. Wisniak, J. The History of Catalysis. From the Beginning to Nobel Prizes. Educ. Química **2010**, 21, 60–69, doi:10.1016/S0187-893X(18)30074-0.
55. Piumetti, M. A Brief History of the Science of Catalysis – I : From the Early Concepts to Single-Site Heterogeneous Catalysts. Chim. Oggi - Chem. Today **2014**, 32(6), 22–27.
56. Anastas, .P. T.; Warner J.C. Green Chemistry:Theory and Practice; Oxford University Press, 1998; ISBN 0198502346, 9780198502340.
57. Chorkendorff, I.; Niemantsverdriet, J.W. Surface Reactivity. In WILEY-VCH Verlag GmbH & Co. KGaA, Weinheim; 2003; pp. 215–266 ISBN 3527305742.
58. Chorkendorff, I.; Niemantsverdriet, J.W. Concepts of Modern Catalysis and Kinetics. In Adsorption Journal Of The International Adsorption Society; WILEY-VCH Verlag GmbH & Co. KGaA, Weinheim, 2003, ISBN 3527305742.
59. Othman, M.S. Catalysts of the Preparation and Industrial Importance of Catalysis and Catalyst Deactivation. Int. J. Adv. Chem. Res. **2020**, 1, 23–27, doi:10.33545/26646781.2019.v1.i2a.12
60. Piet W.N.M, van L. Homogeneous Catalysis: Understanding the Art; 2019; Vol. 53; ISBN 9788578110796.
61. Tathe, A.; Nikalje, A.P.G.; Ghodke, M. Biocatalysis : A Brief Review. Asian J. Res. Chem **2011**, 4(9), 1355–1360.
62. Nikulin, M.; Švedas, V. Prospects of Using Biocatalysis for the Synthesis and Modification of Polymers. Molecules **2021**, 26, 1–37, doi:10.3390/molecules26092750.
63. Pera, L.M.; Baigori, M.D.; Pandey, A.; Castro, G.R. Biocatalysis. Ind. Biorefineries White Biotechnol. **2015**, 391–408, doi:10.1016/B978-0-444-63453-5.00012-4.
64. Sheldon, R.A.; Woodley, J.M. Role of Biocatalysis in Sustainable Chemistry. Chem. Rev. **2018**, 118, 801–838, doi:10.1021/acs.chemrev.7b00203.
65. Kumar, A.; Daw, P.; Milstein, D. Homogeneous Catalysis for Sustainable Energy: Hydrogen AndMethanol Economies, Fuels from Biomass, and Related Topics. Chem.Rev **2022**, 122, 385–441, doi:https://doi.org/10.1021/acs.chemrev.1c00412.
66. Gates, B. C.; Huber, G. W.; Marshall, C. L.; Ross, C. L.; Siirola, J.; Wang, Y. Catalysts for Emerging Energy Applications. MRS Bull. **2008**, 33, 429–435.
67. Norskov, J. K.; Studt, F.; Pedersen, F.A.; Bligaard, T. Fundamental Concepts in Heterogeneous Catalysis; John Wiley & Sons, Inc, 2014; ISBN 9788490225370.
68. Ertl, G., Knözinger, H., Weitkamp, J. Handbook of Heterogeneous Catalysis; 1997; Vol. 2; ISBN 9783527312412.
69. Thomas, J.M. Uniform Heterogeneous Catalysts: The Role of Solid-State Chemistry in Their Development and Design. Angew. Chemie Int. Ed. English **1988**, 27, 1673–1691, doi:10.1002/anie.198816731.
70. Gates, B.C.; Huber, G.W.; Marshall, C.L.; Ross, P.N.; Siirola, J.; Wang, Y. Catalysts for Emerging Energy Applications. MRS Bull. **2008**, 33, 429–435, doi:10.1557/mrs2008.85.
71. Zhao, Y.; Zhong, F.; Tekeei, A.; Suppes, G.J. Modeling Impact of Catalyst Loading on

Polyurethane Foam Polymerization. Appl. Catal. A Gen. **2014**, 469, 229–238, doi:10.1016/j.apcata.2013.09.055.

72. Dworakowska, S.; Bogdał, D.; Zaccheria, F.; Ravasio, N. The Role of Catalysis in the Synthesis of Polyurethane Foams Based on Renewable Raw Materials. Catal. Today **2014**, 223, 148–156, doi:10.1016/j.cattod.2013.11.054.
73. Dias, G.; Prado, M.; Le Roux, C.; Poirier, M.; Micoud, P.; Ligabue, R.; Martin, F.; Einloft, S. Synthetic Talc as Catalyst and Filler for Waterborne Polyurethane-Based Nanocomposite Synthesis. Polym. Bull. **2020**, 77, 975–987, doi:10.1007/s00289-019-02789-w.
74. Liu, L.; Dong, H.; Yu, Y.; Tang, Z.; Bai, C.; Feng, Y.; Chen, H.; Schmidt, T. Polyurethane Latent Catalysts Obtained by Emulsion Solvent Evaporation. Polym. Bull. **2022**, 1–17, doi:10.1007/s00289-022-04225-y.
75. Tesser, R.; Di Serio, M.; Sclafani, A.; Santacesaria, E. Modeling of Polyurethane Foam Formation. J. Appl. Polym. Sci. **2004**, 92, 1875–1886, doi:10.1002/app.20170.
76. Landers, R. ; Modro, H.; Hubel, R. Influencing the Cell Structure of Flexible Polyurethane Foams by Additives. Proc. 2014 Polyurethane Tech. Conf. Dallas, TX, USA **2014**, 22–24.
77. Zhao, Y. Modeling and Experimental Study of Polyurethane Foaming Reactions, Dissertation, University of Missouri-Columbia, 2015.
78. Baser, S.A.; Khakhar.; D. V. Modeling of the Dynamics of R-11 Blown Polyurethane Foam Formation. Polym. Eng. Sci. **1994**, 34, 632–641, doi:10.1002/pen.760340804.
79. Rekha Rao, Lisa Mondy, Kevin Long, Mathew Celina, Christine Roberts, Melissa Soehnel, Nicholas Wyatt, V.B. The Kinetics of Polyurethane Structural Foam Formation: Foaming and Polymerization. AIChE J. **2012**, 59, 215–228, doi:10.1002/aic.
80. Bantu, B..; Pawar, G. M.; Decker, U.; Wurst, K.; Schmidt, A. M.; Buchmeiser, M.R. CO2 and SnII Adducts of N-Heterocyclic Carbenes as Delayed-Action Catalysts for Polyurethane Synthesis. Chem. - A Eur. J. **2009**, 15, 3103–3109, doi:10.1002/chem.200802670.
81. Rossi, F.V. Additives in Composite Materials: Synthesis and Characterization of Innovative Promoters in Polyurethane Blends, 2016.
82. Avraham, L.; Sanguramath, R.A.; Cohen, O.; Perry, L.; Levenberg, S.; Silverstein, M.S. Polysaccharide-Based, Emulsion-Templated, Porous Poly(Urethane Urea)s: Composition, Catalysis, Cell Growth. Eur. Polym. J. **2022**, 169, 111140, doi:10.1016/j.eurpolymj.2022.111140.
83. Ruiduan, L.; Ling, L.; Yanjie, L.; Ben, W.; Jia Jun, Y.; Jibo, Z. Research Progress of Amine Catalysts for Polyurethane. New Materials and Intelligent Manufacturing. **2018**, 1, 54–57, doi:10.26480/icnmim.01.2018.54.57.
84. Sardon, H. ; Chan, J. M. W.; Ono, R. J.; Mecerreyes, D.; Hedrick, J.L. Highly Tunable Polyurethanes: Organocatalyzed Polyaddition and Subsequent Post-Polymerization Modification of Pentafluorophenyl Ester Sidechains. Polym. Chem. **2014**, 5, 3547, doi:10.1039/c4py00262h.
85. Malwitz, N.; Wong, S. W.; Frisch, K. C.; Manis, P.A. Amine Catalysis of Polyurethane Foams. J. Cell. Plast. **1987**, 23, 461–502, doi:10.1177/0021955X8702300505.
86. Rad, A. S.; Ardjmand, M. A. Studying on the Mechanism and Raw Materials Used to Manufacturing Polyurethane. Chem. Technol. an indian J. **2008**, 3, 60–71.
87. Sardon, H.; Engler, A.C.; Chan, J. M. W.; García, J. M.; Coady, D. J.; Pascual, A.; Mecerreyes, D.; Jones, G. O.; Rice, J. E.; Horn, H. W.; Hedrick, J.L. Organic Acid-Catalyzed Polyurethane Formation via a Dual-Activated Mechanism: Unexpected Preference of n-Activation over o-Activation of Isocyanates. J. Am. Chem. Soc. **2013**, 135, 16235–16241, doi:10.1021/ja408641g.
88. Chen, Z.J.; Zhong, W.Q.; Tang, D.L.; Zhang, G.Z. Preparation of Organic Nanoacid Catalyst for Urethane Formation. Chinese J. Chem. Phys. **2017**, 30, 339–342, doi:10.1063/1674-0068/30/cjcp1703060.
89. Dove, A.P. Organic Catalysis for Ring-Opening Polymerization. ACS Macro Lett **2012**, 1, 1409–1412, doi:https://doi.org/10.1021/mz3005956.
90. Nordstrom, D. J.; Stolarski, V.L. Proceedings of Waterborne, High-Solids, and Powder Coatings Symposium. In Proceedings of the Proceedings of Waterborne, High-Solids, and Powder Coatings Symposium; New Orleans, LA; University of Southern Mississippi: Hattiesburg, MS, 1997.

91. Muuronen, M.; Deglmann, P.; Tomović, Ž. Design Principles for Rational Polyurethane Catalyst Development. J. Org. Chem. **2019**, 84, 8202–8209, doi:10.1021/acs.joc.9b01319.
92. Pentamethyldiethylenetriamine | AminCat PMDETA | CAS: 3030-47-5 Available online: https://vestachem.com/chemicals/pentamethyldiethylenetriamine/ (accessed on 6 January 2021).
93. 2-[2-(Dimethylamino)Ethoxy]Ethanol CAS#: 1704-62-7 Available online: https://www.chemicalbook.com/ProductChemicalPropertiesCB5490275_EN.htm (accessed on 6 January 2021).
94. N-(3-Aminopropyl)-Imidazole | 5036-48-6 Available online: https://www.chemicalbook.com/ChemicalProductProperty_EN_CB2724203.htm (accessed on 10 November 2020).
95. CAS 616-47-7 - Amine Catalysts Available online: http://www.newtopchem.com/cas-616-47-7/ (accessed on 9 November 2020).
96. Tris(3-(Dimethylamino)Propyl)-Hexahydro-s-Triazine | CAS: 15875-13-5 Available online: https://vestachem.com/chemicals/tris3-dimethylaminopropyl-hexahydro-s-triazine/ (accessed on 10 November 2020).
97. Hatanaka, M. DFT Analysis of Catalytic Urethanation. Bull. Chem. Soc. Jpn. **2011**, 84, 933–935, doi:.org/10.1246/bcsj.20110144.
98. Wen, Z.; Hu, W.; Chi, X.; Wang, X.; Tian, D.; Wang, M.; Liu, J.; Ma, X.; Pang, A. DFT Study of the Catalytic Mechanism for Urethane Formation in the Presence of Basic Catalyst 1,4-Diazabicyclo[2.2.2]Octane. Commun. Comput. Chem. **2014**, 2, 22–35, doi:10.4208/cicc.2014.v2.n1.3.
99. Kolboe, S. Proton Affinity Calculations with High Level Methods. J tChem Theory Compu . 2014 Aug 12;10(8)3123-8. **2014**, 10, 3123–3128, doi:10.1021/ct500315c.
100. Szycher, M. Rigid Polyurethane Foams; 2012; ISBN 9781439863138.
101. Ivdre, A.; Abolins, A.; Volkovs, N.; Vevere, L.; Paze, A.; Makars, R.; Godina, D.; Rizikovs, J. Rigid Polyurethane Foams as Thermal Insulation Material from Novel Suberinic Acid-Based Polyols. Polymers (Basel). **2023**, 15, doi:10.3390/polym15143124.
102. Amundarain, I.; Miguel-Fernández, R.; Asueta, A.; García-Fernández, S.; Arnaiz S. Synthesis of Rigid Polyurethane Foams Incorporating Polyols from Chemical Recycling of Post-Industrial Waste Polyurethane Foams. Polymers (Basel). **2022**, 14, 1157, doi:10.3390/polym14061157.
103. Paciorek-Sadowska, J.; Czupryłski, B.; Liszkowska J. Glycolysis of Rigid Polyurethane-Polyisocyanurate Foams with Reduced Flammability. J. Elastomers Plast. **2016**, 48, 340–353, doi:10.1177/0095244315576244.
104. Akindoyo, J. O.; Beg, M. D. H. ; Ghazali, S.; Islam, M. R.; Jeyaratnam, N.; Yuvarajc, A.R. Polyurethane Types, Synthesis and Applications-a Review. RSC Adv. **2016**, 6, 114453–114482, doi:10.1039/c6ra14525f.
105. Miguel-Fernández, R.; Amundarain, I.; Asueta, A.; García-Fernández, S.; Arnaiz, S.; Miazza, L. N.; Montón, E.; Rodríguez-García, B.; Bianca-Benchea E. Recovery of Green Polyols from Rigid Polyurethane Waste by Catalytic Depolymerization. Polymers (Basel). **2022**, 14, 2936, doi:10.3390/polym14142936.
106. Defonseka, C. Practical Guide to Flexible Polyurethane Foams. Smithers Group Company; Smithers Group Company, 2013, ISBN 9781847359759.
107. Lumcharoen, D.; Saravari, O. Preparation and Characterization of Flexible Polyurethane Foams from Palm Oil-Based Polyol. Adv. Mater. Res. **2014**, 911, 352–356, doi:10.4028/www.scientific.net/AMR.911.352.
108. De Carvalho Pinto, P.C.; Da Silva, V.R.; Yoshida, M.I.; De Oliveira, M.A.L. Synthesis of Flexible Polyurethane Foams by the Partial Substitution of Polyol by Steatite. Polimeros **2018**, 28, 323–331, doi:10.1590/0104-1428.10417.
109. American Chemistry Council Inc. Flexible Polyurethane Foam. **2019**, 1, 1–7.
110. Wilkinson, A.N.; Fithriyah, N.H.; Stanford, J.L.; Suckley, D. Structure Development in Flexible Polyurethane Foam-Layered Silicate Nanocomposites. Macromol. Symp. **2007**, 256, 65–72, doi:10.1002/masy.200751007.
111. Kraitape, N.; Thongpin, C. Influence of Recycled Polyurethane Polyol on the Properties of Flexible Polyurethane Foams. Energy Procedia **2016**, 89, 186–197, doi:10.1016/j.egypro.2016.05.025.

112. Andersson, A.; Lundmark, S.; Magnusson, A.; Maurer, F.H.J. Shear Behavior of Flexible Polyurethane Foams Under Uniaxial Compression. J. Appl. Polym. Sci. **2009**, 111, 2290–2298, doi:10.1002/app.
113. Lin, Y-C.; Huff, H-E., Hsieh S-H. Flexible Polyurethane Foam Extended With Corn Starch; Cereals: Novel Uses and Processes, 1997, ISBN 978-1-4757-2675-6.
114. Osman, A.F.; Martin, D.J. Thermoplastic Polyurethane (TPU) / Organo- Fluoromica Nanocomposites for Biomedical Applications: In Vitro Fatigue Properties. Electron. Packag. Interconnect Technol. Symp. **2019**, 701, 1–8, doi:10.1088/1757-899X/701/1/012056.
115. Gao, Z.; Wang, Z.; Liu, Z.; Fu, L.; Li, X.; Eling, B.; Pöselt, E.; Schander, E.; Wang, Z. Hard Block Length Distribution of Thermoplastic Polyurethane Determined by Polymerization-Induced Phase Separation. Polymer (Guildf). **2022**, 256, 125236, doi:10.1016/j.polymer.2022.125236.
116. Yilgör, I.; Yilgör, E.; Wilkes, G.L. Critical Parameters in Designing Segmented Polyurethanes and Their Effect on Morphology and Properties: A Comprehensive Review. Polymer (Guildf). **2015**, 58, A1–A36, doi:10.1016/j.polymer.2014.12.014.
117. Barikani, M.; Barmar, M. Thermoplastic Polyurethane Elastomers: Synthesis, and Study of Effective Structural Parameters. Iran. Polym. J. (English Ed. **1996**, 5, 231–235.
118. Jung, Y.S.; Lee, S.; Park, J.; Shin, E.J. One-Shot Synthesis of Thermoplastic Polyurethane Based on Bio-Polyol (Polytrimethylene Ether Glycol) and Characterization of Micro-Phase Separation. Polymers (Basel). **2022**, 14, doi:10.3390/polym14204269.
119. Charlon, M.; Heinrich, B.; Matter, Y.; Couzigné, E.; Donnio, B.; Avérous, L. Synthesis, Structure and Properties of Fully Biobased Thermoplastic Polyurethanes, Obtained from a Diisocyanate Based on Modified Dimer Fatty Acids, and Different Renewable Diols. Eur. Polym. J. **2014**, 61, 197–205, doi:10.1016/j.eurpolymj.2014.10.012.
120. Dieterich, D.; Keberle, W.; Witt, H. Polyurethane Ionomers, a New Class of Block Polymers. Angew. Chemie Int. Ed. English **1970**, 9, 40–50, doi:10.1002/anie.197000401.
121. Król, P.; Król, B. Structures, Properties and Applications of the Polyurethane Ionomers. J. Mater. Sci. **2020**, 55, 73–87, doi:10.1007/s10853-019-03958-y.
122. Król, P. Synthesis Methods, Chemical Structures and Phase Structures of Linear Polyurethanes. Properties and Applications of Linear Polyurethanes in Polyurethane Elastomers, Copolymers and Ionomers. Prog. Mater. Sci. **2007**, 52, 915–1015, doi:10.1016/j.pmatsci.2006.11.001.
123. Jaudouin, O.; Robin, J.J.; Lopez-Cuesta, J-M; Perrin, D.; Imbertb, C. Ionomer-Based Polyurethanes: A Comparative Study of Properties and Applications. Polym. Inter- Natl. Wiley **2012**, 4, 1–17, doi:10.1002/pi.4156.
124. Davletbaeva, I. M.; Sazonov, O. O.; Fazlyev, A. R.; Davletbaev, R. S. ; Efimov, S. V.; Klochkovc, V. Polyurethane Ionomers Based on Amino Ethers of: Ortho -Phosphoric Acid. RSC Adv. **2019**, 9, 18599, doi:10.1039/c9ra03636a.
125. Bullermann, J.; Spohnholz, R.; Friebel, S.; Salthammer, T. Synthesis and Characterization of Polyurethane Ionomers with Trimellitic Anhydride and Dimethylol Propionic Acid for Waterborne Self-Emulsifying Dispersions. J. Polym. Sci. Part A Polym. Chem. **2014**, 52, 680–690, doi:10.1002/pola.27049.
126. Honarkar, H. Waterborne Polyurethanes: A Review. J. Dispers. Sci. Technol. **2018**, 39, 507–516, doi:10.1080/01932691.2017.1327818.
127. Cakić, S.M.; Špírková, M.; Ristić, I.S.; B-Simendić, J.K.; M-Cincović, M.; Poręba, R. The Waterborne Polyurethane Dispersions Based on Polycarbonate Diol: Effect of Ionic Content. Mater. Chem. Phys. **2013**, 138, 277–285, doi:10.1016/j.matchemphys.2012.11.057.
128. García-Pacios, V.; Costa, V.; Colera, M.; Martín-Martínez, J.M. Waterborne Polyurethane Dispersions Obtained with Polycarbonate of Hexanediol Intended for Use as Coatings. Prog. Org. Coatings **2011**, 71, 136–146, doi:10.1016/j.porgcoat.2011.01.006.
129. Madbouly, S.A. Waterborne Polyurethane Dispersions and Thin Films: Biodegradation and Antimicrobial Behaviors. Molecules **2021**, 26, 961, doi.org/10.3390/molecules26040961.
130. Zhou, X.; Fang, C.; Chen, J.; Li, S.; Li, Y.; Lei, W. Correlation of Raw Materials and Waterborne Polyurethane Properties by Sequence Similarity Analysis. J. Mater. Sci. Technol. **2016**, 32, 687–694, doi:10.1016/j.jmst.2016.02.006.
131. Daniel 1980-, M.A. Polyurethane Binder Systems for Polymer Bonded Explosives. **2006**, DSTO-

GD-0492.
132. Laitar, Robert A, Gomez, E. Polyurethane Binder Compositions and Process for Their Preparation. European Patent, 1986. EU 0177871.
133. Bestuzheva, V. V.; Nalimova, N.K.; Tselinskii, I. V. Polyurethane Binders for Condensed High-Energy-Content Systems. Russ. J. Appl. Chem. **2001**, 74, 1551–1553, doi:10.1023/A:1013773622585.
134. Polyurethane Binders for Sports , Safety and Landscape Surfaces. The Dow Chemical Company Global, **2003**, 1-4.
135. Forrest, M.J. Chemical Characterisation of Polyurethanes.; United Kingdom: Rapra Technology Limited. **1999**, 9, 12, ISBN 088-3144.
136. Saunders, K.J. Polyurethanes. Organic Polymer Chemistry. In; Springer, Dordrecht, 1988, 358–387, ISBN 978-94-017-2506-4.
137. Burke, A., Hasirci, N. Polyurethanes in Biomedical Applications.2004, vol 553. Springer, Boston, MA, ISBN978-0-306-48584-8.
138. Kausar, A. Polyurethanes/Epoxy Interpenetrationg Polymer Network. In; ntechOpen, 2017, DOI: 10.5772/67678
139. Gooch, J.W. Urethane Polymers. Encycl. Dict. Polym. **2011**, 1937, 785–785, doi:10.1007/978-1-4419-6247-8_12399.
140. K. Janischewski and D. Reichel Aqueous Two Component Polyurethane Coatings, Preparation Thereof and Use Thereof. **2000**, U.S. Patent No. 6,048,926.
141. Petrović, Z.S.; Wan, X.; Bilić, O. Zlatanić, A.; Hong, J.; Javni, I.; Ionescu, M.; Milić, J.; Degruson, D. Polyols and Polyurethanes from Crude Algal Oil. JAOCS, J. Am. Oil Chem. Soc. **2013**, 90, 1073–1078, doi:10.1007/s11746-013-2245-9.
142. Segura, D.M.; Nurse, A.D.; McCourt, A.; Phelps,R.; Segura A. Chemistry of Polyurethane Adhesives and Sealants. In Handbook of Adhesives and Sealants; Elsevier Ltd, 2005; pp. 101–162 ISBN 9780080445540.
143. Frisch, K.C. Chemistry and Technology Ofpolyurethane Adhesives. In Adhesion Science and Engineering; Elsevier B.V., 2002; pp. 759–812 ISBN 9780444511409.
144. Chattopadhyay, D.K.; Raju K.V.S.N. Structural Engineering of Polyurethane Coatings for High Performance Applications. Prog. Polym. Sci. **2007**, 32, 352–418, doi:10.1016/j.progpolymsci.2006.05.003.
145. Li, S.; Xu, C.; Yang, W.; Tang, Q. Thermoplastic Polyurethanes Stemming from Castor Oil: Green Synthesis and Their Application in Wood Bonding. Coatings **2017**, 7, 159, doi:10.3390/coatings7100159.
146. Lee, W-J.; Lin, M-S. Preparation and Application of Polyurethane Adhesives Made from Polyhydric Alcohol Liquefied Taiwan Acacia and China Fir. J. Appl. Polym. Sci. **2008**, 109, 23–31, doi:10.1002/app.
147. Dutta, S.; Karak,N. Synthesis, Characterization of Poly(Urethane Amide) Resins from Nahar Seed Oil for Surface Coating Applications. Prog. Org. Coatings **2005**, 53, 147–152, doi:10.1016/j.porgcoat.2005.02.003.
148. Deng, R.; Davies, P.; Bajaj, A.K. Flexible Polyurethane Foam Modelling and Identification of Viscoelastic Parameters for Automotive Seating Applications. J. Sound Vib. **2003**, 262, 391–417, doi:10.1016/S0022-460X(03)00104-4.
149. Elliott, A. N. A. Automotive Application of Polymers II.i Smithers Rapra Publishing, 1991, 5, ISBN 9780080417455.
150. Murakami, S.; Saiki, K.; Hayashi, M.; Satou, T.; Fukami, T. A Newly Developed MDI-Based Polyurethane Flexible Foam for Automotive Seat Cushion Having Both Superior Static and Dynamic Properties. J. Cell. Plast. **2001**, 37, 249–261, doi:10.1106/TA7J-5UMG-XA00-WRJQ.
151. Barkoula, N.M.; Alcock, B.; Cabrera, N.O.; Peijs, T. Flame-Retardancy Properties of Intumescent Ammonium Poly(Phosphate) and Mineral Filler Magnesium Hydroxide in Combination with Graphene. Polym. Polym. Compos. **2008**, 16, 101–113, doi:10.1002/pc.
152. Panaitescu, I.; Koch, T.; Archodoulaki, V.M. Accelerated Aging of a Glass Fiber/Polyurethane Composite for Automotive Applications. Polym. Test. **2019**, 74, 245–256, doi:10.1016/j.polymertesting.2019.01.008.
153. Zdrahala, R.J.; Zdrahala, I. J. Biomedical Applications of Polyurethanes: A Review of Past

Promises, Present Realities, and a Vibrant Future. J. Biomater. Appl. **1999**, 14, 67–90, doi:org/10.1177/0885328299014001.
154. Pivec, T.; Sfiligo. S. M.; Gašparič, P.; Kleinschek, K.S. Polyurethanes for Medical Use. Tekstilec **2017**, 60, 182–197, doi:10.14502/tekstilec2017.60.182-197.
155. Naeem, M.; cao, J.; choi, M.; Kim, W.S.; Moon, H.R.; lee, B.L.; Kim, M-S.; Jung, Y.; Yoo, J-W. Enhanced Therapeutic Efficacy of Budesonide in Experimental Colitis with Enzyme/PH Dual-Sensitive Polymeric Nanoparticles. Colloids Surfaces B Biointerfaces **2015**, 10, 4565–4580, doi:10.1016/j.colsurfb.2014.09.026.
156. Vermette, P.; Griesser, H. J.; Laroche, G.; Guidoin, R. Biomedical Applications of Polyurethanes; 2001; ISBN 158706023X.
157. Wang, Y.; Hong, Q.; Chen, Y.; Lian, X.; Xiongb, Y. Surface Properties of Polyurethanes Modified by Bioactive Polysaccharide-Based Polyelectrolyte Multilayers. Colloids Surfaces B Biointerfaces **2012**, 100, 77–83, doi:10.1016/j.colsurfb.2012.05.030.
158. Davis, F.J.; Mitchell, G.R. Polyurethane Based Materials with Applications in Medical Devices. Bio-Materials Prototyp. Appl. Med. **2008**, 27–48, doi:10.1007/978-0-387-47683-4_3.
159. Akita, S.; Akino, K.; Imaizumi, T.; Tanaka, K.; Anraku, K.; Yano, H.; A. Hirano, A. A Polyurethane Dressing Is Beneficial for Split-Thickness Skin-Graft Donor Wound Healing. Burns **2006**, 32, 447–451, doi:10.1016/j.burns.2005.11.015.
160. Alferiev, I.S.; Connolly, J.M.; Stachelek, S.J.; Ottey, A.; Rauova, L.; Levy, R.J. Surface Heparinization of Polyurethane via Bromoalkylation of Hard Segment Nitrogens. Biomacromolecules **2006**, 7, 317–322, doi:10.1021/bm0506694.
161. Wang W, Wang C. Polyurethane for Biomedical Applications: A Review of Recent Developments. Elsevier Masson SAS, **2012**, doi:org/10.1533/9781908818188.115.
162. Guan, J.; Fujimoto, K. L.; Sacks, M. S.; Wagnera,W.R. Preparation and Characterization of Highly Porous, Biodegradable Polyurethane Scaffolds for Soft Tissue Applications. Biomaterials **2005**, 26, 3961–3971, doi:10.1016/j.biomaterials.2004.10.018.
163. Yamaoka, T.; Makita, Y.; Sasatani, H.; Kim, S.I.; Kimura, Y. Linear Type Azo-Containing Polyurethane as Drug-Coating Material for Colon-Specific Delivery: Its Properties, Degradation Behavior, and Utilization for Drug Formulation. J. Control. Release **2000**, 66, 187–197, doi:10.1016/S0168-3659(99)00270-9.
164. Raza, Z.A.; Rehman, A.; Masood, R. Polyurethane Based Finishing of Cotton Fabric for Imparting Multifunctional Properties by Using Central Composite Design. Pigment Resin Technol. **2016**, 45, 444–449, doi:10.1108/PRT-11-2015-0110.
165. Cardamone, J.M. Reacting Cotton Cellulose with Lignin-Based Polyurethane. Text. Res. J. **1992**, 62, 371–381, doi:10.1177/004051759206200702.
166. Polyurethanes for Textile Coating. **2018**, Impraperm for MVP textile coating.
167. Xinrong, S.; Nanfang, W.; Kunyang, S.; Sha, D.; Zhen, C. Synthesis and Characterization of Waterborne Polyurethane Containing UV Absorption Group for Finishing of Cotton Fabrics. J. Ind. Eng. Chem. **2014**, 20, 3228–3233, doi:10.1016/j.jiec.2013.12.003.
168. Muzaffar, S.; Bhatti, I.A.; Zuber, M.; Bhatti, H.N.; Shahid, M. Synthesis, Characterization and Efficiency Evaluation of Chitosan-Polyurethane Based Textile Finishes. Int. J. Biol. Macromol. **2016**, 93, 145–155, doi:10.1016/j.ijbiomac.2016.08.068.
169. Mazzon, G.; Zahid, M.; Heredia-Guerrero, J.A.; Balliana, E.; Zendri, E.; Athanassiou, A.; Bayer, I.S. Hydrophobic Treatment of Woven Cotton Fabrics with Polyurethane Modified Aminosilicone Emulsions. Appl. Surf. Sci. **2019**, 490, 331–342, doi:10.1016/j.apsusc.2019.06.069.
170. Wang, H.H.; Gen, C.T. Synthesis of Anionic Water-Borne Polyurethane with the Covalent Bond of a Reactive Dye. J. Appl. Polym. Sci. **2002**, 84, 797–805, doi:10.1002/app.10336.
171. Evrard, P.D. and G. Accelerated Ageing of Polyurethanes for Marine Applications. Polym. Degrad. Stab. **2007**, 92, 1455–1464, doi:10.1016/j.polymdegradstab.2007.05.016.
172. Xiao, P.; Dudal, Y.; Corvini, P.F.X.; Pieles, U.; Shahgaldian, P. Cyclodextrin-Based Polyurethanes Act as Selective Molecular Recognition Materials of Active Pharmaceutical Ingredients (APIs). Polym. Chem. **2011**, 2, 1264–1266, doi:10.1039/c1py00114k.
173. Covered, T.; Resins, E.; Resins, P. Epoxy and Polyurethane Coating Systems for Marine Applications. **2020**,1–5.

174. Makama, Z.; Doble, I.; Nicolson, D.; Webb, M.E.; Beech, I.B.; Campbell, S.A.; Smith, J.R. Surface Preparation of Stainless Steel 316L, Bronze CW451K and Titanium Ti6Al4V for Bonding to Polyurethane in Marine Cable Connector Assemblies. Trans. Inst. Met. Finish. **2011**, 89, 237–243, doi:10.1179/174591911X13125496893308.
175. Nasiri, S.; Alizadeh, N. Synthesis and Adsorption Behavior of Hydroxypropyl-β-Cyclodextrin-Polyurethane Magnetic Nanoconjugates for Crystal and Methyl Violet Dyes Removal from Aqueous Solutions. RSC Adv. **2019**, 9, 24603–24616, doi:10.1039/c9ra03335a.
176. Joseph, J. The Durability of Polyurethane Protective Coatings for Sub-Marine Applications. **2019**, Dissertation, University of Portsmouth.
177. Chin, Y.P.; Mohamad, S.; Radzi, M.; Abas, B. Removal of Parabens from Aqueous Solution Using β-Cyclodextrin Cross-Linked Polymer. OPEN ACCESS Int. J. Mol. Sci **2010**, 11, 11, doi:10.3390/ijms11092459.
178. Olszewski, A.; Kosmela, P.; Piszczyk, Ł. Synthesis and Characterization of Biopolyols through Biomass Liquefaction of Wood Shavings and Their Application in the Preparation of Polyurethane Wood Composites. Eur. J. Wood Wood Prod. **2022**, 80, 57–74, doi:10.1007/s00107-021-01755-6.
179. Chen, Y.H.; Wu, C.H.; Chen, Y.C. Optimized Condition for Eco-Friendly Wood Composites Manufactured from Castor Oil-Based Polyurethane. Constr. Build. Mater. **2021**, 306, 124789, doi:10.1016/j.conbuildmat.2021.124789.
180. Shaaban, A.; Se, S.M.; Ibrahim, I.M.; Ahsan, Q. Preparation of Rubber Wood Sawdust-Based Activated Carbon and Its Use as a Filler of Polyurethane Matrix Composites for Microwave Absorption. Xinxing Tan Cailiao/New Carbon Mater. **2015**, 30, 167–175, doi:10.1016/S1872-5805(15)60182-2.
181. Olszewski, A.; Kosmela, P.; Piszczyk, Ł. A Novel Approach in Wood Waste Utilization for Manufacturing of Catalyst-Free Polyurethane-Wood Composites (PU-WC). Sustain. Mater. Technol. **2023**, 36, e00619, doi:10.1016/j.susmat.2023.e00619.
182. Zhang, R.; Dai, H.; Smith, G.D. Investigation of the High Temperature Performance of a Polyurethane Adhesive Used for Structural Wood Composites. Int. J. Adhes. Adhes. **2022**, 116, 102882, doi:10.1016/j.ijadhadh.2021.102882.
183. Lashkaripour, A. Introduction to Quantum Chemistry : The Schrödinger Equation. **2021**.
184. Galler, A.; Canfield, J.; Freericks, J.K. Schrödinger's Original Quantum-Mechanical Solution for Hydrogen. Eur. J. Phys. **2021**, 42, doi:10.1088/1361-6404/abb9ff.
185. Kozlowski, M. The Schrödinger Equation A History. Phys. Institute, Maria Skłodowska-Curie Univ. Lublin , Pol. **2019**, 1-70.
186. Luis Levada, C.; Maceti, H.; Lautenschleguer, I.J.; Levada, C.L. Review of the Schrödinger Wave Equation. IOSR J. Appl. Chem. (IOSR-JAC **2018**, 11, 1–07, doi:10.9790/5736-1104010107.
187. Petrosyan, P.L.· D. Fundamentals OfQuantum Optics and Quantum Information; 2016; ISBN 2013206534.
188. Tamás Veszprémi, M.F. Quantum Chemistry: Fundamentals to Applications; Springer Science & Business Media, 2012; ISBN 1461541891, 9781461541899.
189. Sherrill, D. A Brief Review of Elementary Quantum Chemistry. Sch. Chem. Biochem. Georg. Inst. Technol. **2001**, 2017-1.
190. Sherrill, C.D. An Introduction to Hartree-Fock Molecular Orbital Theory. Sch. Chem. Biochem. Georg. Inst. Technol. **2000**, 1–8.
191. Gardner, M.; Wheeler, J.A. Quantum Theory and Measurement. 1979, 842, ISBN 9780691641027.
192. Fern, F.M. The Born-Oppenheimer Approximation. **2019**, doi:10.13140/RG.2.2.21650.91840.
193. Cancès, E.; Defranceschi, M.; Kutzelnigg, W.; Le Bris, C.; Maday, Y. Computational Quantum Chemistry: A Primer. Handb. Numer. Anal. **2003**, 10, 3–270, doi:10.1016/S1570-8659(03)10003-8.
194. Young, D.C. Computational Chemistry: A Practical Guide for Applying Techniques to Real-World Problems.**2001**, 9, ISBN 0471333689.
195. Leszczynski, J. Handbook of Computational Chemistry; illustrate.; Springer Science & Business Media, 2102; ISBN 9400707118, 9789400707115.

196. Dykstra, C.; Frenking, G.; Kim, K.; Scuseria, G. Theory and Applications of Computational Chemistry: The First Forty Years; 2005, ISBN 978-0-444-51719-7.
197. Jensen, F. Introduction to Computational Chemistry; John Wiley & Sons Ltd, 2007; ISBN ISBN: 978-0-470-05804-6.
198. Einstein, A. The Concept of the Potential Energy Surface; Springer, Boston, MA, 2004; ISBN 9789048138623.
199. Ptáček, P.; Šoukal,F.Š.; Opravil,T. Introduction to the Transition State Theory. In Introducing the Effective Mass of Activated Complex and the Discussion on the Wave Function of this Instanton; IntechOpen, 2018; Vol. 11, p. 13 ISBN 0000957720.
200. Schlegel, H.B. Exploring Potential Energy Surfaces for Chemical Reactions : An Overview of Some Practical Methods. **2003**, 5–7.
201. Corchado, J.C. Constructing Potential Energy Surfaces for Polyatomic Systems: Recent Progress and New Problems. **2012**, doi:10.1155/2012/164752.
202. Foresman, J.B.; Frisch, A.Exploring Chemistry with Electronic Structure Methods Third Edition. **2015**, Gaussian Inc.ISBN: 978-1-935522-03-4.
203. Hill, T.L. An Introduction to Statistical Thermodynamics; Dover Publications, **1987**; ISBN 978-0486652429.
204. Sethna, J.P. Entropy, Order Parameters, and Complexity. **2021**, Laboratory of Atomic and Solid State Physics, Cornell University, Ithaca, NY 14853-2501
205. Moeller, T.; Bailar Jr, J-C.; Kleinberg, J.; Guss, C-O.; Castellion, M-E.; Metz, C. Thermochemistry. Chemistry, With Inorganic Qualitative Analysis. **1980**, 119-136, doi:org/10.1016/B978-0-12-503350-3.50010-X
206. Sőzbilir, M. Students ' Ideas and Misunderstandings of Enthalpy and Spontaneity : A Review of Selected Researches. Hacettepe Üniversitesi E¤itim Fakültesi Dergisi 26, **2004**, 155-159.
207. Eyube, E.S.; Notani, P.P.; Samaila, H. Analytical Prediction of Enthalpy and Gibbs Free Energy of Gaseous Molecules. Chem. Thermodyn. Therm. Anal. **2022**, 6, 100060, doi:10.1016/j.ctta.2022.100060.
208. Kenny B. Lipkowitz, Thomas R. Cundari, D.B.B. Reviews in Computational Chemistry; John Wiley & Sons, Inc, 2008; ISBN 9780470388396.
209. Lewars, E.G. Computational Chemistry; Springer International Publishing Switzerland, 2016; ISBN 9783319309149.
210. Lipkowitz, Kenny, D.B.B. Computational Chemistry Keviews in Computational Chemistry; John Wiley & Sons, Inc., 1996; Vol. I; ISBN 1560816198.
211. Hehre, W.J.; Radom, L.; Schleyer, P. V-R. Pople, J.. Ab Initio Molecular Orbital Theory. Wiley, **1986**, 576, ISBN 978-0-471-81241-8.
212. Moshinsky, M. How Good Is the Hartree-Fock Approximation. **1993**, 52, 52–53, doi:10.1119/1.1974410.
213. Hantsch, F.C.. The Hartree – Fock Equations in Quantum Mechanics. Dissertation, University of Stuttgart, **2012**, doi:org/10.18419/opus-5082
214. Umeno, Y.; Pokluda, J. Progress in Materials Science Ab Initio Calculations of Mechanical Properties : Methods and Applications. **2015**, 73, 127–158, doi:10.1016/j.pmatsci.2015.04.001.
215. Bartlett, R.J.; Stanton, J.F. Applications of Post-Hartree-Fock Methods : A Tutorial. In Reviews in Computational Chemistry; VCH Publishers, Inc. New York, 1994; Vol. V, pp. 65–169.
216. Shikano, Y.; Watanabe, H.C.; Nakanishi, K.M.; Ohnishi, Y. Post-Hartree–Fock Method in Quantum Chemistry for Quantum Computer. Eur. Phys. J. Spec. Top. **2021**, 230, 1037–1051, doi:10.1140/epjs/s11734-021-00087-z.
217. Marsman, M.; Grüneis, A.; Paier, J.; Kresse, G.; Marsman, M.; Grüneis, A.; Paier, J.; Kresse, G. Second-Order Møller – Plesset Perturbation Theory Applied to Extended Systems . I . Within the Projector-Augmented-Wave Formalism Using a Plane Wave Basis Set Second-Order Møller – Plesset Perturbation Theory Applied to Extended Systems . I . Within the P. **2010**, 184103, 0–10, doi:10.1063/1.3126249.
218. Bishop, R.F.; Kümmel,H.G. The Coopled-Closter Method. Phys. Today **1987**, 40, 52–60, doi:10.1063/1.881103.
219. Bartlett, R. J.; Musiał, M. Coupled-Cluster Theory in Quantum Chemistry. Rev. Mod. Phys. **2007**, 79, 291–352, doi:10.1103/RevModPhys.79.291.

220. Hohenbergt, P.; Kohn,W. Inhomogeneous Electron Gaa. Phys. Rev. **1964**, 136, B864, doi:10.1103/PhysRev.136.B864.
221. Sholl, D.S.; Steckel, J.A. Density Functional Theory. A Practical Introduction; John Wiley & Sons, Inc, 2009; ISBN 9780470447710.
222. Cohen, A.J.; Mori-s, P.; Yang, W. Challenges for Density Functional Theory. **2012**, 289–320, doi:org/10.1021/cr200107z
223. Parr, R.G. Density Functional Theory. Ann. Rev. Phys. Cher **1983**, 34, 631–656, doi:org/10.1146/annurev.pc.34.100183.003215
224. Armiento, R. The Many-Electron Energy in Density Functional Theory, Royal Institute of Technology in Stockholm, 2005, ISBN: 9171781501.
225. Burke, K. Perspective on Density Functional Theory. J. Chem. Phys. **2012**, 150901, 150901, doi:10.1063/1.4704546.
226. Sousa, S.F.; Fernandes, P. A.; Ramos, M .J. General Performance of Density Functionals. . Phys. Chem. A 2007, 111, 42, 10439–10452, doi:org/10.1021/jp0734474.
227. Perdew, J.P.; Schmidt, K.; Perdew, J.P.; Schmidt, K. Jacob ' s Ladder of Density Functional Approximations for the Exchange- Correlation Energy. **2013**, 1, doi:10.1063/1.1390175.
228. Slater, J. C. A Simplificationof the Hartree-Fock Method. Phys. Rev. **1951**, 81, 385, DOI:https://doi.org/10.1103/PhysRev.81.385.
229. Palafox, M.A. DFT Computations on Vibrational Spectra : Scaling Procedures to Improve the Wavenumbers Abstract : Phys. Sci. Rev. **2018**, doi:10.1515/psr-2017-0184.
230. Perdew, J. P.; Tao, J.; Staroverov, V. N.; Scuseria,G.E. Meta-Generalized Gradient Approximation : Explanation of a Realistic Nonempirical Density Functional. J. Chem. Phys. **2004**, 120, 6898–6911, doi:10.1063/1.1665298.
231. Perdew, J.P.; Yue, W. Accurate and Simple Density Functional for the Electronic Exchange Energy: Generalized Gradient Approximation. **1986**, 33, 12–14.
232. Becke, A.D. Density-Functional Thermochemistry. III. The Role of Exact Exchange. J. Chem. Phys. **1993**, 98, 5648–5652, doi:10.1063/1.464913.
233. Peng, H.; Yang, Z.; Perdew, J.P.; Sun, J. Versatile van Der Waals Density Functional Based on a Meta-Generalized Gradient Approximation. **2016**, 041005, 1–15, doi:10.1103/PhysRevX.6.041005.
234. Nakamura, K.; Oshiyama, A. Comparative Study of Hybrid Functionals Applied to Structural and Electronic Properties of Semiconductors and Insulators. **2014**, doi:10.1103/PhysRevB.84.075205.
235. Zhao, Y.; Truhlar, D.G. The M06 Suite of Density Functionals for Main Group Thermochemistry , Thermochemical Kinetics , Noncovalent Interactions , Excited States , and Transition Elements : Two New Functionals and Systematic Testing of Four M06-Class Functionals and 12 Other Fun. **2008**, 215–241, doi:10.1007/s00214-007-0310-x.
236. Kohn, W.; Becke, A.D.; Parr, R.G. Density Functional Theory of Electronic Structure. **1996**, 0, 12974–12980, doi:10.1021/jp960669l.
237. Becke, A.D. A New Mixing of Hartree-Fock and Local Density-Functional Theories. J. Chem. Phys. **1993**, 98, 1372–1377, doi:10.1063/1.464304.
238. Perlt, E. ed. Basis Sets in Computational Chemistry; Springer Cham, **2021**; ISBN 9783030672614.
239. Lipkowitz, K.B.;Boyd, D.B. eds. Reviews in Computational Chemistry; VCH, **1995**., ISBN 9780470399545.
240. Ramachandran, K. I. ; Gopakumar, D.; Namboori, K. Computational Chemistry and Molecular Modeling; Springer Berlin, Heidelberg, **2008**; ISBN 9783540773047.
241. Davidson, E.R.; Feller, D. Basis set selection for molecular calculations. Chemical Reviews. **1986**, 1;86(4):681-96, doi:org/10.1021/cr00074a002.
242. Rassolov, V.A.; Ratner, M.A.; Pople, J.A.; Redfern, P.C.; Curtiss, L.A. 6-31G ∗ Basis Set for Third-Row Atoms. Wiley, **2001**, 22, 976–984, doi:org/10.1002/jcc.1058
243. Schäfer, A.; Horn, H.; Ahlrichs, R. Fully Optimized Contracted Gaussian Basis Sets for Atoms Li to Kr. **1992**, 2571, doi:10.1063/1.463096.
244. Weigenda, F.; Ahlrichsb, R. Balanced Basis Sets of Split Valence, Triple Zeta Valence and Quadruple Zeta Valence Quality for H to Rn: Design and Assessment of Accuracy. Phys. Chem.

Chem. Phys., **2005**,7, 3297-3305, doi:org/10.1039/B508541A.
245. Weber, R.; Wilson, A.K. Do Composite Methods Achieve Their Target Accuracy ? Comput. Theor. Chem. **2015**, 1072, 58–62, doi:10.1016/j.comptc.2015.08.015.
246. Redfern, P.C. Gaussian-3 ( G3 ) Theory for Molecules Containing First- and Second-Row Atoms. **2014**, 3, doi:10.1063/1.477422.
247. Bachrach, S.M. Computational Organic Chemistry. 2nd Edition John Wiley & Sons, Inc, **2007**; ISBN 9780471713425.
248. Szori, M.; Abou-Abdo, T.; Fittschen, C.; Csizmadia, I.G.; Viskolcz, B. Allylic Hydrogen Abstraction II. H-Abstraction from 1,4 Type Polyalkenes as a Model for Free Radical Trapping by Polyunsaturated Fatty Acids (PUFAs). Phys. Chem. Chem. Phys. **2007**, 9, 1931–1940, doi:10.1039/b613048h.
249. Waleed, H. Q.; Viskolcz, B.; Fejes, Z.; Fiser, B. Urethane Formation in the Presence of 2 , 2-Dimorpholinodiethylether ( DMDEE ) and 1 , 4-Dimethylpiperazine ( DMP ) – A Combined Experimental and Theoretical Study. Comput. Theor. Chem. **2023**, 1221, 114045, doi:10.1016/j.comptc.2023.114045.
250. Waleed, H.Q.; Pecsmány, D.; Csécsi, M.; Farkas, L.; Viskolcz, B.; Fejes, Z.; Fiser, B. Experimental and Theoretical Study of Cyclic Amine Catalysed Urethane Formation. Polmers **2022**, 14, 2859, doi:https://doi.org/10.3390/polym14142859.
251. Waleed, H.Q.; Hadjadj, R.; Viskolcz, B.; Fiser, B. Effect of Morpholine, and 4-Methylmorpholine on Urethane Formation: A Computational Study. Sci. Rep. **2023**, 13, 1–8, doi:10.1038/s41598-023-44492-x.
252. Waleed, H. Q.; Csécsi, M.; Konyhás, V.; Boros, Z. R. ; Viskolcz, B.; Fejes, Z.; Fiser, B. Aliphatic Tertiary Amine Catalysed Urethane Formation – a Combined Experimental and Theoretical Study. Phys. Chem. Chem. Phys **2022**, 24, 20538, doi:10.1039/D2CP00728B.
253. Waleed, H. Q.; Csécsi, M.; Hadjadj, R.; Thangaraj, R.; Pecsmány, D.; Owen, M.; Szőri, M.; Fejes, Z.; Viskolcz, B.; Fiser, B. Computational Study of Catalytic Urethane Formation. Polymers (Basel). **2022**, 14, 1–11, doi:10.3390/polym14010008.
254. Waleed, H. Q.; Csécsi, M.; Hadjadj, R.; Thangaraj, R.; Owen, M.; Szőri, M.; Fejes, Z.; Viskolcz, B.; Fiser, B. The Catalytic Effect of DBU on Urethane Formation – A Computational Study. Mater. Sci. Eng. **2021**, 46, 70–77, doi:http://doi.org/10.32974/mse.2021.008 THE.
255. M. J. Frisch, et al Gaussian 09, Revision E.01 **2013**.
256. Chai, J. Da; Head-Gordon, M. Long-Range Corrected Hybrid Density Functionals with Damped Atom-Atom Dispersion Corrections. Phys. Chem. Chem. Phys. **2008**, 10, 6615–6620, doi:10.1039/b810189b.
257. Ditchfield, R.; Hehre, W.J.; Pople, J.A. Self-Consistent Molecular-Orbital Methods. IX. An Extended Gaussian-Type Basis for Molecular-Orbital Studies of Organic Molecules. J. Chem. Phys. **1971**, 54, 720–723, doi:10.1063/1.1674902.
258. Rassolov, V.A.; Pople, J.A.; Ratner, M.A.; Windus, T.L. 6-31G* Basis Set for Atoms K through Zn. J. Chem. Phys. **1998**, 109, 1223–1229, doi:10.1063/1.476673.
259. Petersson, G.A.; Bennett, A.; Tensfeldt, T.G.; Al-Laham, M.A.; Shirley, W.A.; Mantzaris, J. A Complete Basis Set Model Chemistry. I. The Total Energies of Closed-Shell Atoms and Hydrides of the First-Row Elements. J. Chem. Phys. **1988**, 89, 2193–2218, doi:10.1063/1.455064.
260. Szori, M.; Fittschen, C.; Csizmadia, I.G.; Viskolcz, B. Allylic H-Abstraction Mechanism: The Potential Energy Surface of the Reaction of Propene with OH Radical. J. Chem. Theory Comput. **2006**, 2, 1575–1586, doi:10.1021/ct600140b.
261. Izsák, R.; Szori, M.; Knowles, P.J.; Viskolcz, B. High Accuracy Ab Initio Calculations on Reactions of OH with 1-Alkenes. The Case of Propene. J. Chem. Theory Comput. **2009**, 5, 2313–2321, doi:10.1021/ct900133v.
262. Janoschek, R.; Rossi, M.J. Thermochemical Properties of Free Radicals from G3MP2B3 Calculations. Int. J. Chem. Kinet. **2002**, 34, 550–560, doi:10.1002/kin.10082.
263. Wada, G.; Tamura, E.; Okina, M. ; Nakamura, M. On the Ratio of Zwitterion Form to Uncharged Form of Glycine at Equilibrium in Various Aqueous Media. Bull. Chem. Soc. Jpn. **1982**, 55, 3064–3067, doi.org/10.1246/bcsj.55.3064
264. Fiser, B.; Jojart, B.; Szőri, M.; Lendvay, G.; Csizmadia, I. G.; Viskolcz, B. Glutathione as a Prebiotic Answer to α-Peptide Based Life. J. Phys. Chem. B, **2015**, 119, 3940–3947,

doi:10.1021/jp511582m.
265. Zhang, J.; Zhang, H.; Wu, T.; Wang, Q.; Spoel, D.V.D. Comparison of Implicit and Explicit Solvent Models for the Calculation of Solvation Free Energy in Organic Solvents. J. Chem. Theory Comput. **2017**, 13, 1034–1043, doi:10.1021/acs.jctc.7b00169.
266. Tomasi, J.; Mennucci, B.; Cammi, R. Quantum Mechanical Continuum Solvation Models. Chem. Rev. **2005**, 105, 2999–3093, doi:10.1021/cr9904009.
267. Norjmaa, G.; Ujaque, G.; Lledós, A. Beyond Continuum Solvent Models in Computational Homogeneous Catalysis. Top. Catal. **2022**, 65, 118–140, doi:10.1007/s11244-021-01520-2.
268. Onufriev, A. Implicit Solvent Models in Molecular Dynamics Simulations: A Brief Overview. Annu. Rep. Comput. Chem. **2008**, 4, 125–137, doi:10.1016/S1574-1400(08)00007-8.
269. Rivail, G.M. and J.L. Solvent Effects in Quantum Chemistry. In Handbook of Computational Chemistry; Springer Science+Business Media B.V., 2017; pp. 727–739 ISBN 9783319272825.
270. Marenich, A. V.; Cramer, C.J.; Truhlar, D.G. Universal Solvation Model Based on Solute Electron Density and on a Continuum Model of the Solvent Defined by the Bulk Dielectric Constant and Atomic Surface Tensions. J. Phys. Chem. B **2009**, 113, 6378–6396, doi:10.1021/jp810292n.
271. Cossi, M.; Barone, V.; Cammi, R.; Tomasi, J. Ab Initio Study of Solvated Molecules: A New Implementation of the Polarizable Continuum Model. Chem. Phys. Lett. **1996**, 255, 327–335, doi:10.1016/0009-2614(96)00349-1.
272. Pliego, J. R.J.; Riveros, J.M. Hybrid Discrete-Continuum Solvation Methods. Wiley Interdiscip. Rev. Comput. Mol. Sci. **2020**, 1–25, doi:10.1002/wcms.1440.
273. Simm, G. N.; Türtscher, P. L.; Reiher, M.R. Systematic Microsolvation Approach with a Cluster-Continuum Scheme and Conformational Sampling. J. Comput. Chem. **2020**, 1–12, doi:10.1002/jcc.26161.
274. Anandakrishnan, R.; Drozdetski, A.; Walker, R.C.; Onufriev, A. V. Speed of Conformational Change: Comparing Explicit and Implicit Solvent Molecular Dynamics Simulations. Biophys. J. **2015**, 108, 1153–1164, doi:10.1016/j.bpj.2014.12.047.
275. Bordado, . L. Silva and J. C. Recent Developments in Polyurethane Catalysis: Catalytic Mechanisms Review. Catal. Rev. - Sci. Eng. **2004**, 46, 31–51, doi:10.1081/CR-120027049.
276. Beran, R.; Zarybnicka, L.; Machova, D. Recycling of Rigid Polyurethane Foam: Micro-Milled Powder Used as Active Filler in Polyurethane Adhesives. J. Appl. Polym. Sci. **2020**, 137, 1–11, doi:10.1002/app.49095.
277. Chuayjuljit, S.; Maungchareon, A.; SARAVARI, O. Preparation and Properties of Palm Oil-Based Rigid Polyurethane Nanocomposite Foams. J. Reinf. Plast. Compos. **2010**, 29, 218–225, doi:10.1177/0731684408096949.
278. Liyanage, .P. Samarappuli and I N. M. V. K. Evaluation of the Suitability of 1, 4-Dimethylpiperazine as a Substitute Catalyst in Polyurethane Foam Production. Moratuwa Eng. Res. Conf. Eval. **2018**, 282–287, doi:10.1109/MERCon.2018.8421986.
279. Raden, D.S.; Weiner, M.A.; Hill, D. W. Catalyst Combination for Polyurethanes. US Patent, US4141862A, **1972**.
280. El Ghobary, H.; Muller, L. Process for Preparing Polyurethane Foam. US Patent, US6395796B1, 2000.
281. NIST Chemistry WebBook Available online: https://webbook.nist.gov/chemistry/ (accessed on 13 April 2021).
282. Hunter, E. P. L.; Lias, S. G.Evaluated Gas Phase Basicities and Proton Affinities of Molecules : An Update. J. Phys. Chem. Ref. Data **1998**, 27, 413–656, doi:org/10.1063/1.556018.
283. Schwetlick, K.; Noack, R . Kinetics and Catalysis of Consecutive Isocyanate Reactions. Formation of Carbamates, Allophanates and Lsocyanurates. J. Chem. Soc., Perkin Trans **1995**, 2, 395–402, doi:org/10.1039/P29950000395.
284. PU Catalyst DMDEE ( 2,2-Dimorpholinodiethylether ) Cas No 6425-39-4 Manufacturer - Sinocure Chemical Group Available online: https://www.sinocurechem.com/product/synocat-dmdee/ (accessed on 12 December 2022).
285. N,n'-DIMETHYLPIPERAZINE Available online: http://www.chemicalland21.com/specialtychem/perchem/n,n'-DIMETHYLPIPERAZINE.htm (accessed on 13 December 2022).

286. Some Organic Solvents, Resin Monomers and Related Compounds, Pigments and Occupational Exposures in Paint Manufacture and Painting, IARC Working Group on the Evaluation of Carcinogenic Risks to Humans, Lyon, **1988**, ISBN 92 832 1247 9.
287. Https://Www.Ccdc.Cam.Ac.Uk/Solutions/about-the-Csd/.
288. Oswald, I. D. H., Motherwell, W. D. S. & Parsons, S. Acta crystallogr. Sect. B Struct. Sci. 61, 46, 2005..
289. Emamian, S.R.; Domingo, L.R.; Tayyari, S.F. Tautomerism in Pyridazin-3(2H)-One: A Theoretical Study Using Implicit/Explicit Solvation Models. J. Mol. Graph. Model. **2014**, 49, 47–54, doi:10.1016/j.jmgm.2014.01.006.

# Appendix

**Urethane formation reactions of phenyl isocyanate and methanol without and in the presence of amine catalysts**

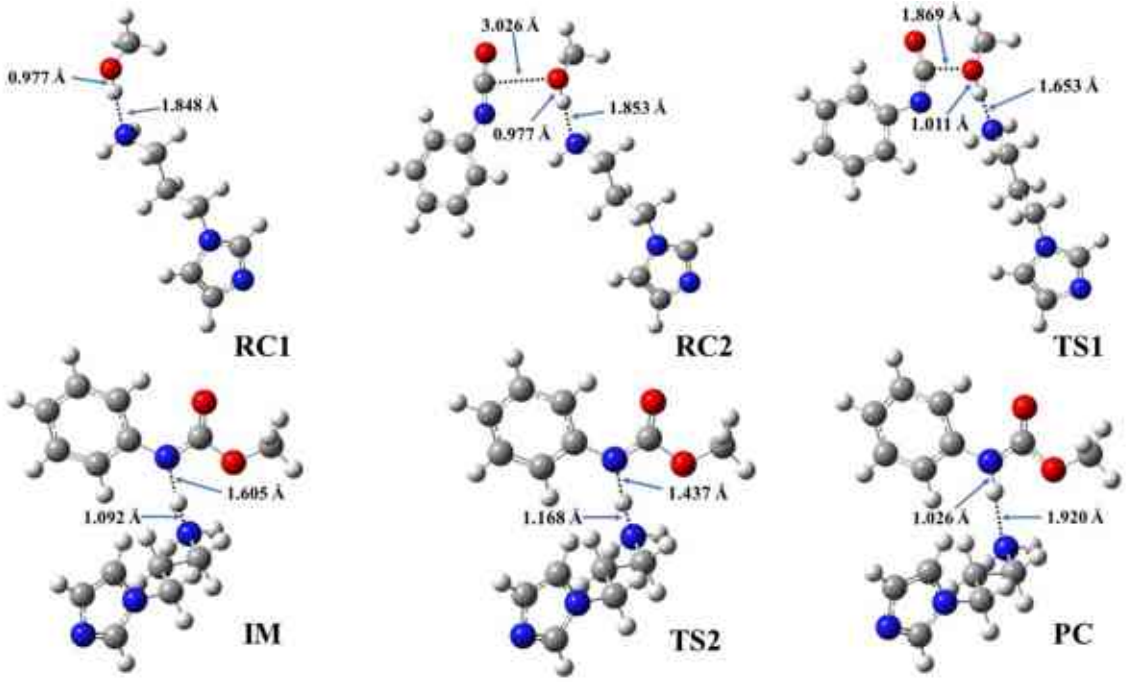


***Figure A1.*** *Optimized structures along the reaction pathway between phenyl isocyanate (PhNCO) and methanol in the presence of 1-(3-aminopropyl)imidazole (APIM) calculated at the BHandHLYP/6-31G(d) level of theory in acetonitrile at 298.15 K and 1 atm. RC – reactant complex, TS – transition state, IM – intermediate, PC – product complex.*

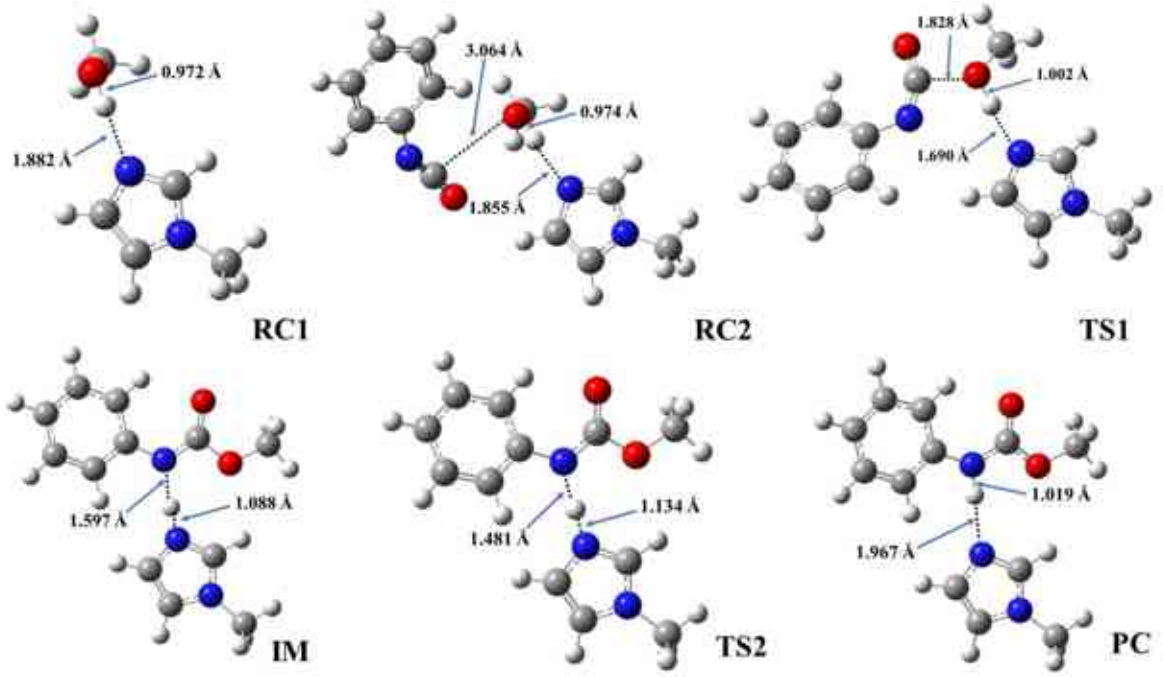


***Figure A2.*** *Optimized structures along the reaction pathway between phenyl isocyanate (PhNCO) and methanol in the presence of 1-methylimidazole (1-MIM) calculated at the BHandHLYP/6-31G(d) level of theory in acetonitrile at 298.15 K and 1 atm. RC – reactant complex, TS – transition state, IM – intermediate, PC – product complex.*

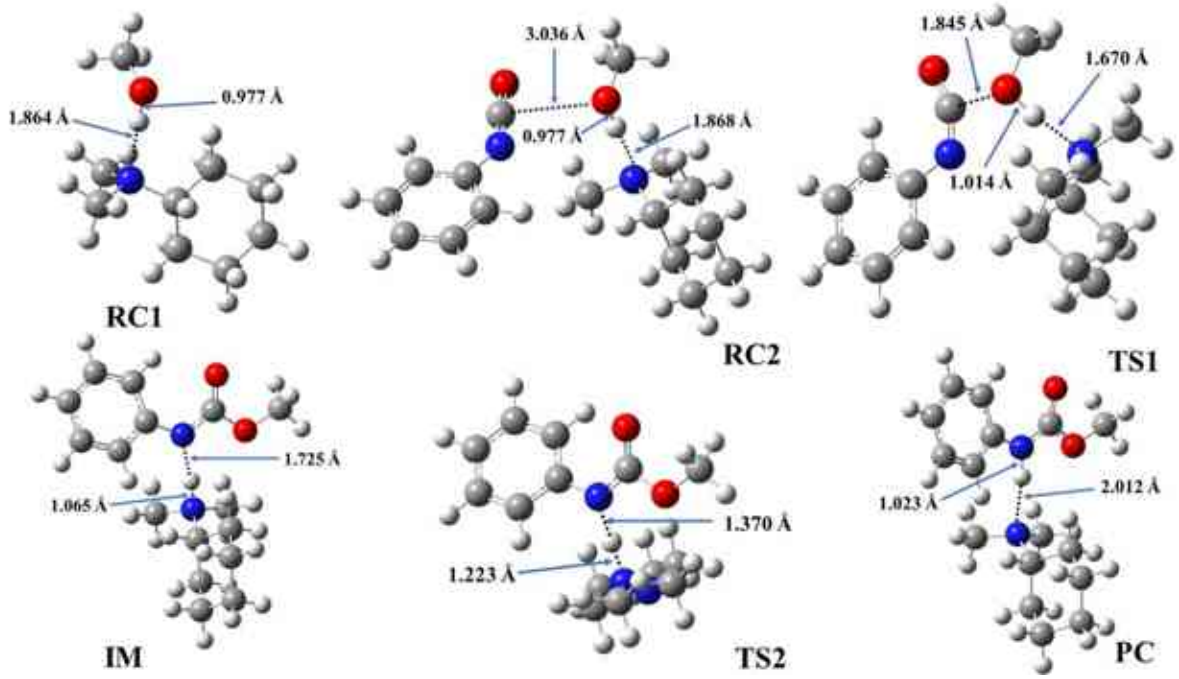


***Figure A3.*** *Optimized structures along the reaction pathway between phenyl isocyanate (PhNCO) and methanol in the presence of N,N-dimethylcyclohexanamine (DMCHA) calculated at the BHandHLYP/6-31G(d) level of theory in acetonitrile at 298.15 K and 1 atm. RC – reactant complex, TS – transition state, IM – intermediate, PC – product complex.*

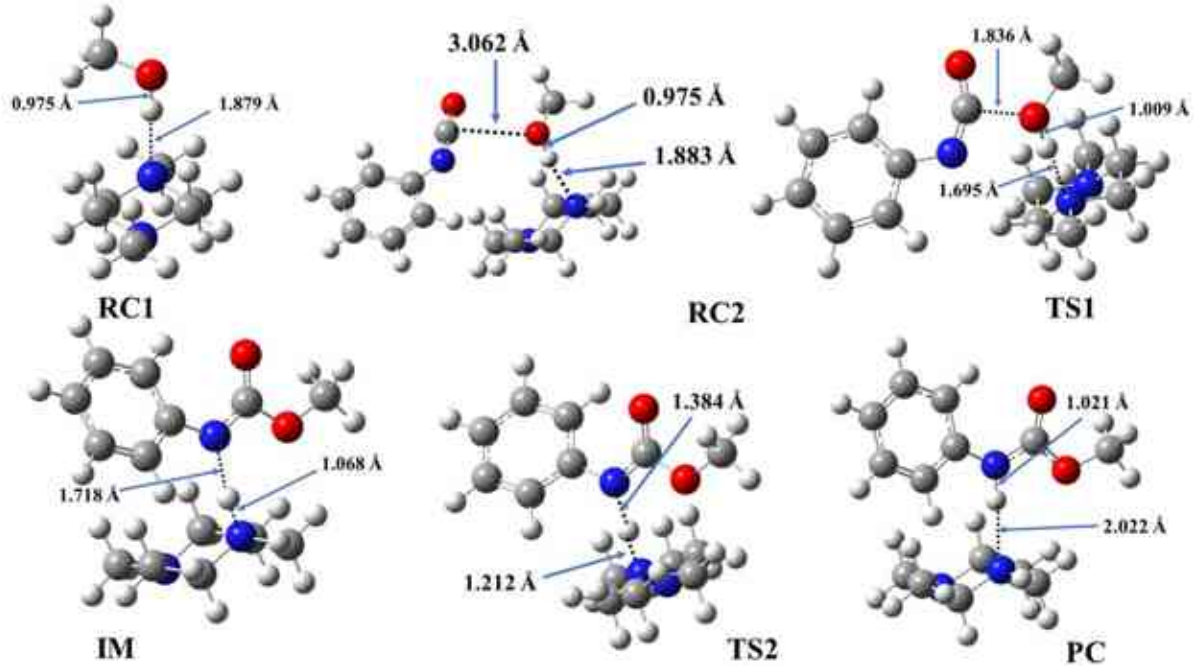


***Figure A4.*** *Optimized structures along the reaction pathway between phenyl isocyanate (PhNCO) and methanol in the presence of 1,4-dimethylpiperazine (DMP) calculated at the BHandHLYP/6-31G(d) level of theory in acetonitrile at 298.15 K and 1 atm. RC – reactant complex, TS – transition state, IM – intermediate, PC – product complex.*

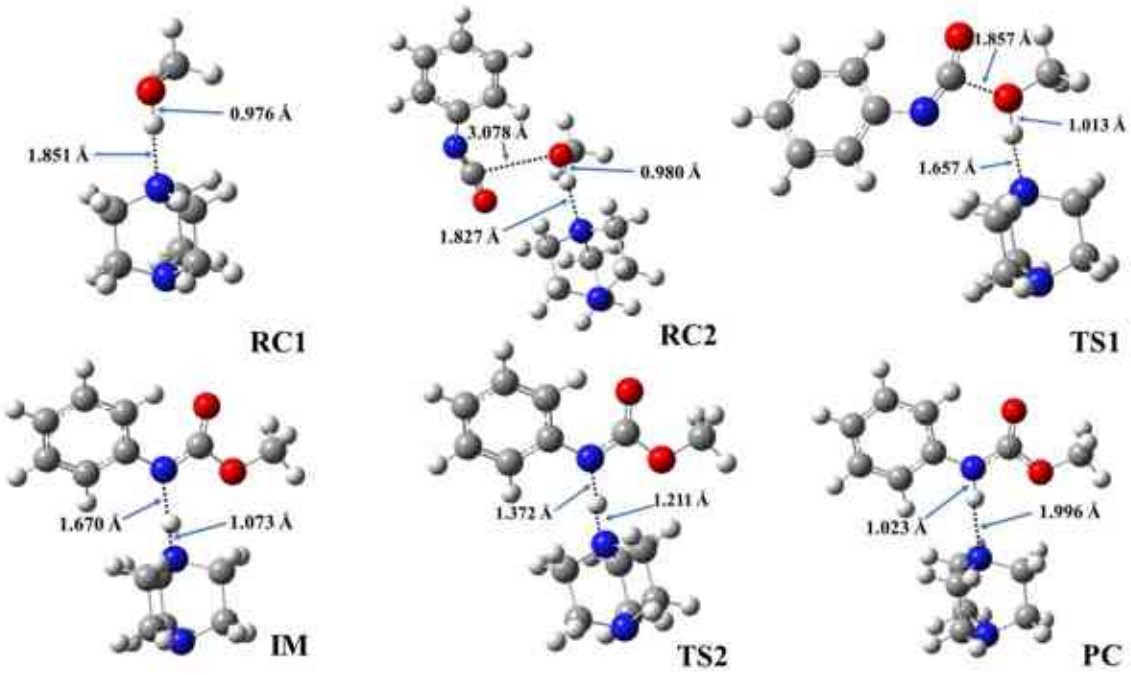


***Figure A5.*** *Optimized structures along the reaction pathway between phenyl isocyanate (PhNCO) and methanol in the presence of 1,4-diazabicyclo[2.2.2]octane (DABCO) calculated at the BHandHLYP/6-31G(d) level of theory in acetonitrile at 298.15 K and 1 atm. RC – reactant complex, TS – transition state, IM – intermediate, PC – product complex.*

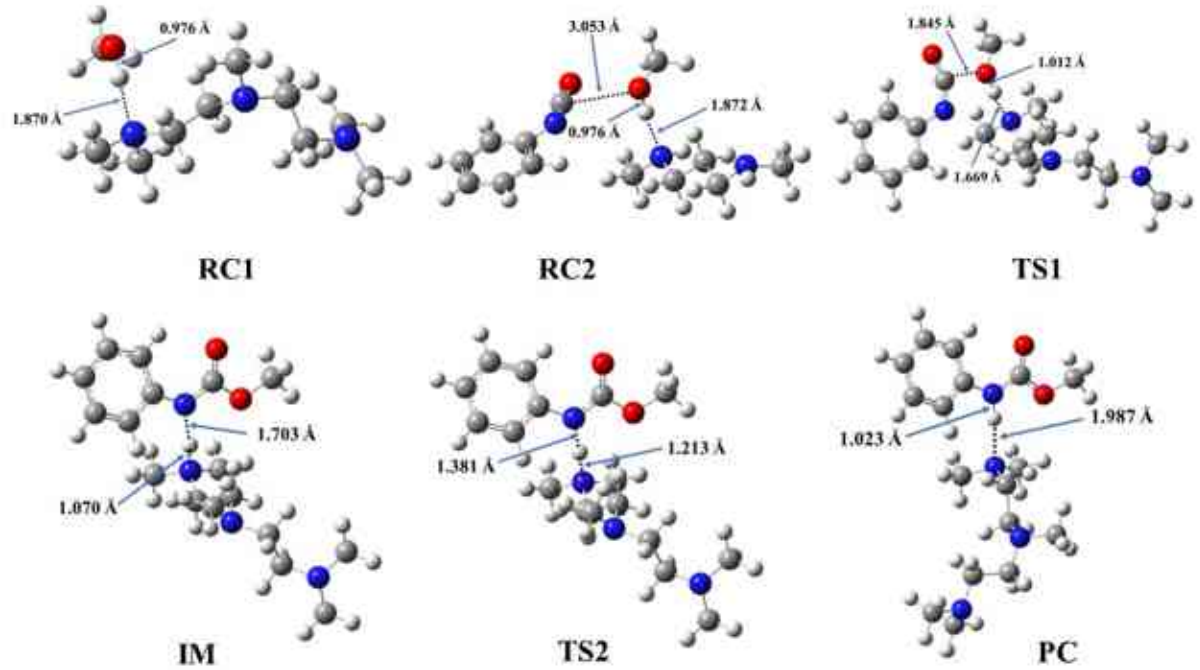


***Figure A6.*** *Optimized structures along the reaction pathway between phenyl isocyanate (PhNCO) and methanol in the presence of N,N,N',N",N"–pentamethyldiethylenetriamine (PMDETA) calculated at the BHandHLYP/6-31G(d) level of theory in acetonitrile at 298.15 K and 1 atm. RC – reactant complex, TS – transition state, IM – intermediate, PC – product complex.*

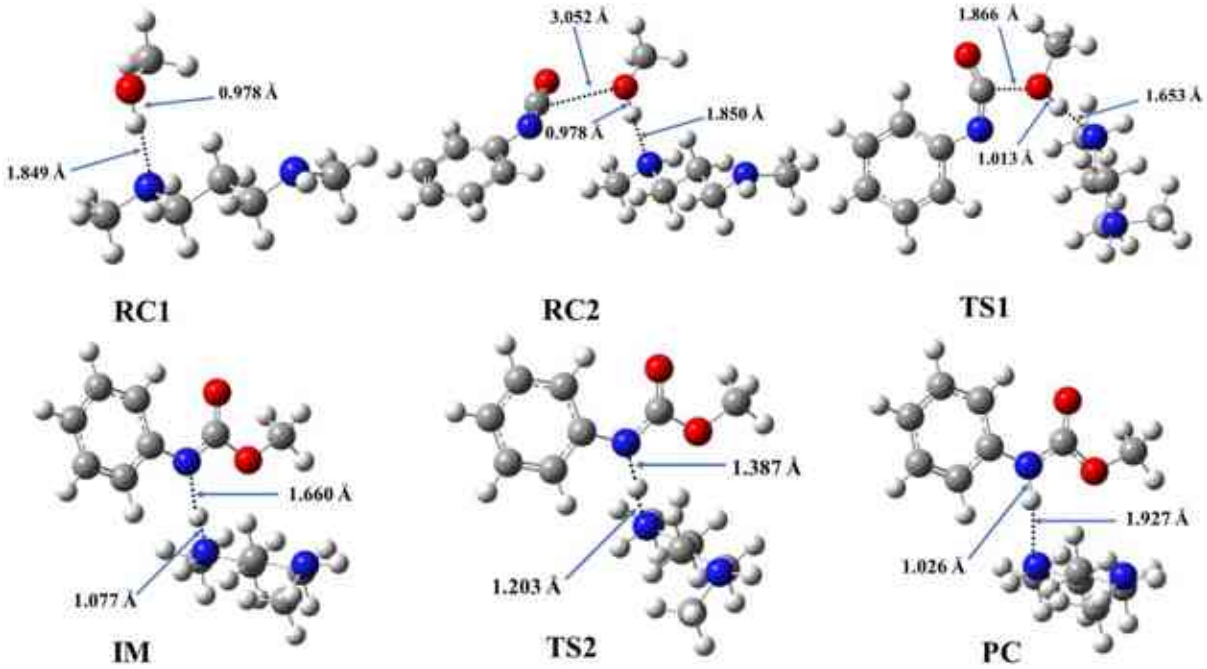


***Figure A7.*** *Optimized structures along the reaction pathway between phenyl isocyanate (PhNCO) and methanol in the presence of N,N-dimethyl-1,3-propanediamine (DMPDA) calculated at the BHandHLYP/6-31G(d) level of theory in acetonitrile at 298.15 K and 1 atm. RC – reactant complex, TS – transition state, IM – intermediate, PC – product complex.*

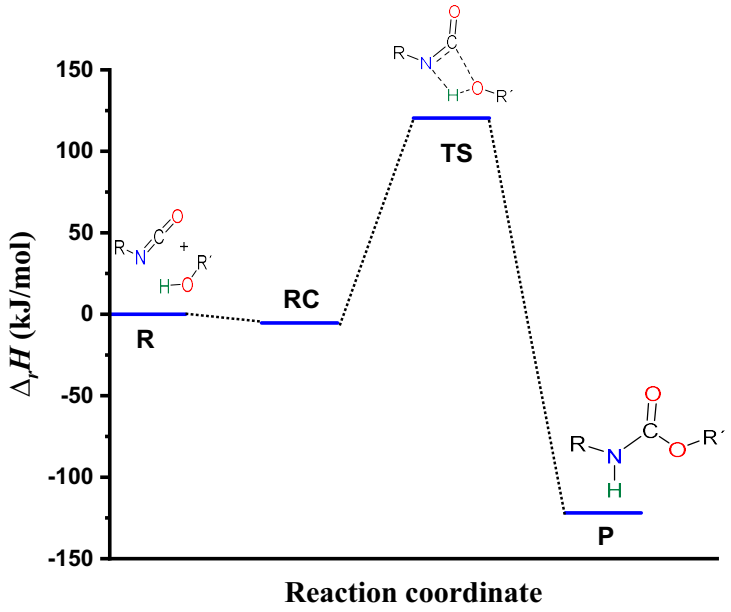


***Figure A8.*** *Energy profile (relative enthalpy, $\Delta_r H$) of the phenyl isocyanate (PhNCO) and methanol reaction calculated at the BHandHLYP/6-31G(d) level of theory in acetonitrile using the SMD implicit solvent model at 298.15 K and 1 atm.*

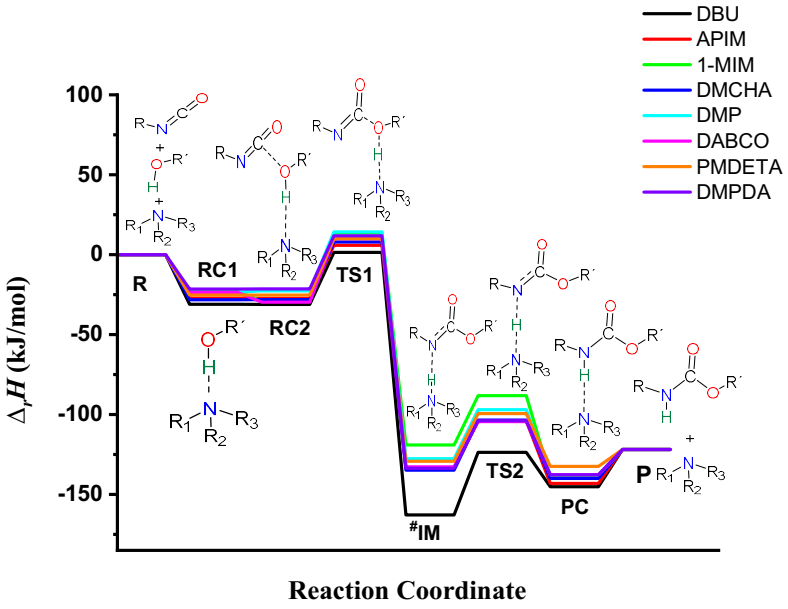


***Figure A9.*** *Energy profile (relative enthalpy, $\Delta_r H$) of the catalyzed urethane formation reactions calculated at the BHandHLYP/6-31G(d) level of theory in acetonitrile using the SMD implicit solvent model at 298.15 K and 1 atm.*

***Table A1.*** *Computed and measured proton affinities (**PA**) in kJ/mol. The calculations have been carried out at the BHandHLYP level of theory in gas phase at 298.15 K and 1 atm.* ***$RNH_2$, $R_2NH$, $R_3N$,*** *and* ***$R_2C$=N-R****: primary, secondary, tertiary amines, and secondary ketimine, respectively. •side, •• middle amine group.*

| Catalysts | $PA_{calc}$ | | | | $PA_{exp}$[281] |
|---|---|---|---|---|---|
| | $RNH_2$ | $R_2NH$ | $R_3N$ | $R_2C$=N-R | |
| **DBU** | - | - | 916.7 | 1065.4 | - |
| **APIM** | 898.5 | 987.5 | 776.3 | - | - |
| **1-MIM** | - | 975.8 | 760.6 | - | 959.6 |
| **DMCHA** | - | - | 983.5 | - | 983.6 |
| **DMP** | - | - | 969.9 | - | - |
| **DABCO** | - | - | 972.4 | - | 963.4 |
| **PMDETA** | - | - | 969.3•<br>965.1•• | - | - |
| **DMPDA** | - | 954.0 | - | - | 1035.2 |

***Table A2.*** *Zero-point corrected relative energies ($\Delta_r E_0$), relative enthalpies ($\Delta_r H$), and relative Gibbs free energies ($\Delta_r G$) of the species in the reaction between phenyl isocyanate (PhNCO) and methanol with and without catalysts, calculated at the BHandHLYP/6-31G(d) level of theory in acetonitrile using the SMD implicit solvent model at 298.15 K and 1 atm. R – reactant, RC – reactant complex, TS – transition state, IM – intermediate, PC – product complex, P – product.*

**$\Delta_r E_0$ (kJ/mol)**

| | R | RC1 | RC2 | TS1 | IM | TS2 | PC | P |
|---|---|---|---|---|---|---|---|---|
| **Catalyst-free system** | 0.00 | - | -9.36’ | 121.87 | - | - | - | -120.67 |
| **DBU** | 0.00 | -31.81 | -37.43 | -0.19 | -125.23 | -123.51 | -146.44 | -120.67 |
| **APIM** | 0.00 | -28.22 | -33.55 | 4.45 | -94.59 | -102.39 | -143.83 | -120.67 |
| **1-MIM** | 0.00 | -24.06 | -35.61 | 12.35 | -80.63 | -86.60 | -140.27 | -120.67 |
| **DMCHA** | 0.00 | -28.72 | -34.24 | 6.51 | -96.81 | -102.68 | -140.90 | -120.67 |
| **DMP** | 0.00 | -24.13 | -29.11 | 12.99 | -89.53 | -96.15 | -138.47 | -120.67 |
| **DABCO** | 0.00 | -24.51 | -36.02 | 8.56 | -94.99 | -104.00 | -138.83 | -120.67 |
| **PMDETA** | 0.00 | -26.16 | -31.66 | 8.88 | -91.15 | -98.69 | -133.29 | -120.67 |
| **DMPDA** | 0.00 | -22.03 | -27.77 | 10.72 | -95.35 | -102.65 | -138.53 | -120.67 |

**$\Delta_r H$ (kJ/mol)**

| | R | RC1 | RC2 | TS1 | IM | TS2 | PC | P |
|---|---|---|---|---|---|---|---|---|
| **Catalyst-free system** | 0.00 | - | -5.32’ | 120.36 | - | - | - | -121.89 |
| **DBU** | 0.00 | -31.03 | -31.09 | 1.41 | -124.70(-162.80#) | -123.70 | -145.15 | -121.89 |
| **APIM** | 0.00 | -27.28 | -27.39 | 5.87 | -95.06(-133.16#) | -103.95 | -143.10 | -121.89 |
| **1-MIM** | 0.00 | -22.90 | -29.10 | 13.55 | -80.95(-119.05#) | -88.19 | -138.95 | -121.89 |
| **DMCHA** | 0.00 | -28.24 | -28.14 | 7.90 | -96.69(-134.79#) | -103.52 | -140.04 | -121.89 |
| **DMP** | 0.00 | -23.37 | -22.60 | 14.21 | -89.50(-127.60#) | -97.02 | -137.66 | -121.89 |
| **DABCO** | 0.00 | -23.60 | -29.75 | 9.99 | -94.64(-132.74#) | -104.39 | -137.64 | -121.89 |
| **PMDETA** | 0.00 | -25.32 | -25.32 | 10.01 | -91.16(-129.26#) | -99.41 | -132.46 | -121.89 |
| **DMPDA** | 0.00 | -21.49 | -21.46 | 11.83 | -95.54(-133.64#) | -103.89 | -137.78 | -121.89 |

**$\Delta_r G$ (kJ/mol)**

| | R | RC1 | RC2 | TS1 | IM | TS2 | PC | P |
|---|---|---|---|---|---|---|---|---|
| **Catalyst-free system** | 0.00 | - | 27.84’ | 171.78 | - | - | - | -71.72 |
| **DBU** | 0.00 | 7.60 | 44.58 | 93.02 | -28.85(-53.75#) | -26.12 | -54.47 | -71.72 |
| **APIM** | 0.00 | 5.95 | 45.17 | 92.13 | 1.39(-23.51#) | -6.63 | -53.18 | -71.72 |
| **1-MIM** | 0.00 | 10.95 | 40.93 | 104.40 | 17.23(-7.67#) | 11.13 | -50.86 | -71.72 |
| **DMCHA** | 0.00 | 12.92 | 47.73 | 100.66 | 2.46(-22.44#) | -0.61 | -44.01 | -71.72 |
| **DMP** | 0.00 | 14.71 | 49.51 | 106.38 | 9.17(-15.73#) | 5.09 | -42.77 | -71.72 |
| **DABCO** | 0.00 | 11.75 | 43.16 | 99.51 | 1.35(-23.55#) | -6.74 | -46.93 | -71.72 |
| **PMDETA** | 0.00 | 11.06 | 47.71 | 103.40 | 7.30(-17.60#) | 1.10 | -38.48 | -71.72 |
| **DMPDA** | 0.00 | 15.49 | 46.44 | 101.26 | -0.19(-25.09#) | -4.74 | -46.91 | -71.72 |

’RC for catalyst-free reaction. # Corrected relative enthalpy and relative Gibbs free energies calculated according to ref[251,263,264].

***Table A3.*** *Zero-point corrected relative energies ($\Delta_r E_0$), and relative Gibbs free energies ($\Delta_r G$) of the species in the reaction between phenyl isocyanate (PhNCO) and methanol with and without catalysts, calculated at the G3MP2BHandHLYP level of theory in acetonitrile using the SMD implicit solvent model at 298.15 K and 1 atm. Cat. – catalyst, R – reactant, RC – reactant complex, TS – transition state, IM – intermediate, PC – product complex, P – product.*

| | $\Delta_r E_0$ (kJ/mol) | | | | | | | |
|---|---|---|---|---|---|---|---|---|
| | **R** | **RC1** | **RC2** | **TS1** | **IM** | **TS2** | **PC** | **P** |
| **Catalyst-free system** | 0.00 | - | −8.22’ | 120.18 | - | - | - | −90.33 |
| **DBU** | 0.00 | −27.43 | −40.71 | −2.20 | −112.98 | −116.72 | −125.14 | −90.33 |
| **APIM** | 0.00 | −16.27 | −25.95 | 17.72 | −74.79 | −82.97 | −111.38 | −90.33 |
| **1-MIM** | 0.00 | −19.99 | −29.04 | 16.33 | −65.63 | −72.68 | −112.74 | −90.33 |
| **DMCHA** | 0.00 | −26.81 | −38.76 | −1.96 | −99.90 | −109.55 | −125.82 | −90.33 |
| **DMP** | 0.00 | −25.77 | −38.73 | 3.84 | −92.55 | −103.27 | −123.31 | −90.33 |
| **DABCO** | 0.00 | −25.85 | −37.16 | 2.85 | −92.53 | −103.34 | −120.54 | −90.33 |
| **PMDETA** | 0.00 | −26.88 | −39.61 | −1.08 | −96.15 | −106.49 | −116.42 | −90.33 |
| **DMPDA** | 0.00 | −19.03 | −30.45 | 9.63 | −88.89 | −97.52 | −117.25 | −90.33 |
| | $\Delta_r G$ (kJ/mol) | | | | | | | |
| | **R** | **RC1** | **RC2** | **TS1** | **IM** | **TS2** | **PC** | **P** |
| **Catalyst-free system** | 0.00 | - | 28.99’ | 170.09 | - | - | - | -41.38 |
| **DBU** | 0.00 | 11.97 | 41.31 | 91.02 | -16.60(-41.50#) | -19.33 | -33.17 | -41.38 |
| **APIM** | 0.00 | 17.91 | 52.76 | 105.40 | 21.19(-3.71#) | 12.79 | -20.74 | -41.38 |
| **1-MIM** | 0.00 | 15.02 | 47.50 | 108.38 | 32.23(7.33#) | 25.05 | -23.33 | -41.38 |
| **DMCHA** | 0.00 | 14.97 | 43.36 | 92.34 | -0.50(-25.40#) | -7.34 | -28.79 | -41.38 |
| **DMP** | 0.00 | 13.07 | 39.88 | 97.22 | 6.15(-18.75#) | -2.04 | -27.61 | -41.38 |
| **DABCO** | 0.00 | 10.41 | 42.02 | 93.80 | 3.80(-21.10#) | -6.07 | -28.64 | -41.38 |
| **PMDETA** | 0.00 | 11.83 | 41.26 | 94.94 | 3.80(-21.10#) | -5.20 | -20.12 | -41.38 |
| **DMPDA** | 0.00 | 18.64 | 43.92 | 100.33 | 6.42(-18.48#) | 0.55 | -25.48 | -41.38 |

’RC for catalyst-free reaction. # Corrected relative enthalpy and relative Gibbs free energies calculated according to ref.[179], [259], [260].

**Urethane formation reactions of phenyl isocyanate and butan-1-ol without and in the presence of cyclic amine catalysts**

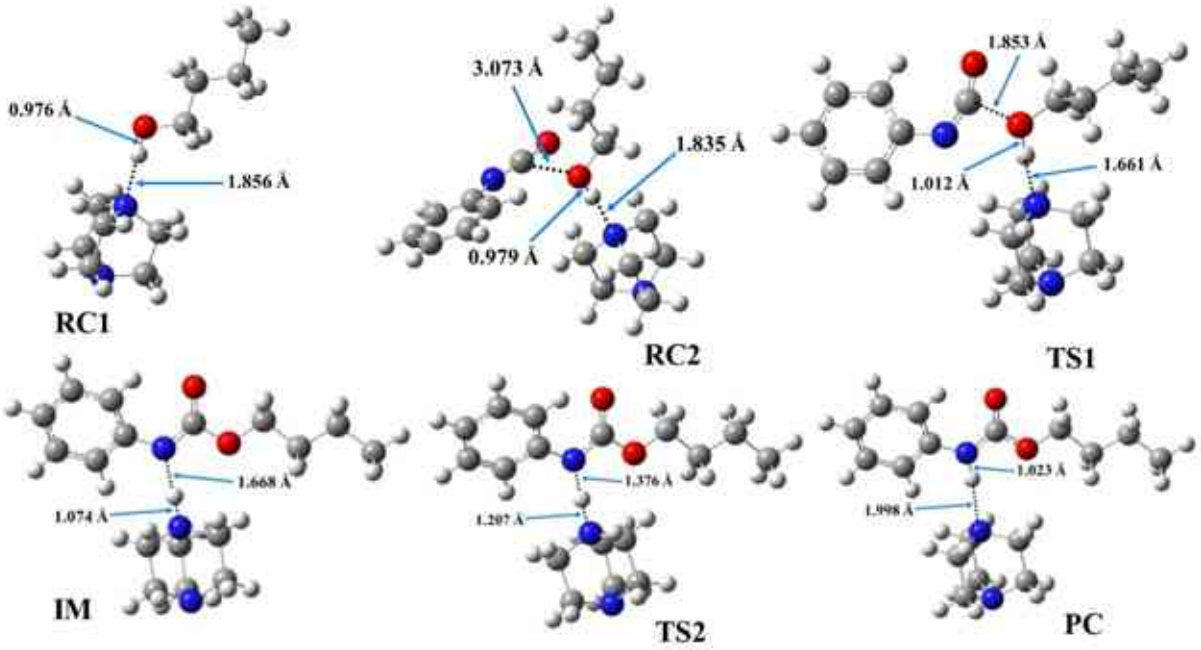


***Figure B1.*** *Optimized structures along the reaction pathway between phenyl isocyanate and butan-1-ol in the presence of 1,4-diazabicyclo[2.2.2]octane (DABCO) catalyst, calculated at the BHandHLYP/6-31G(d) level of theory in acetonitrile at 298.15 K and 1 atm. RC—reactant complex, TS—transition state, IM—intermediate, and PC—product complex.*

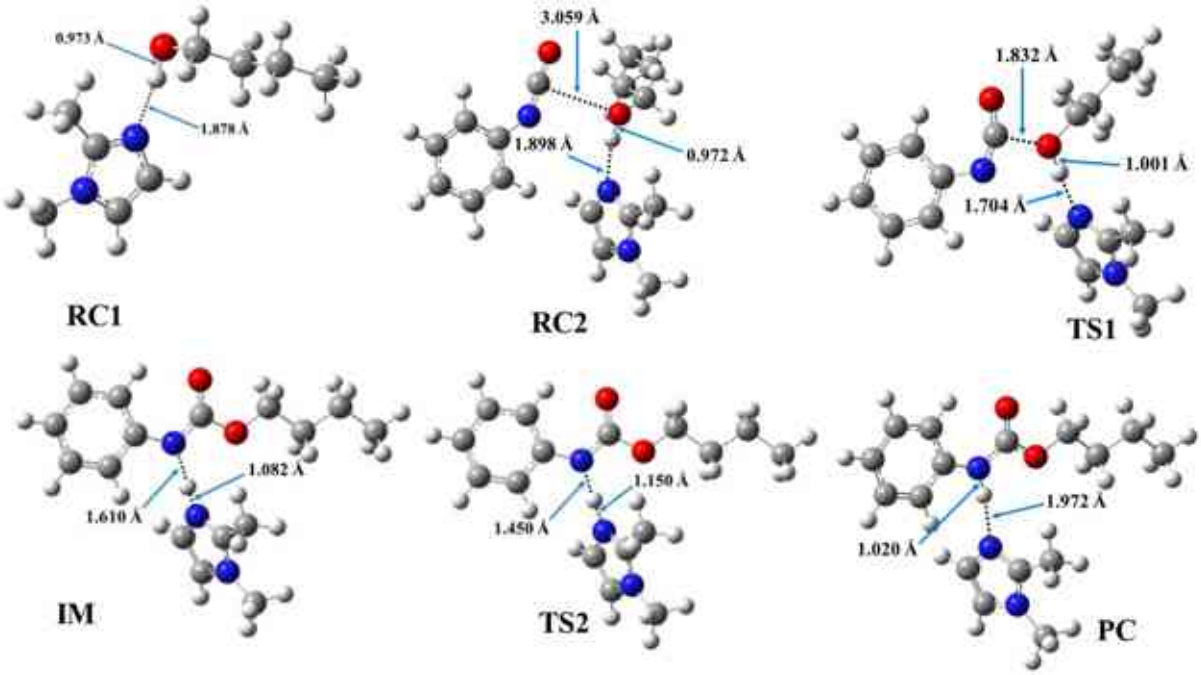


***Figure B2.*** *Optimized structures along the reaction pathway between phenyl isocyanate and butan-1-ol in the presence of 1,2-dimethylimidazole (1,2-DMI) catalyst, calculated at the BHandHLYP/6-31G(d) level of theory in acetonitrile at 298.15 K and 1 atm. RC—reactant complex, TS—transition state, IM—intermediate, and PC—product complex.*

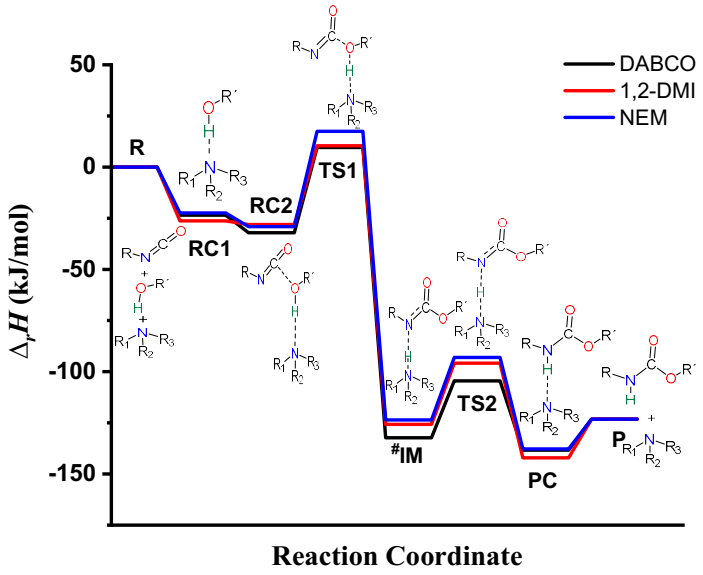


***Figure B3.*** *Energy profile (zero-point corrected, $\Delta E_0$) of the studied catalyzed urethane formation reactions calculated at the BHandHLYP/6-31G(d) level of theory in acetonitrile using the SMD implicit solvent model at 298.15 K and 1 atm.*

***Table B1.*** *Zero-point corrected relative energies ($\Delta_r E_0$), and relative Gibbs free energies ($\Delta_r G$) of the reaction between phenyl isocyanate and butan-1-ol in the presence of the studied catalysts, 1,4-diazabicyclo[2.2.2]octane (DABCO), 1,2-dimethylimidazole (1,2-DMI), and N-ethylmorpholine (NEM), calculated at the G3MP2BHandHLYP level of theory in acetonitrile using the SMD implicit solvent model at 298.15 K and 1 atm. R—reactant; RC—reactant complex; TS—transition state; IM—intermediate; PC—product complex; P—product.*

| | $\Delta_r E_0$ (kJ/mol) | | | | | | | |
|---|---|---|---|---|---|---|---|---|
| | **R** | **RC1** | **RC2** | **TS1** | **IM** | **TS2** | **PC** | **P** |
| **Catalyst-free system** | 0.0 | - | −11.2’ | 119.1 | - | - | - | −92.6 |
| **DABCO** | 0.0 | −26 | −46.6 | −0.9 | −96.2 | −107.6 | −124.7 | −92.6 |
| **1,2-DMI** | 0.0 | −21.8 | −33.5 | 7.2 | −78.4 | −86.9 | −119.9 | −92.6 |
| **NEM** | 0.0 | −28.7 | −49.1 | −0.2 | −95.9 | −106 | −132.2 | −92.6 |
| | $\Delta_r G$ (kJ/mol) | | | | | | | |
| | **R** | **RC1** | **RC2** | **TS1** | **IM** | **TS2** | **PC** | **P** |
| **Catalyst-free system** | 0.0 | - | 28.9’ | 170 | - | - | - | −41.5 |
| **DABCO** | 0.0 | 14.5 | 28 | 91.5 | 2.2(-22.7#) | −6.9 | −28.8 | −41.5 |
| **1,2-DMI** | 0.0 | 19.5 | 46.7 | 103.1 | 19.7(-5.2#) | 14.9 | −24.6 | −41.5 |
| **NEM** | 0.0 | 13.3 | 34.6 | 100.7 | 9.1(-15.8#) | −0.9 | −33.9 | −41.5 |

’RC for catalyst-free reaction. # Corrected relative Gibbs free energies calculated according to ref.[179], [259], [260].

***Table B2.*** *Zero-point corrected relative energies ($\Delta_r E_0$), relative enthalpies ($\Delta_r H$), and relative Gibbs free energies ($\Delta_r G$), of the reaction between phenyl isocyanate and butan-1-ol in presence of the studied catalysts, 1,4-diazabicyclo[2.2.2]octane (DABCO), 1,2-dimethylimidazole (1,2-DMI), and N-ethylmorpholine (NEM), calculated at the BHandHLYP/6-31G(d) level of theory in acetonitrile using the SMD implicit solvent model at 298.15 K and 1 atm. R – reactant, RC – reactant complex, TS – transition state, IM – intermediate, PC – product complex, P – product.*

| $\Delta_r E_0$ (kJ/mol) | | | | | | | | |
|---|---|---|---|---|---|---|---|---|
| | **R** | **RC1** | **RC2** | **TS1** | **IM** | **TS2** | **PC** | **P** |
| **Catalyst-free system** | 0.0 | - | -10.5’ | 122.8 | - | - | - | -120.9 |
| **DABCO** | 0.0 | -24.1 | -37.2 | 9.5 | -93.5 | -102.9 | -138.4 | -120.9 |
| **1,2-DMI** | 0.0 | -27.6 | -32.1 | 10.4 | -87.3 | -94.2 | -142.4 | -120.9 |
| **NEM** | 0.0 | -23.8 | -33.8 | 18.2 | -84.2 | -91.2 | -137.8 | -120.9 |
| $\Delta_r H$ (kJ/mol) | | | | | | | | |
| | **R** | **RC1** | **RC2** | **TS1** | **IM** | **TS2** | **PC** | **P** |
| **Catalyst-free system** | 0.0 | - | -8.2’ | 120.13 | - | - | - | -123.2 |
| **DABCO** | 0.0 | -23.5 | -32.1 | 9.6 | -94.2(-132.3[#]) | -104.5 | -138.3 | -123.2 |
| **1,2-DMI** | 0.0 | -26.3 | -28.1 | 10.4 | -87.6(-125.7[#]) | -95.9 | -142.1 | -123.2 |
| **NEM** | 0.0 | -22.4 | -29.1 | 17.5 | -85.5(-123.6[#]) | -93.1 | -137.8 | -123.2 |
| $\Delta_r G$ (kJ/mol) | | | | | | | | |
| | **R** | **RC1** | **RC2** | **TS1** | **IM** | **TS2** | **PC** | **P** |
| **Catalyst-free system** | 0.0 | - | 29.7’ | 173.7 | - | - | - | -69.9 |
| **DABCO** | 0.0 | 15.5 | 37.4 | 101.9 | 4.9(-19.9[#]) | -2.2 | -42.5 | -69.9 |
| **1,2-DMI** | 0.0 | 13.8 | 47.2 | 106.2 | 10.9(-13.9[#]) | 7.6 | -47.2 | -69.9 |
| **NEM** | 0.0 | 18.2 | 49.9 | 119.1 | 20.8(-4.1[#]) | 13.9 | -39.5 | -69.9 |

’RC for catalyst-free reaction. # Corrected relative enthalpy and relative Gibbs free energies calculated according to ref.[179], [259], [260].

**Urethane formation reactions of phenyl isocyanate and butan-1-ol without and in the presence of aliphatic tertiary amine catalysts**

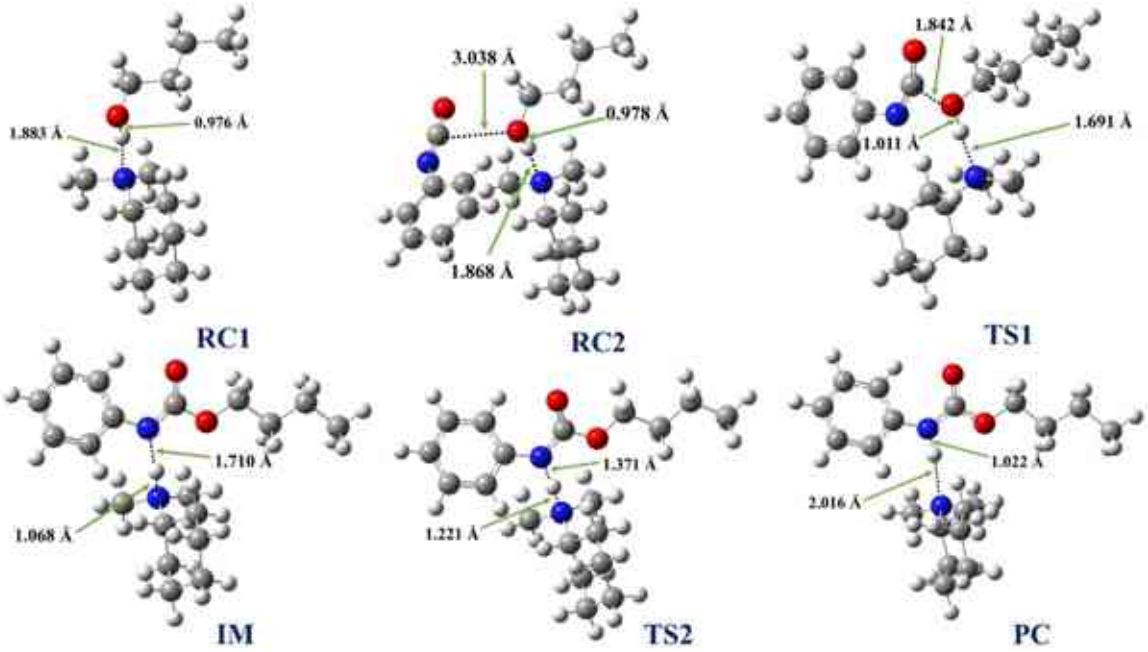


***Figure C1.*** *Optimized structures along the reaction pathway between phenyl isocyanate (PhNCO) and butan-1-ol in the presence of N,N-dimethylcyclohexylamine (DMCHA) calculated at the BHandHLYP/6-31G(d) level of theory in acetonitrile at 298.15 K and 1 atm. RC – reactant complex, TS – transition state, IM – intermediate, PC – product complex.*

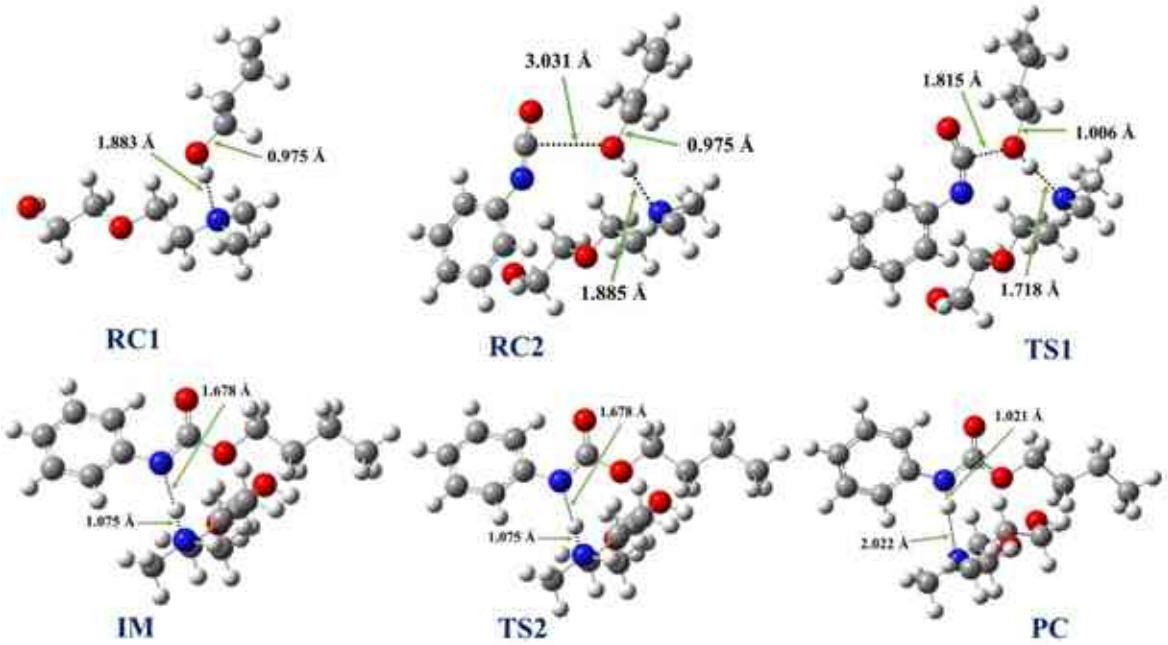


***Figure C2.*** *Optimized structures along the reaction pathway between phenyl isocyanate (PhNCO) and butan-1-ol in the presence of DMEE calculated at the BHandHLYP/6-31G(d)*

*level of theory in acetonitrile at 298.15 K and 1 atm. RC – reactant complex, TS – transition state, IM – intermediate, PC – product complex.*

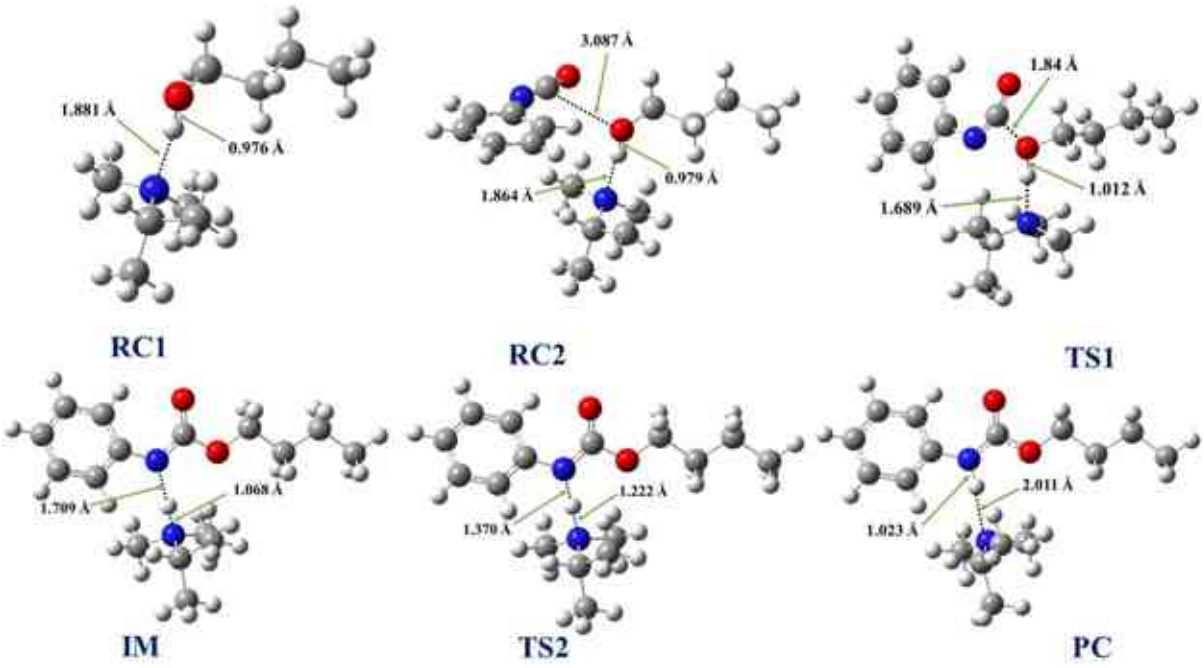


***Figure C3.*** *Optimized structures along the reaction pathway between phenyl isocyanate (PhNCO) and butan-1-ol in the presence of N,N-dimethylpropane-2-amine (DMIPA) calculated at the BHandHLYP/6-31G(d) level of theory in acetonitrile at 298.15 K and 1 atm. RC – reactant complex, TS – transition state, IM – intermediate, PC – product complex.*

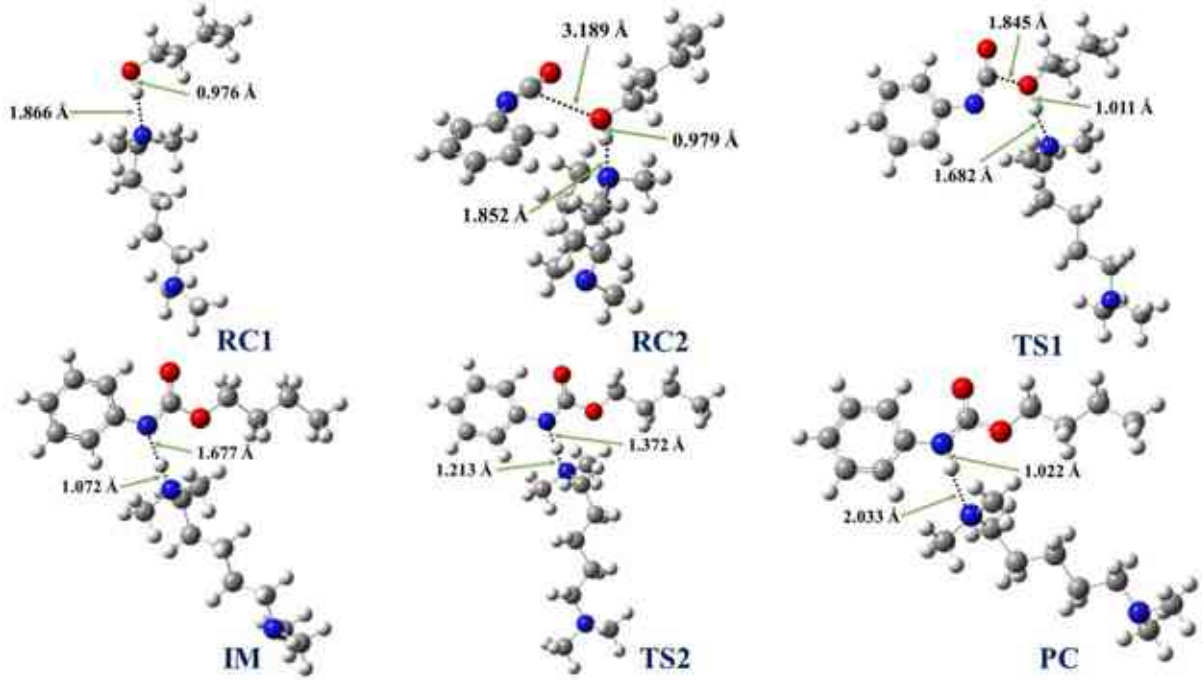


***Figure C4.*** *Optimized structures along the reaction pathway between phenyl isocyanate (PhNCO) and butan-1-ol in the presence of N,N,N',N'-tetramethylpentane-1,5-diamine (TMPD) calculated at the BHandHLYP/6-31G(d) level of theory in acetonitrile at 298.15 K and 1 atm. RC – reactant complex, TS – transition state, IM – intermediate, PC – product complex.*

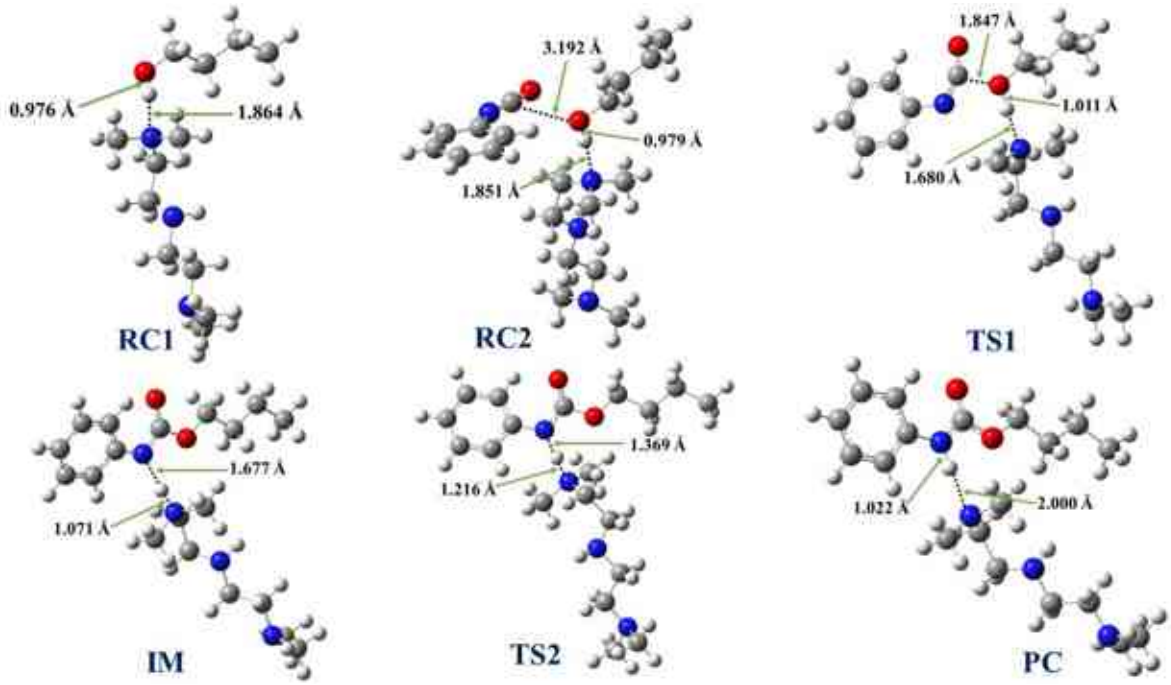


***Figure C5.*** *Optimized structures along the reaction pathway between phenyl isocyanate (PhNCO) and butan-1-ol in the presence of N-[2-(dimethylamino)ethyl]-N',N'-dimethylethane-1,2-diamine (DMAEDMED) calculated at the BHandHLYP/6-31G(d) level of theory in acetonitrile at 298.15 K and 1 atm. RC – reactant complex, TS – transition state, IM – intermediate, PC – product complex.*

***Table C1.*** *Zero-point corrected relative energies ($\Delta_r E_0$), and relative Gibbs free energies ($\Delta_r G$) of the reaction between phenyl isocyanate and butan-1-ol with and without catalysts, calculated at the G3MP2BHandHLYP composite method in acetonitrile using the SMD implicit solvent model at 298.15 K and 1 atm. R – reactant, RC – reactant complex, TS – transition state, IM – intermediate, PC – product complex, P – product. * RC for catalyst-free reaction.*

| $\Delta_r E_0$ (kJ/mol) | | | | | | | | |
|---|---|---|---|---|---|---|---|---|
| | **R** | **RC1** | **RC2** | **TS1** | **IM** | **TS2** | **PC** | **P** |
| **Catalyst-free system** | 0.00 | - | -11.22' | 119.11 | - | - | - | -92.58 |
| **DMCHA** | 0.00 | -29.29 | -51.48 | -5.40 | -104.97 | -114.39 | -130.52 | -92.58 |
| **DMEE** | 0.00 | -28.40 | -48.88 | -4.40 | -96.65 | -105.58 | -131.06 | -92.58 |
| **DMAEE** | 0.00 | -29.04 | -43.57 | -3.07 | -100.93 | -109.33 | -127.63 | -92.58 |
| $\Delta_r G$ (kJ/mol) | | | | | | | | |
| | **R** | **RC1** | **RC2** | **TS1** | **IM** | **TS2** | **PC** | **P** |
| **Catalyst-free system** | 0.00 | - | 28.91' | 170.05 | - | - | - | -41.54 |
| **DMCHA** | 0.00 | 15.24 | 36.85 | 95.68 | -4.69(-29.59[#]) | -9.41 | -30.65 | -41.54 |
| **DMEE** | 0.00 | 14.19 | 37.24 | 97.24 | 5.81(-19.09[#]) | -1.05 | -39.88 | -41.54 |
| **DMAEE** | 0.00 | 12.64 | 40.66 | 94.20 | -1.46(-26.36[#]) | -6.62 | -26.62 | -41.54 |

'RC for catalyst-free (cat.-free) reaction. # Corrected relative Gibbs free energies calculated according to ref.[179], [259], [260].

***Table C2.*** *Zero-point corrected relative energies ($\Delta_r E_0$), relative enthalpies ($\Delta_r H$), and relative Gibbs free energies ($\Delta_r G$),of the reaction between phenyl isocyanate and butan-1-ol in presence of catalysts, calculated at the G3MP2BHandHLYP/6-31G(d) level of theory in acetonitrile using the SMD implicit solvent model at 298.15 K and 1 atm. R – reactant, RC – reactant complex, TS – transition state, IM – intermediate, PC – product complex, P – product.*

| | | | | $\Delta E_0$ (kJ/mol) | | | | |
|---|---|---|---|---|---|---|---|---|
| | **R** | **RC1** | **RC2** | **TS1** | **IM** | **TS2** | **PC** | **P** |
| **DMCHA** | 0.00 | -29.29 | -51.48 | -5.40 | -104.97 | -114.39 | -130.52 | -92.58 |
| **DMIPA** | 0.00 | -27.11 | -45.91 | -2.33 | -101.87 | -110.46 | -127.51 | -92.58 |
| | | | | **$\Delta\Delta E_0$ = 3.07** | | | | |
| **DMAEE** | 0.00 | -29.04 | -43.57 | -3.07 | -100.93 | -109.33 | -127.63 | -92.58 |
| **TMPD** | 0.00 | -29.61 | -43.80 | -3.16 | -103.10 | -111.06 | -127.87 | -92.58 |
| **DMAEDMED** | 0.00 | -29.72 | -43.79 | -3.88 | -103.73 | -111.26 | -127.48 | -92.58 |
| | | | | **$\Delta\Delta E_0$*= 0.09** | | | | |
| | | | | **$\Delta\Delta E_0$ = 0.81** | | | | |
| | | | | $\Delta H$ (kJ/mol) | | | | |
| | **R** | **RC1** | **RC2** | **TS1** | **IM** | **TS2** | **PC** | **P** |
| **DMCHA** | 0.00 | -28.14 | -47.16 | -5.94 | -105.63(-143.73#) | -116.14 | -130.65 | -94.84 |
| **DMIPA** | 0.00 | -25.93 | -41.37 | -2.48 | -102.78(-140.88#) | -112.44 | -127.55 | -94.84 |
| | | | | **$\Delta\Delta_r H$ = 3.46** | | | | |
| **DMAEE** | 0.00 | -27.59 | -38.67 | -3.20 | -101.62(-139.72#) | -111.10 | -127.92 | -94.84 |
| **TMPD** | 0.00 | -27.92 | -38.90 | -3.53 | -104.08(-142.18#) | -112.97 | -127.83 | -94.84 |
| **DMAEDMED** | 0.00 | -27.85 | -38.70 | -3.96 | -104.44(-142.54#) | -113.22 | -127.35 | -94.84 |
| | | | | **$\Delta\Delta_r H$*= 0.33** | | | | |
| | | | | **$\Delta\Delta_r H$ = 0.76** | | | | |
| | | | | $\Delta G$ (kJ/mol) | | | | |
| | **R** | **RC1** | **RC2** | **TS1** | **IM** | **TS2** | **PC** | **P** |
| **DMCHA** | 0.00 | 15.24 | 36.85 | 95.68 | -4.69(-29.59#) | -9.41 | -30.65 | -41.54 |
| **DMIPA** | 0.00 | 15.92 | 38.62 | 93.96 | -0.79(-25.69#) | -6.37 | -29.69 | -41.54 |
| **DMAEE** | 0.00 | 12.64 | 40.66 | 94.20 | -1.46(-26.36#) | -6.62 | -26.62 | -41.54 |
| **TMPD** | 0.00 | 8.59 | 38.23 | 94.85 | -3.36(-28.26#) | -7.33 | -30.72 | -41.54 |
| **DMAEDMED** | 0.00 | 7.08 | 38.39 | 93.25 | -6.71(-31.61#) | -6.94 | -31.83 | -41.54 |

* ($\Delta\Delta E_0$= $TS1_{DMAEE}$ - $TS1_{TMPD}$). # Corrected relative enthalpy and relative Gibbs free energies calculated according to ref.[251,263,264].

## Urethane formation in the presence of 2,2-dimorpholinodiethylether (DMDEE) and 1,4-dimethylpiperazine (DMP)

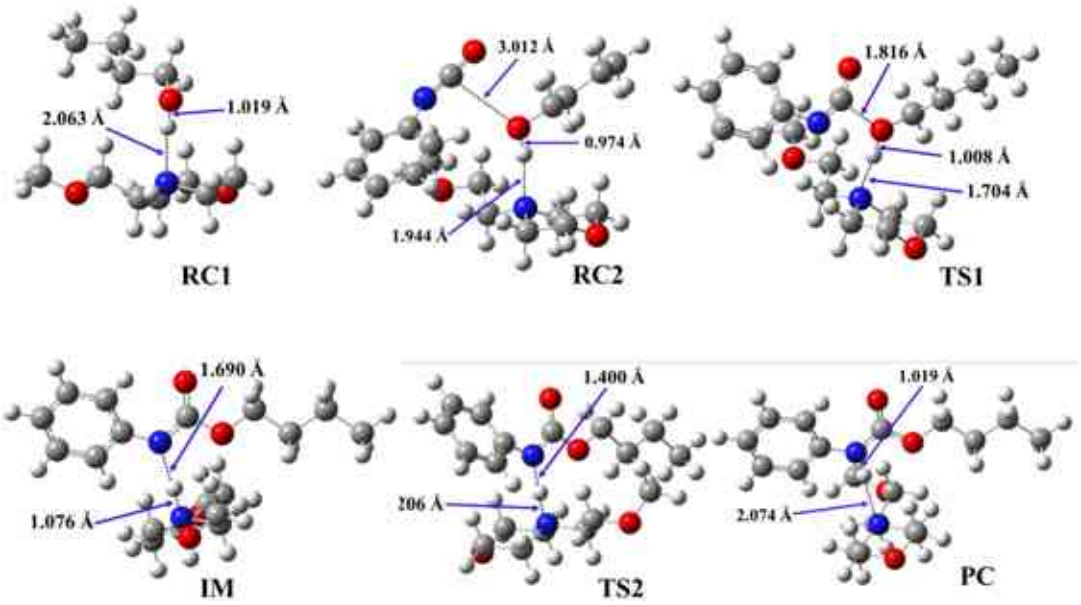


***Figure D1.*** *Optimised structures along the reaction pathway between phenyl isocyanate and butan-1-ol in the presence of truncated model structure calculated at the BHandHLYP/6-31G(d) level of theory in acetonitrile at 298.15 K and 1 atm. RC—reactant complex; TS—transition state; IM—intermediate; PC—product complex.*

***Table D1.*** *Zero-point corrected relative energies ($\Delta_r E_0$), and relative Gibbs free energies ($\Delta_r G$), of the reaction between phenyl isocyanate and butan-1-ol without and in the presence of the studied catalysts, 2,2-dimorpholinodiethylether (DMDEE), and 1,4-dimethylpiperazine (DMP), calculated at the G3MP2BHandHLYP level of theory in acetonitrile using the SMD implicit solvent model at 298.15 K and 1 atm. R—reactant; RC—reactant complex; TS—transition state; IM—intermediate; PC—product complex; P—product.*

| $\Delta_r E_0$ (kJ/mol) | | | | | | | | |
|---|---|---|---|---|---|---|---|---|
| | **R** | **RC1** | **RC2** | **TS1** | **IM** | **TS2** | **PC** | **P** |
| **Catalyst-free system** | 0.00 | - | -11.22' | 119.11 | - | - | - | -92.58 |
| ***DMDEE** | 0.00 | -28.73 | -58.82 | -5.01 | -94.15 | -107.42 | -135.63 | -92.58 |
| **DMP** | 0.00 | -28.02 | -40.90 | -2.38 | -96.71 | -107.45 | -129.19 | -92.58 |
| $\Delta_r G$ (kJ/mol) | | | | | | | | |
| | **R** | **RC1** | **RC2** | **TS1** | **IM** | **TS2** | **PC** | **P** |
| **Catalyst-free system** | 0.00 | - | 28.91' | 170.05 | - | - | - | -41.54 |
| ***DMDEE** | 0.00 | 11.24 | 34.07 | 92.65 | 11.29(-13.61[#]) | -0.44 | -34.72 | -41.54 |
| **DMP** | 0.00 | 13.07 | 39.92 | 94.44 | 5.09(-19.81[#]) | -3.56 | -30.82 | -41.54 |

'RC for catalyst-free reaction. *calculated using the qG3MP2BHandHLYP workflow. # Corrected relative Gibbs free energies calculated according to ref.[251,263,264].

***Table D2.*** *Zero-point corrected relative energies ($\Delta_r E_0$), relative enthalpies ($\Delta_r H$), and relative Gibbs free energies ($\Delta_r G$), of the reaction between phenyl isocyanate and butan-1-ol in presence of the studied catalysts, 2,2-dimorpholinodiethylether (DMDEE), and 1,4-dimethylpiperazine (DMP), calculated at the BHandHLYP/6-31G(d) level of theory in acetonitrile using the SMD implicit solvent model at 298.15 K and 1 atm. R – reactant, RC – reactant complex, TS – transition state, IM – intermediate, PC – product complex, P – product.*

| $\Delta_r E_0$ (kJ/mol) | | | | | | | | |
|---|---|---|---|---|---|---|---|---|
| | **R** | **RC1** | **RC2** | **TS1** | **IM** | **TS2** | **PC** | **P** |
| **Catalyst-free system** | 0.00 | - | -10.48' | 122.75 | - | - | - | -120.94 |
| **DMDEE** | 0.00 | -23.29 | -36.12 | 16.94 | -79.40 | -87.04 | -137.31 | -120.94 |
| **DMP** | 0.00 | -25.03 | -28.54 | 14.58 | -88.03 | -95.33 | -138.65 | -120.94 |
| $\Delta_r H$ (kJ/mol) | | | | | | | | |
| | **R** | **RC1** | **RC2** | **TS1** | **IM** | **TS2** | **PC** | **P** |
| **Catalyst-free system** | 0.00 | - | -8.23' | 120.13 | - | - | - | -123.20 |
| **DMDEE** | 0.00 | -21.82 | -31.95 | 16.92 | -80.27(-118.37[#]) | -88.91 | -137.01 | -123.20 |
| **DMP** | 0.00 | -23.43 | -23.44 | 14.16 | -88.91(-13.61[#]) | -97.14 | -138.69 | -123.20 |
| $\Delta_r G$ (kJ/mol) | | | | | | | | |
| | **R** | **RC1** | **RC2** | **TS1** | **IM** | **TS2** | **PC** | **P** |
| **Catalyst-free system** | 0.00 | - | 29.65' | 173.69 | - | - | - | -69.89 |
| **DMDEE** | 0.00 | 16.69 | 56.77 | 114.60 | 26.04(1.14[#]) | 19.94 | -36.40 | -69.89 |
| **DMP** | 0.00 | 16.07 | 52.28 | 111.40 | 13.77(-11.13[#]) | 8.57 | -40.27 | -69.89 |

'RC for catalyst-free (cat.-free) reaction. # Corrected relative enthalpy and relative Gibbs free energies calculated according to ref.[251,263,264].

## Stoichiometric reaction and catalytic effect of 2-dimethylaminoethanol in urethane formation

***Table E1.*** *Zero-point corrected relative energies ($\Delta_rE_0$), enthalpies ($\Delta_rH$), and relative Gibbs free energies ($\Delta_rG$), of the reaction between phenyl isocyanate and butan-1-ol in the presence 2-dimethylaminoethanol (DMEA) (catalytic system), and reaction between 2-dimethylaminoethanol (DMEA) and phenyl isocyanate (PhNCO) (stoichiometric), calculated at the BHandHLYP/6-31G(d) level of theory in acetonitrile using the SMD implicit solvent model at 298.15 K and 1 atm. R—reactant; RC—reactant complex; TS—transition state; IM—intermediate; PC—product complex; P—product.*

| $\Delta_rE_0$ (kJ/mol) | | | | | | | | |
|---|---|---|---|---|---|---|---|---|
| | **R** | **RC1** | **RC2** | **TS1** | **IM** | **TS2** | **PC** | **P** |
| **Catalyst-free system** | 0.00 | - | -10.48' | 122.75 | - | - | - | -120.94 |
| **Catalytic system** | 0.00 | -25.35 | -37.91 | 13.59 | -86.98 | -96.11 | -138.33 | -120.94 |
| **Stoichiometric system** | 0.00 | -17.68 | - | 44.49 | -46.78 | -52.21 | - | -118.02 |
| $\Delta_rH$ (kJ/mol) | | | | | | | | |
| | **R** | **RC1** | **RC2** | **TS1** | **IM** | **TS2** | **PC** | **P** |
| **Catalyst-free system** | 0.00 | - | -8.23' | 120.13 | - | - | - | -123.20 |
| **Catalytic system** | 0.00 | -24.04 | -33.85 | 13.04 | -88.21 (-126.31[#]) | -98.45 | -138.50 | -123.20 |
| **Stoichiometric system** | 0.00 | -15.89 | - | 40.03 | -51.44 (-89.54[#]) | -57.40 | - | -121.32 |
| $\Delta_rG$ (kJ/mol) | | | | | | | | |
| | **R** | **RC1** | **RC2** | **TS1** | **IM** | **TS2** | **PC** | **P** |
| **Catalyst-free system** | 0.00 | - | 29.65' | 173.69 | - | - | - | -69.89 |
| **Catalytic system** | 0.00 | 16.44 | 49.00 | 111.31 | 15.66 (-9.24[#]) | 8.69 | -41.55 | -69.89 |
| **Stoichiometric system** | 0.00 | 24.04 | - | 100.13 | 12.68 (-12.22[#]) | 7.88 | - | -64.77 |

'RC for catalysts-free reaction. # Corrected relative enthalpy and relative Gibbs free energies calculated according to ref[263,264].

***Table E2.*** *Zero-point corrected relative energies ($\Delta_rE_0$), and relative Gibbs free energies ($\Delta_rG$) of the reaction between phenyl isocyanate (PhNCO) and butan-1-ol in the presence 2-dimethylaminoethanol (DMEA) (catalytic system), and DMEA with PhNCO (stoichiometric system), calculated at the G3MP2BHandHLYP level of theory at (298.15 K and 1 atm) in acetonitrile using the SMD implicit solvent model. R—reactant; RC—reactant complex; TS—transition state; IM—intermediate; PC—product complex; P—product.*

| $\Delta_rE_0$ (kJ/mol) | | | | | | | | |
|---|---|---|---|---|---|---|---|---|
| | **R** | **RC1** | **RC2** | **TS1** | **IM** | **TS2** | **PC** | **P** |
| **Catalyst-free system** | 0.00 | - | -11.22' | 119.11 | - | - | - | -92.58 |
| **Catalytic system** | 0.00 | -26.96 | -42.13 | -2.00 | -94.27 | -104.16 | -126.62 | -92.58 |
| **Stoichiometric system** | 0.00 | -23.98 | - | 43.09 | -46.53 | -52.07 | - | -91.93 |
| $\Delta_rG$ (kJ/mol) | | | | | | | | |
| | **R** | **RC1** | **RC2** | **TS1** | **IM** | **TS2** | **PC** | **P** |
| **Catalyst-free system** | 0.00 | - | 28.91' | 170.05 | - | - | - | -41.54 |
| **Catalytic system** | 0.00 | 14.83 | 44.78 | 95.72 | 8.38(-16.52[#)] | 0.64 | -29.84 | -41.54 |
| **Stoichiometric system** | 0.00 | 17.74 | - | 98.73 | 12.93(-11.97[#)] | 8.01 | - | -38.68 |

'RC for catalysts-free reaction. # Corrected relative Gibbs free energies calculated according to ref.[263,264].

**Urethane formation in the presence of 4-[2-(dimethylamino)ethyl]morpholine, and *N,N*-dimethylbenzylamine**

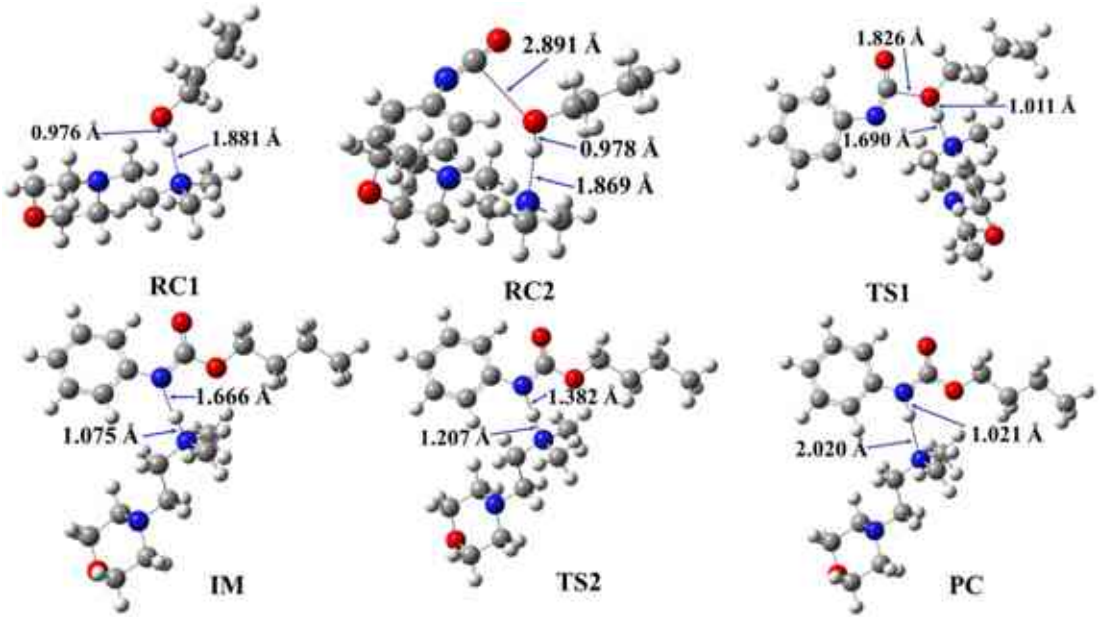


***Figure F1.*** *Optimised structures along the reaction pathway between phenyl isocyanate and butan-1-ol in the presence of 4-[2-(dimethylamino)ethyl]morpholine (DMAEM-2N) calculated at the BHandHLYP/6-31G(d) level of theory in acetonitrile. 2N—aliphatic nitrogen, RC—reactant complex, TS—transition state, IM—intermediate, PC—product complex.*

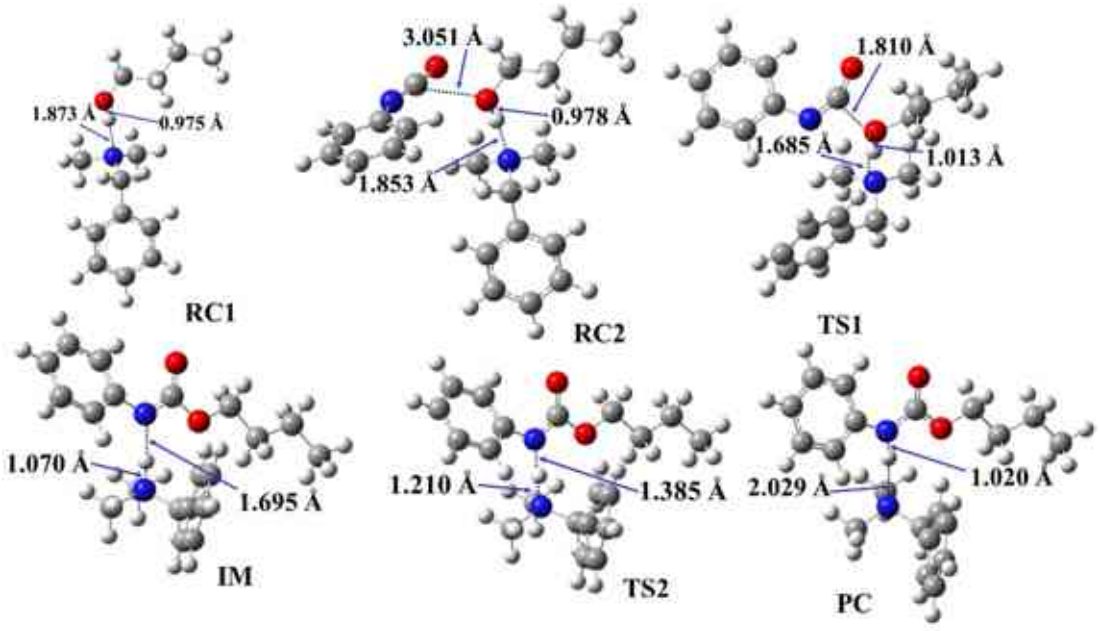


***Figure F2.*** *Optimised structures along the reaction pathway between phenyl isocyanate and butan-1-ol in the presence of N,N-dimethylbenzylamine (DMBA)calculated at the BHandHLYP/6-31G(d) level of theory in acetonitrile. RC—reactant complex, TS—transition state, IM—intermediate, PC—product complex.*

***Table F1.*** *Zero-point corrected relative energies ($\Delta_r E_0$), relative enthalpies ($\Delta_r H$), and relative Gibbs free energies ($\Delta_r G$), of the reaction between phenyl isocyanate and butan-1-ol with and without catalysts, calculated using the BHandHLYP composite method in acetonitrile, using the SMD implicit solvent model at 298.15 K and 1 atm. 1N— aromatic nitrogen, 2N— aliphatic nitrogen, R—reactant, RC—reactant complex, TS—transition state, IM—intermediate, PC—product complex, and P—product.*

| $\Delta_r E_0$ (kJ/mol) | | | | | | | | |
|---|---|---|---|---|---|---|---|---|
| | **R** | **RC1** | **RC2** | **TS1** | **IM** | **TS2** | **PC** | **P** |
| **Catalyst-free system** | 0.00 | - | -10.48’ | 122.75 | - | - | - | -120.94 |
| **DMAEM-1N** | 0.00 | -23.58 | -34.16 | 16.90 | -82.39 | -85.98 | -133.13 | -120.94 |
| **DMAEM-2N** | 0.00 | -21.49 | -32.48 | 17.59 | -87.42 | -94.71 | -134.63 | -120.94 |
| **DMBA** | 0.00 | -18.91 | -30.77 | 17.72 | -88.37 | -95.35 | -138.08 | -120.94 |
| $\Delta_r H$ (kJ/mol) | | | | | | | | |
| | **R** | **RC1** | **RC2** | **TS1** | **IM** | **TS2** | **PC** | **P** |
| **Catalyst-free system** | 0.00 | - | -8.23’ | 120.13 | - | - | - | -123.20 |
| **DMAEM-1N** | 0.00 | -22.22 | -29.91 | 16.66 | -83.35(-121.45#) | -87.77 | -133.22 | -123.20 |
| **DMAEM-2N** | 0.00 | -20.18 | -28.05 | 17.13 | -88.17(-126.27#) | -96.45 | -134.55 | -123.20 |
| **DMBA** | 0.00 | -17.48 | -26.17 | 16.86 | -89.40(-127.50#) | -97.18 | -138.30 | -123.20 |
| $\Delta_r G$ (kJ/mol) | | | | | | | | |
| | **R** | **RC1** | **RC2** | **TS1** | **IM** | **TS2** | **PC** | **P** |
| **Catalyst-free system** | 0.00 | - | 29.65’ | 173.69 | - | - | - | -69.89 |
| **DMAEM-1N** | 0.00 | 21.10 | 57.03 | 114.42 | 21.43(-3.47#) | 20.77 | -32.41 | -69.89 |
| **DMAEM-2N** | 0.00 | 22.22 | 55.42 | 117.25 | 14.33(-10.57#) | 10.34 | -36.52 | -69.89 |
| **DMBA** | 0.00 | 22.57 | 52.95 | 117.59 | 14.84(-10.06#) | 8.81 | -38.89 | -69.89 |

’RC for catalysts-free reaction; # Corrected relative enthalpy and relative Gibbs free energies according to ref.[251,263,264].

***Table F2.*** *Zero-point corrected relative energies ($\Delta_r E_0$), and relative Gibbs free energies ($\Delta_r G$) of the reaction between phenyl isocyanate and butan-1-ol with and without catalysts, calculated using the G3MP2BHandHLYP composite method in acetonitrile, using the SMD implicit solvent model at 298.15 K and 1 atm. 1N— aromatic nitrogen, 2N— aliphatic nitrogen, R—reactant, RC—reactant complex, TS—transition state, IM—intermediate, PC—product complex, and P—product.*

| $\Delta_r E_0$ (kJ/mol) | | | | | | | | |
|---|---|---|---|---|---|---|---|---|
| | **R** | **RC1** | **RC2** | **TS1** | **IM** | **TS2** | **PC** | **P** |
| **Catalyst-free system** | 0.00 | - | -11.22' | 119.11 | - | - | - | -92.58 |
| **DMAEM-1N** | 0.00 | -28.92 | -56.65 | -7.16 | -98.52 | -104.55 | -129.76 | -92.58 |
| **DMAEM-2N** | 0.00 | -22.57 | -47.04 | 3.36 | -93.74 | -102.81 | -120.13 | -92.58 |
| **DMBA** | 0.00 | -25.04 | -42.04 | -3.00 | -101.08 | -111.38 | -132.77 | -92.58 |
| $\Delta_r G$ (kJ/mol) | | | | | | | | |
| | **R** | **RC1** | **RC2** | **TS1** | **IM** | **TS2** | **PC** | **P** |
| **Catalyst-free system** | 0.00 | - | 28.91' | 170.05 | - | - | - | -41.54 |
| **DMAEM-1N** | 0.00 | 15.76 | 34.53 | 90.37 | 5.31($^{-}$19.59$^{\#}$) | 2.19 | -29.03 | -41.54 |
| **DMAEM-2N** | 0.00 | 21.14 | 40.87 | 103.02 | 8.01($^{-}$16.89$^{\#}$) | 2.24 | -22.02 | -41.54 |
| **DMBA** | 0.00 | 16.44 | 41.68 | 96.86 | 2.13($^{-}$22.77$^{\#}$) | -7.22 | -33.58 | -41.54 |

'RC for catalysts-free reaction; # Corrected relative Gibbs free energies calculated according to ref.[251,263,264].

**Urethane formation in the presence of acid catalysts**

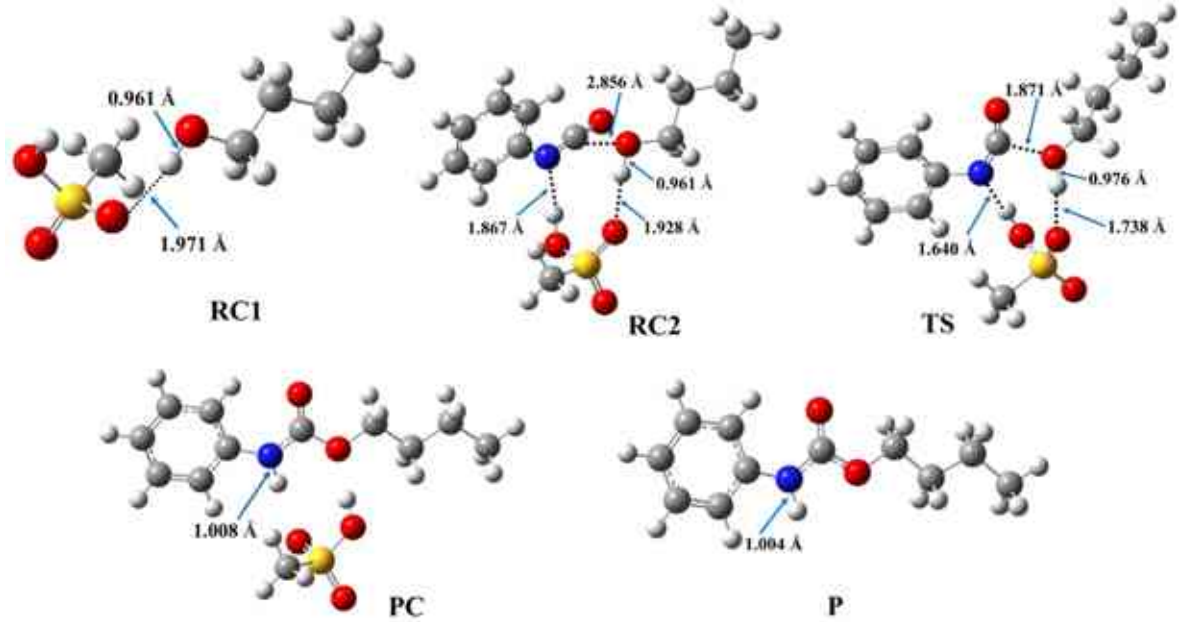


***Figure G1.*** *Optimised structures along the reaction pathway between phenyl isocyanate and butan-1-ol in the presence of methanesulfonic acid (MSA) calculated at the BHandHLYP/6-31G(d) level of theory in acetonitrile. RC—reactant complex, TS—transition state, PC—product complex, and P—product.*

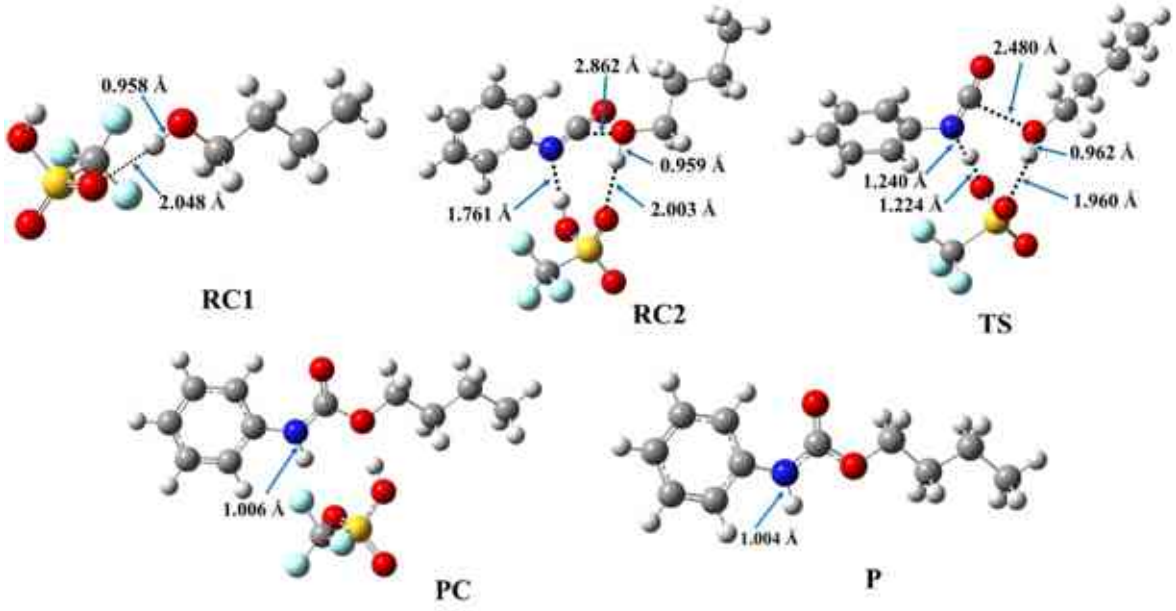


***Figure G2.*** *Optimised structures along the reaction pathway between phenyl isocyanate and butan-1-ol in the presence of trifluoromethanesulfonic acid (TFMSA) calculated at the BHandHLYP/6-31G(d) level of theory in acetonitrile. RC—reactant complex, TS—transition state, PC—product complex, and P—product.*

***Table G1.*** *Zero-point corrected relative energies ($\Delta_r E_0$), relative enthalpies ($\Delta_r H$), and relative Gibbs free energies ($\Delta_r G$), of the reaction between phenyl isocyanate and butan-1-ol in presence of the studied catalysts, dimethyl hydrogen phosphate (DMHP), methanesulfonic acid (MSA), and trifluoromethanesulfonic acid (TFMSA) calculated at the BHandHLYP/6-31G(d) level of theory in acetonitrile using the SMD implicit solvent model at 298.15 K and 1 atm. R – reactant, RC – reactant complex, TS – transition state, IM – intermediate, PC – product complex, P – product.*

| $\Delta_r E_0$ (kJ/mol) | | | | | | |
|---|---|---|---|---|---|---|
| | **R** | **RC1** | **RC2** | **TS1** | **PC** | **P** |
| **Catalyst-free system** | 0.0 | - | -10.48’ | 122.75 | - | -120.94 |
| **DMHP** | 0.0 | -21.67 | -41.77 | -7.93 | -151.94 | -120.94 |
| **MSA** | 0.0 | -13.19 | -34.19 | 0.53 | -144.67 | -120.94 |
| **TFMSA** | 0.0 | -9.95 | -35.97 | -25.77 | -146.28 | -120.94 |
| **$\Delta_r H$ (kJ/mol)** | | | | | | |
| | **R** | **RC1** | **RC2** | **TS1** | **PC** | **P** |
| **Catalyst-free system** | 0.0 | - | -8.23’ | 120.13 | - | -123.20 |
| **DMHP** | 0.0 | -19.32 | -38.12 | -9.40 | -153.13 | -123.20 |
| **MSA** | 0.0 | -11.42 | -30.82 | -1.35 | -145.96 | -123.20 |
| **TFMSA** | 0.0 | -7.28 | -32.57 | -24.36 | -147.11 | -123.20 |
| **$\Delta_r G$ (kJ/mol)** | | | | | | |
| | **R** | **RC1** | **RC2** | **TS1** | **PC** | **P** |
| **Catalyst-free system** | 0.0 | - | 29.65’ | 173.69 | - | -69.89 |
| **DMHP** | 0.0 | 13.78 | 43.57 | 92.46 | -51.18 | -69.89 |
| **MSA** | 0.0 | 25.74 | 52.01 | 98.52 | -45.29 | -69.89 |
| **TFMSA** | 0.0 | 30.20 | 56.17 | 67.24 | -47.89 | -69.89 |

’RC for catalyst-free reaction.

***Table G2.*** *Zero-point corrected relative energies ($\Delta_r E_0$), and relative Gibbs free energies ($\Delta_r G$), of the reaction between phenyl isocyanate and butan-1-ol in presence of the studied catalysts, dimethyl hydrogen phosphate (DMHP), methanesulfonic acid (MSA), and trifluoromethanesulfonic acid (TFMSA) calculated at the G3MP2BHandHLYP/6-31G(d) level of theory in acetonitrile using the SMD implicit solvent model at 298.15 K and 1 atm. R – reactant, RC – reactant complex, TS – transition state, IM – intermediate, PC – product complex, P – product.*

| $\Delta E_0$ (kJ/mol) | | | | | | |
|---|---|---|---|---|---|---|
| | **R** | **RC1** | **RC2** | **TS1** | **PC** | **P** |
| **Catalyst-free system** | 0.0 | - | -11.22’ | 119.11 | - | -92.58 |
| **DMHP** | 0.0 | -20.44 | -51.44 | -13.84 | -131.93 | -92.58 |
| **MSA** | 0.0 | -10.44 | -44.68 | -6.57 | -123.71 | -92.58 |
| **TFMSA** | 0.0 | -9.61 | -49.35 | -44.25 | -129.63 | -92.58 |
| **$\Delta G$ (kJ/mol)** | | | | | | |
| | **R** | **RC1** | **RC2** | **TS1** | **PC** | **P** |
| **Catalyst-free system** | 0.0 | - | 28.91’ | 170.05 | - | -41.54 |
| **DMHP** | 0.0 | 15.02 | 33.91 | 86.56 | -31.17 | -41.54 |
| **MSA** | 0.0 | 28.50 | 41.53 | 91.43 | -24.33 | -41.54 |
| **TFMSA** | 0.0 | 30.54 | 42.80 | 48.75 | -31.24 | -41.54 |

’RC for catalyst-free reaction.